## TOPICS IN HETEROCYCLIC CHEMISTRY

Series Editor R. R. Gupta
Volume Editor L. Strekowski

# Heterocyclic Polymethine Dyes

Synthesis, Properties and Applications



# 14 Topics in Heterocyclic Chemistry

Series Editor: R. R. Gupta

#### **Editorial Board:**

D. Enders · S. V. Ley · G. Mehta · K. C. Nicolaou R. Noyori · L. E. Overman · A. Padwa

#### **Topics in Heterocyclic Chemistry**

Series Editor: R. R. Gupta

#### Recently Published and Forthcoming Volumes

#### **Bioactive Heterocycles VI**

Flavonoids and Anthocyanins in Plants, and Latest Bioactive Heterocycles I Volume Editor: N. Motohashi Volume 15, 2008

#### Heterocyclic Polymethine Dyes

Synthesis, Properties and Applications Volume Editor: L. Strekowski Volume 14, 2008

#### Synthesis of Heterocycles via Cycloadditions II

Volume Editor: A. Hassner Volume 13, 2008

#### Synthesis of Heterocycles via Cycloadditions I

Volume Editor: A. Hassner Volume 12, 2008

#### Bioactive Heterocycles V

Volume Editor: M. T. H. Khan Volume 11, 2007

#### **Bioactive Heterocycles IV**

Volume Editor: M. T. H. Khan Volume 10, 2007

#### **Bioactive Heterocycles III**

Volume Editor: M. T. H. Khan Volume 9, 2007

#### **Bioactive Heterocycles II**

Volume Editor: S. Eguchi Volume 8, 2007

#### **Heterocycles from Carbohydrate Precursors**

Volume Editor: E. S. H. El Ashry Volume 7, 2007

#### Bioactive Heterocycles I

Volume Editor: S. Eguchi Volume 6, 2006

#### Marine Natural Products

Volume Editor: H. Kiyota Volume 5, 2006

#### **QSAR** and Molecular Modeling Studies

in Heterocyclic Drugs II Volume Editor: S. P. Gupta Volume 4, 2006

#### **QSAR and Molecular Modeling Studies**

in Heterocyclic Drugs I Volume Editor: S. P. Gupta

Volume Editor: S. P. Gupta Volume 3, 2006

#### **Heterocyclic Antitumor Antibiotics**

Volume Editor: M. Lee Volume 2, 2006

#### Microwave-Assisted Synthesis of Heterocycles

Volume Editors: E. Van der Eycken, C. O. Kappe

Volume 1, 2006

## Heterocyclic Polymethine Dyes Synthesis, Properties and Applications

Volume Editor: Lucjan Strekowski

With contributions by

B. A. Armitage · Y. Chen · M. P. Dobhal · M. Henary · N. James B. Jędrzejewska · J. Kabatc · J. Kim · M. Mojzych · H. Nakazumi J. Paczkowski · R. K. Pandey · G. Patonay · V. Z. Shirinian A. A. Shimkin · V. F. Traven · A. Watson · S. Yagi



The series *Topics in Heterocyclic Chemistry* presents critical reviews on "Heterocyclic Compounds" within topic-related volumes dealing with all aspects such as synthesis, reaction mechanisms, structure complexity, properties, reactivity, stability, fundamental and theoretical studies, biology, biomedical studies, pharmacological aspects, applications in material sciences, etc. Metabolism will be also included which will provide information useful in designing pharmacologically active agents. Pathways involving destruction of heterocyclic rings will also be dealt with so that synthesis of specifically functionalized non-heterocyclic molecules can be designed.

The overall scope is to cover topics dealing with most of the areas of current trends in heterocyclic chemistry which will suit to a larger heterocyclic community.

As a rule contributions are specially commissioned. The editors and publishers will, however, always be pleased to receive suggestions and supplementary information. Papers are accepted for *Topics in Heterocyclic Chemistry* in English.

In references Topics in Heterocyclic Chemistry is abbreviated Top Heterocycl Chem and is cited as a journal.

Springer WWW home page: springer.com Visit the THC content at springerlink.com

ISBN 978-3-540-79063-1 e-ISBN 978-3-540-79064-8 DOI 10.1007/978-3-540-79064-8

Topics in Heterocyclic Chemistry ISSN 1861-9282

Library of Congress Control Number: 2008923961

© 2008 Springer-Verlag Berlin Heidelberg

This work is subject to copyright. All rights are reserved, whether the whole or part of the material is concerned, specifically the rights of translation, reprinting, reuse of illustrations, recitation, broadcasting, reproduction on microfilm or in any other way, and storage in data banks. Duplication of this publication or parts thereof is permitted only under the provisions of the German Copyright Law of September 9, 1965, in its current version, and permission for use must always be obtained from Springer. Violations are liable to prosecution under the German Copyright Law.

The use of general descriptive names, registered names, trademarks, etc. in this publication does not imply, even in the absence of a specific statement, that such names are exempt from the relevant protective laws and regulations and therefore free for general use.

Cover design: WMXDesign GmbH, Heidelberg Typesetting and Production: le-tex publishing services oHG, Leipzig

Printed on acid-free paper

9876543210

springer.com

#### **Series Editor**

Prof. R. R. Gupta<sup>†</sup>

10A, Vasundhara Colony Lane No. 1, Tonk Road Jaipur-302 018, India rrg\_vg@yahoo.co.in

#### **Volume Editor**

Prof. Lucjan Strekowski

Professor of Chemistry Department of Chemistry Georgia State University P.O. Box 4098 Atlanta, GA 30302-4098 USA lucjan@gsu.edu

#### **Editorial Board**

Prof. D. Enders

RWTH Aachen Institut für Organische Chemie D-52074, Aachen, Germany enders@rwth-aachen.de

Prof. Steven V. Ley FRS

BP 1702 Professor and Head of Organic Chemistry University of Cambridge Department of Chemistry Lensfield Road Cambridge, CB2 1EW, UK svl1000@cam.ac.uk

Prof. G. Mehta FRS

Director
Department of Organic Chemistry
Indian Institute of Science
Bangalore- 560 012, India
gm@orgchem.iisc.ernet.in

#### Prof. K.C. Nicolaou

Chairman
Department of Chemistry
The Scripps Research Institute
10550 N. Torrey Pines Rd.
La Jolla, California 92037, USA
kcn@scripps.edu
and
Professor of Chemistry
Department of Chemistry and Biochemistry
University of California
San Diego, 9500 Gilman Drive
La Jolla, California 92093, USA

VI Editorial Board

#### Prof. Ryoji Noyori NL

President
RIKEN (The Institute of Physical and Chemical Research)
2-1 Hirosawa, Wako
Saitama 351-0198, Japan
and
University Professor
Department of Chemistry
Nagoya University
Chikusa, Nagoya 464-8602, Japan
noyori@chem3.chem.nagoya-u.ac.jp

#### Prof. Larry E. Overman

Distinguished Professor Department of Chemistry 516 Rowland Hall University of California, Irvine Irvine, CA 92697-2025 leoverma@uci.edu

#### Prof. Albert Padwa

William P. Timmie Professor of Chemistry Department of Chemistry Emory University Atlanta, GA 30322, USA chemap@emory.edu

## Topics in Heterocyclic Chemistry Also Available Electronically

For all customers who have a standing order to Topics in Heterocyclic Chemistry, we offer the electronic version via SpringerLink free of charge. Please contact your librarian who can receive a password or free access to the full articles by registering at:

springerlink.com

If you do not have a subscription, you can still view the tables of contents of the volumes and the abstract of each article by going to the SpringerLink Homepage, clicking on "Browse by Online Libraries", then "Chemical Sciences", and finally choose Topics in Heterocyclic Chemistry.

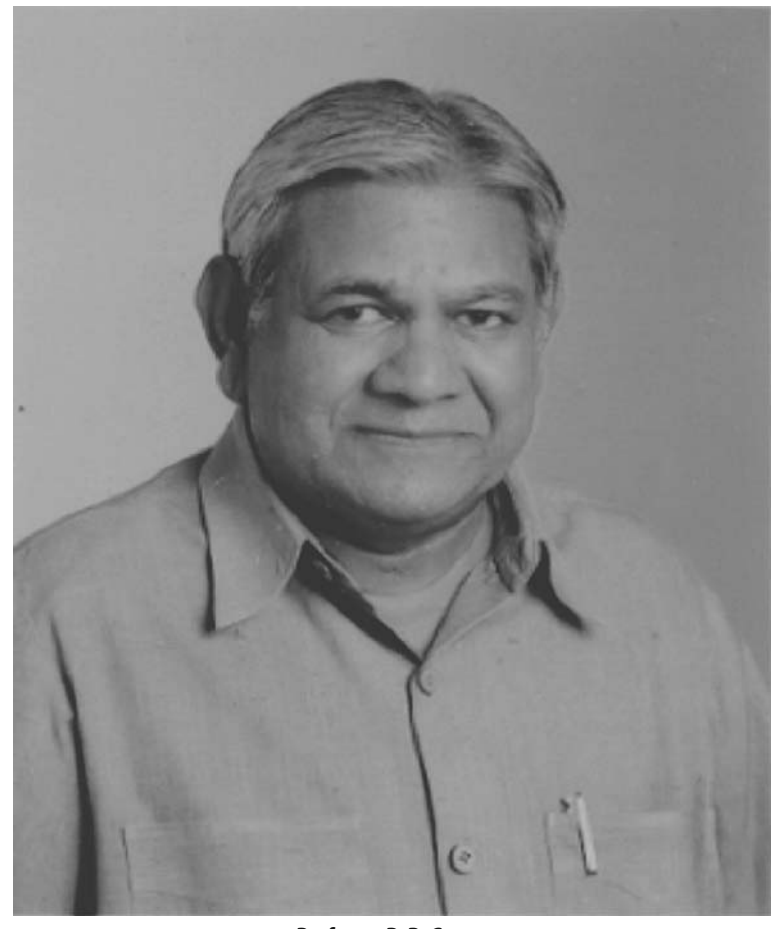
You will find information about the

- Editorial Board
- Aims and Scope
- Instructions for Authors
- Sample Contribution

at springer.com using the search function.

Color figures are published in full color within the electronic version on SpringerLink.

#### Obituary Professor R. R. Gupta (1941–2008)



Professor R. R. Gupta Great Heterocyclic Chemist Highly Spiritual Person

R. R. Gupta, distinguished professor, eminent scientist, founding editor of International Journal of Heterocyclic Communications, founding editor of the well-known series *Topics in Heterocyclic Chemistry* (Springer), editor of volumes within the Landolt-Bærnstein series, and author as well as co-author of several research monographs and books, passed away suddenly on 8<sup>th</sup> March 2008 due to cardiac arrest.

Prof. Gupta was born on the 18th Aug 1941 in Rajgarh, a small town of the Alwar district in Rajasthan state of India. He received his MSc and PhD in Chemistry from the University of Rajasthan, Jaipur, India. After receiving his PhD degree Prof. Gupta joined the Chemistry Department of the University of Rajasthan as an Assistant Professor in 1968. Prof. Gupta had a distinguished career not only in science but in education, too. He served University of Rajasthan for 33 years as an Assistant Professor, Associate Professor, and Professor. He was a highly distinguished faculty member who was loved and admired by colleagues and students alike.

Prof. Gupta was a prominent scientist who contributed commendable work in chemical research. The areas of research interest included heterocyclic and theoretical chemistry (diamagnetism and chemical bonding).

Prof. Gupta made significant contributions to the field of heterocyclic chemistry. He introduced an international journal of heterocyclic chemistry called *Heterocyclic Communications* (published by Freund Publishing House, London) and served as Editor-in-Chief in collaboration with the regional editors from the US, France, and Japan and an international editorial board of nearly 80 eminent scientists from all over the world. Prof. Gupta introduced an international series in heterocyclic chemistry *Topics in Heterocyclic Chemistry*, published by Springer, with an International editorial board of five distinguished professors and eminent scientists including Nobel Laureate Prof. R. Noyori (Japan). Fifteen volumes of *Topics in Heterocyclic Chemistry* have already been published on different recent and emerging topics of heterocyclic chemistry and five to six volumes are in process of publication.

Prof. Gupta authored, co-authored, and edited nearly 15 volumes on NMR spectral data of different elements in the most prestigious and oldest series of chemistry, the Landolt-Bærnstein series, published by Springer. Prof. Gupta also edited three volumes on "Diamagnetic Susceptibility and Anisotropy of Organic and Organo-metallic Compounds" in the Landolt-Bærnstein series. Two volumes have already been published and a third volume is to appear soon.

Prof. Gupta edited a handbook on *Physical Methods in Heterocyclic Chemistry* (published by Wiley, New York) to which top ranking distinguished scientists from all over the world contributed. He edited a book *Phenothiazines and 1,4-Benzothiazines: Chemical and Biomedical Aspects* (published by Elsevier, Amsterdam); also to this volume a number of distinguished scientists contributed their research articles.

Prof. Gupta not only contributed research monographs to self-edited books, but also to books edited by other renowned scientists. He contributed to the prestigious series *Chemistry of Functional Groups* edited by S. Patai and published by Wiley. He also contributed a chapter to the CRC *Handbook of Chemistry and Physics* in its 59th Edition.

Prof. Gupta authored not only a number of reference books and monographs relating to his research field, but also authored text books on heterocyclic chemistry published by Springer, which are used in Indian and foreign universities at post-graduate level.

Prof. Gupta was Chairman and Member of several national and international committees. He visited 28 countries for his scientific research and delivered plenary and invited lectures and chaired scientific sessions at international conferences. He also organized as chairman an international conference sponsored by the International Union of Pure and Applied Chemistry (IUPAC) "Phenothiazine and Related Psychotropic Drugs" in 1996 held at Jaipur, India. He was a member of the International Advisory Board for an international conference on "Reversal of Drug Resistance" (Szeged, Hungary). He was also a member of the International Advisory Board of the International Society of Antimicrobial Activity of Non-Antibiotics and organized the 2nd international conference in Denmark. Prof. Gupta was a member of the Advisory Council of the International Biographical Centre (Cambridge, England), and a member of the International Society of Heterocyclic Chemistry. For his service to science and to education, Prof. Gupta was included among the top 100 scientists of the world by the International Biographical Centre (England). Prof. Gupta was a member of the UGC committee (UGC, New Delhi) which framed the chemistry syllabus for UG and PG classes in Indian universities.

Prof. Gupta supervised more than 30 students for their Doctorate degree. He published nearly 250 scientific articles in journals of international repute (including ACS Journals). Prof. Gupta was awarded an International Fellowship by the International Union against Cancer (UICC, Switzerland) to carry out research work in the cancer research laboratory of the Medical School of Auckland University in New Zealand. He was awarded fellowships for Post-Doctoral research work in Marseille (France) and Munich (Germany).

R. R. Gupta retired in 2001 and remained active in research as a distinguished editor until his death. Though quite healthy till the end, he passed away rather suddenly. Personally, we have lost our respected father and Guru. It is a great loss to his family, friends, well wishers, and of course the scientific community which benefited from his significant contributions.

We've never been cold here in your shadow because we've had your sunlight on our faces... but you weren't content to shine... You wouldn't dare leave us behind so..... we've had a part in all of your glories, now we share a part of your strengths. Your beautiful face... for so long. The beautiful smile that hid your pain. It might have appeared to have gone unnoticed... but we've got it all here in our hearts. We want you to know, we know the truth... Of course we know... We might have been nothing without you. Did you ever know that you were our hero? You were all of those things we're striving to be... Now we can climb toward that higher mark... Because you were the wind beneath our wings. WE THANK GOD FOR YOU with much love.

Dr. Vandana Gupta (Editor-in-Chief) Heterocyclic Communications, A-13, Jai Jawan Colony-I, Tonk Road Jaipur-302018, India, e-mail: *dr vandana27@yahoo.co.in* 

#### **Preface**

This treatise pertains to dyes composed of a central polymethine moiety and two cyclic terminal subunits. The polymethine linker can be unsubstituted or substituted, and at least one terminal subunit is a heterocyclic system. The classes of compounds reviewed range from classical cyanines, first synthesized in the 1850s, to hemicyanines, to styryl dyes, to merocyanines, to coumarin polymethines, and to squarylium dyes that were synthesized for the first time in the 1960s. These structurally diverse classes of compounds have one common denominator, namely electron conjugation that involves the terminal heterocyclic/aromatic subunits and the central polymethine linker of the molecule. Such conjugated molecules show absorption and fluorescence that are a function of the structure of the three moieties. By changing the length and substitution of the polymethine linker and/or the structures of the terminal moieties, molecules can be designed with absorption and fluorescence ranging from the blue visible region (> 400 nm) to the near-infrared region (> 700 nm) of the electromagnetic spectrum. The synthetic developments of the last decade are reviewed and references to older but important work are provided to help design a dye of interest for a desired specific application. It is the fluorescence properties that are most important for a large array of modern applications of the dyes, especially in biotechnology. Some of the applications are clearly visible from the titles of the individual chapters, and additional features can be found upon inspection of the corresponding tables of contents. The subject index should be consulted for other properties and applications of the dyes that could not be elaborated on extensively in this relatively short review book. The authors took excellent care of such information by providing leading references on the additional subjects. I wish to thank the authors for their outstanding contributions. Thanks are also due to Ms. Birgit Kollmar-Thoni of Springer and Ms. Cornelia Gründer of le-tex publishing services oHG who effortlessly and with grace coordinated the technical aspects of the total project.

Atlanta, May 2008

Lucjan Strekowski

#### **Contents**

Synthesis of Cyanine Dyes M. Mojzych · M. Henary	1
Cyanine Dye-Nucleic Acid Interactions B. A. Armitage	11
Near-Infrared Cyanine Dye-Protein Interactions J. Kim · A. Watson · M. Henary · G. Patonay	31
Cyanine Dye-Based Compounds for Tumor Imaging With and Without Photodynamic Therapy R. K. Pandey · N. James · Y. Chen · M. P. Dobhal	41
Merocyanines: Synthesis and Application V. Z. Shirinian · A. A. Shimkin	75
Coumarin Polymethines, Their Boron Complexes and Analogs V. F. Traven	107
Squarylium Dyes and Related Compounds S. Yagi · H. Nakazumi	133
Polymethine Dyes as Fluorescent Probes and Visible-Light Photoinitiators for Free Radical Polymerization J. Paczkowski · J. Kabatc · B. Jędrzejewska	183
Stability and Reactivity of Polymethine Dyes in Solution M. Henary · M. Mojzych	221
Subject Index	239

#### **Synthesis of Cyanine Dyes**

Mariusz Mojzych¹ · Maged Henary² (☒)

1	Introduction	1
2	Synthesis	2
2.1	Monomethine Cyanines	2
2.2	Trimethine Cyanines	3
2.3	Pentamethine Cyanines	4
2.4	Heptamethine Cyanines	6
Dofo	rancas	ç

**Abstract** Recent developments in the general synthesis of cyanine dyes are reviewed. This short chapter provides a background to the subsequent reviews of applications of cyanines.

**Keywords** Heptamethine cyanines  $\cdot$  Monomethine cyanines  $\cdot$  Pentamethine cyanines  $\cdot$  Synthesis  $\cdot$  Trimethine cyanines

#### 1 Introduction

Classical cyanine dyes are cationic molecules in which two terminal nitrogen heterocyclic subunits are linked by a polymethine bridge as shown by the general structure 1.

Their common names denote the number of methine groups in the polyene chain. For example, compounds 1 with n=0 and n=3 are referred to as monomethine and heptamethine cyanines, respectively. The end subunits containing a nitrogen atom may be identical or different. Hemicyanines may be represented by a general structure 2, and particular derivatives with the shortest bridge (n=1) are often called styryl dyes. The first member of cyanine compounds was synthesized in 1856. Several cyanine dyes are natural products [1]. The monomethine and trimethine cyanines generally show absorption in the visible region, and each extension of the chromophore by one vinylene moiety (CH = CH) causes a bathochromic shift of about 100 nm [2]. Depending on substituents, absorption of pentamethine derivatives can reach a near-infrared region (>700 nm), and heptamethine cyanines may show absorption beyond 1000 nm. Cyanine dyes have narrow absorption bands and

<sup>&</sup>lt;sup>1</sup>Department of Chemistry, University of Podlasie, 08-110 Siedlce, Poland

<sup>&</sup>lt;sup>2</sup>Department of Chemistry, Georgia State University, Atlanta, Georgia 30302-4098, USA chemmh@langate.gsu.edu

$$X \stackrel{+}{\stackrel{-}{R^1}}$$

1

 $X \stackrel{+}{\stackrel{-}{R^1}}$ 
 $X \stackrel{+}{\stackrel{-}{R^1}}$ 
 $X \stackrel{+}{\stackrel{-}{R^1}}$ 
 $X \stackrel{+}{\stackrel{-}{R^1}}$ 

extremely high extinction coefficients, often reaching  $200\,000\,\mathrm{M^{-1}}\,\mathrm{cm^{-1}}$ . Cyanine dyes are mildly fluorescent in solution and the fluorescence quantum yield decreases with increasing length of the polymethine chain [3]. The fluorescence efficiency is greatly increased upon binding of the dyes with nucleic acids or proteins as a result of the rigidization of the fluorophore.

A large number of cyanine dyes have been synthesized and reviewed [1–10]. The most recent synthetic methodologies are briefly summarized in this chapter and an additional recent synthetic work is described in the chapters Cyanine Dye – Based Compounds for Tumor Imaging With and Without Photodynamic Therapy and Stability and Reactivity of Polymethine Dyes in Solution. The older reviews mentioned above should be consulted for a complete picture of the preparation of cyanine dyes.

In general, structural diversity is reached through varying the polyene chain, the nitrogen substituents, or the heterocycles themselves. However, this general approach is not compatible with some reactive groups that are required for a fine tuning of the solubility, reactivity, and spectroscopic properties of the cyanine dyes, as may be necessary for a wide range of modern applications. In fact, only carboxylic and sulfonic acid groups are completely inert toward the reagents and reaction conditions used for synthesis of cyanine dyes. This major drawback can be by-passed by an alternative synthetic approach based on the preparation of a precursor of the target functionalized cyanine dye, a so-called "convertible cyanine dye", and the subsequent post-synthetic chemical transformations to give the molecule bearing the desired substituents.

#### 2 Synthesis

#### Monomethine Cyanines

Highly fluorescent derivatives of this class of compounds have been developed as molecular probes that bind strongly with nucleic acids [11–17] and proteins [18]. Additional information can be found in the respective Chapters Cyanine Dye – Nucleic Acid Interactions and Cyanine Dye – Based Compounds for Tumor Imaging With and Without Photodynamic Therapy. A novel method for the preparation of symmetrical and asymmetrical monomethine cyanine dyes 3 was developed by Deligeorgiev et al. [19]. The

#### **Equation 1**

chemistry is illustrated in Eq. 1 and it involves melting under basic conditions of a quaternary heterocyclic salt containing a 2- or 4-methyl group and a 2-sulfobetaine derived from a cationic heterocyclic system. The applicability of this method depends on the melting points of the substrates and their thermal stabilities.

## 2.2 Trimethine Cyanines

The classical orthoester approach to trimethine cyanines involves condensation under basic conditions of orthoesters with quaternary heterocyclic salts substituted with an activated methyl group [20]. The methodology is illustrated in Eq. 2 by the preparation of a water-soluble sulfonated dye 4 [21]. In similar transformations, a central one-carbon component of the trimethine bridge is derived from N,N'-diphenylformamidine [22, 23] or iodoform [23]. The diphenylformamidine method allows for the synthesis of unsymmetrical dyes containing two different end-heterocyclic subunits or two different N-substituents at the identical heterocyclic systems [24]. The central methine moiety of the trimethine bridge in dyes 6 and 7 can also be supplied by a novel Vilsmeier-type reagent derived from N,N-dimethylformamide and hydrogen bromide (Scheme 1) [25].

#### **Equation 2**

A post-synthetic modification at a meso position of a meso-methylsubstituted trimethine dye is illustrated in Eq. 3 by condensation with an aldehyde to give dye 8. An ethyl analogue undergoes a similar condensation at the  $\alpha$  position of the ethyl group [26].

**Equation 3** 

#### 2.3 **Pentamethine Cyanines**

A major synthetic route to this class of compounds involves condensation of cationic heterocyclic compounds containing an activated methyl group with derivatives of malondialdehyde. Recent synthetic examples are shown in Eq. 4 by the preparation of a water soluble dye 9 [21] and in Scheme 2 by the preparation of a dye 10 containing two different N-substituents [27]. A modification of the latter synthetic route for the synthesis of a different penthamethine dye has also been published [24]. A series of cyanines substituted with methyl and ethoxycarbonyl groups at the pentamethine chain

#### **Equation 4**

#### Scheme 2

have been synthesized by using ethyl 3-oxobutanoate as a precursor to the substituted pentamethine chain [28] (not shown).

Highly polar dyes, such as **9** and **10**, are difficult to purify. Crystallization seldom furnishes pure compounds, and a substantial amount of the dye is irreversibly adsorbed by using classical silica gel chromatography. The purification method of choice is reverse-phase chromatography using a commercial C18 adsorbent. This and similar adsorbents are currently quite inexpensive and can be used in low-pressure reverse-phase column chromatography for purification of highly polar compounds on a several-gram scale. Dye **10** was purified by using this method [27].

## 2.4 Heptamethine Cyanines

Currently there is an immense interest in the chemistry of heptamethine cyanines due to their application as fluorescence markers in biological sciences. A separate chapter *Cyanine Dye-Based Compounds For Tumor Imaging With and Without Photodynamic Therapy* has been devoted to this topic. A vast majority of such dyes contain a six-membered carbocyclic subsystem as part of the heptametine chain, such as in compound 13 (Eq. 5), which increases rigidity of the molecule for an increased quantum yield of fluorescence. For steric reasons, this structural feature also decreases aggregation of dye molecules in solution.

CI 
$$\xrightarrow{PhHh}$$
 NHPh  $\stackrel{\uparrow}{R^2}$  NHPh  $\stackrel{\downarrow}{R^2}$  NHPh  $\stackrel{\downarrow}{R^2}$  NHPh  $\stackrel{\downarrow}{R^2}$  11:  $R^1 = H, X = CI, Br$  13

#### **Equation 5**

The first dyes of this class were synthesized about 30 years ago [29] by condensation of Vielsmeier–Haack reagent 11 derived from cyclohexanone and a heterocyclic salt (mostly an iodide) containing an activated methyl group. An analogue of 11 derived from cyclopentanone is sometimes used for the preparation of the corresponding analogues of 13 [30]. Strekowski has introduced recently an ethoxycarbonyl-substituted reagent 12 for a facile functionalization of the corresponding dyes 13 (R<sup>1</sup> = COOEt) [31]. He also has shown that the chloro-substituted dyes 13 can additionally be functionalized at the meso position by the reaction with nucleophiles that are good single-electron donors [30]. The mechanism, scope, and limitations of this

efficient transformation are discussed in more detail in the chapter *Stability* and *Reactivity of Polymethine Dyes in Solution* of this book. It is important to note that amino derivatives of **103** (X = SUDSTILLE = SUD

Strekowski and coworkers reported for the first time the synthesis of a novel class of near-infrared bis(heptamethine cyanine) (BHmC) dyes containing a flexible polymethylene linker between the two cyanine subunits [35, 36]. Such bis-cyanines may be of significant bioanalytical utility due to their negligible fluorescence in aqueous solution and a strong increase in fluorescence (~1000 fold) upon binding with a protein. More specifically, the bisdyes form an intramolecular stacking complex in solution, which quenches fluorescence, and the complex opens-up upon binding of the dye with protein, which greatly increases the fluorescence efficiency. The synthesis of dyes BHmCs is presented in Scheme 3. Briefly, indolenine 14 was quaternized with

#### Scheme 3

an  $\alpha$ ,  $\omega$ -dibromoalkane to yield a bis-indolium salt 15, which was subsequently condensed with a half dye 17. Compound 17 was obtained by using excess of the Vielsmeier reagent 11 relative to the indolium salt 16.

#### References

- 1. Reichardt C (1995) J Phys Org Chem 8:761
- 2. Mishra A, Behera RK, Behera PK, Mishra BK, Behera GB (2000) Chem Rev 100:1973
- 3. Haughland RP (2002) Molecular Probes. Handbook of Fluorescent Probes and Research Chemicals, 9th ed. Molecular Probes Inc, Eugene, OR
- 4. Fabian J, Nakazumi H, Matsuoka M (1992) Chem Rev 92:1179
- 5. Matsuoka M (1990) Infrared Absorbing Dyes. Plenum Press, New York, NY
- Matsuoka M (1990) Absorption Spectra of Dyes for Diode Lasers. Bunshin Publishing Co., Tokyo
- 7. Hammer FM (1964) The Cyanine Dyes and Related Compounds. Wiley, New York
- 8. Tyutyulkov N, Fabian J, Mehlhorn A, Dietz F, Tadjer A (1991) Polymethine Dyes: Structure and Properties. St. Kliment Ohridski University Press, Sofia, Bulgaria
- 9. James TH (1977) The Theory of the Photographic Process. Macmillan, New York
- 10. Raue R (1990) Methine Dyes and Pigments. In: Ullman's Encyclopedia of Industrial Chemistry, vol. A16, 5th edn. Wiley, Weinheim, p 487
- 11. Deligeorgiev TG, Zaneva DA, Kim SH, Sabnis RW (1998) Dyes Pigm 37:205
- 12. Gadjev NI, Deligeorgiev TG, Kim SH (1999) Dyes Pigm 40:181
- Deligeorgiev TG, Gadjev NI, Timtcheva II, Maximova VA, Katerinopoulos HE, Foukaraki E (1999) Dyes Pigm 44:131
- 14. Gadjev NI, Deligeorgiev TG, Timcheva I, Maximova V (2003) Dyes Pigm 57:161
- Rye HS, Yue S, Wemmer DE, Quesada MA, Haugland RP, Maties RA, Glazer AN (1992) Nucleic Acids Res 20:2803
- 16. Stark D, Hamed AA, Pedersen EB, Jacobsen JP (1997) Bioconjugate Chem 8:869
- 17. Jacobsen JP, Pedersen JB, Hansen LF, Wemmer DE (1995) Nucleic Acids Res 23:753
- 18. Yarmoluk SM, Kryvorotenko DV, Balanda AO, Losytskyy MY, Kovalska VB (2001) Dyes Pigm 51:41
- 19. Deligeorgiev TG, Zaneva DA, Katerinopoulos HE, Kolev VN (1999) Dyes Pigm 41:49
- Peng Z-H, Qun L, Zhou X-F, Carroll S, Geise HJ, Peng B-X, Dommisse R, Carleer R (1996) J Mater Chem 6:559
- 21. Mujumdar SR, Mujumdar RB, Grant CM, Waggoner AS (1996) Bioconjugate Chem 7:356
- 22. Peng Z-H, Geise HJ, Zhou X-F, Peng B-X, Carleer R, Dommisse R (1997) Liebigs Ann Recueil, p 27
- 23. De Rossi U, Moll J, Spieles M, Bach G, Daehne S (1995) J Pract Chem 337:203
- 24. Jung ME, Kim W-J (2006) Bioorg Med Chem 14:92
- 25. El-Shishtawy RM, Almeida P (2006) Tetrahedron 62:7793
- 26. Mitekura H, No T, Suzuki K, Satake K, Kimura M (2002) Dyes Pigm 54:113
- 27. Chipon B, Clavé G, Bouteiller C, Massonneau M, Renard P-Y, Romieu A (2006) Tetrahedron Lett 47:8279
- 28. Mahmoud R, El-Aal A (2002) Dyes Pigm 52:129
- 29. Makin SM, Boiko II, Shavrygina OA (1977) Zh Org Khim 13:1189
- 30. Strekowski L, Lipowska M, Patonay G (1992) J Org Chem 57:4578
- 31. Lipowska M, Patonay G, Strekowski L (1995) Heterocycl Commun 1:427

- 32. Zhou Li-Ch, Zhao G-J, Liu J-F, Han K-L, Wu Y-K, Peng X-J, Sun M-T (2007) J Photochem Photobiol A 187:305
- 33. Peng X, Song F, Lu E, Wang Y, Zhou W, Fan J, Gao Y (2005) J Am Chem Soc 127:4170
- 34. Lee H, Mason JC, Achilefu S (2008) J Org Chem 73:72335
- 35. Patonay G, Kim JS, Kodaghally R, Strekowski L (2005) Appl Spectrosc 59:682
- 36. Kim JS, Kodagahally R, Strekowski L, Patonay G (2005) Talanta 67:947

#### **Cyanine Dye-Nucleic Acid Interactions**

#### Bruce A. Armitage

Department of Chemistry, Carnegie Mellon University, 4400 Fifth Avenue, Pittsburgh, PA 15213-3890, USA army@andrew.cmu.edu

1	Introduction	12
2	Symmetrical Cyanines	14
2.1	Noncovalent Binding	14
2.2	Covalent Binding	16
3	Unsymmetrical Cyanines	17
3.1	Noncovalent Binding	17
3.1.1	Insights into Photophysics	17
	New Unsymmetrical Dyes	18
	Applications	21
3.2	Covalent Binding	23
3.2.1	DNA-Conjugated Dyes	24
	PNA-Conjugated Dyes	25
	Peptide- and Protein-Conjugated Dyes	26
4	Conclusions	27
Refer	rences	28

**Abstract** Cyanine dyes are widely used in biotechnology due to their ability to form fluorescent complexes with nucleic acids. This chapter describes how the structure of the dye determines the mode in which it binds to nucleic acids as well as the fluorescence properties of the resulting complexes. Related dyes, such as hemicyanines and styryl dyes, are briefly described as well. In addition, covalent conjugates of cyanines with nucleic acids or with nucleic acid-binding ligands allow fluorescent labeling and probing of DNA/RNA structure and function. Several examples of different types of conjugates and their applications are described.

**Keywords** Cyanines · Dyes · Fluorescence · Intercalation · Nucleic Acids

#### **Abbreviations**

A Adenine C Cytosine

DNA Deoxyribonucleic acid

FRET Förster resonance energy transfer

G Guanine

HOMO Highest occupied molecular orbital

LUMO Lowest unoccupied molecular orbital

PNA Peptide nucleic acid RNA Ribonucleic acid T Thymine

### Introduction

The cyanines are among the oldest synthetic dyes commonly used today. The name "cyanine" comes from the first member of this class, which was reported by Williams in 1856 and was blue in color [1]. In the ensuing 150+ years, thousands more cyanines have been synthesized due to demand based on diverse applications of these versatile dyes [2]. Their ease of synthesis and rich palette of colors initially motivated the use of cyanines in the textile industry. Later, the cyanines became important components of photographic films, making possible the development of vibrant color images. Both of these applications rely on the ability of cyanines to efficiently absorb light at specific wavelengths in the visible region. Most recently, the cyanines have found a third home in the biotechnology sector that relies on their ability to emit light, i.e., fluoresce. In particular, cyanine dyes have become widely used as fluorescent labels and sensors for bioimaging and detection applications. Many of these applications involve the interaction between the dyes and nucleic acids (DNA and RNA), which is the subject of this chapter. A brief summary of the structural and spectroscopic properties of the cyanines is in order.

The general structure for a cyanine is shown in Fig. 1. In these dyes, two nitrogen-containing heterocycles are linked by a polymethine bridge containing an odd number of carbons, which allows resonance delocalization of a positive charge between the two nitrogens. Variation of the length of the polymethine bridge and the identity of the heterocycles allows tuning

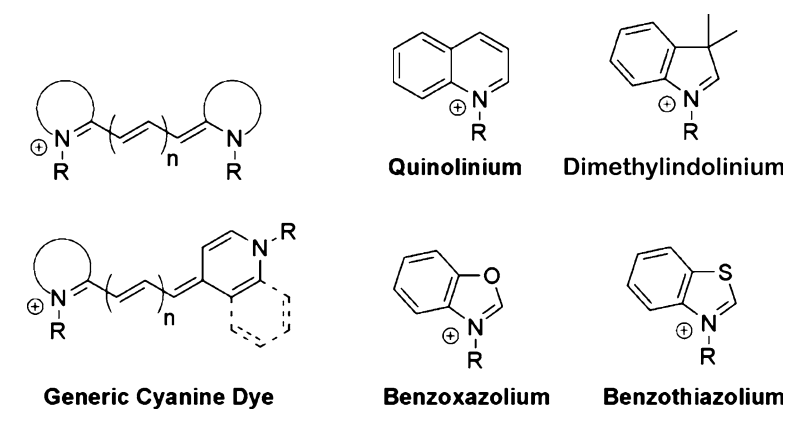
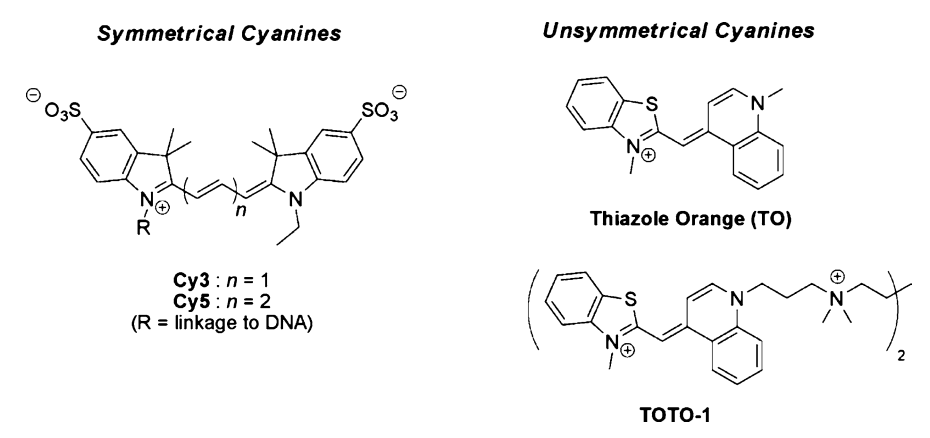


Fig. 1 Generic structures of cyanine dyes and typical heterocyclic components

of the absorption and emission spectra throughout the visible and near-infrared regions of the electromagnetic spectrum. For example, addition of two extra methine units typically causes a ca. 100 nm spectral shift to a longer wavelength. Meanwhile, dyes based on dimethylindole and benzo-thiazole heterocycles have comparable absorption and emission wavelengths, whereas benzoxazole-containing dyes absorb at shorter wavelengths. Adding substituents to one or both rings allows further fine-tuning of the spectra.

Cyanines can be categorized structurally as being either *symmetrical* or *unsymmetrical*, examples of which are shown in Fig. 2. This chapter will consider these two structural classes separately, since they often exhibit vastly different spectral and nucleic acid binding behavior, which leads to distinct applications. For example, the fluorescent DNA labels Cy3 and Cy5 are symmetrical cyanines, while the commonly used fluorescent DNA stain thiazole orange (TO) and the dimeric analogue TOTO-1 are unsymmetrical cyanines (the latter with respect to the chromophore, not the overall structure).



**Fig. 2** Commonly used symmetrical and unsymmetrical cyanine dyes. (Counterions are not shown; these are typically iodide, bromide, or tosylate.)

This introduction concludes with a brief description of nucleic acid binding modes. Cyanine dyes typically associate noncovalently with double-helical DNA in one of two ways: (1) intercalation, in which the dye inserts between two adjacent base pairs resulting in a  $\pi$ -stacked sandwich complex, or (2) minor groove binding, in which the dye inserts lengthwise into the narrower of the two grooves present in the DNA structure. Methods for determining DNA binding modes are reviewed elsewhere [3] and so will not be discussed here. For additional information, interested readers are also referred to recent detailed reviews of the interactions between cyanine dyes and DNA [4,5]. This chapter will focus on how the dye structure relates to nucleic acid binding mode and photophysical behavior, with emphasis on both fundamental properties and applications.

#### 2 Symmetrical Cyanines

## 2.1 Noncovalent Binding

The earliest report of a cyanine dye–DNA interaction was published by Lerman in his classic paper proposing the intercalation binding mode for planar, cationic dyes that were commonly used to stain DNA for microscopic observation [6]. The dye, pinacyanol, caused a decrease in the viscosity of a DNA solution, in contrast to acridine dyes, which increased the viscosity of the same solutions. Intercalation necessarily causes the DNA to lengthen, leading to the observed increased viscosity, so Lerman concluded that pinacyanol bound in a nonintercalative manner and this conclusion was supported by later studies. However, simply decreasing the bridge length of the dye by two methines yields pseudoisocyanine, which unequivocally binds to DNA by intercalation at low dye to DNA ratios [7]. Another example is provided by the tricationic dye DiSC<sub>3+</sub>(5), which binds to various types of DNA by intercalation as well as by minor groove binding as either a monomer or a cofacial dimer [8].

$$n = 1$$
: Pinacyanol  $n = 0$ : Pseudoisocyanine DiSC<sub>3+</sub>(5):  $R = (CH_2)_3N(CH_3)_3$ 

An interesting class of symmetrical cyanines features substitution of the methine bridge. For example, Yarmoluk and coworkers synthesized Cyan2, an analogue of  $DiSC_1(3)$  bearing a methyl group at the beta (i.e., central) carbon of the trimethine bridge [9]. Under identical conditions, the unsubstituted dye exhibits a <5-fold increase in fluorescence in the presence of DNA while the  $\beta$ -methyl analogue displays a ca. 100-fold fluorescence enhancement (Table 1) [9, 10]. The difference can be traced to the background fluorescence

Dye	F (Buffer)	F (DNA)	Enhancement
$DiSC_1(3)$	560	2570	4.6
Cyan2	24.5	4350	178
1	8.6	610	71
2	5.4	1120	207

Table 1 Fluorescence enhancements for symmetrical cyanines in the presence of DNA

of the two dyes in the absence of DNA. A similarly large enhancement is observed for the  $\beta$ -methyl dye in the presence of RNA as well. The origin of this behavior has been attributed to a change in the stereochemistry of the trimethine bridge [11]. In the unsubstituted dye, the strongly fluorescent all-*trans* isomer should be favored. However, substitution on the bridge is expected to lead to *cis* isomers, which are nonfluorescent (Fig. 3). Whether binding of **Cyan2** to DNA or RNA induces isomerization to the all-*trans* form or promotes fluorescence by another mechanism is unclear. Regardless of the mechanism, the fact that the  $\beta$ -methyl dye has a low fluorescence quantum yield in solution allows it to exhibit a large enhancement upon nucleic acid binding. The idea of using fluorogenic dyes as indicators for the presence of nucleic acids will also be an important theme for the unsymmetrical cyanines described later in this chapter.

**Fig. 3** Effect of a *meso* alkyl substituent on conformation and fluorescence of a symmetrical cyanine dye

Nonfluorescent

The same group studied the impact of substituents at carbon 6 of the benzothiazole ring system for trimethine dyes bearing unsubstituted or  $\beta$ -substituted bridges [10]. Bulky benzoylamino groups at these positions (e.g., dyes 1 and 2) led to improved fluorescence enhancements in the presence of DNA, relative to  $DiSC_1(3)$  and Cyan2 (Table 1). In both cases, the larger fluorescence enhancement is due to lower fluorescence in buffer rather than higher fluorescence in DNA. The likely explanation for these results is enhanced formation of nonfluorescent aggregates by the 6,6'-substituted dyes

in the absence of DNA rather than to a change in the inherent photophysical properties of the dye. The peripheral amide substituents also increase the selectivity for DNA over RNA and bovine serum albumin, a protein that is known to bind organic dyes via hydrophobic interactions.

The complexity of noncovalent DNA binding by symmetrical cyanines has led to very few applications. One exception is the monocationic dye  ${\bf DiSC_2(5)}$ , which was found to assemble into helical aggregates in the presence of a hybrid duplex composed of complementary DNA and peptide nucleic acid (PNA) strands [12]. (Like many symmetrical cyanines [13,14],  ${\bf DiSC_2(5)}$  also aggregates in water, but only at higher concentrations than were used in the assay.) Aggregation of  ${\bf DiSC_2(5)}$  in the presence of PNA–DNA duplexes leads to a 120-nm shift to shorter wavelength of the absorption spectrum, resulting in a visible blue-to-purple color change. Thus, the PNA oligomer and cyanine dye constitute a simple qualitative sensor for the presence of specific DNA sequences. Several subsequent reports described improvements on the original assay [15–17].

## 2.2 Covalent Binding

In contrast to the dearth of applications involving noncovalent binding of symmetrical cyanines to DNA or RNA, covalently bound versions of these dyes, particularly Cy3 and Cy5 [18], are among the most widely used fluorescent labels in biotechnology. For example, in DNA/RNA microarray experiments, captured target strands are usually detected using Cy3 (green) or Cy5 (red) fluorescence, where the dye is introduced either in the form of a Cylabeled secondary probe strand that hybridizes to the captured target or by enzymatic synthesis of a Cy-labeled DNA strand complementary to the target, with subsequent capture of the fluorescent strand on the array.

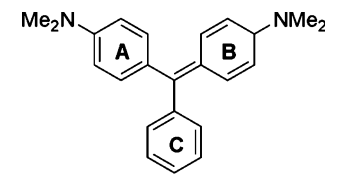
Two structural features of Cy3 and Cy5 are evident (Fig. 2): the dimethylindole heterocycles and the peripheral anionic sulfonate substituents are present to suppress intercalation into DNA as well as dye aggregation, which is a concern for multiply labeled probes. These properties help to give the "CyDyes" high fluorescence quantum yields (and, therefore, sensitive detection) without interfering with DNA hybridization.

#### 3 Unsymmetrical Cyanines

## 3.1 Noncovalent Binding

### 3.1.1 Insights into Photophysics

The unsymmetrical cyanines such as thiazole orange (TO, Fig. 2) are best known for their fluorogenic behavior in the presence of DNA and RNA. These dyes exhibit very low fluorescence quantum yields in aqueous solution but 10<sup>2</sup>-10<sup>3</sup>-fold enhancements upon binding to nucleic acids [19]. The fluorescence response has long been attributed to restricted torsional motion of the dye excited state when intercalated into DNA [20]. Recent ultrafast time-resolved experiments by Ernsting and colleagues were consistent with a twisting motion leading to nonradiative relaxation of TO in fluid solution [21]. In addition, calculations by Yaron and coworkers indicate that twisting beyond an interplanar angle of 60° is required before nonradiative relaxation becomes efficient [22]. Thus, TO and presumably other unsymmetrical cyanines need not be planar in order to exhibit a large fluorescence enhancement: rigidification with an interplanar angle less than 60° should also lead to strong fluorescence from the dye. This phenomenon has also been observed in the case of the fluorogenic dye malachite green bound to a specific RNA aptamer: the interplanar angle between the A and B rings is 57° [23], yet the fluorescence is increased more than 1000-fold upon binding to the RNA [24].



Malachite Green

The unsymmetrical cyanines typically bind to DNA with  $K_{\rm d}$  values in the low to mid micromolar range, depending on the ionic strength of the medium and the charge state of the dye [25]. This means that nucleic acids present at nanomolar or lower concentrations will not be detected by the fluorogenic dye. In order to improve the affinity and, therefore, sensitivity of DNA/RNA detection, a series of bis-cyanine dyes such as TOTO-1 (Fig. 2) have been synthesized [26]. The presence of two intercalating groups as well as four positive charges leads to binding at nanomolar concentrations.

Vauthey and coworkers showed that the maximum fluorescence enhancements observed for bis-intercalating cyanines are lower than those for the corresponding monointercalating analogues [27]. This is not due to differences in the quantum yields of the bound dyes, which are very similar. Rather, in the absence of DNA, the two chromophores of a bis-intercalating cyanine dye can  $\pi$ -stack, yielding an intramolecular dimer. The authors propose that stacking of the two chromophores actually suppresses the twisting motion that leads to deactivation of the dye excited state. Thus, where fluorophore dimerization is often associated with reduced fluorescence, in the case of the bis-cyanines dimerization enhances fluorescence, albeit only slightly. Since the quantum yield in the absence of DNA is higher for the bis dyes, they exhibit smaller enhancements upon intercalating into DNA. In practice, the significantly higher affinity of the bis-intercalators usually outweighs the lower fluorescence enhancement, so dyes such as TOTO-1 are more widely used than monointercalating analogues.

#### 3.1.2 New Unsymmetrical Dyes

Synthetic efforts are continuing to focus on new fluorogenic dyes for detecting DNA and/or RNA. Deligeorgiev and coworkers recently reported several interesting new unsymmetrical cyanines [28]. The novel feature of these dyes is an expanded heterocyclic system that includes the benzothiazole normally found in **TO** derivatives, such as in compound **3**. These dyes also substitute a nitrogen atom for one of the CH groups in the polymethine bridge. Dye **3** exhibited a 360-fold fluorescence enhancement in the presence of double-stranded DNA.

Silva and coworkers synthesized several TO analogues bearing electron-withdrawing fluorine and trifluoromethyl groups on the benzothiazole or quinoline ring systems (Fig. 4, [22]). These substituents significantly alter the HOMO-LUMO gap, leading to predictable spectral shifts. For example, fluorination of the benzothiazole system results in blue-shifted absorption and emission spectra. This is because the HOMO is spread over both rings but the LUMO is localized on the quinoline. Therefore, electron-withdrawing fluor-

Fig. 4 Fluorinated thiazole orange derivatives

ine substituents on the benzothiazole will stabilize the HOMO more than the LUMO, leading to the observed blue-shift. These authors also reported that while increased fluorination resulted in improved photostability (as observed previously for a symmetrical cyanine dye [29]), DNA binding affinity was reduced.

The *hemicyanines* can be classified as unsymmetrical dyes due to the fact that only one of the two nitrogens is part of a heterocyclic system. Hemicyanine 4 was synthesized and characterized by Kostenko and coworkers [30]. This dye is similar to **TO** in that it has a benzothiazole group and a single methine in the bridge between the two ring systems, although the longer conjugation in 4 leads to absorption and emission at longer wavelengths. The dye exhibits a 10–15-fold fluorescence enhancement in the presence of double-stranded DNA. The weaker fluorogenic behavior compared to **TO** appears to be due to stronger fluorescence of 4 in the absence of DNA. Based on the computational study by Yaron described above [22], it would be interesting to determine whether the torsional barrier in the excited state is lower for 4 than for **TO**.

Another mechanism for enhancing fluorescence in hemicyanines was described in the same paper by Kostenko [30]. A precursor dye possessing an exocyclic methyl ether instead of an amine was synthesized and exhibited ca. 100–150-fold lower fluorescence than 4, both in aqueous buffer and in the presence of DNA. However, in situ reaction with a primary amine led to substitution of the methoxy group and concomitant enhancement of fluores-

cence. This reaction was used to label a protein with the dye, but could also be extended to labeling of other biomolecules and probes.

A hemicyanine dye has also found use as a reporter for guanine (G) quadruplex DNA. Quadruplexes are the subject of increasing scrutiny due to their suspected involvement in regulating gene expression at multiple levels, including transcription, splicing, and translation [31]. Dye-peptide conjugate 5 was discovered by screening of a combinatorial library for binding to a DNA quadruplex structure modeled on the human telomeric DNA sequence [32]. The dye bound to the quadruplex at low micromolar concentrations and exhibited greater than 600-fold lower affinity for double-stranded DNA. The same dye was subsequently used to monitor the unfolding kinetics of a DNA quadruplex [33]. The DNA was covalently labeled with tetramethylrhodamine, which served as the energy acceptor in a Förster resonance energy transfer (FRET) assay where noncovalently bound 5 was the donor. Unfolding of the quadruplex and trapping by a complementary DNA oligonucleotide resulted in release of the hemicyanine donor and loss of FRET. The results are significant because the dynamics of quadruplex folding/unfolding as well as the interconversion between different quadruplex polymorphs are likely to be intimately associated with the biological functions of these intriguing structures.

5

The styryl dyes are similar to unsymmetrical cyanines in that they have two heterocyclic nitrogen atoms and are cationic, but the charge is not delocalized as effectively by resonance as in the cyanines. Nevertheless, these dyes can exhibit substantial shifts and enhancements in fluorescence in response to environmental changes. Recently, Chang and coworkers screened a combinatorial library of styryl dyes for selective RNA staining and obtained three useful compounds [34]. The best dye 6 exhibits more than 50-fold enhancement of fluorescence upon binding to ribosomal RNA from *Escherichia coli*. Both green and red fluorescence were observed, depending on the dye structure, and effective staining of intracellular RNA was observed by confo-

cal microscopy. The dearth of selective labels for RNA makes this work highly significant and it will be interesting to learn the specific interactions the dye uses to recognize RNA.

## 3.1.3 Applications

An interesting application for the intercalating unsymmetrical cyanines was recently reported by Benvin and coworkers [35]. Whereas most applications of these dyes involve detection of the DNA or RNA into which they intercalate, these investigators used a DNA-dye assembly to fluorescently label other things, such as mammalian cells and polystyrene beads. The concept is shown in Fig. 5: intercalating dyes bind to the DNA template at high densities, creating very bright fluorescent objects (where "brightness" is defined as the product of the molar extinction coefficient and the fluorescence quantum yield). By virtue of having so many dyes bound to the same DNA template, the overall assembly has a very large extinction coefficient. (A similar concept was proposed by Glazer in a patent [36]; the main innovation in the pub-

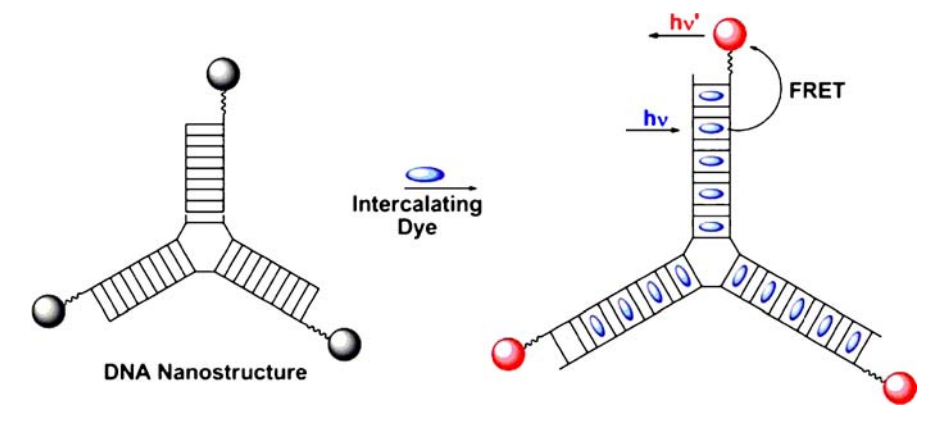


**Fig. 5** Illustration of the DNA nanotag concept. Intercalating dye is an unsymmetrical cyanine such as a high-affinity thiazole orange or oxazole yellow analogue. Branched DNA substrates allow assembly of high-density fluorophore arrays

lished work is the use of a branched DNA template to increase the density of fluorophores.) This supramolecular fluorophore, referred to as a "DNA nanotag", can be functionalized with various groups that allow its attachment to a wide variety of substrates, imparting an intensely fluorescent label. Furthermore, additional attachment of longer-wavelength energy acceptor dyes leads to efficient FRET. This allows large separation between the excitation and emission wavelengths, which should improve image quality due to reduced background fluorescence from the sample. The main drawback to the system is that the dyes are noncovalently bound to the DNA template, meaning they are free to dissociate and bind to other molecules in the sample. Nevertheless, straightforward chemistry is available that allows dyes to be covalently attached to DNA, so this problem should be readily addressed.

The binding of various small molecules to DNA is typically studied under decidedly nonbiological conditions with respect to the nucleic acid. Genomic DNA generally exists in highly compacted states when packaged into cellular nuclei, and an important question concerns how this affects DNA binding of dyes that are used for microscope imaging. Åkerman and coworkers approached this question by studying the association of four different unsymmetrical cyanines with genomic DNA packaged into protein capsids of bacteriophage T5 [37]. The dyes varied with respect to overall charge (+1 to +4) and DNA binding mode (intercalation vs minor groove binding). Binding of the dyes to the packaged capsid DNA was compared to the same DNA extracted from the capsid. The binding kinetics were considerably slower, particularly for the tetracationic bisintercalator, YOYO-1. In addition, the affinities of the dyes were ca. fivefold lower for the capsid DNA. Possible explanations for these results include conformational constraints imposed by packaging of the DNA into the capsid, which is expected to im-

pact intercalation because of the structural distortion imposed on the DNA by the dye, and competition with multivalent cations that are present inside the capsid to help balance the high negative charge density compared with extended DNA in solution. Another intriguing result from this study was the tendency of the dication intercalator (YO-PRO-1) and groove binder (BOXTO-PRO [38]) to induce aggregation of the bacteriophage. The authors suggest that this is due to association of the dyes with the phage tails by electrostatic attraction, resulting in cross-linking of the phage and assembly into clusters.

## 3.2 Covalent Binding

The large fluorescence enhancements exhibited by **TO** and related dyes upon binding to DNA and RNA has led to their widespread use in the laboratory over the past two decades. While much is known about the photophysics of these dyes, a lingering question concerns the sequence dependence of fluorescence. Early work by Netzel and coworkers revealed that both **TO-PRO-1** and **YO-PRO-1**, dicationic analogues of **TO** and **YO**, respectively, exhibited ca. 50–80% greater fluorescence in alternating G-C versus alternating A-T sequences [39]. Even in the simplified DNA copolymers used for those experiments, uncertainty exists about the dye binding site since there are two distinct intercalation sites, e.g., 5'-A-T-3' or 5'-T-A-3'.

The challenge in further refining our understanding of how sequence determines fluorogenic response is controlling where the dye binds. In an attempt to address this, Seitz and coworkers synthesized a series of PNA oligomers in which the central base was replaced by **TO** and was flanked by various combinations of bases [40]. The PNA-**TO** conjugates were then hybridized with their corresponding perfectly matched and mismatched single-

**PNA-TO Conjugate** 

stranded DNA oligonucleotides. (A thymine was always placed directly across from the **TO**.) In contrast to the earlier report by Netzel et al., the highest quantum yields ( $\phi_f = 0.20$ –0.27) were observed when at least one of the flanking base pairs was A-T/T-A. When both flanking base pairs were G-C or C-G,  $\phi_f = 0.13$ –0.16. Whether the lower quantum yields in G-C/C-G intercalation sites reflect a less restrictive environment or partial quenching by a competitive mechanism such as electron transfer is unknown. Similar experiments in which **TO** is forced to intercalate at a specific site within DNA–DNA duplexes would also be interesting because the different helical parameters for DNA–DNA and PNA–DNA could lead to different fluorogenic responses by the dye in homologous sequence contexts.

## 3.2.1 DNA-Conjugated Dyes

The fluorogenic properties of unsymmetrical cyanines have been exploited in several different conjugation formats, where a dye is covalently attached to a nucleic acid, protein, or other molecule. If the dye conjugate binds to another molecule and the local environment of the dye is substantially changed in the resulting complex, a change in fluorescence might be observed allowing sensing of the binding event. The first example of this concept was reported by Ishiguro and coworkers, who attached oxazole yellow to a DNA oligonucleotide at an internal position [41]. (The dye was linked to the phosphorus in the internucleotide linker, so no base was replaced.) Hybridization of the YO–DNA conjugate to a complementary DNA resulted in a ca. 20-fold fluorescence enhancement. This effect was attributed to intercalation of the dye into the DNA double helix.

More recently, Lartia and Asseline investigated a large number of cyanine–DNA conjugates [42]. Several different monomethine dyes were attached to either internal or terminal positions on DNA oligonucleotides. Surprisingly, most of the conjugates exhibited *lower* fluorescence after hybridization to complementary DNA strands. This insensitivity to hybridization could arise from stacking of the dye with the nucleobases in the single-stranded conjugate, leading to substantial fluorescence even in the absence of the complementary strand. A similar effect has been noted for conjugates of these dyes with PNA, described in more detail in the next section.

The same research group also reported on the behavior of DNA probes labeled at the 5' end with TO [43]. Once again, the hybridized probes exhibited lower fluorescence than the single-stranded probe, but the significant finding was that hybridization to oligonucleotides having single mismatches resulted in greater fluorescence than for perfectly matched complements. The reason for this discrimination is unclear, although one possibility is that the mismatched base pair allows the DNA to adapt better to the TO intercalator, creating a more effective binding site for the dye.

# 3.2.2 PNA-Conjugated Dyes

The high affinity and sequence selectivity of PNA for complementary DNA and RNA targets [44] has generated great interest in its use in a wide variety of hybridization-based applications [45]. Thiazole orange, oxazole yellow, and other analogues have been conjugated to the ends of PNA oligomers [46]. The resulting PNA-TO conjugates have been commercialized as "LightUp® probes" and have found use as reporters in real-time PCR assays that measure viral loads in patients infected by cytomegalovirus and SARS coronavirus [47].

LightUp® probes have been used primarily to detect specific DNA or RNA target sequences. A slightly different application involves using the fluorescence enhancement of the conjugated TO to report on successful hybridization of a PNA to a desired nucleic acid. For example, Peteanu and coworkers developed a FRET assay for RNA splicing, a posttranscriptional process that deletes internal regions of RNA (introns) and connects the flanking regions (exons) [48]. PNA probes labeled with fluorescent donor and acceptor dyes were designed to hybridize to the exons on either side of an intron. Splicing deletes the intron and links the exons, bringing the donor- and acceptor-labeled PNAs into close proximity and leading to a large increase in FRET efficiency (Fig. 6). TO-labeled probes were used initially to demonstrate that both PNAs bound to the large, folded RNA target. In the FRET experiments, TO was retained as the donor fluorophore while an Alexa dye was conjugated to the acceptor PNA. Splicing resulted in >75% FRET efficiency and was detected both in bulk solution and by using single molecule microscopy.

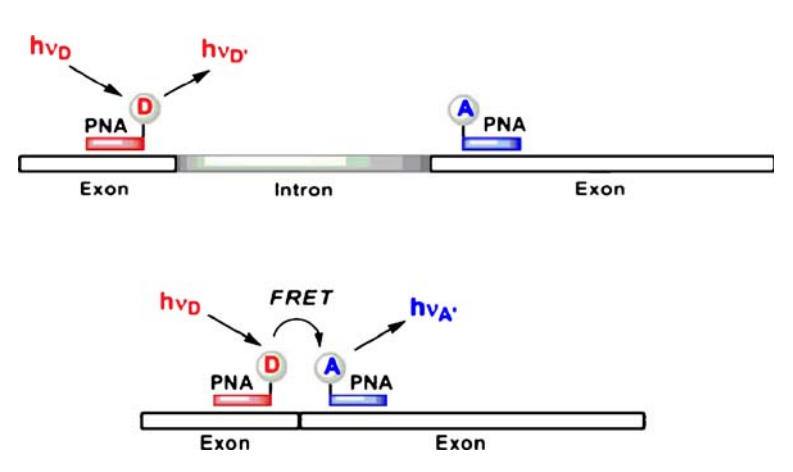


**Fig. 6** Use of fluorescent PNA probes to assay RNA splicing. Unsymmetrical cyanine dyes exhibit fluorogenic responses upon hybridization, verifying RNA labeling. Increased FRET indicates splicing

26 B.A. Armitage

The fluorogenic dye used in hybridization probes need not be attached to a terminal position. As described earlier, Seitz and coworkers have synthesized PNA probes in which TO was attached directly to the backbone at an internal site [40]. The resulting PNA-TO conjugates are called "forced intercalation" (FIT) probes due to the fact that TO, like other intercalators such as ethidium bromide [49], binds only weakly to PNA-DNA hybrids. These probes can be hybridized to complementary DNA targets having any base opposite the TO [50]. Good mismatch discrimination was observed when the dye was attached to the PNA via a short linker extending from the quinoline ring. Fluorescence enhancements of 10–20-fold were observed upon hybridization to perfectly matched targets, whereas lower enhancements result from targets having single mismatches directly adjacent to the TO site. Comparison of a series of linker lengths and conjugation site revealed that an acetyl linker to the quinoline ring gave the best results, with tenfold greater fluorescence than the same linker to the benzothiazole ring.

# 3.2.3 Peptide- and Protein-Conjugated Dyes

The fluorogenic properties of the unsymmetrical cyanines have also been exploited for studying DNA-binding peptides and proteins. For example, Kelley and coworkers synthesized a series of TO-conjugated cationic peptides and studied their binding to calf thymus DNA [51]. Substantial fluorescence enhancements were seen in most cases, with conjugation of the peptide to the quinoline ring leading to ca. threefold greater quantum yields than conjugation to the benzothiazole ring. The better performance of the quinoline-linked conjugate is similar to that reported for the FIT probes described in the preceding paragraph, and it will be interesting to see if similar results are obtained for other types of TO conjugates.

Along similar lines, Thompson synthesized conjugates where **YO** was attached to sequence-specific DNA binding peptides [52]. In the presence of double-stranded DNA containing a binding site for the peptide, the peptide-conjugated dye exhibited a fluorescence quantum yield of 0.37 and an estimated enhancement factor of 770, values that compare well with those of DNA-bound **YO** (i.e., without the peptide): 0.44 and 920, respectively. However, the peptide enhances the affinity of the dye for the DNA by ca. 200-fold ( $K_d = 10 \text{ nM}$  for the conjugate versus 2  $\mu$ M for the free dye).

While the two preceding examples demonstrate that peptide-dye conjugates can bind to and signal the presence of DNA via fluorescence enhancement, they lack the ability to recognize any predetermined sequence. To achieve this goal, a general DNA recognition module is needed. The minor groove binding polyamides developed over the past decade by Dervan's group are capable of high affinity and sequence-specific recognition of virtually any target sequence [53]. Conjugation of TO to three different polyamides

did not alter their specific recognition sequences [54]. Fluorescence enhancement values of >1000 were observed for specific targets and these were at least tenfold greater than for mismatched sequences. The affinities were in the expected range for the polyamides ( $K_{\rm d}={\rm ca.~10~nM}$ ). In addition, DNA footprinting experiments verified that the polyamide domain bound in the minor groove while plasmid relaxation assay demonstrated unwinding of the DNA, indicating that the **TO** chromophore intercalates into the DNA. Thus, the polyamide–**TO** conjugates could be useful for detecting specific sequences of DNA in the low nanomolar concentration regime.

Genomic DNA is highly compacted into nucleosome particles consisting of double-helical DNA wrapped around cationic histone proteins. A fluorogenic reporter dye could allow study of the structure and dynamics of nucleosome assembly. Woodbury and coworkers reported the conjugation of TO to a cysteine residue in the histone H3 protein to provide a sensor for the protein–DNA interactions [55]. Assembly of the labeled histone with DNA to form reconstituted nucleosomes resulted in a ca. 20-fold enhancement of fluorescence when performed at low salt concentration. Reconstitution at higher ionic strength leads to somewhat lower enhancement and the reason for this difference is unclear. The probe also exhibits different enhancements based on the sequence and length of the DNA used to reconstitute the nucleosomes.

In summary, conjugating cyanine dyes to various oligonucleotides, peptides, proteins, or their analogues can yield useful fluorescent labels, probes, and sensors for biological imaging and detection. The desired application dictates the dye selection, with symmetrical dyes such as Cy3 or Cy5 ideally suited for labeling because their fluorescence quantum yields are relatively insensitive to changes in environmental conditions. The unsymmetrical dyes such as TO are more useful in sensing schemes due to their fluorogenic behavior.

#### 4 Conclusions

The popularity of cyanine dyes has never been greater than it is now, with applications in nucleic acid detection leading the way. A strong foundation of fundamental knowledge concerning how the dye structure influences DNA binding and the mechanisms for fluorogenic behavior assists in the design of new dyes with improved properties. An area for future growth lies in the development of RNA-specific dyes. The need for such probes grows seemingly on a daily basis, with each new discovery of RNA involvement in regulating gene expression. The ability to detect and track these short RNAs as they maneuver through the cell could dramatically increase our knowledge of these critical biological pathways.

28 B.A. Armitage

**Acknowledgements** The author gratefully acknowledges the hard work and intellectual contributions of an outstanding group of students and collaborators who have studied the fundamentals and developed applications of cyanine dye–nucleic acid interactions. Research in the author's lab was made possible by generous financial support from the US National Science Foundation and National Institutes of Health, the American Chemical Society, and Carnegie Mellon University.

### References

- 1. Williams CG (1856) Trans R Soc Edinb 21:377
- 2. Mishra A, Behera RK, Behera PK, Mishra BK, Behera GB (2000) Chem Rev 100:1973
- 3. Suh D, Chaires JB (1995) Bioorg Med Chem 3:723
- 4. Armitage BA (2005) Top Curr Chem 253:55
- 5. Ihmels H, Otto D (2005) Top Curr Chem 258:161
- 6. Lerman LS (1961) J Mol Biol 3:18
- 7. Nordén B, Tjerneld F (1977) Biophys Chem 6:31
- 8. Cao R, Venezia CF, Armitage BA (2001) J Biomol Struct Dyn 18:844
- Yarmoluk SM, Kovalska VB, Lukashov SS, Slominskii YL (1999) Bioorg Med Chem Lett 9:1677
- Kovalska VB, Volkova KD, Losytskyy MY, Tolmachev OI, Balanda AO, Yarmoluk SM (2006) Spectrochim Acta A 65:271
- 11. West W, Pearce S, Grum F (1967) J Phys Chem 71:1316
- 12. Smith JO, Olson DA, Armitage BA (1999) J Am Chem Soc 121:2686
- 13. West W, Pearce S (1965) J Phys Chem 69:1894
- 14. Herz AH (1974) Photogr Sci Eng 18:323
- 15. Komiyama M, Ye S, Liang X, Yamamoto Y, Tomita T, Zhou J-M, Aburatani H (2003) J Am Chem Soc 125:3758
- Wilhelmsson LM, Nordén B, Mukherjee K, Dulay MT, Zare RN (2002) Nucleic Acids Res 30:e3
- 17. Sforza S, Scaravelli E, Corradini R, Marchelli R (2005) Chirality 17:515
- Mujumdar RB, Ernst LA, Mujumdar SR, Lewis CJ, Waggoner AS (1993) Bioconjug Chem 4:105
- 19. Lee LG, Chen C, Liu LA (1986) Cytometry 7:508
- 20. Nygren J, Svanvik N, Kubista M (1998) Biopolymers 46:39
- 21. Karunakaran V, Lustres JLP, Zhao L, Ernsting NP, Seitz O (2006) J Am Chem Soc 128:2954
- 22. Silva GL, Ediz V, Armitage BA, Yaron D (2007) J Am Chem Soc 129:5710
- 23. Flinders J, DeFina SC, Brackett DM, Baugh C, Wilson C, Dieckmann T (2004) Chem-BioChem 5:62
- 24. Babendure JR, Adams SR, Tsien RY (2003) J Am Chem Soc 125:14716
- 25. Petty JT, Bordelon JA, Robertson ME (2000) J Phys Chem B 104:7221
- 26. Rye HS, Yue S, Wemmer DE, Quesada MA, Haugland RP, Mathies RA, Glazer AN (1992) Nucleic Acids Res 20:2803
- 27. Fürstenburg A, Julliard MD, Deligeorgiev TG, Gadjev NI, Vasilev AA, Vauthey E (2006) J Am Chem Soc 128:7661
- 28. Deligeorgiev TG, Gadjev NI, Vasilev AA, Maximova VA, Timcheva II, Katerinopoulos HE, Tsikalas GK (2007) Dyes Pigm 75:466
- 29. Renikuntla BR, Rose HC, Eldo J, Waggoner AS, Armitage BA (2004) Org Lett 6:909

- Kostenko OM, Kovalska VB, Volkova KD, Shaytanov P, Kocheshev IO, Slominskiy YL, Pisareva IV, Yarmoluk SM (2006) J Fluoresc 16:589
- 31. Neidle S, Balasubramanian S (eds) (2006) Quadruplex nucleic acids. Royal Society of Chemistry, Cambridge
- 32. Schouten JA, Ladame S, Mason SJ, Cooper MA, Balasubramanian S (2003) J Am Chem Soc 125:5594
- 33. Green JJ, Ladame S, Ying L, Klenerman D, Balasubramanian S (2006) J Am Chem Soc 128:9809
- 34. Li Q, Kim Y, Namm J, Kulkarni A, Rosania GR, Ahn Y-H, Chang Y-T (2006) Chem Biol 13:615
- 35. Benvin AL, Creeger Y, Fisher GW, Ballou B, Waggoner AS, Armitage BA (2007) J Am Chem Soc 129:2025
- 36. Glazer AN, Mathies RA, Peck K (1998) US Patent 5763162
- 37. Eriksson M, Härdelin M, Larsson A, Bergenholtz J, Åkerman B (2007) J Phys Chem B 111:1139
- 38. Karlsson HJ, Eriksson M, Perzon E, Åkerman B, Lincoln P, Westman G (2003) Nucleic Acids Res 31:6227
- 39. Netzel TL, Nafisi K, Zhao M, Lenhard JR, Johnson I (1995) J Phys Chem 99:17936
- 40. Jarikote DV, Krebs N, Tannert S, Röder B, Seitz O (2007) Chem Eur J 13:300
- 41. Ishiguro T, Saitoh J, Yawata H, Otsuka M, Inoue T, Sugiura Y (1996) Nucleic Acids Res 24:4992
- 42. Lartia R, Asseline U (2006) Chem Eur J 12:2270
- 43. Asseline U, Chassignol M, Aubert Y, Roig V (2006) Org Biomol Chem 4:1949
- 44. Egholm M, Buchardt O, Christensen L, Behrens C, Freier SM, Driver DA, Berg RH, Kim SK, Nordén B, Nielsen PE (1993) Nature 365:566
- 45. Nielsen PE (ed) (2004) Peptide nucleic acids: protocols and applications. Horizon Bioscience, Norfolk, p 318
- 46. Svanvik N, Westman G, Wang D, Kubista M (2000) Anal Biochem 281:26
- 47. Leijon M, Mousavi-Jazi M, Kubista M (2006) Mol Aspects Med 27:160
- 48. Robertson KL, Yu L, Armitage BA, Lopez AJ, Peteanu LA (2006) Biochemistry 45:6066
- 49. Wittung P, Kim SK, Buchardt O, Nielsen PE, Nordén B (1994) Nucleic Acids Res 22:5371
- 50. Köhler O, Jarikote DV, Seitz O (2005) ChemBioChem 6:69
- 51. Carreon JR, Mahon KPJ, Kelley SO (2004) Org Lett 6:517
- 52. Thompson M (2006) Bioconjug Chem 17:507
- 53. Dervan PB, Edelson BS (2003) Curr Opin Struct Biol 13:284
- 54. Fechter EJ, Olenyuk B, Dervan PB (2005) J Am Chem Soc 127:16685
- 55. Babendure J, Liddell PA, Bash R, LoVullo D, Schiefer TK, Williams M, Daniel DC, Thompson M, Taguchi AKW, Lohr D, Woodbury NW (2003) Anal Biochem 317:1

### **Near-Infrared Cyanine Dye-Protein Interactions**

Junseok Kim · Amy Watson · Maged Henary · Gabor Patonay (≥)

Department of Chemistry, Georgia State University, Atlanta, GA 30302-4098, USA cheggp@langate.gsu.edu

1	Introduction	31
2	Protein Labeling	32
2.1	Covalent Labeling	33
2.2	Noncovalent Interaction	36
References		

**Abstract** Recent developments in the applications of near-infrared cyanine dyes involving their interactions with proteins are briefly reviewed.

 $\textbf{Keywords} \quad \text{Fluorescence} \cdot \text{Covalent labeling} \cdot \text{Near-infrared dyes} \cdot \text{Noncovalent labeling} \cdot \text{Protein}$ 

#### 1 Introduction

Dyes have been used extensively in biological research throughout the last several decades. When examining the published literature, it is important to note that this research has always been dictated by dye availability as well as detector technology. Because visible dyes were made available much earlier than their longer wavelength counterparts, a significant part of the literature focuses only on dyes exhibiting absorption and emission in the visible region of the electromagnetic spectrum. Despite the numerous advantages of using near-infrared (NIR) dyes, the limitations of earlier detection methods made the utilization of the longer wavelength range (700–1200 nm) less attractive. However, with the advent of both semiconductor detectors and laser excitation sources in the 1980s, instruments working within the NIR region began to emerge. The use of the compact and inexpensive GaAlAs laser diode with its high power output and long lifetime (≥ 100 000 h) opened up opportunities for researchers that had not previously been available. Since then a large number of research groups have been actively utilizing the NIR spectral region for a broad range of biological applications.

Heptamethine cyanine dyes commonly absorb in the NIR region. In recent years, such NIR dyes have been used to study proteins in solution. Few biomolecules absorb and fluoresce within the NIR region and, as a result, Raman and Rayleigh light scattering are greatly reduced in this region. Con-

J.S. Kim et al.

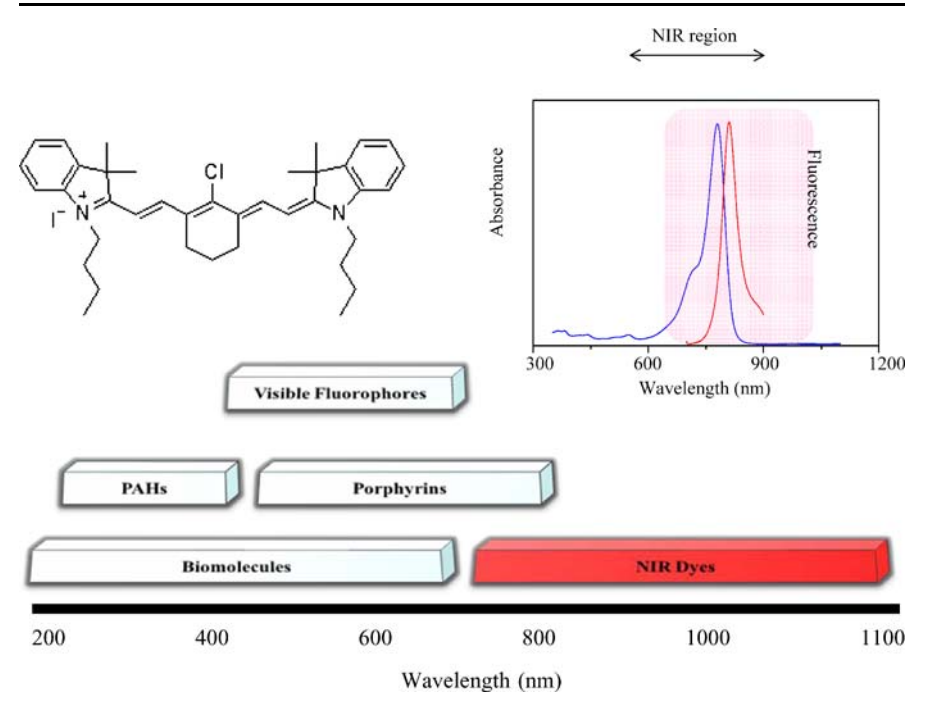


**Fig. 1** Typical ranges of absorption and fluorescence of common classes of compounds. The *inset* shows the absorption (*left*) and fluorescence (*right*) spectra of the indicated cyanine dye

sequently, improved signal-to-noise ratios are typically observed in the NIR region. In addition, typical impurities need not be considered because such species are not detected at longer wavelengths.

The main spectral advantage of NIR dyes is illustrated in Fig. 1. Proteins that may be present in their natural environment, especially in in vivo studies, have significant absorption and fluorescence in the visible spectral range. By moving detection to the longer wavelength spectrum, the detection becomes virtually free from background interference and, hence, is limited only by the detector technology.

### 2 Protein Labeling

Protein labeling or probe technology involves the attachment of a chromophore to a biomolecule either covalently or noncovalently. Labeling allows for much higher sensitivity and better detection limits because the detection of the extrinsic chromophore has a much higher molar absorptivity than the protein's intrinsic chromophore. As previously mentioned, greater sensitivity

is also achieved when studies are performed in the more advantageous NIR region of the electromagnetic spectrum. For both qualitative and quantitative analysis either covalent labeling or noncovalent labeling techniques can be employed [1–5].

# 2.1 Covalent Labeling

Although many NIR dyes containing reactive groups are commercially available, the majority of covalent labels must be synthesized for specific biological

Fig. 2 Covalent labeling of amine and thiol groups of proteins R<sup>2</sup>NH<sub>2</sub> and R<sup>2</sup>SH

J.S. Kim et al.

applications. Reactive moieties on the protein that are targeted by dyes for conjugation by the reaction with functionalized dyes are mostly primary amines and thiols [6]. Dyes functionalized with an isothiocyanate (SCN) group or N-hydroxysuccinimidyl (NHS) ester are used to target a lysine moiety. In addition, dyes derivatized with iodoacetamide or maleimide can be reacted with protein thiols. Hydrazide or amine groups on dyes have been used for the attachment to carboxylic acid groups on proteins. Figure 2 shows the reactive pathways of some common labeling reagents, and Fig. 3 shows selected NIR reagents for labeling of proteins at the amino group [7,8]. Reactions involving lysine moieties of proteins occur easily and cleanly with a variety of commercially available reagents. Covalently labeled complexes are usually stable, and the probability for nonspecific interactions is greatly minimized. Some fluorescent covalent labels in particular exhibit good photostability, water solubility, and favorable photophysical properties. Due to the specificity which can be achieved with covalent labeling, it is often the labeling method of choice in quantitative analysis. In quantitative studies, the number of reactive sites or at least the degree of substitution can be determined [9]. This particular feature of covalent labeling is useful in determining the number of functional groups (e.g., amines) present on the surface of

NCS 
$$X = O, S$$
  $SO_3Na$   $O_3S$   $X = O, S$   $SO_3Na$   $SO_3NA$ 

Fig. 3 Typical NIR cyanine dyes for covalent labeling of proteins at an amino group

a protein of interest. Covalent labeling schemes can be quite time consuming and require laborious purification steps. Often, covalent labeling reactions also require harsh, sometimes denaturing, conditions such as elevated pH [6]. In addition, band broadening in chromatographic applications can be observed as a result of analyte/dye heterogeneity [10].

Frangioni's research group has studied intraoperative NIR fluorescence imaging systems for small-animal surgery. Thus, human serum albumin (HSA) was covalently labeled with IRDye78 to produce an HSA-dye conjugate as a fluorescent lymph tracer [11, 12]. This tracer is adequate for use in the intraoperative NIR fluorescence imaging study since it is nontoxic and the excitation light source is safe for animals. Furthermore, the tracer exhibits clearly resolved images. Frangioni has also compared the utility of NIR probes with that of quantum dots (QDs) and found that the former probes are clearly superior [13].

IRDye78-NHS

NIR dyes have found application in capillary electrophoresis (CE) of proteins. The most attractive feature of covalent labeling is that very low limits of detection (LODs) can be achieved by CE with laser-induced fluorescence (LIF) detection [14]. Less than an attomole range of detection can be achieved when NIR dyes are used with this technique. In conjunction with immunoassays, CE-LIF is particularly beneficial [15]. An antibody labeled with a NIR dye reduces the LOD for an antigen. The role of antibodies is important in that the antibody has a specific binding site and this specificity allows for only a particular antigen. The combination of the selectivity of immunoassays with the sensitivity of NIR detection makes combining the two techniques quite desirable for protein analysis [15]. Note that the relationship of antibody and antigen is a type of ligand–receptor relationship; thus, it is a type of noncovalent interaction. Furthermore, the use of immunoassays in CE an-

J.S. Kim et al.

alysis is a type of affinity capillary electrophoresis (ACE) because the mobility of unbound fluorescence tagged antibody is quite different from that of the antigen-bound covalently labeled antibody [16].

Patonay investigated the detection of biomolecules with a fluorescent fiber-optic immunosensor (FFOI) [17]. In this analysis, anti-immunoglobulin G (anti-IgG) was immobilized on the tip of the FFOI so that the antigen-antibody complex was formed. Then, NIR dye-labeled secondary antibody was introduced to generate a fluorescence signal. This type of immunoassay is called a sandwich assay.

#### 2.2 Noncovalent Interaction

Some of the drawbacks of covalent labeling can be minimized in noncovalent labeling techniques. Noncovalent labeling is fast with little or no pH dependence. Also, the functional activity of labeled protein is affected to a lesser extent than with covalent labels [18]. Noncovalent labels are affected by a series of neighboring subunits in the protein binding site. Thus, before any binding studies are performed, one needs to consider protein-dye binding equilibria characteristics such as stoichiometry, association constants, and cooperativity. Both homogenous and heterogeneous ligand binding can be affected by cooperative binding effects [19]. Therefore, cooperativity must be investigated if more than 1:1 stoichiometry is determined. Although noncovalent labeling minimizes this concern, the effects of ligand binding on structure and function must be closely monitored. Experimentally, circular dichroism (CD) and X-ray crystallography are commonly used for this purpose [19–21]. In the sections that follow, the methods for the determination of stoichiometry and binding equilibria will be discussed further.

In order to fully appreciate the infinite utility of noncovalent labels, binding equilibria must be understood in detail. Several methods for the determination of stoichiometry have been introduced. The Hummel-Dreyer method was originally developed to explain the stoichiometry between a macrobiomolecule and small ligands in gel filtration [22, 23]. Ultracentrifugation [24] was used in another method for measuring stoichiometry. For these techniques, the diffusion or sedimentation coefficients were used. Unfortunately, equilibrium dialysis, gel filtration, and sedimentation analysis require relatively large samples. Therefore, excitation and emission spectroscopy has been the preferred method for determining binding parameters. The molar ratio method uses the spectral changes observed upon protein-dye complex formation to determine binding parameters [25-27]. Other methods that use spectroscopic changes to determine association constants include Scatchard, modified Scatchard, Hill, and Job's plots. The Hill's plot method is typically used to measure cooperativity of a protein-ligand complex. And because Scatchard plot analysis requires the spectral data of unbound and bound molecules with two different absorbance maxima, Job's plot is often a more useful method for determining binding stoichiometry when the spectra are not well separated [19].

In 1962, Hummel and Dreyer introduced a valuable theory for the separation of macromolecules and small ligands using gel filtration [23]. In this method, the separation is dependent not only on the size of the free ligand and complex, but also on the sieving material. Nowadays, with the increasing use of CE in the areas of chemistry and biology, the Hummel–Dreyer method has been reapplied. In CE, a tiny sample is generally separated in a few minutes with high detection response. The separation is based on the charge-to-mass ratio of a molecule, so that the bound ligand and free ligand, possessing different charges and mass inside the capillary, can be readily separated.

In CE, there are generally five methods of binding analysis: Hummel-Dreyer (HD), vacancy peak (VP), frontal analysis (FA), affinity capillary electrophoresis (ACE), and vacancy affinity capillary electrophoresis (VACE) [28-30]. In the HD method, the capillary is filled with a ligand dissolved in running buffer and a protein prepared in the same buffer is injected. This method is useful when the mobilities of unbound protein and the protein-ligand complex are identical. The negative, or vacant, peak corresponds to the absence of unbound ligand when the ligand binds to a protein; the positive peak represents the protein-ligand complex. In order to quantify the bound ligand, a simple relationship between the negative and positive peaks using either peak area or peak height can be employed. Either an internal or external standard is used for these measurements [31]. In the VP method, the complex is prepared in running buffer and the concentration of the ligand is changed. Two negative peaks are observed with the first peak corresponding to the complex and the second representing the free ligand. Using internal calibration, the concentration of bound ligand can be calculated. It is important to note that in this method the mobility of the protein and the complex is nearly identical [30]. In FA, the capillary is filled only with buffer and the sample plug contains unbound ligand, unbound protein, and the protein-ligand complex. During analysis, the components are separated based on their mobilities. The mobility of bound and unbound protein is nearly identical, but the mobility of the unbound ligand is sufficiently different. Therefore, by using a calibration curve, the concentration of bound ligand can be calculated. The experimental setup for the ACE method is the same as for the HD method, but the mobilities of the free protein and bound protein are different. Diffusion or sedimentation coefficient analysis can also be used to determine binding parameters. The drawback of methods utilizing sedimentation or diffusion is that a ligand must have a relatively large mass. Otherwise, a protein or macromolecule bound to a small ligand will be not be distinguishable.

Increased LODs can be achieved with noncovalent labeling using CE with LIF [32]. Colyer and coworkers have studied noncovalent labeling using CE-

38 J.S. Kim et al.

LIF extensively [1, 28, 33, 34]. With the help of several NIR dyes they have successfully separated HSA, bovine serum albumin (BSA),  $\beta$ -lactoglobulin A, and trypsinogen.

The propensity of cyanine dyes to form aggregates in polar solution has been extensively reported [35–37]. The type of aggregate is dependent upon several factors, such as dye structure, concentration, solvent polarity, pH, ionic strength, and temperature [38]. The phenomenon of achiral cyanine dyes spontaneously forming chiral J-aggregates has gained much attention in recent years for its potential to increase the spectral sensitivity of photographic emulsions [39–41]. The formation of J-aggregates has recently been extended to using biomolecules, such as proteins [42–44] and DNA [45, 46], as templates for aggregate formation.

#### References

- 1. Welder F, Paul B, Nakazumi H, Yagi S, Colyer CL (2003) J Chromatogr B 793:93
- 2. Patonay G, Salon J, Sowell J, Strekowski L (2004) Molecules 9:40
- 3. Fukushima T, Usui N, Santa T, Imai K (2003) J Pharm Biomed Anal 30:1655
- 4. Patonay G, Kim JS, Kodagahally R, Strekowski L (2005) Appl Spectrosc 59:682
- 5. Kim JS, Kodagahally R, Strekowski L, Patonay G (2005) Talanta 67:947
- Garman A (1997) Non-radioactive labelling: a practical introduction. Academic, San Diego
- 7. Williams RJ, Lipowska M, Patonay G, Strekowski L (1993) Anal Chem 65:601
- 8. Narayanan N (2003) Cyanine dye compounds and labeling methods. US Patent 6593148
- 9. Jacobsen C (1975) Int J Pept Protein Res 7:161
- 10. Craig DB, Dovichi NJ (1998) Anal Chem 70:2493
- 11. Parungo CP, Ohnishi S, De Grand AM, Laurence RG, Soltesz EG, Colson YL, Kang PM, Mihaljevic T, Cohn LH, Frangioni JV (2004) Ann Surg Oncol 11:1085
- 12. Nakayama A, Del Monte F, Hajjar RJ, Frangioni JV (2002) Mol Imaging 1:365
- 13. Ohnishi S, Lomnes SJ, Laurence RG, Gogbashian A, Mariani G, Frangioni JV (2005) Mol Imaging 4:172
- 14. Baars M, Patonay G (1999) Anal Chem 71:667
- 15. Sowell J, Parihar R, Patonay G (2001) J Chromatogr B 752:1
- 16. Schou C, Heegaard NH (2006) Electrophoresis 27:44
- 17. Daneshvar MI, Peralta JM, Casay GA, Narayanan N, Evans L, Patonay G (1999) J Immunol 226:119
- 18. Williams RJ, Lipowska M, Patonay G, Strekowski L (1993) Anal Chem 65:601
- 19. Holde KEV, Johnson WC, Ho PS (2006) Principles of physical biochemistry, 2nd edn. Pearson, New Jersey, p 605
- Drenth J (2007) Principles of protein X-ray crystallography, 3rd edn. Springer Science, New York
- 21. Bulheller BM, Rodger A, Hirst JD (2007) Phys Chem Chem Phys 9:2020
- 22. Soltes L (2004) Biomed Chromatogr 18:259
- 23. Hummel JP, Dreyer WJ (1962) Biochim Biophys Acta 63:530
- 24. Boudier C, Bieth JG (1992) J Biol Chem 267:4370
- 25. Meyer AS, Ayres GH (1957) J Am Chem Soc 79:49

- 26. Chriswell CD, Schilt AA (1975) Anal Chem 47:1623
- 27. Wang H, Li WR, Guo XF, Zhang HS (2007) Anal Bioanal Chem 387:2857
- 28. Yan W, Colyer CL (2006) J Chromatogr A 1135:115
- 29. Busch MHA, Kraak JC, Poppe H (1997) J Chromatogr A 777:329
- Busch MHA, Carels LB, Boelens HFM, Kraak JC, Poppe H (1997) J Chromatogr A 777:311
- 31. Kraak JC, Busch S, Poppe H (1992) J Chromatogr 608:257
- 32. Benito I, Marina ML, Saz JM, Diez-Masa JC (1999) J Chromatogr A 841:105
- 33. McCorquodale EM, Colyer CL (2001) Electrophoresis 22:2403
- 34. Moody ED, Viskari PJ, Colyer CL (1999) J Chromatogr B 729:55
- 35. Min H, Park J, Yu J, Kim D (1998) Bull Korean Chem Soc 19:650
- 36. Green MD, Patonay G, Ndou T, Warner IM (1992) J Inclus Phenom Mol Recognit Chem 13:181
- 37. Mishra A, Behera RK, Behera PK, Mishra BK, Behera GB (2000) Chem Rev 100:1973
- 38. Herz A (1977) Adv Colloid Interface Sci 8:237
- 39. Kirstein S, Von Berlepsch H, Bottcher C, Burger C, Ouart A, Reck G, Dahne S (2000) ChemPhysChem 1:146
- 40. Spitz C, Dahne S, Ouart A, Abraham HW (2000) J Phys Chem B 104:8664
- 41. Neumann B, Pollmann P (2001) Phys Chem Chem Phys 3:943
- 42. Tatikolov AS, Panova IG (2005) High Energy Chem 39:232
- 43. Zhang YZ, Xiang JF, Tang YL, Xu GZ, Yan WP (2007) ChemPhysChem 8:224
- 44. Tatikolov AS, Costa SMB (2004) Biophys Chem 107:33
- 45. Seifert JL, Connor RE, Kushon SA, Wang M, Armitage BA (1999) J Am Chem Soc 121:2987
- Ogul'chansky TY, Losytskyy MY, Kovalska VB, Lukashov SS, Yashchuk VM, Yarmoluk SM (2001) Spectrochim Acta A 57:2705

# Cyanine Dye-Based Compounds for Tumor Imaging With and Without Photodynamic Therapy

Ravindra K. Pandey (⋈) · Nadine James · Yihui Chen · Mahabeer P. Dobhal

Photodynamic Therapy Center, Department of Cell Stress Biology, Roswell Park Cancer Institute, Buffalo, NY 14263, USA ravindra.pandey@roswellpark.org

1	Introduction	42
2	Modified ICG Analogs with Enhanced Stability	45
3	Water-Soluble Cyanine Dyes	46
4	Tumor-Targeted Cyanine Dyes	48
4.1	Cyanine Dye-Small Peptide Conjugates	49
4.2	Hydrophilic Cyanine Dyes With and Without Carbohydrate Moieties	51
4.3	Cyanine Dye-Arg-Gly-Asp sequence (RGD) Conjugates	54
4.4	Cyanine Dye-Endostatin Conjugates	58
4.5	Cathepsin-D-Sensitive Cyanine Dyes	59
4.6	Tricarbocyanine-Cholesteryl Laurates	60
4.7	Cyanine Dye-Folic Acid Conjugates	61
5	Cyanine Dyes for Photodynamic Therapy (PDT)	62
6	Porphyrin-Based Photosensitizer-Cyanine Dye Conjugates	
	as Bifunctional Agents: a "See and Treat" Approach	63
6.1	In Vivo Fluorescence Imaging of Glioma Tumors and PDT Efficacy	67
7	Conclusions	69
Refe	rences	70

**Abstract** Among the near-infrared (NIR) dyes, cyanine dyes in general have shown enormous potential for optical imaging. Efforts are underway to increase their tumor-targeted specificity by conjugating these fluorophores with those targeting moieties known to bind certain receptors having high expression in tumor cells. Attempts are also underway to develop "multifunctional dyes" with nuclear, magnetic resonance (MR) and optical imaging properties. Recent studies have shown that certain tumor-avid photosensitizers conjugated with cyanine dyes can be used as "bifunctional agents" for tumor imaging and photodynamic therapy (PDT). Such compounds, which effectively function as imaging and therapeutic agents, would create an entirely new paradigm for tumor diagnosis and therapy. In this review article, the synthesis, imaging and therapeutic potential of selected cyanine dyes are briefly summarized.

**Keywords** 3-(1'-Hexyloxyethyl)-3-devinyl-pyropheophorbide-a  $\cdot$  Fluorodeoxyglucose  $\cdot$  Indocyanine green  $\cdot$  Magnetic resonance  $\cdot$  Near-infrared fluorescence  $\cdot$  Photodynamic therapy

#### **Abbreviations**

CDF CaD sensitive peptide [Gly-Pro-Ile-Cys (Et)-Phe-Phe-Arg-Leu-Gly-Lys(FITC)-Cys-NHal

FDG Fluorodeoxyglucose

FH Familial hypercholesterolemia FITC Fluorescein isothiocyanate

FR Folate receptor

HPPH 3-(1'-Hexyloxyethyl)-3-devinyl-pyropheophorbide-a

ICG Indocyanine green
LDL Low-density lipoprotein
MPEG Methoxy poly(ethyleneglycol)

MR Magnetic resonance
NIRF Near-infrared fluorescence

PDB Protein Data Bank PDT Photodynamic therapy

PET Positron emission tomography PGC Protected graft copolymer RGD Arg-Gly-Asp sequence

RIF Radiation-induced fibrosarcoma DTPA diethylenetriaminepentaaceticacid

### 1 Introduction

A large number of articles dealing with the synthesis [1–4], self-aggregation [5–7], nonlinear optical properties [8–10], adsorption [11–14], photodimerization [15–18], *cis-trans* isomerization [19–21], photocoloration [22], photodynamic therapy (PDT) [23, 24], solvatochromism [25, 26], fluorescent labeling [27], photography [28], optical data storage [29], and proteomics [30] of cyanine dyes have been reported. This chapter is focused on tumor imaging and PDT applications of certain cyanine dyes and their porphyrin-based conjugates. The reviewed dyes are classical cyanines 1 and merocyanines 2. The syntheses of certain dyes are also briefly discussed.

Among the cyanine dyes, indocyanine green (ICG) 3 [31] has generated great attention in the academic and industrial world. It is a tricarbocyanine type of dye exhibiting long-wavelength absorption near 800 nm with little or no absorption in the visible region of the electromagnetic spectrum. Shortly after its introduction by Fox et al. (1957) [138], ICG was adopted and used for recording dye dilution curves, particularly in the determination of cardiac output. When dissolved in blood, ICG binds to proteins such as human serum albumin and lipoproteins. The absorption maximum shifts to 805 nm, but the fluorescence wavelength stays at 830 nm and the fluorescent intensity depends on its concentration. Although ICG is a nonspecific agent that is

cleared rapidly from the blood, it tends to collect in regions of dense vascularity through extravasation.

In recent years, ICG and the related analogs have been explored for their capability of detecting tumors by fluorescence imaging. Tumor detection via fluorescence is a consequence of a complex series of events that occur at the molecular level [32]. The net effect is that a fluorescent molecule absorbs light within a molecular-specific absorption band and subsequently emits light isotropically at a longer wavelength. The wavelength shift accompanying fluorescence emission and the isotropic nature of these emissions facilitate discriminating between excited and emitted light in fluorescence measurements [33].

Multiple complementary techniques for tumor detection, including magnetic resonance (MR), scintigraphic, and optical imaging are under active development [34–59]. Each approach has particular strengths and advantages. Optical imaging includes measurement of absorption of endogenous molecules (e.g., hemoglobin) or administered dyes [60, 61], detection of bioluminescence in preclinical models [62], and detection of fluorescence from endogenous fluorophores or from targeted exogenous molecules [63–67]. Fluorescence, which involves absorption of light and re-emission at a longer wavelength, can be highly sensitive: a typical cyanine dye with a lifetime of 0.6 ns can emit up to  $10^{32}$  photons/s/mol [68]. A sensitive optical detector can image  $<10^3$  photons/s. Thus even with low excitation power, low concentrations of fluorescent molecular beacons can be detected.

As with other noninvasive techniques, fluorescence imaging has the potential for in vivo diagnosis in situ, with real-time display of the resulting information [69]. Optical tomographic techniques are being devised to visualize the fluorescent probes within tissue volumes [70]. Optical imaging instruments may be simpler and less expensive to operate than those required for other imaging technologies, thus facilitating their future incorporation in less specialized medical centers. Therapeutically (especially in applications

such as endoscopic examination), fluorescence imaging can allow precise assessment of the location and size of a tumor and provide information on its invasiveness. During debulking surgery, where malignant loci can be difficult to identify, the presence of a fluorescent signal might assist the surgeon in identifying the diseased site.

Fluorescence techniques are attractive because they are highly sensitive, and we are capable of detecting picomoles of light-emitting fluorophores in heterogenous media. As a result, aberrant molecular events that indicate early manifestation of diseases can be assessed by tissue-specific fluorescent biomolecules. A variety of such target-specific molecules has been developed for in vitro and in vivo studies. Optical imaging has a number of advantages over radionuclide-based functional imaging techniques. It is relatively inexpensive, the optical imaging probes can be stored, and radioactivity is not a concern. Furthermore, because a fluorophore is not annihilated upon radiation emission, as is a radiotracer, there is potentially greater signal available for imaging.

The optimal wavelength range for in vivo fluorescence excitation and emission is determined by tissue optical properties [71]. Hemoglobin has strong

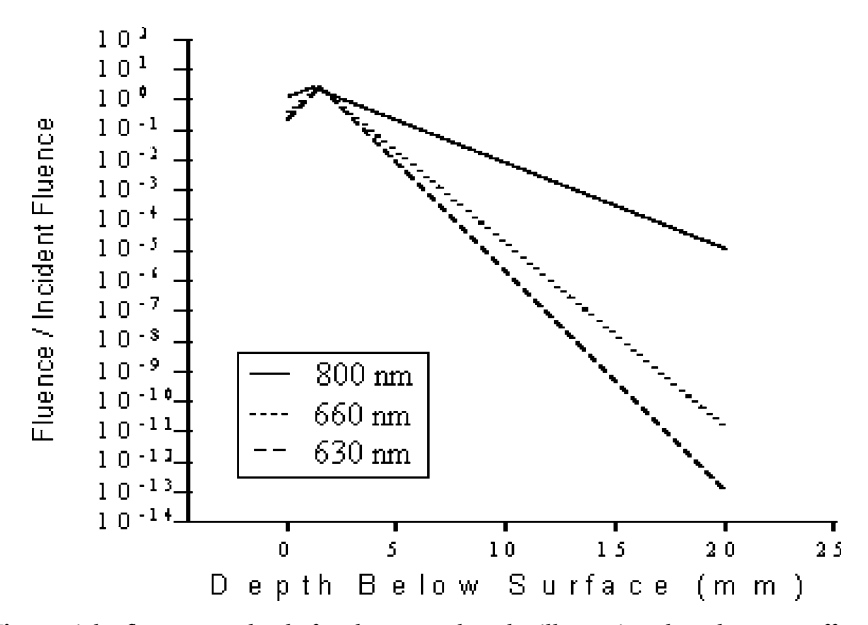


**Fig. 1** Light fluence vs. depth for three wavelengths illustrating the advantage offered by long-wavelength sensitizers. The graph is a measure of the total light dose available for absorption by a sensitizer at different depths below the surface (i.e., the number of photons (of a given wavelength) per square centimeter that pass through an imaginary infinitesimal surface at that point). The *curves* are calculated from measurements of the attenuation of light in rat brain, but similar results are obtained in other tissues

absorption at wavelengths less than about 600 nmand there can be significant background fluorescence from endogenous biomolecules up to about 680 nm. At longer wavelengths into the near-infrared (NIR), tissue absorption and scattering decrease with increasing wavelength [71]. As shown in Fig. 1, there is a large increase in light penetration as wavelengths increase from  $\sim\!600$  to 800 nm. Although tissue penetration is limited compared to NIR dyes, fluorophores with visible (red) excitation may provide high-resolution delineation of infiltrating tumor cells adjacent to tumor excision margins. Because of the possibility of detecting both dye and photosensitizer fluorescence, our multifunctional agents can allow excitation and detection at both red and NIR wavelengths.

In addition, the difference between the fluorophore's absorption and emission bands (Stokes shift) should be at least 20 nm, to readily discriminate between the excitation and emission light. Many NIR fluorescent dyes are based on carbocyanine molecules such as ICG, an FDA-approved agent with 730 nm excitation and 830 nm emission maxima. Various novel ICG analogs have been evaluated because of the high biocompatibility and desirable spectral properties of the carbocyanines.

### 2 Modified ICG Analogs with Enhanced Stability

Since the discovery of ICG, cyanine dyes have found widespread use as fluorescent labels for biomolecules. The appeal of this class of fluorophore derives from their straightforward syntheses, broad wavelength tenability, large molar extinction coefficients, and moderate-to-high fluorescence quantum yields. ICG with its 778–830 nm excitation/emission maxima was an early contrast agent used as a blood-pooling agent for assessing hypervascularity and "leaky" angiogenic vessels of high permeability. However, two common problems encountered by cyanine dyes and numerous other fluorophores are (a) their susceptibility to form nonfluorescent aggregates and (b) their tendency to undergo photobleaching.

Armitage and coworkers [72] have reported the synthesis of certain polyfluorinated cyanine dyes with substantially improved resistance to both aggregation and photobleaching as well as enhanced fluorescence quantum yield. Synthesis of the octafluorinated thiadicarbocyanine dye 6 was accomplished in two steps from the precursor 2-methyl-4,5,6,7-tetrafluorobenzothiazole 4 through the intermediary of 5. Alkylation of the heterocycles was achieved by reaction with diethyl sulfate, and the resulting benzothiazolium salt converted directly to the cyanine dye without isolation (Scheme 1).

A series of ten pentamethine indocyanine dyes 7–16 were synthesized [73], and the photophysical characteristics relevant to applications in cell biology and single molecule detection were analyzed. It was observed that substitu-

Scheme 1

tions in the polymethine chain increased the nonradiative energy dissipation of the excited singlet state and decreased the fluorescence quantum yield, relative to the unsubstituted compound. For substituents at the aromatic rings, the fluorescence quantum yield was found to be negatively correlated with the position of the substituents in the auxochromic series –  $SO_3$ , – H, – F and –  $CH_3$ . Compounds with sulfonic acid groups and halogen atoms attached to the indolenine systems had the highest fluorescence quantum yields.

### 3 Water-Soluble Cyanine Dyes

During the past decade, intensive research efforts have been devoted to the design and synthesis of water-soluble fluorescent dyes for life science applications [74]. Among these dyes, pentamethine and heptamethine cyanine dyes are in general more important, due to their long wavelength absorptions in the NIR region. Among these cyanine dyes, Cy5.5 and Cy7.0 are two that are widely used. Despite its good optical properties in the NIR region, the sul-

fobenzoindocyanine 17 is prepared in low yield from a poorly reproducible synthetic route. Major synthetic difficulties are related to poor solubility. This synthesis problem and the drastic reaction conditions are the main reasons that a limited number of derivatives are commercially available. As far as the heptamethine cyanine dye 18 is concerned, its poor chemical stability limits its use as a fluorescent marker. To overcome this problem, numerous studies have shown that incorporating a rigid cyclohexenyl ring in the polymethine chain increases the stability of the resulting Cy7.0 analog. The substituted ring system also provides an opportunity to incorporate desired functionality for structure–activity relationship studies and target specificity. Recently,

Scheme 2

Renard, Romieu and coworkers have reported the synthesis of two novel NIR cyanine fluorophores 21 and 22, which are analogs of Cy5.5 and Cy7, respectively (Scheme 2) [75]. These dyes display absorption and emission maxima in the NIR region, large extinction coefficients, excellent solubility and no tendency to self-aggregate. The utility of these agents is illustrated by the preparation of an internally quenched fluorescent probe of caspase-3 protease 23.

Strekowski et al. [76] have also reported an efficient approach for the preparation of water-soluble NIR cyanine dyes functionalized with [(succinimido)oxy]carbonyl group. The desired dye 25 (Eq. 1) was obtained by esterification of the respective carboxylic acid 24 with disuccinimido carbonate in a pure form by simple crystallization from a crude reaction mixture. The high polarity of ester makes these dyes soluble in water, which is desirable for labeling of water-soluble molecules containing a primary amino group. These dyes exhibit large Stokes' shifts (>30 nm) and can be excited by using commercially available diode lasers.

**Equation 1** 

### 4 Tumor-Targeted Cyanine Dyes

A challenge is to deliver fluorescent dyes selectively and in high enough concentration to detect small tumors. Use of ICG alone to image hypervascular or "leaky" angiogenic vessels around tumors has been disappointing due to the dye's limited intrinsic tumor selectivity. Multiple approaches have been employed to improve optical probe localization, including administering it in a quenched form that is activated within tumors or coupling the fluorescent agents to antibodies or small molecules such as receptor ligands. Recent studies have focused on developing dye conjugates of small bioactive molecules to improve rapid diffusion to target tissue, incorporate combinatorial and high throughput strategies to identify and optimize new probes, and enhance in vivo stability of the compounds. Some of the peptide and folic acid analogs of certain ICG derivatives have shown some tumor specificity and are at initial stages of preclinical studies.

# 4.1 Cyanine Dye-Small Peptide Conjugates

In an attempt to prepare target-specific fluorescent agents, Achilefu et al. [77] and Bugaj et al. [78] conjugated cyanine dye to small peptides for targeting somatostatin (SST) and bombesin receptors. A commercial nuclear diagnostic agent, Octreoscan, is based on targeting the SST receptor, which is over-expressed in neuroendocrine tumors. In Achilefu's approach, to prepare the target-specific cyanine dye 28, the macrocyclic molecule 26 was incorporated to the C-terminus of a cyclic SST receptor avid octapeptide 27 (Eq. 2). The spectral properties of 28 (absorption at 792 nm, emission at 811 nm) are similar to those of the nonpeptide analog 26.

#### **Equation 2**

In a parallel study, Licha et al. [79] also evaluated SST receptor-specific peptide H<sub>2</sub>N-(D-Phe)-cyclo[Cys-Phe-(D-Trp)-Lys-Thr-Cys]-Thr-OH, which was labeled with a carboxylated indodicarbo and an indotricarbocyanine dye at the N-terminal amino group. The preparation was performed by automatic solid-phase synthesis, with subsequent attachment of the cyanine dye and cleavage of the entire conjugate from the resin (Scheme 3).

The ability of these agents 36-39 to target the SST receptor was demonstrated by flow cytometry in vitro. To evaluate the effect of incorporating lysine at the C-terminus and subsequent macrocyclization of the peptide, receptor-binding assays of these compounds were performed. The IC $_{50}$  values were quite close and showed that the binding of the peptide to the dye retained its receptor binding affinity.

In a similar study, Becker et al. [80] reported the in vivo diagnostic use of a peptide-dye conjugate consisting of a cyanine dye and the SST analog octreotate agent for optical tumor imaging. In their approach indocarbocyanine dye (IDCC) or indotricarbocyanine (ITCC) was coupled to octreotate, a stabilized analog of SST. An IDCC-SST-14 conjugate was also prepared for comparison with the native ligand. When used in whole-body in vivo imaging of mouse xenografts, ITCC accumulated in tumor tissue. Tumor fluorescence rapidly increased and was more than threefold higher than that of normal tis-

#### Scheme 3

sue from 3 to 24 h after application. Primary human neuroendocrine tumor cells specifically internalized the targeting conjugate.

In another study involving peptide conjugation, Zaheer et al. [81] conjugated a biophosphonate derivative, pamidronate, which exhibits specific binding to hydroxypatite to an indocyanine dye to image bone structure in hairless mice. The system may be capable of NIR detection of osteoblastic

activity, enabling NIR imaging of skeletal development, coronary atherosclerosis and other diseases.

In a related study Brock and coworkers [82] conjugated the indocyanine dye with SINFEKL (MHC class I epitope) and EQKLISEEDL (myc-tag) peptides. The dye-labeled peptide did not show any aggregation and produced specific binding to tissue culture cells and proteins. The dye is therefore an attractive new fluorophore for in vitro and cell-based detection of receptor ligand interaction at nanomolar concentrations by flow cytometry, fluorescence correlation spectroscopy, and laser scanning microscopy.

# 4.2 Hydrophilic Cyanine Dyes With and Without Carbohydrate Moieties

A few years ago, Licha, Chance and coworkers [83] synthesized a group of glucamine- and glucosamine-substituted cyanine dyes 42–45 structurally related to ICG. In brief, the symmetric dicarboxylated ITCC 40 and the non-symmetric monocarboxy derivative 41 served as key substrates for further reactions. The carboxylic acid groups of 40 and 41 were readily converted into amides. To provide high hydrophilicity, two different amino-sugar derivatives, D-glucamine and D-glucosamine, were used to synthesize the four different iodotricarbocyanines 42–45. These compounds exhibited increased hydrophilicity and less plasma protein binding with respect to ICG. For deriva-

$$R_1 \xrightarrow{P} R_2$$

$$SO_3 \xrightarrow{P} SO_3 = R_2$$

$$SO_3 \xrightarrow{P} R_2$$

$$SO_3 = R_2 = R_2$$

$$SO_3 = R_3$$

$$SO_3 = R$$

tives with the highest hydrophilicity the efflux from tumor and normal tissue was monitored by intensity-modulated diffuse optical spectroscopy in tumor-bearing rats. In comparison with ICG, 45 exhibited a considerably enhanced tissue-efflux half-life (73 min versus less than 10 min for ICG in tumor tissue) and a twofold higher initial tissue absorption compared to ICG. It also generated an elevated tumor-to-tissue concentration gradient up to 1 h after injection.

Both enhanced fluorescence quantum yields in physiological media and a slower tissue efflux in vivo are considered to be important features of an optical contrast agent that is not directed against molecular targets but utilizes tumor physiological properties. Polyhydroxyl moiety between hydrophobic groups enhanced the solubility and probably minimized aggregation in aqueous media. The preliminary results of the in vivo distribution of 45 in normal nude mice showed that conjugate 45 rapidly clears from blood and is predominantly excreted by the hepatibiliary system within 5 min after injection. The fast clearance from blood reduces background fluorescence, thereby enabling rapid visualization of target tissue.

A new NIR fluorescent molecular probe 48 derived from indocarbocyanine and galactose was prepared by Achilefu and coworkers [84] (Scheme 4). The presence of a nonionic polyhydroxyl moiety between hydrophobic groups enhances solubility and minimizes aggregation in aqueous solutions.

Scheme 4

Lysosomes are membranous organelles found in almost all mammalian cells. Recent studies demonstrated that lysosomes can play a pivotal role in cancer cell invasion and metastasis because several crucial proteolytic enzymes, such as cathepsin D, B and L, which actively participate in the digestion of extracellular matrix (ECM) proteins, are sequestered in lysosomal vesicles [85]. Moreover, under the conditions of acidic extracellular pH, which are frequently found in the tumor environment, cells with a high degree of malignancy exhibit larger lysosome sizes and increased nucleus–lysosome distances than poorly metastatic cells. Therefore, assessing lysosomal morphology and trafficking in vivo by using NIR optical imaging probes should help elucidate the role of lysosomal parameters in cancer invasion and metastasis and may provide a novel means of diagnosing malignant lesions in their early stages.

Bhujwalla, Glunde and coworkers [86] synthesized two novel NIR fluorescent probes by linking a carbocyanine fluorophore and glucosamine through different linkers (Scheme 5). These probes 52 and 53 demonstrated a high quantum yield, low cytotoxicity, reversible pH dependent fluorescence in the physiological pH range, and a decreased aggregation tendency in aqueous solutions. In vitro NIR optical imaging studies revealed cellular uptake and strong intracellular NIR fluorescence of these two probes in four breast epithelial cell lines.

#### Scheme 5

Although radionuclide imaging has several advantages, including intrinsically high sensitivity, capability of quantitation and clinical translation, it

often suffers from relatively low spatial resolution, high cost and limited radiation to personnel. Moreover, positron emission tomography (PET) imaging often requires an on site cyclotron and a radiochemistry laboratory to produce short half-life radionuclides and radiolabeled agents. Therefore optical imaging has emerged as an attractive imaging modality to study the biological/molecular events in both cell culture and small living objects. Considering the extensive applications of [18F] fluorodeoxyglucose (FDG) in nuclear medicine and the rapid advancement in optical imaging, the development of near-infrared fluorescence (NIRF) deoxyglucose analog 55 developed by Gambhir and coworkers [87] may serve as novel probes with the ability to evaluate the glucose metabolic rate of tumors (Eq. 3). These probes could be useful for (a) the accurate detection of abnormalities such as tumors and (b) the noninvasive monitoring of the therapeutic efficacy of drugs in small living animals. Gambhir and coworkers have recently synthesized a series of FDG-Cypate analogs Cy5.5-2DG and Cy5.5-NHS. Both demonstrated tumortargeting abilities in cell culture and living mice but not through the glucose transporters/hexokinase pathway [88, 89].

**Equation 3** 

# 4.3 Cyanine Dye-Arg-Gly-Asp sequence (RGD) Conjugates

Integrin is a family of transmembrane cell adhesion receptors that control cell-cell and cell-ECM) interactions [90]. They recruit many ECM molecules as their ligands and the interactions between integrins and their ligands are essential for many biological functions of cells. Integrins are heterodimeric, consisting of one  $\alpha$ -subunit and one  $\beta$ -subunit that are bound noncovalently (Fig. 2). Twenty four integrins have being identified; they are composed of  $24\alpha$ - and  $9\beta$ -subunits. Integrin  $\alpha V \beta 3$  has been demonstrated to promote angiogenic processes or formation of neovasculature. It has been used as a marker for tumor angiogenesis. Many of these findings strongly suggest that

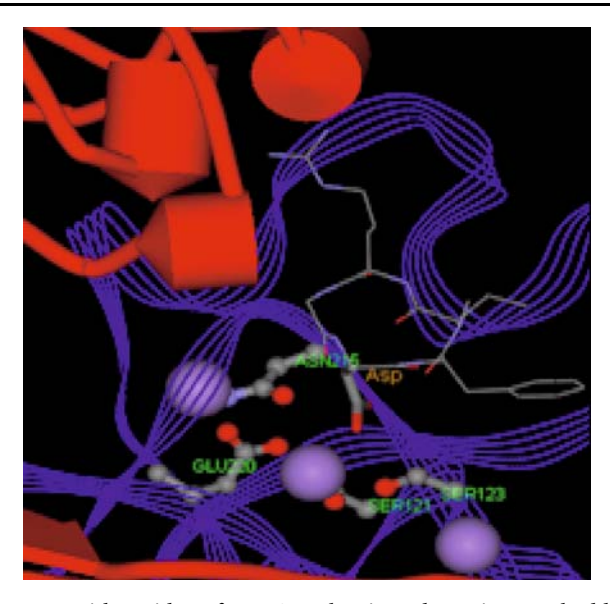


**Fig. 2** Asp interacts with residues from  $\beta 3$  subunit and Mn ions embedded in  $\beta 3$  subunit. Especially, the middle Mn ion is directly coordinated with Asp side chain (COO –) group. In turn, this Mn ion is coordinated by Ser 121, Ser 123, and Glu 220. These residues in turn are coordinated to two other Mn ions, which form additional coordination with other residues from the  $\beta 3$  subunit. The Asp side chain of Arg-Gly-Asp sequence (RGD) peptide also makes a direct interaction with Asn 215. This network of interaction involving three Mn ions seems to be a very important stabilizing factor

this endothelial integrin is a valuable target for developing therapeutic agents for cancer diagnosis, treatment and prognosis [91].

Sequence analysis of the integrin  $\alpha_{\rm V}$  subunit from various organisms (human, mouse, bull, chicken, frog, and zebrafish) using T-Coffee and ClustalW multiple sequence alignment programs shows high degree of conservations, especially among the mammals. Similar results are also perceived for the  $\beta_3$  subunit from the sequence analyses of various organisms (human, rat, mouse, chicken, frog, and zebrafish). From the sequence alignment results, it is clear that the ligand binding regions are well conserved [92]. Several crystal structures are available at the Protein Data Bank (PDB). For integrin  $\alpha V \beta_3$ , three crystal structures of the extracellular segment are available [93]. IJV2 is the crystal structure of the extracellular segment of  $\alpha V \beta_3$  in complex with an Arg-Gly-Asp (RGD) ligand. 1M1X is the crystal structure of extracellular segment of  $\alpha V \beta_3$  bound to Mn<sup>2+</sup>. Another  $\alpha V \beta_3$  plexin-semaphorin-integrin (PSI) domain crystal structure is also available at the PDB (1U8C).

To understand the interaction and recognition between  $\alpha V \beta 3$  and its antagonists, integrin  $\alpha V \beta 3$  with an RGD ligand was chosen to be the template

for studying the specific interaction of photosensitizer conjugate with  $\alpha V \beta 3$ . The crystal structure of the  $\alpha V \beta 3$ -RGD peptide complex indicates that the RGD peptide binds at the interface of  $\alpha_V$  and  $\beta_3$  subunits while three Mn cations in  $\beta_3$  seem to play an important role in the ligand binding (Fig. 3).

It is believed that integrins, especially integrin  $\alpha v \beta 3$ , play an important role in tumor progression, angiogenesis, and metastasis [94]. Integrin  $\alpha_v \beta_3$  in tumor cells binds to matrix metalloprotease-2 in a proteolytically active form and facilitates cell-mediated collagen degradation and invasion. An increase in its expression is correlated with increased malignancy in melanomas. A critical role is played by  $\alpha_v \beta_3$  in angiogenesis, and it is upregulated in vascular cells within human tumors. Significant overexpression of  $\alpha_v \beta_3$  is reported in colon, lung, pancreas, brain and breast carcinomas, and the expression of  $\alpha_v \beta_3$  was significantly higher in tumors of patients with metastases than in those without metastases. Integrin  $\alpha v \beta_3$  binds factors such as vitronectin that contain the RGD amino acid sequence and this binding appears to be critical in mediating the ligation signal, allowing endothelial cells to attach to the ECM, thus supporting endothelial survival and growth. The important role of  $\alpha v \beta_3$  in tumor angiogenesis and metastasis suggests that integrins could be an excellent diagnostic and therapeutic target in cancer.

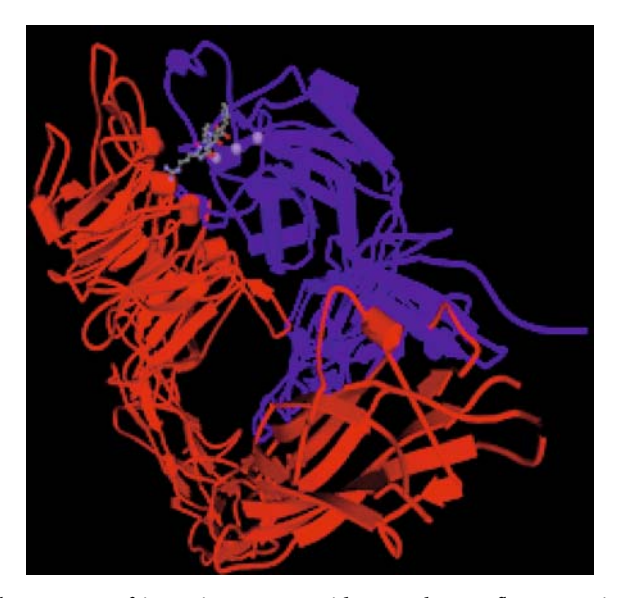


**Fig. 3** Crystal structure of integrin RGD peptide complex. A *flat arrow* indicates the  $\beta$  strand and a cylinder the  $\alpha$  helix. *Red* is used for the  $\alpha$ v subunit and *blue* for the  $\beta$ 3 subunit. Integrin RGD peptide, Arg-Gly-Asp-D-Phe-N-methyl Val is located between the  $\alpha$ v and  $\beta$ 3 subunits shown in the ball and stick figure. The Mn ions located near the RGD peptide are shown as *purple spheres* 

In a recent study, Chen and coworkers [95] synthesized a series of NIRF imaging agents in which the cyanine dye (Cy7) was attached to mono-, di-, and tri-RGD moieties 57–59 (Scheme 6). Mice bearing subcutaneous U87MG tumor were intravenously injected with these conjugates at a dose of 500 pmol/mouse and these mice were imaged at 30 min, 1, 2, 4 and 24 h post injection. Among these conjugates, the RGD-conjugated cypate moieties showed enhanced tumor imaging ability. The sulfonic acid groups attached to the cyanine dye made a significant difference in the clearance of the fluorophore from the tumor.

Scheme 6

In a similar study Li and coworkers [96] evaluated Cy5.5-RGD conjugate 61 (Eq. 4) in mice bearing human melanoma M21 (integrin+) and M21L (integrin-) tumors. Fluorescence intensity in the tumors of mice was 2.3 and 1.3 times that of normal tissue, respectively. Dynamic imaging revealed that Cy5.5-C(KRGDf) was rapidly taken up by KS1767 tumor immediately after bolus injection. The rate of its uptake in tumor was reduced by preinjection of C(KRGDf) in an interval time-dependent manner. These studies suggest that NIRF imaging may be applied to the detection of tumors expressing  $\alpha$ vb3.

#### **Equation 4**

Chen and coworkers have also followed this approach previously for in vivo NIRF imaging of brain tumor xenograft mice [97].

# 4.4 Cyanine Dye-Endostatin Conjugates

The angiogenesis inhibitor endostatin is a 20 kDa C-terminal fragment of collagen XVIII, a proteoglycan/collagen found in vessel walls and basement membranes. The endostatin fragment was originally identified in conditioned media from a murine endothelial tumor cell line. Endostatin inhibits endothelial cell migration in vitro and appears to be highly effective in murine in vivo studies. The molecular mechanisms behind the inhibition of angiogenesis have not yet been elucidated. Studies of the crystal structure of endostatin have shown a compact globular fold, with one face particularly rich in arginine residues acting as a heparin-binding epitope [98, 99]. It was initially suggested that zinc binding was essential for the antiangiogenic mechanism, but later studies indicate that zinc has a structural rather than a functional role in endostatin. The generation of endostatin or endostatin-like collagen

XVIII fragments is catalyzed by proteolytic enzymes, including cathepsin L and matrix metalloproteases, that cleave peptide bonds within the protease-sensitive hinge region of the C-terminal domain [100]. The processing of collagen XVIII to endostatin may represent a local control mechanism for the regulation of angiogenesis. Citrin et al. [101, 102] conjugated endostatin to a NIR probe (Cy5.5) monofunctional dye and injected it into mice bearing Lewis lung carcinoma tumors. Mice were imaged at various time points while under sedation. The best images were observed at 48 h post injection. No signal was emitted from mice injected with unlabeled endostatin or Cy5.5 dye alone or those that received no injection. This study suggests that the NIR- labeled endostatin can provide translational information, noninvasive tumor imaging, and basic mechanistic information in an in vivo animal model.

# 4.5 Cathepsin-D-Sensitive Cyanine Dyes

A variety of proteases are overexpressed or activated during pathogenesis and represent important targets for therapeutic drugs [103–111]. Cathepsin D is an aspartic proteinase that is normally localized in lysosomes of various mammalian tissues. Its main function is in protein catabolism; however, a 2- to 50-fold increase in enzyme levels has been reported in breast cancers, demonstrated by immunohistochemistry and in situ hybridization.

High cathepsin D levels in tumors have also been associated with higher metastatic potential, invasion, angiogenesis, degradation of basement membrane and activation of other proteolytic enzymes as part of the metastatic cascade. In the Tung and Weissleder approach [112], a NIR cyanine fluorophore serving as the optical reporter was attached to the amino terminal of an 11-amino-acid peptide sequence with specificity for cathepsin D. The peptide was subsequently attached to a synthetic graft polymer for efficient tumoral delivery (Scheme 7). Cell culture experiments using a rodent tumor cell line stably transfected with human cathepsin D confirmed enzyme-specific activation within cells. This sequence, but not a scrambled control sequence, showed enzyme specificity in vitro. The development of a biocompatible, enzyme-activatable NIRF imaging probe 67 represents a critical step toward development of in vivo molecular optical imaging. This technique is cur-

Scheme 7

**Fig. 4** Schematic structure of near-infrared fluorescence (NIRF) probes. The *undulating line* represents the enzyme-specific peptide. The Cy5.5 fluorochrome is depicted as a *dark circle* and fluorescein isothiocyanate (FITC) as an *open triangle*. The cleavage position by target protease is indicated by the *arrows* (see [103]). *MPEG* Methoxy poly(ethyleneglycol)

rently being applied by Weissleder and other researchers to other enzymes, including matrix metalloproteinases, caspases and prostate-specific antigen, etc. (Fig. 4).

# 4.6 Tricarbocyanine-Cholesteryl Laurates

For monitoring low-density lipoprotein receptors (LDLr) in tumors and in livers of patients with familial hypercholesterolemia (FH) [113] treated with gene therapy, a series of tricarbocyanine cholesteryl laurates were synthesized with the cholesteryl laurate moiety serving as a lipid-chelating anchor of LDL. The conjugate **70** was successfully used to label LDL and its preparation is illustrated in Scheme 8.

To confirm the selective delivery of the conjugate to tumors via LDLr-mediated endocytosis, a low temperature 3-D redox scanner was used as a NIR fluorescent imager on a LDLr overexpressed tumor model, HepG<sub>2</sub>. A strong fluorescence signal of the fluorescent agent was detected only inside the tumor tissue, demonstrating that the LDL conjugate 70 was selectively internalized into the tumor [105]. Because of its target specificity and its high sensitivity, this approach could be useful for monitoring LDLr in tu-

$$H_3C(H_2C)_{10}$$
 $H_3C(H_2C)_{10}$ 
 $H_3C(H_2C)_{10}$ 
 $H_3C(H_2C)_{10}$ 
 $H_3C(H_2C)_{10}$ 
 $H_3C(H_2C)_{10}$ 
 $H_3C(H_2C)_{10}$ 
 $H_3C(H_2C)_{10}$ 

#### Scheme 8

mors overexpressing LDLr and in the liver of FH patients treated with gene therapy.

# 4.7 Cyanine Dye-Folic Acid Conjugates

Tung, Weissleder and coworkers [114] reported the preparation of cyanine dye-folic acid conjugate 74 with a goal of determining whether a fairly abundant receptor on tumor cells could serve as a target for NIRF-enhanced optical imaging. The folate receptor (FR) was ideally suited for this study because it overexpresses in several cancers such as breast, lung, cervical, ovarian, colorectal, renal, and nasopharyngeal cancers. Additionally, it has low expression

#### Scheme 9

in normal tissues, thus facilitating the use of MR and nuclear imaging. The conjugate was prepared by following the approach shown in Scheme 9.

The conjugate 74 was evaluated for in vivo NIRF imaging, specifically on tumor enhancement characteristics as a function of time and comparison of the folate and NIRF conjugate to the NIR fluorochrome alone. The results revealed that the folate-cyanine dye conjugate has potential applications in improved detection of FR-positive tumors. Compared to nontargeted dye, intravenous injection of the targeting probe was shown to significantly increase tumor contrast 4–48 h in the nude mouse xenograft model.

# 5 Cyanine Dyes for Photodynamic Therapy (PDT)

Photodynamic therapy (PDT) uses photosensitizing agents and light to kill cancer cells [115]. Once incorporated in the body, time is allowed for the drug to localize in the tumor in high concentration, and then a light source is applied to the treated area. The light causes the drug to react with oxygen, producing singlet oxygen, a cytotoxic agent that kills the cancer cells. PDT may also work by destroying the blood vessels that feed the cancer cells and by alerting the immune system to attack the cancer. This novel treatment has several advantages over traditional cancer treatments like surgery, chemotherapy, radiation and/or hormone therapy. Patients have fewer, if any, long-term side effects, the treatment is less invasive, it can be precisely targeted and can be repeated several times at the same site if necessary. PDT has been approved by the FDA and is used worldwide for early- and late-stage lung cancer, obstructive esophageal cancer, high-grade dysplasia associated with Barrett's esophagus, age-related macular degeneration and actinic keratoses [116–124].

Certain cyanine dyes such as merocyanines and ketocyanines have been studied extensively as potential photosensitizers for PDT [23, 125] and radiation sensitizers [126] for the treatment of solid tumors. Merocyanine 540 (75) showed a selective recognition for leukemia cells and has also been proposed as a reagent for both diagnosis and treatment of early stage leukemia by PDT. The intracellular dyes 75–81 act as a phototoxin to destroy the host cells under illumination due to a long-lived triplet excited state of the dye, which plays an active role in the whole process [127]. The dominant photoprocess involves isomerization from the first excited singlet state progressing to an all-trans configuration to a long-lived cis-isomer. Therefore for merocyanine derivatives to be clinically useful, it is necessary that (a) photoisomerization, which competes with intersystem crossing and radiation deactivation, is inhibited, and (b) highly fluorescent dye is photobleached in cellular media to recognize leukemia. Photobleaching occurs via oxidative attack of singlet oxygen produced from the long-lived triplet excited state on the poly-

methine chain [128]. Thus, a group of merocyanine dyes giving no triplet state, and therefore useful for detection purposes, and another group of such dyes displaying high triplet yield, and therefore useful as phototoxins, are needed.

For a series of merocyanine derivatives it was observed that the presence of heavy atoms enhances the triplet yield by spin-orbit coupling and changes the rate and yield of isomerization [129]. Among these compounds, merocyanine 80, containing Se, was shown to be a potent sensitizer [130]. The lipophilicity increases by the inclusion of heavy atoms and it possesses high toxicity toward leukemia cells due to high intracellular solubilization and the faster rate of uptake into infected cells improves biological activity. Benniston et al. [131] investigated a series of these dyes 75–81 in depth and suggested that the presence of heavy Se atom 80 is more effective for PDT than replacing the Se with an O atom as in 81 for diagnosis.

### 6 Porphyrin-Based Photosensitizer-Cyanine Dye Conjugates as Bifunctional Agents: a "See and Treat" Approach

The cyanine dyes related to ICG, Cy5.5 and Cy7.0 are excellent candidates for optical imaging of tumors, but do not produce singlet oxygen, and are therefore not suitable as photosensitizers for PDT (Pandey RK et al [132]).

Porphyrin-based photosensitizers (porphyrins, chlorins, bacteriochlorins and phthalocyanines) generally fluoresce and the fluorescence properties of these porphyrins in vivo has been exploited by several investigators for the detection of early-stage cancers in the lung, bladder and various other sites. In addition, for treatment of early disease or for deep-seated tumors the fluorescence can be used to guide the activating light [115–124]. However, photosensitizers are not optimal fluorophores for tumor detection for several

reasons. First, they have low quantum yields. Because the excited state energy is transferred to the triplet state and then to molecular oxygen, efficient photosensitizers tend to have lower fluorescence efficiency (quantum yield) than compounds designed to be fluorophores, such as cyanine dyes. Second, they have small Stokes' shifts. Porphyrin-based photosensitizers have a relatively small difference between the long-wavelength absorption band and the fluorescence wavelength (Stokes' shift), which makes it technically difficult to separate the fluorescence from the excitation wavelength. Third, they have relatively short fluorescent wavelengths, which are not optimal for deep tissue penetration.

Pandey and coworkers [133, 134] have shown the utility of tumor-avid photosensitizers in the corresponding bifunctional conjugates (83) to target the NIR fluorophores to the tumor. The function of the fluorophore is to visualize the tumor location and treatment site. The presence of the photosensitizer allows subsequent tumor ablation. A compound that effectively functions both as a fluorescence imaging agent and a photosensitizer would create an entirely new paradigm for tumor detection and therapy. The optical imaging allows the clinician performing PDT to continuously acquire and display patient data in real time. This "see and treat" approach may determine where to treat superficial carcinomas and how to reach deep-seated tumors, in sites such as the breast, with optical fibers delivering the photoactivating light.

Cyanine dye, Imaging Agent

The bifunctional conjugates provide an opportunity to independently select appropriate photosensitizers and fluorophores. For treating large and deeply seated tumors, photosensitizers exhibiting long-wavelength absorption in the range of 780–800 nm and higher tumor avidity than 3-(1'-hexyloxyethyl)-3-devinyl-pyropheophorbide-a (HPPH) (a chlorophylla based photosensitizer developed in our laboratory and currently in Phase II human clinical trials) [98–102, 122–124] will be conjugated with NIR fluorophores. As shown in Figs. 5–7, the conjugate 83 can achieve high tumor localization and effective photodynamic activity. By varying parameters such as lipophilicity, it may further optimize the pharmacokinetics, biodistribution and tumor selectivity of the conjugates by modifying the tumor avidity

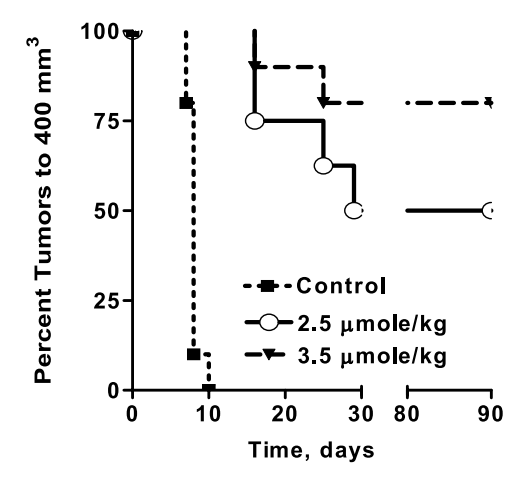


**Fig. 5** In vivo photosensitizing efficacy of conjugate **83** in mice (C3H) implanted with radiation induced fibrosarcoma (RIF) tumors at drug concentrations of 2.5 and  $3.5 \,\mu \text{mol/kg}$  (ten mice/group). The tumors were exposed to light (665 nm,  $130 \,\text{J/cm}^2$ ) at 24 h post injection

#### 24 h post-injection of PDT-IRD

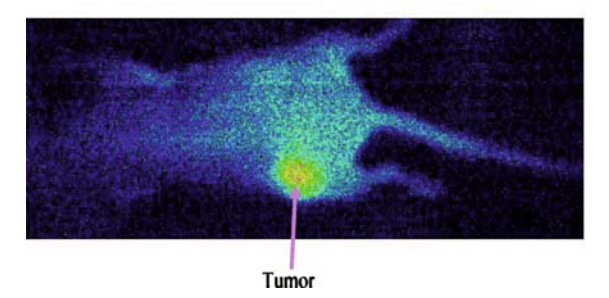
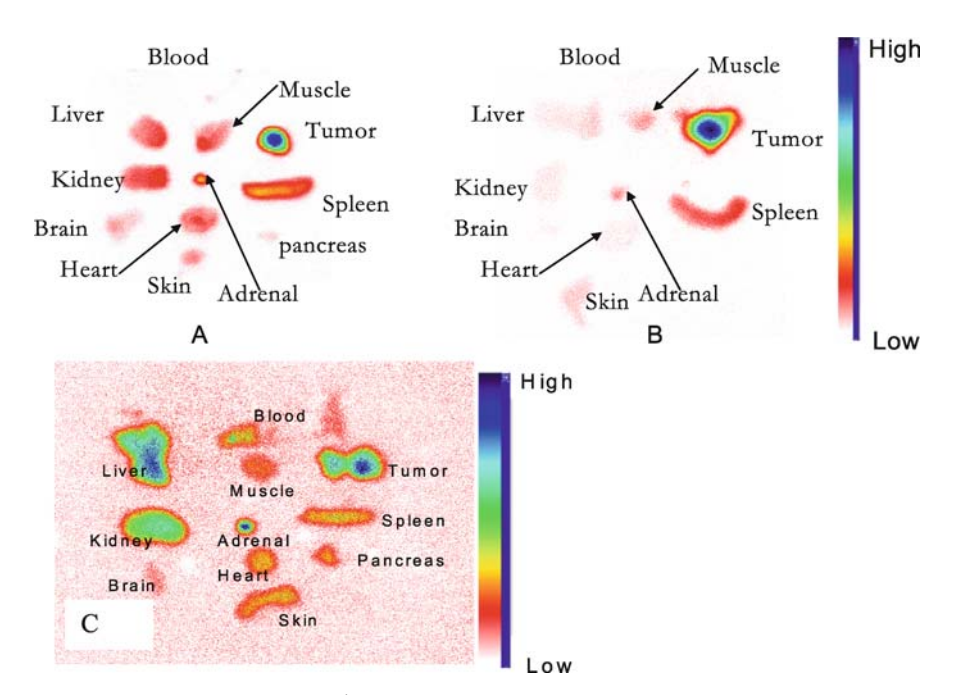


Fig. 6 Localization of the conjugate 83 in a live mouse 24 h after injection (drug dose  $0.3 \, \mu mol/kg)$ 

and photophysical characteristics. For example, to produce a conjugate with only tumor-imaging capability without photosensitization, the singlet oxygen ( $^{1}O_{2}$ )-producing capability can be eliminated or reduced by introducing certain quenchers (e.g., carotenoids) or by using the Cu(II) photosensitizers.

In initial studies investigating the utility of a tumor-avid photosensitizer as a vehicle to target imaging moieties to tumors, HPPH was conjugated with a non-tumor-specific cyanine-dye-based fluorophore to visualize the tumor by optical imaging. The presence of the photosensitizer allows subsequent tumor ablation. The resulting conjugate 83 was an effective photosensitizer both in vitro and in vivo (Fig. 5). At a therapeutic/imaging dose the conjugate did not show significant skin phototoxicity (a major drawback associated with most porphyrin-based photosensitizers). The conjugate 83 also was found to be a promising imaging agent even at low doses (Fig. 6).

Results of the whole body fluorescence imaging in radiation-induced fibrosarcoma (RIF) tumor-bearing C3H mice with excitation of the fluorescent cyanine dye ( $780_{\rm ex}$  and  $865_{\rm em}$  in vivo) 24 h post injection are shown in Fig. 7. Even at a dose of 0.3  $\mu$ mol/kg, which was later found to be eight- to tenfold less than the therapeutic dose, the conjugate showed significant tumor imaging capability. Under similar conditions, unconjugated cyanine dye had no



**Fig. 7** Accumulation of a 3-(1'-hexyloxyethyl)-3-devinyl-pyropheophorbide-a (HPPH)+ dye **83** in various organs **A** 48 hr, **B** 72, and **C** 24 h post injection from RIF-tumor-bearing mice

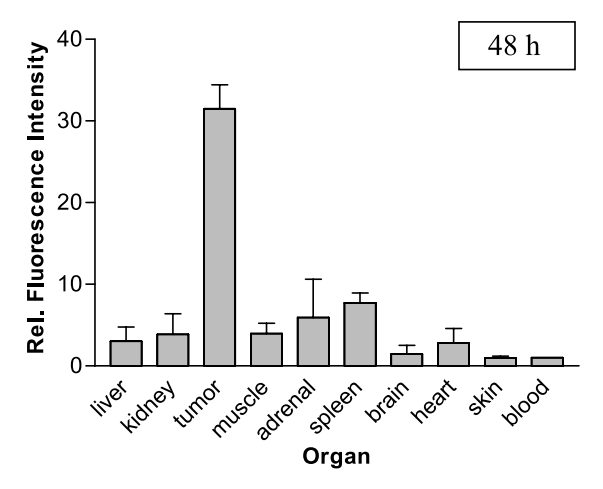


Fig. 8 In vivo biodistribution of conjugate 83

tumor localization. For optical biodistribution experiments the organs were removed, dried, weighed, placed on a black surface and imaged.

The ability to determine fluorescence from individual organs is depicted in Fig. 8. The fluorescence distribution was averaged over multiple mice, as shown for three mice; the data are relative to blood. At 48 and 72 h, there was more than eight- to tenfold more HPPH dye in the tumor than in the blood, muscle, skin, liver and kidney (Fig. 8).

In a parallel study, Pandey and coworkers also showed that porphyrin-based compounds linked to Gd(III)DTPA conjugates are successful as combination tumor MR imaging and PDT agents. In their initial work, HPPH was used as a vehicle to deliver the Gd(III) chelates to tumor cells. Insertion of paramagnetic metals (e.g., Cu) in the HPPH portion of the conjugate eliminated its singlet oxygen producing capability without any significant effect on its imaging capability. Thus, this approach is quite versatile and shows an enormous potential for developing tumor-imaging agents with and without PDT efficacy.

# 6.1 In Vivo Fluorescence Imaging of Glioma Tumors and PDT Efficacy

Malignant gliomas are the most common primary brain tumor and are responsible for approximately 2.5% of all cancer deaths [135]. Surgery, radiation therapy and chemotherapy offer palliation of neurologic symptoms and prolongation of survival. For glioblastoma multiforme, however, mean survival is still less than 1 year [136]. Since local control remains inadequate, there is a strong rationale for the development of adjunctive treatments to enhance destruction of tumor cells beyond the margins of resection. Selectivity for

tumor tissue is a vital element of this strategy. The prognosis for patients with malignant brain tumors is linked to the completeness of tumor removal. However, the borders of such tumors are often indistinguishable from surrounding brain tissue, making completeness of tumor removal highly dependent upon the neurosurgeon's judgment. The information provided by tumor-targeted multifunctional photosensitizers allows for an additional localization of the tumor as well as assessment of therapeutic effect, thus assisting the neurosurgeon in performing tumor resection more completely. Fluorophores with long-wavelength absorptions and a significant Stokes' shift (>50 nm) provide the means to localize deeply seated nests of tumor cells that are otherwise difficult to locate [135]. The conjugate 83 fulfills these requirements nicely. Its imaging and therapeutic potential was evaluated in mice bearing U87 tumors.

The tumor images at variable time points are shown in Fig. 9 with excitation of the fluorescent cyanine dye moiety of conjugate 83. In initial experiments, the imaging and therapeutic doses were kept the same. It is exciting to note that even at a dose of  $0.3~\mu mol/kg$ , which was 10- to 12-fold less than the therapeutic dose, the conjugate 83 shows significant tumor-imaging capability. To visualize the actual localization of the conjugate in the tumor versus the skin over the tumor, the tumor was surgically removed from the original site and placed away from the original site. Upon imaging, a prominent fluorescence intensity of 83 was found in the tumor compared to the normal skin.

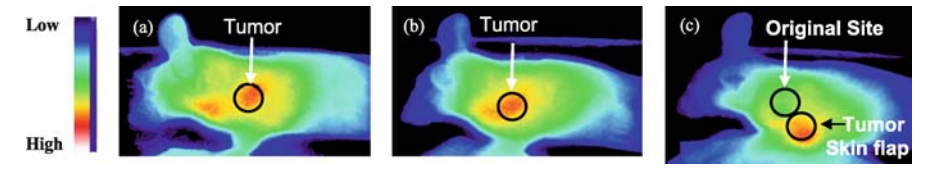


**Fig. 9** Fluorescence images of male athymic nude mice (CD-1, nu/nu) implanted with U87 tumor on the shoulder with the conjugate **83** at variable time points in the therapeutic dose (3.5  $\mu$ mol/kg,  $\lambda$ <sub>ex</sub> = 782 nm;  $\lambda$ <sub>em</sub> = 865 nm). Skin was removed and flapped back to expose the tumor at **a** 24 h, **b** 48 h, and **c** 48 h post injection

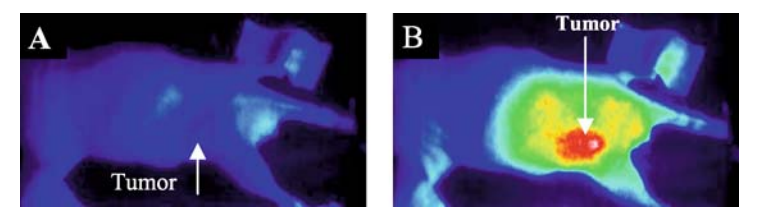


**Fig. 10** Nude mice bearing U87 tumors on the right flank. **A** Before injecting the drug. **B** Fluorescence image at 72 h post injection. Imaging agent: the HPPH-cyanine conjugate **83** (0.3 μmol/kg)

The imaging potential of the conjugate 83 in nude mice bearing U87 (glioma) tumors (three mice/group) at a dose of  $0.3 \,\mu\text{mol/kg}$  at 24, 48, and 72 h post injection was found to be quite promising. The fluorescence images of mice before and after injecting the imaging agent are shown in Fig. 10.

For in vivo photosensitizing efficacy, nude mice were implanted subcutaneously with U87 tumors and the conjugate 83 was evaluated for PDT efficacy at various drug doses (0.5, 1.0, 2.5 and 3.5  $\mu$ mole/kg) with a constant light dose (135 J/cm², 75 mW/cm²). Under these treatment conditions, at a dose of 3.5  $\mu$ moles/kg, the conjugate 83 was found to be quite effective with 60% of the mice (6/10 mice) being tumor-free on day 60.

### 7 Conclusions

Fluorescence-enhanced imaging has been known for a long time in evaluating the spatial distribution as well as the pharmacokinetics of porphyrinbased photosensitizers in PDT. Most of the monopyrrole-reduced porphyrin systems exhibit long-wavelength absorptions in the range 650-700 nm with highly efficient fluorescence. The long-wavelength absorption can further be extended (750-800 nm) by reducing two pyrrole rings, which are diagonal to each other. Such systems are known as bacteriochlorins [137]. Both series of compounds are known for their photosensitizing capability and high singlet oxygen producing efficiency. However, compared to porphyrins and chlorins, the bacteriopurpurinimide analogs are less fluorescent. One of the main problems with most of the porphyrin-based compounds (including chlorins and bacteriochlorins) is a small Stokes' shift between the absorption and emission peaks, which limits their application in fluorescence imaging. On the other hand, most of the cyanine dyes exhibit strong fluorescence and a large Stokes' shift with limited tumor avidity. Therefore, the recent approaches for developing target-specific fluorophores by conjugating them with various target-specific moieties have created enormous interest in optical imaging. One of the problems in fluorescence imaging is quantitation, which may be resolved by conjugating the fluorophores with various nuclides or MR imaging agents, and such studies are currently underway at various laboratories.

Some of the cyanine dyes (e.g., merocyanine 540 analogs) have been investigated for PDT, but their utility is quite limited due to low tumor avidity, isomerization and singlet oxygen quenching characteristics. Compared to merocyanines, cyanine dyes (Cy5.5, Cy7 etc.) exhibit longer wavelength absorptions. Therefore, a recent report by Pandey and coworkers [134] in which the modified cyanine dye (IR 820) was conjugated with HPPH is of particular interest. The impressive in vivo tumor imaging (fluorescence) and PDT data suggest the utility of this approach in developing bifunctional agents. As re-

ported by the same authors, this approach can further be extended toward the development of target-specific multifunctional agents in which target-specific cyanine dyes are conjugated with photosensitizers with and without radionuclide-attached functionalities. Consequently, development of more stable cyanine dyes will certainly enhance their applicability in the area of cancer detection, thus enabling physicians to treat early-stage cancer patients.

**Acknowledgements** Financial support from the NIH (CA55791, CA109914B and CA114053A) and the Oncologic Foundation of Buffalo is gratefully acknowledged. A partial support from the shared resources of the RPCI support grant (P30CA16056) is also appreciated. Dr. M.P. Dobhal is thankful to Dr. N.K. Jain, Vice-Chancellor, University of Rajasthan, Jaipur, India for the study-leave award.

#### References

- 1. Hamer FM (1964) The cyanine dyes and related compounds. In: Weissberger A (ed) Chemistry of Heterocyclic Compounds. Wiley Interscience, New York
- 2. Mishra A, Behera RK, Behera PK, Mishra BK, Behera GB (2000) Chem Rev 100:1973
- 3. Mason SJ, Hake JJ, Nairne J, Cummins WJ, Balasubramanian S (2005) J Org Chem 70:2939
- 4. Lee H, Masson C, Achilefu S (2006) J Org Chem 71:7862
- 5. Vaidyanathan S, Patterson LK, Mobius D, Gruniger HR (1985) J Phys Chem 11:390
- Rotermund F, Weigand R, Hoizer W, Wittermann M, Penzkofer A (1997) J Photochem Photobiol A: Chem 110:75
- Reindl S, Penzkofer A, Gong SH, Landthaler M, Szeimies RM, Abel C, Baumler W (1997) J Photochem Photobiol A: Chem 105:65
- 8. Prasad P, Williams DJ (1991) Introduction to Non-Linear Optical Effects in Molecules and Polyners. Wiley, New York
- 9. Kuhn H, Robillard J (eds) (1992) Non-Linear Optical Materials. CRC Press, Boca Raton
- 10. Ashwell GL, Hargreaves RC, Baldwin CE, Bahra GS, Brown CR (1992) Nature 357:393
- 11. Chen C, Zhou B, Lu D, Xu G (1995) J Photograph Sci 41:134
- 12. Fassler D, Baezold M (1995) Proc Indian Acad Sci 107:743
- 13. Ozelik S, Axins DL (1997) Appl Phys Lett 71:3057
- 14. Kemnitz K, Yoshihara K, Tani T (1990) J Phys Chem 94:3099
- 15. Shindo Y, Ohta Y, Hasegawa M (1996) J Photopolym Sci Technol 9:59
- 16. Lenhard JR, Parton RL (1997) J Am Chem Soc 109:5808
- 17. Oehling H, Baer F (1977) Org Magn Reson 9:465
- 18. Parton RL, Lenhard JR (1990) J Org Chem 55:49
- Ischenko AA, Mushkalo IL, Sogulyave YA, Agafonova GA, Ibraev NK (1994) Opt Spectrosc 77:353
- 20. Chibisov AK, Zakharoca GV, Gorner H, Tonmachev AI (1995) Appl Spectrosc 62:58
- 21. Chibisov AK, Zakharova GV, Corner H (1996) J Chem Soc Faraday Trans 92:4917
- 22. Serpone N, Sahyun MR (1994) J Phys Chem 98:734
- 23. Gomer C (1991) J Photochem Photobiol 54:1093
- 24. Redmond RW, Srichai MB, Bllitz JM, Schlomer DD, Kreig M (1994) Photochem Photobiol 60:348
- 25. Soper SA, Mattingly QL (1994) J Am Chem Soc 116:3744

- 26. Banerjee D, Laha AK, Bagchi S (1995) Ind J Chem 34A:94
- 27. Hirata T, Kogiso H, Morimoto K, Miyamoto S, Taue H, Sano S, Muguruma N, Ito S, Nagao Y (1998) Bioorg Med Chem 6:2179
- 28. James TH (1986) Adv Photochem 13:329
- 29. Spitler MT, Ehret A, Kietzmann R, Willing F (1997) J Phys Chem B 101:2552
- 30. Tonge R, Shaw J, Middleton B, Rowlinson R, Rayner S, Young J, Pognan F, Hawkins E, Currie I, Davison M (2001) Proteomics 1:377
- 31. Leevy CM, Smith F, Longueville J (1967) J Am Med Assoc 200:236
- 32. Sevick-Muraca EM, Kuwana E, Godavarty A, Houston JP, Thompson AB, Roy R (2002) Near infrared fluorescence imaging and spectroscopy in random media and tissues. In: Vo-Dinh T (ed) Biomedical photonics handbook. CRC Press, Boca Raton
- 33. Cohn GE, Domanik R (2002) In vitro clinical diagnostic instrumentation. In: Vo-Dinh T (ed) Biomedical photonics handbook. CRC Press, Boca Raton
- 34. Harisingham MG, Willenberg J, Weissleder R (2003) Primer of diagnostic imaging, 3rd edn. Elsevier, New York
- 35. Artemov D, Mori N, Okolie B, Bhujwala ZM (2003) Magn Reson Med 49:403
- 36. Pathak AP, Artemov D, Solaiyappan M, Bhujwala ZM (2003) Diagnostic Imaging 25:25
- 37. Aboayge E, Bhujwalla ZM, He Q, Glickson JD (1998) Radiat Res 150:38
- 38. Ntziachristos V, Yodh AG, Schnall M, Chance B (2000) Proc Natl Acad Sci USA 97:2767
- 39. Thompson AB, Hawrysz DJ, Sevick-Muraca EM (2003) Appl Opt 42:4125
- Eppstein MJ, Hawrysz DJ, Godavarty A, Sevick-Muraca EM (2002) Proc Natl Acad Sci USA 99:9619
- 41. Ebert B, Sukowski U, Grosenick D, Wabnitz H, Moesta KT, Licha K, Becker A, Semmler W, Schlag PM, Rinneberg HJ (2001) Biomed Opt 6:134
- 42. Ntziachristos V, Schellenberger EA, Ripoll J, Yessayan D, Graves E, Bogdanov A Jr, Josephson L, Weissleder R (2004) Proc Natl Acad Sci USA 101:12294
- 43. Blasberg RG (2003) Nucl Med Biol 30:879
- 44. Thompson AB, Sevick-Muraca EM (2002) J Biomed Opt 8:111
- Petrovsky A, Schllenberger L, Josephson R, Weissleder R, Bogdanov A (2003) Cancer Res 63:1936
- 46. Chen Y, Zheng G, Zhang ZH, Blessington D, Zhang M, Li H, Liu Q, Zhou L, Intes X, Achilefu S, Chance B (2003) Opt Lett 28:2070
- 47. Josephson L, Mahmood U, Wunderbaldinger P, Tang Y, Weissleder R (2003) Mol Imaging 2:18
- 48. Song LM, Wang KK (2003) Technol Cancer Res Treatment 2:289
- 49. Gambhir SS (2002) Nat Rev Cancer 2:883
- 50. Wisner ER, Ferrara KW, Short RE, Ottoboni TB, Gabe JD, Patel D (2003) Invest Radiol 36:358
- 51. Rubens DJ (2004) Radiol Clin N Am 42:257
- 52. Nalcioglu O (2003) J Magn Reson Imaging 18:467
- 53. Partridge SC, Gibbs JE, Lu Y, Esserman LJ, Sudilovsky D, Hylton NM (2002) Am J Roentgenol 179:1193
- 54. Guillem JG, Moore HG, Akhurst T, Klimstra DS, Ruo L, Mazumdar M, Minsky BD, Saltz L, Wong WD, Larson S (2004) J Am Coll Surgeons 199:1
- 55. Galons JP, Morse DL, Jeannings DR, Gillies RJ (2003) Isr J Chem 43:91
- 56. Brenner W, Conrad EU, Eary JF (2004) Eur J Nucl Med Mol 31:189
- 57. Tzika AA, Cheng LL, Goumnerova L, Madsen JR, Zurakowski D, Astrakas LG, Zarifi MK, Scott RM, Anthony DC, Gonzalez RG, Black PM (2002) J Neurosurg 96:1023

58. Collier TL, Lecomte R, McCarthy TJ, Meikle S, Ruth TJ, Scopinaro F, Signore A, Vanbrocklin H, Van de Wiele C, Waterhouse RN (2002) Dis Markers 18:211

- 59. Spincemaille P, Nguyen TD, Wang Y (2004) Magn Reson Med 52:461
- 60. Chance B, Cope M, Gratton E, Ramanujan N, Tromberg B (1998) Rev Sci Instrum 689:3457
- 61. Chance B (1997) Ann New Acad Sci 838:29
- 62. Choy G, Choyke P, Libutti SK (2003) Mol Imaging 2:303
- 63. Achilefu S, Dorshow RB, Bugaj JE, Rajagopalan R (2000) Invest Radiol 35:479-485
- 64. Choi H, Choi SR, Zhou R, Kung HF, Chen IW (2004) Acad Radiol 11:996
- 65. Kelly K, Alencar H, Funovics M, Mahmood U, Weissleder R (2004) Cancer Res 64:6247
- 66. Gao X, Cui Y, Levenson RM, Chung LW, Nie S (2004) Nat Biotechnol 22:969
- 67. Sevick-Muraca EM, Kuwana E, Godavarty A, Houston JP, Thompson AB, Roy R (2003) Near-infrared fluorescence imaging and spectroscopy in random media and tissues. In: Vo-Dinh T (ed) Biomedical photonics handbook. CRC Press, Boca Raton
- 68. Garfinkel M, Thomson AB, Ralston W, Troy TL, Moore AL, Moore TA, Gust JD, Tatman D, Pandey RK, Reynolds JS, Muggenburg B, Nikula K, Mayer RH, Hawrysz DJ, Sevick-Muraca EM (2000) Photochem Photobiol 72:94
- 69. Ntziachristos V, Bremer C, Graves EE, Ripoll J, Weissleder R (2002) Mol Imaging 1:82
- 70. Chen Q, Wilson B, Patterson M, Chopp M, Hetzel F (1991) Proc SPIE 1426:156
- 71. Lobel J, MacDonald IJ, Ciesielski MJ, Barone T, Potter WR, Pollina J, Plunkett RJ, Fenstermaker RA, Dougherty TJ (2001) Laser Surg Med 29:397
- 72. Renikuntla BR, Rose HC, Eldo J, Waggoner AS, Armitage BA (2004) Org Lett 8:909
- 73. Mader O, Reiner K, Egelhaaf HJ, Fischer R, Brock R (2004) Bioconjugate Chem 15:70
- 74. Haugland RP (2002) Handbook of fluorescence probes and research products, 9th edn. Molecular Probes, Eugene, Oregon, USA
- 75. Chipon B, Clave G, Bouteiller C, Massonneau M, Renard PY, Romieu A (2006) Tetrahedron Lett 47:8279
- 76. Strekowski L, Mason CJ, Lee H, Gupta R, Sowell J (2003) J Heterocycl Chem 40:913
- 77. Ye Y, Li WP, Anderson CJ, Kao J, Nikiforovich GV, Achilefu S (2003) J Am Chem Soc 125:7766
- 78. Bugaj JE, Achilefu S, Dorshow RB, Rajgopalan R (2001) J Biomed Opt 6:122
- 79. Licha K, Hessenius C, Becker A, Henklein P, Bauer M, Wisniewski S, Wiedenmann B, Semmler W (2001) Bioconjugate Chem 12:44
- 80. Becker A, Licha H, Krese M, Riefke B, Sukowski U, Ebert B, Rinneberg H, Sennler W (1999) Proc SPIE 142:3600
- 81. Zaheer A, Lenkinski RE, Mahmood A, Jones AG, Cantly LC, Frangioni JV (2001) Nat Biotechnol 19:1148
- 82. Mader O, Reiner K, Egelhaaf HJ, Fischer R, Brock R (2004) Bioconjugate Chem 15:70
- 83. Licha K, Riefke B, Niziachristos V, Becker A, Chance B, Semmler W (2000) Photochem Photobiol 72:392
- 84. Zhang Z, Achilefu S (2004) Org Lett 6:2067
- 85. Cherqui S, Kalatzis V, Trugnan G (2001) J Biol Chem 276:13314
- 86. Li C, Greenwood TR, Bhujwalla ZV, Glunde K (2006) Org Lett 8:3623
- 87. Cheng Z, Levi J, Xiong Z, Gheysens O, Keren S, Chen X, Gambhir SS (2006) Bioconjugate Chem 17:662
- 88. Warburg O (1931) The metabolism of tumors. Richard R Smith, New York
- 89. Levi J, Cheng Z, Gheysens O, Patel M, Chen CT, Wang Y, Namavari M, Gambhir SS (2007) Bioconjugate Chem 18:628

- 90. Xiong JP, Stehle T, Zhang R, Joachimiak A, Frech M, Goodman SL, Arnaout MA (2002) Science 296:151
- 91. Brooks PC, Clark RA, Cheresh DA (1994) Science 264:569
- 92. Kumar CC (2003) Curr Drug Targets 4:123
- 93. Brooks PC, Stromblad S, Sanders LC, von Schalscha TL, Aimes RT, Stetler-Stevenson WG, Quigley JP, Cheresh DA (1996) Cell 85:683
- 94. Chen X, Conti PS, Moats RA (2004) Cancer Res 64:8009
- 95. Chen X, Park R, Hou Y, Khankaldyyan V, Tohme M, Bading JR, Laug WE, Conti PS (2004) Eur J Nucl Med Mol Imaging 31:1081
- 96. Ke S, Wen X, Gurfinkel M, Charnsangavej C, Wallace S, Sevick-Muraca EM, Li C (2003) Cancer Res 63:7870
- 97. Chen Y, Ohkubo K, Zhang M, Wenbo E, Liu W, Pandey SK, Ciesielski M, Baumann H, Erin T, Fukuzumi S, Kadish KM, Fenestermaker R, Oseroff A, Pandey RK (2207) Photochem Photobiol Sci 6:1257–1267
- 98. Wickstrom S, Alitalo K, Keski-Oja J (2002) Cancer Res 62:5580
- 99. Kim Y, Hwang S, Kim Y (2002) J Biol Chem 31:27872
- 100. Karumanchi S, Jha V, Ramachandran R (2001) Mol Cell 7:811
- 101. Citrin D, Lee AK, Scott T, Sproull M, Menard C, Tofilon PJ, Camphausen K (2004) Mol Cancer Ther 3:481
- Citrin D, Scott T, Sproull M, Menard C, Toflon PJ, Camphausen K (2004) Int J Radiat Oncol 58:536
- 103. Escot C, Zhao Y, Pusch C, Rochefort H (1996) Breast Cancer Res Treatment 38:216
- 104. Roger R, Montcourrier P, Maudeloride T, Brouilet JP, Pages A, Laffargue F, Rochefort H (1994) Hum Pathol 25:863
- 105. Garcia M, Derocq D, Pujol P, Rochefort H (1990) Oncogene 5:1809
- 106. Leto G, Gebbia N, Rausa L, Tumminello F (1992) Anticancer Res 12:235
- 107. Tedone T, Correale M, Barbarossa G, Casavola V, Paradiso A, Reshkin SJ (1997) FASEB J 11:785
- 108. Keppler D, Saneni M, Moin K, Mikkelsen T, Digilo C, Sloane B (1996) Biochem Cell Biol 74:799
- 109. Liaudet E, Derocq D, Rochefort H, Garcia M (1995) Cell Growth Differ 6:1045
- 110. Peterson JJ, Meares CF (1998) Bioconjugate Chem 9:618
- 111. Weisslerder R, Tung CH, Mahmood U, Bogdanov AJ (1997) Drug Target 4:321
- 112. Tung CH, Bredow S, Mahmood U, Weissleder R (1999) Bioconjugate Chem 10:892
- 113. Zheng G, Li H, Yang K, Blessington D, Licha K, Lund-Katz S, Chance B, Glickson JD (2002) Bioorg Med Chem Lett 12:1485
- 114. Moon WK, Lin Y, O'Loughlin T, Tang Y, Kim DE, Weissleder R, Tung CH (2003) Bioconjugate Chem 14:539
- 115. Dougherty TJ (1987) Photochem Photobiol 45:879
- 116. Dolmans DE, Fukumura D, Jain RK (2003) Nat Rev Cancer 3:380
- 117. Dougherty TJ, Gomer CJ, Henderson BW, Jori G, Kessel D, Korbelik M, Moan J, Peng QJ (1998) Natl Cancer Inst 90:889
- 118. Henderson BW, Dougherty TJ (1992) Photochem Photobiol 55:145
- 119. Kessel D (2004) Adv Drug Deliver Rev 56:7
- 120. Pandey RK, Zheng G (2000) Porphyrins as photosensitizers in photodynamic therapy. In: Kadish K, Guiland R, Smith KM (eds) The porphyrin handbook, vol 6. Academic, Boston, p 157
- 121. Pandey RK, Goswami LN, Chen Y, Gryshuk A, Missert JR, Oseroff A, Dougherty TJ (2006) Laser Surg Med 38:445

122. Henderson BW, Gollnick SO (2003) Mechanistic principles of photodynamic therapy. In: Horspool W, Lenci F (eds) Handbook of organic photochemistry and photobiology. CRC Press, Boca Raton

- 123. Dougherty TJ, Levy JG (2003) Clinical applications of photodynamic therapy. In: Horspool W, Lenci F (eds) Handbook of organic photochemistry and photobiology. CRC Press, Boca Raton
- 124. Jori G (2004) Photodynamic therapy: basic and preclinical aspects. In: Horspool W, Lenci F (eds) Handbook of organic photochemistry and photobiology. CRC Press, Boca Raton
- 125. Krieg M, Redmond RW (1993) Photochem Photobiol 7:472
- 126. Harriman A, Shoute LC, Neta P (1991) J Phys Chem 95:2415
- 127. Salma G, Mordar M (1976) Science 191:485
- 128. Frank B, Schneider U (1992) Photochem Photobiol 56:271
- 129. Benniston AC, Gulliya KS, Harriman A (1997) J Chem Soc Faraday Trans 93:2491
- 130. Bonnett R, Harriman A, Kozyrev AN (1992) J Chem Soc Faraday Trans 88:763
- 131. Benniston AC, Harriman A, McAvoy C (1997) J Chem Soc Faraday Trans 93:3653
- 132. Pandey RK et al., personal communication
- 133. Chen Y, Grushuk A, Achilefu S, Ohulchanskyy T, Potter W, Zhong T, Morgan J, Chance B, Prasad P, Henderson BW, Oseroff A, Pandey RK (2004) Bioconjugate Chem 8:1105
- 134. Chen Y, Ohkubo K, Zhang M, Wenbo E, Liu W, Pandey SK, Ciesielski M, Baumann H, Tracy E, Fukuzumi S, Kadish KM, Fenstermaker R, Oseroff A, Pandey RK (2007) Photochem Photobiol Sci 6:1257
- 135. Central Brain Tumor Registry of the United States (1997) Annual Report, Brain Tumor Society, 124 Watertown Street, Suite 3H, Watertown MA 02472
- 136. Wallner KE, Galicich JH, Krol G, Arbit E, Malkin MG (1989) Int J Radiat Oncol Bio Phys 16:1405
- 137. Chen Y, Li G, Pandey RK (2004) Curr Org Chem 8:1105
- 138. Fox IJ et al. (1957) Proc Staff Meetings Mayo Clin 32(18):478-484

### **Merocyanines: Synthesis and Application**

Valerii Z. Shirinian (⋈) · Alexey A. Shimkin

N. D. Zelinsky Institute of Organic Chemistry, RAS, 47, Leninsky prosp., 119991 Moscow, Russia

shir@ioc.ac.ru

1	Introduction	76
2	Synthesis	77
2.1	Simple Merocyanines	78
2.2	Merocarbocyanines	79
2.3	Long-Bridge Merocyanines	86
3	Structure and Isomerization	89
4	Properties and Applications	91
4.1	Solvatochromism	91
4.2	Ion Sensors	93
4.3	Molecular Aggregation	94
4.4	Non-Linear Optics	97
4.5	Solar Cells and Hydrogen Energy	98
4.6	Medicine	99
5	Conclusions	101
Refe	prences	101

**Abstract** The rapid progress of information technology continues to stimulate the exploration of innovative materials and architectures for digital processing. Merocyanine dyes appear to be potential candidates for the realization of future data-elaboration, -storage, and -communication devices. While the early stages of this research have been mainly concerned with applications in the fields of photography and medicine, most of the current work on these dyes involves investigation of moderate-to-large intermolecular aggregates, including both red-shifted "J" and blue-shifted "H" aggregates, optical and fluorescent sensors, and applications in solar engineering and medicine. This review summarizes advances in the synthesis, structure, and applications of merocyanine dyes over the last decade.

**Keywords** Dye · Merocyanine · Polymethine · Review · Synthesis

#### **Abbreviations**

CNDO/S Complete neglect of differential overlap/spectroscopic

DBU 1,8-Diazabicyclo[5.4.0]undecene-7

DMF N,N-Dimethylformamide

DMF-DMA N,N-Dimethylformamide dimethyl acetal

EFISH Electric-field-induced-second-harmonic

Het Heteroary

IWFO Integrated waveguide fluorescence optodes

LB Langmuir-Blodgett (films)

LOX Lipoxygenases MC Merocyanine

MNDO Modified neglect of differential overlap

NIR Near-infrared NLO Non-linear optics

NOE Nuclear Overhauser effect P3HT Poly(3-hexylthiophene-2,5-diyl)

PDT Photodynamic therapy

PM3/COSMO Parameterization method 3/conductor-like screening model

PR Photorefractive
PVC Poly(vinyl chloride)
SAM Self-assembled monolayer
SHG Second-harmonic generation

THF Tetrahydrofuran

#### 1 Introduction

Merocyanines (I) are neutral unsymmetrical polymethine dyes comprised of two fragments—nitrogen donor and oxygen acceptor connected by an ethylene or polyethylene chain. The transfer of charge from donor to acceptor through the polyene chain gives rise to the deep coloration that depends both on chain length and nature of donor and acceptor groups that usually belong to carbo- or heterocycles (II).

Advances in computer science and nanotechnology in the last decade have provoked new interest in dye chemistry including merocyanines. Merocyanine dyes have found wide application in various areas of science and technology. They are used as optical sensors, spectral sensitizers for silver halide photography [1–3], and recording medium in optical disks. Their potential application as photosensitizers for photodynamic therapy (PDT) [4–6] and radiation sensitizers for solid tumor treatment [7] has been extensively studied. Merocyanine dyes are promising materials for future technological applications, including nonlinear optics, solar and hydrogen energy, laser technology, and nanotechnology. It is worthy of special attention that mero-

cyanines (often called photomerocyanines) are obtained during the UV irradiation or heating of spiropyrans [8–10]. Their photo- and thermochromic properties are of considerable interest, and spiropyrans have been proposed for optical memory and switches [11], metal ions extraction [12, 13], photocontrollable ferromagnetics [14, 15], and optical and fluorescence sensors on metal ions and biological objects [16–18]. Some merocyanine dyes are so well known that they have specific names; for example, Brooker's merocyanine and MC540, the former showing remarkable solvatochromism and the latter being used in a number of medicinal applications.

This review covers the literature over the last decade concerning synthesis, structure, properties and application of merocyanine dyes. Though some data on merocyanines has been presented in a number of reviews [19–23] concerning color chemistry and polymethine dyes, no work summarizing data exclusively on merocyanines has been published over the last decade.

Although in the last few years papers have appeared dealing with "merocyanine-type" dyes [24–26], traditional merocyanines are the most widespread. So, this work is focused on classical dyes of general structure II. The data for photomerocyanines will not be given except for the case of structure discussion, since significant efforts have been made for the determination of their structures. Special emphasis is given to merocarbocyanine dyes (II, n=1) because of their prevalence and importance among other merocyanines as well as the multiplicity of synthetic methods.

### 2 Synthesis

The methods for the synthesis of merocyanines vary depending on the bridge length (number of methyne groups, n). The merocyanines can be divided into three groups, namely simple merocyanines (n = 0), merocarbocyanines (n = 1), and meropolycarbocyanines (n > 1). There are specific synthetic methods applied for the particular group of compounds, as well as common methods. The chemistry of merocyanine dyes is rather conservative, and the methods used for the synthesis of the first merocyanines [27] are widely utilized now.

### 2.1 Simple Merocyanines

The simplest merocyanines (n=0) are commonly prepared by the reaction of nitrogen heterocycles containing a leaving group in the 2- or 4-position with active methylene bases. In this way merocyanines, precursors to rhodacyanine dyes, were prepared [28–30]. The condensation of 2-(methylmercapto)benzothiazole with rhodanine in acetonitrile in the presence of triethylamine at  $10-15\,^{\circ}\text{C}$  results in merocyanine 1 in 87% yield (Eq. 1). A number of merocyanines were prepared starting from salts of other heterocycles such as pyridine, benzoxazole, naphthothiazole, and thiazoline.

#### **Equation 1**

A similar method was used for the synthesis of merocyanines based on the pyrazolin-5-one system [31]. The reaction of 2-chloroisatin 2 with pyrazolones 3 in boiling THF leads to merocyanines 4 in about 50% yields (Eq. 2).

#### **Equation 2**

The key stage in the synthesis of Brooker's merocyanine analog is the reaction of 2-(4-hydroxyphenyl)-substituted pyrylium tetrafluoroborate 5 with aniline resulting in pyridinium salt 6, which after treating with solid sodium hydroxide gives merocyanine 7 [32] (Scheme 1).

The construction of thioxopyrrolidine-2,3-dione ring by the reaction of a pyridinium salt 8 with oxalyl chloride is a convenient approach to the synthesis of merocyanines such as 9 [33] (Eq. 3).

Oxidation of indoxyls 10 is used for the preparation of famous indigo dyes 11 that have been highly valued since ancient times [34] (Eq. 4). It is interesting that 6,6′-dibromoindigo, best known as Tyrian, or Royal purple, was so expensive that it was used exclusively by the richest and most powerful men [35], and later, in Imperial Roman times, a purple cloak distinguished Emperors.

#### Scheme 1

#### **Equation 3**

#### **Equation 4**

Air oxygen is usually used as the oxidation agent though to oxidize other heterocyclic ketones, the use of stronger oxidants may be necessary. Thus, FeCl<sub>3</sub> was used for the synthesis of indigo analogue 12 (pyrazole blue) [31].

# 2.2 Merocarbocyanines

Methods for the preparation of merocarbocyanines (n = 1) or their higher vinylogues are much more varied. The classical route for the synthesis of merocarbocyanine dyes is a reaction of heterocyclic enamines or corresponding salts with hydroxybenzaldehydes or their heterocyclic analogs. Recently this method was applied to the synthesis of merocyanines of cumarine

13 [36], 8-hydroxyquinoline 14, 15 [37, 38], chromen-4-one and thiochromen-4-one 16 [39] series (Eq. 5).

R = H, Me, Br, NO<sub>2</sub>

13

$$X = CIO_4$$
 $X = O_1 S$ 

#### **Equation 5**

When quaternary salts are used, the reaction should be carried out in the presence of base (usually triethylamine or piperidine), otherwise merocyanine salts like 17 are formed [38] (Scheme 2). The treatment of the salt 17 with bases such as aqueous ammonia affords dye 18.

Tso 
$$\frac{Cl}{\Delta}$$
  $\frac{EtOH}{\Delta}$   $\frac{Cl}{A}$   $\frac{C$ 

#### Scheme 2

The capability of merocyanines to produce salts was used for their isolation [40]. Tetrafluoroborate 19, that is easily obtained by addition of sodium tetrafluoroborate to a crude solution in water, is readily deprotonated by

the subsequent treatment with alkali to obtain neutral merocyanine dye 20 (Eq. 6).

#### **Equation 6**

A versatile method for the preparation of merocyanine dyes involves the treatment of methyl-substituted quaternary salts of nitrogen heterocycles with anilinomethylene derivatives of heterocyclic ketones. Thus, the condensation of picoline salt 21 with the compounds 22 in ethanol in the presence of piperidine afforded a large series of merocyanines 23 in high yields [41] (Eq. 7).

$$R = CH_{2}CH(OH)CH_{2}OH;$$

$$Het$$

$$Piperidine, EtOH$$

$$R = N$$

#### **Equation 7**

A similar reaction of anilinomethylene derivative of rhodanine 24 with methyl quaternary salts of heterocycles results in the substitution of aniline residue by piperidine yielding product 25 [41] (Eq. 8).

#### **Equation 8**

This result can be explained in terms of the weak electron acceptor properties of the rhodanine ring. Merocyanine dyes based on rhodanine using 24 as starting material can still be prepared in acetic acid in the presence

of DBU [42]. Apparently, the activated acetanilidomethylene derivatives of rhodanine 26 are formed, which subsequently undergo condensation with nitrogen heterocycle salts.

Acetanilidomethylene-substituted heterocycles 27 are useful, versatile synthones, and they have been extensively used for the preparation of merocyanine dyes 28 that are based on rhodanine [28–30], barbituric acid [43] and pyridinedione [43, 44] (Eq. 9). The reaction is carried out in acetic anhydride in the presence of potassium acetate or in acetonitrile with triethylamine.

$$R^{2} = C_{12}H_{25}, ; R_{2} = H, i-Pr;$$

$$R = N$$

$$R$$

#### **Equation 9**

Dimethylaminomethylene derivatives 29 prepared by treatment of carboand heterocyclic ketones with DMF-DMA or with DMF in acetic anhydride have been used for the synthesis of various merocyanine dyes 30 [45-47]

$$X = CMe_2$$
,  $CH=CH$ ;  $A = CMe_2$ ,  $A = CMe_2$ 

#### **Equation 10**

(Eq. 10). Pyridine, ethanol or acetic anhydride are suitable solvents in this reaction depending on substrate nature.

No merocyanine dyes based on pyrazol-3,5-dione were obtained under similar conditions. It was stated that dimethylaminomethylene derivatives of five-membered heterocycles have extremely low activity and could not be utilized in this reaction [45]. However, this very method was successfully used for the preparation of merocyanine dyes of thiophen-3(2*H*)-one, benzothiophen-3(2*H*)-one, pyrazol-5(4*H*)-one, and coumarine series [48] (Scheme 3). The discovered rearrangement of benzothienopyrrole salt 31 to 2*H*-pyrrole derivative 32 allowed investigators to obtain merocyanines of two types 33 and 34 with absorption maxima covering the 500-650 nm range.

#### Scheme 3

This reaction is suitable for the preparation of merocyanines with carbocyclic moieties containing a carbonyl group. When difunctionalized ketones are condensed with two equivalents of quaternary salt, symmetrical ketocyanines 35 ( $R^1 = R^2$ ) are obtained. Non-symmetrical dyes can be prepared by step-by-step addition of different reagents [49, 50]. The yields of ketocyanines

X, Y = CMe<sub>2</sub>, S; R<sub>1</sub>, R<sub>2</sub> = H, OH, COOEt, NHAc, benzo

(52–75%) are significantly higher than those for the reactions of carbocyclic ketones and Fischer's aldehydes [51].

Other leaving groups, for example cyano group, can also be utilized. The reaction of 4-methylquinolinium bromide 36 with (dicyanomethylene)indene 37 results in merocyanine 38 containing cyano group in the methine bridge [52] (Eq. 11).

**Equation 11** 

The transfer of a formyl group from hydroxyaldehyde derivatives to nitrogen containing heterocycles is suitable when the required heterocyclic aldehydes are difficult to obtain. The condensation of aldehydes 39 with active methylene compounds 40 in absolute ethanol [31, 53, 54] or acetic anhydride [55, 56] leads to merocyanines 41 in moderate yields (Eq. 12).

#### **Equation 12**

Aza derivatives of unsaturated heterocyclic aldehydes are the most utilized starting materials for the preparation of merocyanine dyes since the first merocyanine syntheses [27]. To prepare dimer dyes based on barbituric acid anilinomethylene derivatives 42 were used. The reaction is carried out in dichloromethane at ambient temperature leading to merocyanines 43 in 42–89% yields [57] (Eq. 13).

**Equation 13** 

Crown-substituted merocyanines based on tellurazole 45 were prepared by the reaction of acetanilide salts 44 with active methylene compounds [58] (Eq. 14). Rhodanine and dimedone derivatives were best synthesized in pyridine, and the efficient preparation of merocyanines based on barbituric acid required the use of butanol in the presence of piperidine.

RR = O(CH<sub>2</sub>CH<sub>2</sub>O)<sub>4</sub>; Het = 
$$\begin{pmatrix} O & O & O & O \\ Het & S & S & O \end{pmatrix}$$

#### **Equation 14**

Recently, Würthner et al. developed a versatile one-pot synthesis of merocyanines 48 based on multi-step reaction of nitrogen heterocycles 46 with active methylene compounds 47 and DMF in acetic anhydride [45, 59] (Eq. 15). The process is uninfluenced by impurities in starting compounds, including water, and can be used in combinatorial synthesis.

$$X = CMe_2, O, S;$$

$$A6$$

$$A7$$

$$A8$$

$$DMF, Ac_2O$$

$$N$$

$$A8$$

$$A8$$

#### **Equation 15**

The preparation of merocarbocyanines that are vinylogues of indigo dyes by the condensation of pyrrol- or indol-3(2H)-ones with glyoxal in the

presence of inorganic acid generally proceeds in low yield [60]. The modified method using 3-acetoxy-1-methylindole **49** gave dye **50** in 51% yield (Eq. 16).

#### **Equation 16**

A number of methods have been developed for the transformation of chloro-substituted carbocyanine dyes 51 and analogues to ketocyanines, such as 52, the absorption spectra of which are very sensitive to pH [61] (Eq. 17). The best results were achieved when the reaction was catalyzed with succinimide *N*-oxide anion [62].

**Equation 17** 

### 2.3 Long-Bridge Merocyanines

The same methodology as utilized for the synthesis of simple merocyanines was found to be useful for the preparation of their cyclic higher vinilogues. The reaction of 2-methylmercapto-substituted benzisoxazole 53 with thiobarbituric acid derivative 54 in pyridine leads to merodicarbocyanine 55 in 53% yield [63] (Eq. 18). Compound 54 was synthesized by condensation of dibutylthiobarbituric acid with 3,5,5-trimethylcyclohex-2-enone.

**Equation 18** 

The importance of merocyanine MC-540 in medicinal chemistry was briefly mentioned in the Introduction. Analogues 57 were synthesized in 14–25% yields as shown in Eq. 19 [63]. The substrate 56 was obtained from thiobarbituric acid and 1,3,3-triethoxypropene.

O Bu NEt<sub>3</sub> NEt<sub>3</sub> NeOH Na
$$^+$$
 S  $^+$  Na $^+$  $^+$ 

#### **Equation 19**

The methodology was also applied to the synthesis of other analogues of MC540 including sterically hindered **58** [64], barbituric derivative **59** [65], and a series of merocyanine dyes **60**, **61** [66].

The reaction of acetanilide 62 with indoline salt was used for the preparation of merotricarbocyanine 63 [67] (Eq. 20).

#### **Equation 20**

Acetanilino derivative of the vinylogue of Fischer's aldehyde 64 was utilized for the synthesis of the cyclic merocyanine 65 [68] (Eq. 21).

#### **Equation 21**

Anils were also used for the preparation of oxonole **66** [69]. Two molecules of 1,3-dibutyl-2-thiobarbituric acid undergo reaction with one molecule of glutacondialdehyde dianil monohydrochloride to afford the dye **66** in 37% yield (Eq. 22).

**Equation 22** 

# 3 Structure and Isomerization

The structure of merocyanine dyes is of considerable interest both from theoretical and practical aspects. Great attention has been paid to establishing a relationship between structure and properties, in particular the ability to form aggregates and supramolecular assemblies. Merocarbocyanines can exist as four transoid isomers with regard to two double bonds of the bridge fragment. They are usually labeled as TTC, TTT, CTC, and CTT (abbreviations of *cis/trans* configuration for three bridge bonds), but the use of *E,Z*-nomenclature seems to be most proper because in many cases it is not possible to name a compound using *cis/trans* terms. Special attention will be drawn to the study of photomerocyanines (open forms of photochromic spiropyrans) because very limited data are known concerning structures of classical merocyanine dyes.

X-ray diffraction analysis of merocyanine **67** showed that the double bond connected to the isoxazolone moiety has *Z*-configuration [41]. On the other hand, the *E*,*E*-isomer was found for **68** both in crystal and solution [74].

Merocyanines **69–71** studied in the work by Shimkin et al. [48] have *Z*-configuration of the double bond near the benzothiophen-3(2*H*)-one moiety. The *E*,*Z*-structure of the indoline derivative **69** was proved by X-ray diffraction analysis. The 2D NMR study of merocyanine based on 1-benzothieno[3,2-*b*]-

pyrrole **70** showed *E,Z*-isomer as the only detectable form in solution. This conclusion was confirmed by MNDO calculations of the four possible isomers of **70**. The results of the calculations were consistent with the highest stability of the *E,Z*-isomer and the relative low stability of the *E,E*-isomer. Blue-colored dye **71** has been described as *Z,Z*-isomer both in crystal and solution.

$$E,Z-69$$
 $E,Z-70$ 
 $Z,Z-71$ 

Significant efforts were made to determine structures of photomerocyanines that are metastable open forms of photochromic spiropyrans. Quantum mechanics calculations suggested that the E,Z-isomer of photomerocyanines (for example 72, R = H) is the most stable, with E,E form being the second most favorable [70–73]. Experimental data often confirm these results: both in solutions (usually by NOESY) and crystals (by X-ray diffraction analysis) merocyanines commonly exist in E,Z or E,E form or both. For example, merocyanine 72 (R = NO<sub>2</sub>) crystallizes as E,E-isomer though in solution it exists in the major E,Z and the minor E,E forms [74, 75]. Analogous data were obtained for 72 (R = Br) in solution by NOE spectroscopy [76]. The energy difference between E,Z and E,E-isomers was estimated to be E,E0 and E,E1 and the isomerization activation energy barrier of E,E1 and E,E2 and E,E3.

<sup>1</sup>H-NMR study of the protonated dye **73** showed the presence of the *E*,*Z*-isomer only [77], while the *E*,*E* structure was found by X-ray diffraction

$$E,Z$$
 $NO_2$ 
 $NO_2$ 
 $NO_2$ 
 $NO_2$ 
 $NO_2$ 
 $NO_2$ 
 $NO_2$ 
 $NO_2$ 
 $NO_2$ 
 $NO_2$ 

analysis for the protonated form of another photomerocyanine 74 [78]. These data may be only of limited interest because it was revealed that the relative stabilities of isomers for protonated and non-protonated forms of merocyanines are different [78].

Other isomers (Z,Z) and Z,E) are much less stable, though they can be formed by irradiation in the visible absorption band of stable E,Z- or E,E- isomers as a result of *cis-trans* isomerization reaction [71]. The relative stability of the isomers could be changed by the alteration of the structure. Thus, the quantum mechanics calculations suggested that the replacement of the hydrogen atom in position 3 of benzothiazole derivative 75 (R = H) with methyl group (R = Me) results in the strengthening of sterical interactions between substituents leading to stabilization of E,E form [70].

# 4 Properties and Applications

## 4.1 Solvatochromism

Solvatochromic merocyanines exhibit bathochromic or hypsochromic shifts in solvents of various polarities. Other characteristics such as dipole moments [73], fluorescence [79] and Raman [80] spectra, and NLO properties [81] change as well. The solvent effect can be used as a tool to make a dye solution that absorbs at a predetermined wavelength and intensity. Solvatochromic properties of merocyanines have been extensively studied over

the last decade. Among them, Brooker's merocyanine and its analogs (76) are of particular interest [82–85].

It has been postulated that the origin of the large hypsochromic shift in the spectrum of Brooker's merocyanine 76 (R = H) is due to a distinct change in structure from a covalent quinone (A) in pyridine or chloroform to a zwitterion (B) in water or methanol. The extent of this shift is critically dependent on the solvent used for measurement in each case with the highest energy absorption found in water and the lowest one in chloroform with an observed change in color from yellow to blue. Recently the spectroscopic properties of derivatives of Brooker's merocyanine 76 with increased solubility have been studied both experimentally and theoretically using molecular orbital methods [86]. Analysis of <sup>1</sup>H- and <sup>13</sup>C-NMR spectra taken in a range of solvents suggests that merocyanines exist as resonance hybrids that are weighted toward the zwitterion form even in solvents of low dielectric constants. In protic solvents, the large hypsochromic shift observed for merocyanine in the visible region arises from both a dielectric effect and a hydrogen bonding effect. Theoretically, the PM3/COSMO method gives a reasonable account of the structure and spectroscopic shifts of merocyanines in aprotic solvents. The significant shifts observed arise because solvents with large dielectric constants have a much greater stabilizing effect on the more polar ground state of merocyanines than they do on the first excited state. While the same method predicts stable hydrogen-bonded structures for a dihydrate and hexahydrate, it is unable to reproduce the known hypsochromic shift for these solvated species. In contrast, a version of the CNDO/S method does predict the correct trends on hydration though the magnitude of the effect is less than that found experimentally.

Katoh et al. prepared and studied the solvatochromism of bismerocyanine 77 linked by a 1,8-naphthylene skeleton [42]. The absorption band of the bismerocyanine 77 compared to that of the corresponding monomerocyanine was bathochromically shifted in chloroform (568 vs. 551 nm) and hypsochromically in acetonitrile (516 vs. 550 nm). The absorption spectra of 77 in a mixture of dichloromethane and methanol showed both the hypsochromic and bathochromic bands, with the hypsochromic band becoming more intense with an increase in methanol concentration. These data could be interpreted by the existence of equilibrium between *syn* and *anti* conformers of the bismerocyanine 77.

## 4.2 Ion Sensors

Solvatochromic merocyanine dyes are promising candidates for solvent polarity and pH sensors [87, 88] as well as indicators for the presence of transition metal cations [38]. They also were proposed for personal opto-chemical ammonia sensor with sensitivity in the 5-100 ppm range [47]. The design of chemical sensors that are specific for the detection of biologically important cations, such as Na<sup>+</sup>, K<sup>+</sup>, Ca<sup>2+</sup>, and Mg<sup>2+</sup>, continues to be a field of active research. Suzuki and co-workers synthesized and characterized new calcium-sensitive chromogenic crown ethers 78, 79 based on Brooker's merocyanine [89]. The mechanism of calcium ion sensing includes size-selective binding with crown ether and strong electrostatic attraction between the positively charged calcium ion and two negatively charged parts of the dye moieties. The water-soluble dye 78 can be used for calcium ion sensing in solution while lipophilized derivative 79 has been successfully applied to ion-exchange type optode PVC membranes. By using these sensors, calcium ion can be detected in the range of concentration of  $10^{-5}$  –  $10^{-2}$  M without cross-sensitivity for other physiologically important cations (Mg<sup>2+</sup>, Li<sup>+</sup>, Na<sup>+</sup>, and K<sup>+</sup>).

 $R = CH_3 (78); C_{12}H_{25} (79)$ 

A series of novel NIR ketocyanines **80** was synthesized and studied as potential pH fluoroionophores to be used in the development of new integrated waveguide fluorescence optodes (IWFOs). Upon protonation, ketocyanines undergo transformation to *meso*-hydroxy-substituted carbocyanine dyes **81** (Eq. 23). The process is accompanied by a large bathochromic shift (up to 200 nm) of the absorption band as well as significant decrease in fluorescence intensity.

 $X, Y = CMe_2, S; R^1, R^2 = H, OH, COOEt, NH_2, NHAC$ 

#### **Equation 23**

Ketocyanine dyes have demonstrated their suitability for application as acidochromic fluoroionophores in bulk optodes for the development of IWFOs. They exhibit high fluorescence intensities in the far-visible region, an adequate photostability and an optimum pH response [49, 90]. Ketocyanines were also proposed as sensitizers for lithographic printing with image resolution reaching 7  $\mu$ m [51].

### 4.3 Molecular Aggregation

Molecular aggregates are self-assemblies of molecules by non-covalent interactions. They have significant technological applications such as molecular optoelectronic devices, fluorescence probes for mitochondrial membrane, and as models of antenna systems that function to transfer energy and electrons in biological systems [91–93]. Usually two types of aggregates can be formed, the spectra of which contain bathochromically (J-type) and hypsochromically (H-type) shifted bands compared to the spectrum of the nonaggregated monomer species. Generally J-bands are narrow, and H-bands much more broad [94, 95]. Both H- and J-aggregates are one-dimensional molecular arrangements in which the transition moments of individual monomers are aligned perpendicular (H) or parallel (J) to the line joining

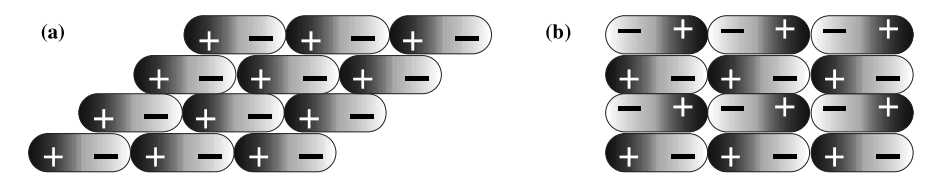


Fig. 1 Molecular arrangement in J- (a) and H-aggregates (b)

their centers (Fig. 1). The arrangement changes the energy difference between ground and excited states of the dye molecule. The H-aggregation increases the difference leading to a hypsochromic shift, and J-aggregation decreases the energy gap resulting in a bathochromic shift. The bands are anisotropic and can be easily distinguished from the band of free dye molecules.

The aggregation of merocyanine with the long alkyl chain McC18 (82) was studied and the formation of J-aggregates in the mixed monolayers and the Langmuir-Blodgett (LB) films with Cd<sup>2+</sup> salts of fatty acids was found [96, 97]. The aggregation number of 40 and the two-dimensional structure were estimated by using the extended dipole model for the spectral shifts [98]. It was also found that McC18 dye in the ternary mixed LB films with cadmium stearate (or arachidate) and octadecane forms the Haggregates, which have been found as the transient state in the compression process in the ternary mixed monolayer of McC18 with methyl arachidate and hexadecane [97–99].

Nakahara et al. have found that merocyanines 82 and 83 form J-aggregates in the presence of arachidic acid and cadmium ions [100, 101]. In LB films, merocyanine 84 is included in J-aggregates in mixture with dyes 82 and 85, although not mixed with other dyes it does not form aggregates. The band of J-aggregate was separated by a difference spectrum method [102]. The studying of the structure of merocyanine dyes 86 by IR spectroscopy shows that the compounds with n = 2, 3, 12-18 form intermolecular hy-

R = H, X = S (82); R = CI, X = S (83); R = H, X = O (84); R = Me, X = S (85)

drogen bonds, while the dyes with medium-length methyne bridge (n = 4–10) form cyclic dimers [103]. The treatment of cast films of merocyanine 86 (n = 18) with NaCl, CaCl<sub>2</sub> or BaCl<sub>2</sub> solution leads to the formation of J-aggregates [104].

A series of merocyanine dye dimers tethered at different sites with spacers ranging from 0 to 5 methylene groups 87, 88 have been synthesized [57]. The formation, structure, and excited state properties of the consequent merocyanine dye "aggregates" in solution and in rigid glass have been studied by UV/visible absorption spectra, steady-state fluorescence, and fluorescence lifetime measurements.

$$O = (CH_2)_n$$
 $O = (CH_2)_n$ 
 $O =$ 

The dimers 87 with 0 and 1 methylene spacers show a very weak and distance-dependent "J"-type exciton coupling, evident in both absorption and fluorescence spectra. For the dimers with 2, 3, and 5 methylene spacers in polar solvents a blue-shifted absorption spectra were observed, suggesting a folded configuration resulting in "H" dimers. Remarkably, both the "J" coupled dimer (n=0) and the dimers having 2–5 methylene groups show a much stronger solvatochromic behavior than the corresponding monomer, which could be attributed to interchromophoric charge-transfer interactions in both ground and excited states.

Aggregation processes of merocyanine dyes on lyposomes (artificial cell membranes) were also studied [105]. Codispersing lipids and J-aggregate forming water-insoluble amphiphilic dye molecules, which do not form liposomes by themselves, are the main features of the method. It is noteworthy that two types of aggregate dispersions were obtained, one that exhibits an absorption band at 635 nm and the other at 600 nm. Upon addition of magnesium or cadmium ions to the dispersions, the long-wavelength absorbing aggregates irreversibly undergo transformation to short-wavelength aggregates, which is accompanied by significant changes in fluorescence and absorption spectra.

### 4.4 Non-Linear Optics

In the search for optically nonlinear organic chromophores and photore-fractive materials [106, 107], a great deal of research has focused upon the molecular engineering requirements to optimize optical nonlinearities in push-pull compounds [41, 108–110]. Merocyanines show NLO properties both in polymer matrix and crystals, though most NLO chromophores normally are difficult to crystallize [111]. Co-crystallization of Brooker's merocyanine with 2,4-dihydroxybenzaldehyde readily provided crystals with the ideal packing for an electro-optic application. Nonlinear optical responses of a self-assembled monolayer (SAM) containing merocyanine chromophore 89 on gold in water and in ethanol were studied by second-harmonic generation (SHG) [112].

The pH dependence of the SHG response clearly showed a solvatochromic change of the merocyanine from a protonated form to a zwitterionic form. A large second-order susceptibility  $\chi_{zzz} = 5.0 \times 10^{-7}$  esu  $(2.1 \times 10^2 \text{ pm/V})$  was found in a basic solution of ethanol where the merocyanine is in the zwitterionic form.

Boxer et al. have reported the results of Stark and electric-field-induced-second-harmonic (EFISH) measurements for a series of merocyanine dyes **90** which demonstrate the correlation between optical nonlinearities and  $|\Delta \gamma|$  along with a large solvent dependence of their electronic structure [113].

A novel supramolecular architecture in which two merocyanine dyes are assembled in a head-to-tail fashion by multiple hydrogen bonds was recently

proposed [114]. The strong geometry of the complex 91 leads to diminishing of the propensity towards antiparallel aggregation. The authors intend to apply this concept to optimized NLO and PR chromophores and to design self-complementary merocyanine dyes.

# 4.5 Solar Cells and Hydrogen Energy

Construction of an efficient system for light energy conversion into chemical energy is one of the most important subjects from the viewpoint of solar light energy utilization. Photocatalytic water splitting into  $H_2$  and  $O_2$  is a promising process for solar energy conversion and storage [115–117], but a satisfactory system workable under visible light irradiation has not yet been established. As a strategy for effective visible light harvesting, spectral sensitization of wide bandgap semiconductors by dye molecules has been studied for photocatalytic  $H_2$  production from water [118–120]. Abe et al. [121, 122] reported the dye-sensitized photocatalysts for efficient hydrogen production from aqueous  $I^-$  solutions under visible light irradiation. It was found that hydrogen production with quantum efficiency of  $\sim$ 2.5% took place using merocyanine or coumarine dye-sensitized Pt/TiO<sub>2</sub> photocatalysts in wateracetonitrile mixed solutions containing iodide electron donor [123, 124].

Dye-sensitized solar cells based on nano-crystalline  $TiO_2$  electrodes have been investigated since the report by Gratzel and co-workers on attaining reasonable conversion efficiencies of high intensity solar light into electric power [125]. Tremendous efforts have been made to improve the conversion efficiency [126–128], the optimization of cell structures and the reliability of the cells, though practical uses seem still quite vague. Takahashi et al. reported that when the photosensitizing merocyanine dye NK2097 (92) was blended into regioregular poly(3-hexylthiophene-2,5-diyl) (P3HT), the performance of the  $TiO_2/P3HT$  solar cell was remarkably improved, resulting in

0.85% of energy conversion yield under the illumination of simulated sunlight with 100 mW/cm<sup>2</sup> intensity [129].

Recently Matsui and co-workers reported the design of multi-colored solar cells sensitized with organic dyes using optimized electrolytes and electrodes with enhanced transparence [130]. The solar cells were assembled using nano-crystalline  ${\rm TiO_2}$  electrodes adsorbing sensitizing dyes, an electrolyte consisting of a mixture of iodine and 1-butyl-3-methylimidazolium iodide in a 0.2:10 molar ratio and the counter platinum electrode to give cells bearing red, purple, blue, green and black colors. The multi-colored solar cells were connected in series, and the assembly exhibited a 2.1% conversion efficiency under  $100~{\rm mW\cdot cm^{-2}}$  irradiation with a total semiconductor area of  $25~{\rm cm^2}$ .

# 4.6 Medicine

The development of new synthetic dye agents and advances in dye chemistry have greatly increased the potential for synthesis of novel drugs based on dyes and dye-containing compounds with applications in medicine. A series of voltage-sensitive cyanine dyes including merocyanines have been studied for the development of methodology for monitoring of multineuronal activity in the intact central nervous system [131]. The simple in vitro method for screening of photoelectric dyes towards their use for retinal prostheses has been proposed [132]. Merocyanine dyes are promising sensitizers in photodynamic therapy (PDT) of cancer [22, 133–135]. They can selectively inactivate neoplastic cells (leukemia, lymphoma, neuroblastoma cells) in autologous bone marrow grafts and also pathogenic viruses in bone marrow and blood fractions [133, 136–138]. Merocyanines localize mainly in the plasma membrane of tumor cells and most of their phototoxicity is attributed to damage occurring in this compartment [136].

Actually, the major part of the work has been carried out on one structure, merocyanine 540 (93, X = O, Y = S). Compound MC540 has been used in the purging of leukemic cells from autologous bone marrow grafts, but its use in the photoinactivation of blood-borne enveloped viruses has also been studied [139]. The chemical structure of MC540 is appealing to the medicinal chemist as it offers much scope for functionalization. Thus, replacing a ring heteroatom with one of higher atomic number (e.g., oxygen for sulfur, 93, X = Y = S) normally leads to increased singlet oxygen yields [140]—

the heavy atom effect—though for cyanine dyes these values are usually low in comparison with, for example, methylene blue. The use of heavy atoms also stabilizes the polymethine chain to photoisomerization (a major deactivation pathway) [6]. As expected, varying the *N*-alkyl side-chains in MC540 causes changes in the lipophilicity of the system [139]. Perhaps the main drawback to the use of merocyanines in PACT (photodynamic antimicrobial chemotherapy) is the inactivation of such compounds by plasma and serum components, although recent work has shown that this effect may be inhibited by the replacement of the ring oxygen with sulfur or selenium [141].

Various derivatives of MC540 of general structure 93 were prepared and studied as intracellular dyes for PDT. They act as phototoxins to destroy the host cells under illumination due to the long-lived triplet excited state of the dye. They display a selective recognition for leukemia cells and have been proposed as reagents for both diagnosis and treatment of early stage leukemia by PDT [141, 142]. The dominant photoprocess involves isomerization from the first excited singlet state possessing an all-*trans* configuration to a long-lived *cis* isomer [143].

A large series of various rhodacyanine dyes 94 was synthesized and evaluated for their properties such as solubility, stability, and antitumor activity [29, 30, 144–146]. The main efforts in these works have been focused on

$$A = \begin{pmatrix} S \\ N \\ R \end{pmatrix}$$
 $A = \begin{pmatrix} S \\ N \\ R \end{pmatrix}$ 
 $A = \begin{pmatrix} S \\ N \\ R \end{pmatrix}$ 
 $A = \begin{pmatrix} S \\ N \\ R \end{pmatrix}$ 
 $A = \begin{pmatrix} S \\ N \\ R \end{pmatrix}$ 
 $A = \begin{pmatrix} S \\ N \\ R \end{pmatrix}$ 
 $A = \begin{pmatrix} S \\ N \\ R \end{pmatrix}$ 
 $A = \begin{pmatrix} S \\ N \\ R \end{pmatrix}$ 
 $A = \begin{pmatrix} S \\ N \\ R \end{pmatrix}$ 
 $A = \begin{pmatrix} S \\ N \\ R \end{pmatrix}$ 
 $A = \begin{pmatrix} S \\ N \\ R \end{pmatrix}$ 
 $A = \begin{pmatrix} S \\ N \\ R \end{pmatrix}$ 
 $A = \begin{pmatrix} S \\ N \\ R \end{pmatrix}$ 
 $A = \begin{pmatrix} S \\ N \\ R \end{pmatrix}$ 
 $A = \begin{pmatrix} S \\ N \\ R \end{pmatrix}$ 
 $A = \begin{pmatrix} S \\ N \\ R \end{pmatrix}$ 
 $A = \begin{pmatrix} S \\ N \\ R \end{pmatrix}$ 
 $A = \begin{pmatrix} S \\ N \\ R \end{pmatrix}$ 
 $A = \begin{pmatrix} S \\ N \\ R \end{pmatrix}$ 
 $A = \begin{pmatrix} S \\ N \\ R \end{pmatrix}$ 
 $A = \begin{pmatrix} S \\ N \\ R \end{pmatrix}$ 
 $A = \begin{pmatrix} S \\ N \\ R \end{pmatrix}$ 
 $A = \begin{pmatrix} S \\ N \\ R \end{pmatrix}$ 
 $A = \begin{pmatrix} S \\ N \\ R \end{pmatrix}$ 
 $A = \begin{pmatrix} S \\ N \\ R \end{pmatrix}$ 
 $A = \begin{pmatrix} S \\ N \\ R \end{pmatrix}$ 
 $A = \begin{pmatrix} S \\ N \\ R \end{pmatrix}$ 
 $A = \begin{pmatrix} S \\ N \\ R \end{pmatrix}$ 
 $A = \begin{pmatrix} S \\ N \\ R \end{pmatrix}$ 
 $A = \begin{pmatrix} S \\ N \\ R \end{pmatrix}$ 
 $A = \begin{pmatrix} S \\ N \\ R \end{pmatrix}$ 
 $A = \begin{pmatrix} S \\ N \\ R \end{pmatrix}$ 
 $A = \begin{pmatrix} S \\ N \\ R \end{pmatrix}$ 
 $A = \begin{pmatrix} S \\ N \\ R \end{pmatrix}$ 
 $A = \begin{pmatrix} S \\ N \\ R \end{pmatrix}$ 
 $A = \begin{pmatrix} S \\ N \\ R \end{pmatrix}$ 
 $A = \begin{pmatrix} S \\ N \\ R \end{pmatrix}$ 
 $A = \begin{pmatrix} S \\ N \\ R \end{pmatrix}$ 
 $A = \begin{pmatrix} S \\ N \\ R \end{pmatrix}$ 
 $A = \begin{pmatrix} S \\ N \\ R \end{pmatrix}$ 
 $A = \begin{pmatrix} S \\ N \\ R \end{pmatrix}$ 
 $A = \begin{pmatrix} S \\ N \\ R \end{pmatrix}$ 
 $A = \begin{pmatrix} S \\ N \\ R \end{pmatrix}$ 
 $A = \begin{pmatrix} S \\ N \\ R \end{pmatrix}$ 
 $A = \begin{pmatrix} S \\ N \\ R \end{pmatrix}$ 
 $A = \begin{pmatrix} S \\ N \\ R \end{pmatrix}$ 
 $A = \begin{pmatrix} S \\ N \\ R \end{pmatrix}$ 
 $A = \begin{pmatrix} S \\ N \\ R \end{pmatrix}$ 
 $A = \begin{pmatrix} S \\ N \\ N \end{pmatrix}$ 
 $A = \begin{pmatrix} S \\ N \\ N \end{pmatrix}$ 
 $A = \begin{pmatrix} S \\ N \\ N \end{pmatrix}$ 
 $A = \begin{pmatrix} S \\ N \\ N \end{pmatrix}$ 
 $A = \begin{pmatrix} S \\ N \\ N \end{pmatrix}$ 
 $A = \begin{pmatrix} S \\ N \\ N \end{pmatrix}$ 
 $A = \begin{pmatrix} S \\ N \\ N \end{pmatrix}$ 
 $A = \begin{pmatrix} S \\ N \\ N \end{pmatrix}$ 
 $A = \begin{pmatrix} S \\ N \\ N \end{pmatrix}$ 
 $A = \begin{pmatrix} S \\ N \\ N \end{pmatrix}$ 
 $A = \begin{pmatrix} S \\ N \\ N \end{pmatrix}$ 
 $A = \begin{pmatrix} S \\ N \\ N \end{pmatrix}$ 
 $A = \begin{pmatrix} S \\ N \\ N \end{pmatrix}$ 
 $A = \begin{pmatrix} S \\ N \\ N \end{pmatrix}$ 
 $A = \begin{pmatrix} S \\ N \\ N \end{pmatrix}$ 
 $A = \begin{pmatrix} S \\ N \\ N \end{pmatrix}$ 
 $A = \begin{pmatrix} S \\ N \\ N \end{pmatrix}$ 
 $A = \begin{pmatrix} S \\ N \\ N \end{pmatrix}$ 
 $A = \begin{pmatrix} S \\ N \\ N \end{pmatrix}$ 
 $A = \begin{pmatrix} S \\ N \\ N \end{pmatrix}$ 
 $A = \begin{pmatrix} S \\ N \\ N \end{pmatrix}$ 
 $A = \begin{pmatrix} S \\ N \\ N \end{pmatrix}$ 
 $A = \begin{pmatrix} S \\ N \\ N \end{pmatrix}$ 
 $A = \begin{pmatrix} S \\ N \\ N \end{pmatrix}$ 
 $A = \begin{pmatrix} S \\ N \\ N \end{pmatrix}$ 
 $A = \begin{pmatrix} S \\ N \\ N \end{pmatrix}$ 
 $A = \begin{pmatrix} S \\ N \\ N \end{pmatrix}$ 
 $A = \begin{pmatrix} S \\ N \\ N \end{pmatrix}$ 
 $A = \begin{pmatrix} S \\ N \\ N \end{pmatrix}$ 
 $A = \begin{pmatrix} S \\ N \\ N \end{pmatrix}$ 
 $A = \begin{pmatrix} S \\ N \\ N \end{pmatrix}$ 
 $A = \begin{pmatrix} S \\ N \\ N \end{pmatrix}$ 
 $A = \begin{pmatrix} S \\ N \\ N \end{pmatrix}$ 
 $A = \begin{pmatrix} S \\ N \\ N \end{pmatrix}$ 
 $A = \begin{pmatrix} S \\ N \\ N \end{pmatrix}$ 
 $A = \begin{pmatrix} S \\ N \\ N \end{pmatrix}$ 
 $A = \begin{pmatrix} S \\ N \\ N \end{pmatrix}$ 
 $A = \begin{pmatrix} S \\ N \\ N \end{pmatrix}$ 
 $A = \begin{pmatrix} S \\ N \\ N \end{pmatrix}$ 
 $A = \begin{pmatrix} S \\ N \\ N \end{pmatrix}$ 
 $A = \begin{pmatrix} S \\ N \\ N \end{pmatrix}$ 
 $A = \begin{pmatrix} S \\ N \\ N \end{pmatrix}$ 
 $A = \begin{pmatrix} S \\ N \\ N \end{pmatrix}$ 
 $A = \begin{pmatrix} S \\ N \\ N \end{pmatrix}$ 
 $A = \begin{pmatrix} S \\ N \\ N \end{pmatrix}$ 
 $A = \begin{pmatrix} S \\ N \\ N \end{pmatrix}$ 
 $A = \begin{pmatrix} S \\ N \\ N \end{pmatrix}$ 
 $A = \begin{pmatrix} S \\ N \\ N \end{pmatrix}$ 
 $A = \begin{pmatrix} S \\ N \\ N \end{pmatrix}$ 
 $A = \begin{pmatrix} S$ 

the structure-activity study of compounds with heteroaromatic substituents that are conjugated to rhodanine moiety. Rhodacyanine dyes **94** composed of benzothiazole (A ring) and pyridinium (B ring) with n = 0 have showed the best activity. The counter-anion had a marked effect on solubility in water, while it had virtually no effect on the biological properties.

Several new rhodacyanine derivatives were found to possess strong in vitro activity against *Plasmodium falciparum* combined with low cytotoxicity [28]. Rhodacyanines were also used in therapy of cancer [147]. In cancer cells, but not in normal cells, they induce release of wild-type p53 from cytoplasmically sequestered p53-mot-2 complexes and rescue its transcriptional activation function.

Würthner and Yao have synthesized and studied various merocyanine dyes containing imide functional groups on hydrogen bonding to melamine receptors [43]. They have demonstrated that the triple hydrogen-bonding coordination to ditopic melamine helps dissolve the highly dipolar dye even in relatively nonpolar solvents, such as methylcyclohexane. On the basis of the optical properties of the resulting solutions, it was concluded that colloidal assemblies are formed by supramolecular polymerization through hydrogen bonding to melamines and dipolar aggregation between the dyes.

# 5 Conclusions

Merocyanine dyes with nitrogen donor and carbonyl acceptor fragments have found a wide application in various areas of science and technology, including optical and fluorescent sensors, silver halide photography, optical data storage, and photodynamic therapy. Over the last decade, both the synthetic potential and application studies have grown significantly.

The synthesis of merocyanines has been reviewed. The combination of the electron donor and acceptor parts allows the preparation of many merocyanines with various properties. Recent progress in computer science and nanotechnology have stimulated new investigations, including the studies of solar and hydrogen energy storage, lasers and biotechnology, non-linear optics, and new areas of medicine.

### References

- 1. Peng Z, Zhou X, Carroll S, Geise HJ, Peng B, Dommisse R, Esmansc E, Carleer R (1996) J Mater Chem 6:1325
- 2. Chen C, Zhou B, Lu D, Xu G (1995) J Photogr Sci 43:134
- 3. Araki T, Ito E, Oichi K, Mitsumoto R, Sei M, Oji H, Yamamoto Y, Ouchi Y, Seki K, Takata Y, Edamatsu K, Yokoyama T, Ohta T, Kitajima Y, Watanabe S, Yamashita K, Tani T (1997) J Phys Chem B 101:10378

- 4. Gomer C (1991) Photochem Photobiol 54:1093
- 5. Krieg M, Redmond RW (1993) Photochem Photobiol 57:472
- Redmond RW, Srichai MB, Bilitz JM, Schlomer DD, Krieg M (1994) Photochem Photobiol 60:348
- 7. Harriman A, Shoute LCT, Neta P (1991) J Phys Chem 95:2415
- 8. Bertelson RC (1999) Spiropyrans. In: Crano JS, Guglielmetti R (eds) Organic Photochromic and Thermochromic Compounds. Plenum Press, New York, p 11
- 9. Minkin VI (2004) Chem Rev 104:2751
- 10. Lukyanov BS, Lukyanova MB (2005) Chem Heterocycl Comp 41:281
- 11. Berkovic G, Krongauz V, Weiss V (2000) Chem Rev 100:1741
- 12. Alfimov MV, Fedorova OA, Gromov SP (2003) J Photochem Photobiol A 158:183
- 13. Kimura K, Sakamoto H, Uda RM (2004) Macromolecules 37:1871
- 14. Taguchi M, Li G, Gu Zh, Sato O, Einada Y (2003) Chem Mater 15:4756
- 15. Kashima I, Okubo M, Qno Y, Itoi M, Kida N, Hikita M, Enomoto M, Kojima N (2005) Synth Metals 155:703
- 16. Evans L III, Collins GE, Shaffer RE, Michelet V, Winkler JD (1999) Anal Chem 71:5322
- Voloshin NA, Chernyshev AV, Metelitsa AV, Besugliy SO, Voloshina EN, Sadimenko LP, Minkin VI (2004) Arkivoc 11:16
- 18. Tomizaki K, Jieb X, Mihara H (2005) Bioorg Med Chem Lett 15:1731
- 19. Zollinger H (2003) Color Chemistry: synthesis, properties and application of organic dyes and pigments, 3rd edn. Wiley, Weinheim
- 20. Christie RM (2001) Colour chemistry. The Royal Society of Chemistry, Cambridge
- 21. Bamfield P (2001) Chromic phenomena. The Royal Society of Chemistry, Cambridge
- 22. Mishra A, Behera RK, Behera PK, Mishra BK, Behera GB (2000) Chem Rev 100:1973
- 23. Sliwa W (1995) Chem Heterocyclic Compounds 31:766
- 24. Rezende MC, Campodonico P, Abuin E, Kossanyi J (2001) Spectrochimica Acta Part A 57:1183
- 25. Kay AJ, Woolhouse AD, Zhao Y, Clays K (2004) J Mater Chem 14:1321
- Shigemitsu Y, Sugimoto M, Itonaga S, Komiya K, Tominaga Y (2003) Dyes Pigm 56:167
- 27. Brooker LGS, Keyes GH, Sprague RH, Van Dyke RH, Van Lare E, Van Zandt G, White FL (1951) J Am Chem Soc 73:5326
- 28. Pudhom K, Kasai K, Terauchi H, Inoue H, Kaiser M, Brun R, Ihara M, Takasu K (2006) Bioorg Med Chem 14:8550
- 29. Kawakami M, Koya K, Ukai T, Tatsuta N, Ikegawa A, Ogawa K, Shishido T, Chen LB (1998) J Med Chem 41:130
- 30. Kawakami M, Koya K, Ukai T, Tatsuta N, Ikegawa A, Ogawa K, Shishido T, Chen LB (1997) J Med Chem 40:3151
- 31. Park S-Y, Oh S-W (2003) Bull Korean Chem Soc 24:569
- 32. Aliaga C, Galdames JS, Rezende MC (1997) J Chem Soc, Perkin Trans 2, p 1055
- 33. Kawakami M, Suzuki M, Kawai H, Ogawa K, Shishido T (1998) Tetrahedron Lett 39:1763
- 34. Clark RJH, Cooksey CJ, Daniels MAM, Withnall R (1993) Endeavour 17:191
- 35. Cooksey CJ (2001) Molecules 6:736
- 36. Traven VF, Miroshnikov VS, Chibisova TA, Barachevsky VA, Venidiktova OV, Strokach YUP (2005) Russ Chem Bull, Int Ed 54:2417
- 37. Kovtun YUP, Prostota YAO, Shandura MP, Poronik YEM, Tolmachev AI (2004) Dyes Pigm 60:215
- 38. Kovtun YUP, Prostota YAO, Tolmachev AI (2003) Dyes Pigm 58:83

- 39. Yagi S, Maeda K, Nakazumi H (1999) J Mater Chem 9:2991
- 40. Khokhlova LV, Lebedeva GK, Lukoshkin VA, Bykova LM (2004) Russ J Gen Chem 74:271
- 41. Kay AJ, Woolhouse AD, Gainsford GJ, Haskell TG, Barnes TH, McKinnie IT, Wyss CP (2001) J Mater Chem 11:996
- 42. Katoh T, Inagaki Y, Okazaki R (1998) J Am Chem Soc 120:3623
- 43. Würthner F, Yao S (2003) J Org Chem 68:8943
- 44. Yao S, Beginn U, Gress T, Lysetska M, Würthner F (2004) J Am Chem Soc 126:8336
- 45. Würthner F (1999) Synthesis, p 2103
- 46. Šimon P, Landl M, Breza M, Kvasnik F (2003) Sens Actuators B 90:9
- 47. Malins C, Doyle A, MacCraith BD, Kvasnik F, Landl M, Šimon P, Kalvoda L, Lukaš R, Puflere K, Babusík I (1999) J Environ Monit 1:417
- 48. Shimkin AA, Shirinian VZ, Nikalin DM, Krayushkin MM, Pivina TS, Troitsky NA, Vorontsova LG, Starikova ZA (2006) Eur J Org Chem 2087
- 49. Miltsov S, Encinas C, Alonso J (2001) Tetrahedron Lett 42:6129
- 50. Puyol M, Encinas C, Rivera L, Miltsov S, Alonso J (2006) Sens Actuators B 115:287
- 51. Gao F, Yang Y (2000) J Photopolym Sci Technol 13:265
- 52. Nesterov VN, Aitov IA, Sharanin YUA, Struchkov YUT (1996) Russ Chem Bull 45:164
- 53. Andreu R, Garín J, Orduna J, Alcalá R, Villacampa B (2003) Org Lett 5:3143
- 54. Park S, Jun K (2005) J Ind Eng Chem 11:688
- 55. Würthner F, Wortmann R, Matschiner R, Lukaszuk K, Meerholz K, DeNardin Y, Bittner R, Bräuchle C, Sens R (1997) Angew Chem Int Ed 36:2765
- 56. Krotko DG, Fedotov KV, Tolmachev AI (2005) Dyes Pigm 65:183
- 57. Lu L, Lachicotte RJ, Penner TL, Perlstein J, Whitten DG (1999) J Am Chem Soc 121:8146
- 58. Ke W, Luo X, Liu X, Xu H (2000) J Heterocycl Chem 37:1321
- 59. Würthner F, Sens R, Etzbach K-H, Seybold G (1999) Angew Chem Int Ed 38:1649
- 60. Fitjer L, Gerke R, Luettke W, Mueller P, Uson I (1999) Tetrahedron 55:14421
- 61. Strekowski L, Mason JC, Lee H, Say M, Patonay G (2004) J Heterocycl Chem 41:227
- 62. Strekowski L, Mason JC, Say M, Lee H, Gupta R, Hojjat M (2005) Heterocycl Commun 11:129
- 63. Benniston AC, Harriman A, McAvoya C (1997) J Chem Soc, Faraday Trans 93:3653
- 64. Benniston AC, Harriman A (1998) J Chem Soc, Faraday Trans 94:1841
- 65. Benniston AC, Harriman A, McAvoya C (1998) J Chem Soc, Faraday Trans 94:519
- 66. Toutchkine A, Kraynov V, Hahn K (2003) J Am Chem Soc 125:4132
- 67. Davidenko NA, Derevyanko NA, Ishchenko AA, Kulinich AV, Melenevskii DA (2004) J Appl Spectroscopy 71:641
- 68. Davidenko NA, Derevyanko NA, Ishchenko AA, Kuvshinsky NG, Kulinich AV, Neiland OYA, Plotniece MV (2004) Russ Chem Bull 53:1674
- 69. Benniston AC, Harriman A, McCulloch IE, Mehrabi M, Rostron SA, Sams CA (2004) J Photochem Photobiol A 163:61
- 70. Toman P, Bartkowiak W, Nešpùrek S, Sworakowski J, Zaleśny R (2005) Chem Phys 316:267
- 71. Wohl CJ, Kuciauskas D (2005) J Phys Chem B 109:22186
- Sheng Y, Leszczynski J, Garcia AA, Rosario R, Gust D, Springer J (2004) J Phys Chem B 108:16243
- 73. Wojtyk JTC, Wasey A, Kazmaier PM, Hoz S, Buncel E (2000) J Phys Chem A 104:9046
- 74. Hobley J, Malatesta V, Millini R, Parker WO Jr (2000) Mol Cryst Liq Cryst 345:329
- 75. Hobley J, Malatesta V, Millini R, Montanan L, Parker WO Jr (1999) Phys Chem Chem Phys 1:3259

- 76. Hobley J, Malatesta V (2000) Phys Chem Chem Phys 2:57
- 77. Gabbutt CD, Hepworth JD, Heron BM (1999) Dyes Pigm 42:35
- 78. Raymo FM, Giordani S, White AJP, Williams DJ (2003) J Org Chem 68:4158
- 79. Abdel-Halim ST, Awad MK (2005) J Mol Struct 754:16
- 80. Leng W, Würthner F, Kelley AM (2005) J Phys Chem A 109:1570
- 81. Albert IDL, Marks TJ, Ratner MA (1996) J Phys Chem 100:9714
- 82. Brooker LGS, Keys CH, Sprague RH, Van Dyke RH, Van Zandt E, White FL, Cressman HWJ, Dent SG (1951) J Am Chem Soc 73:5332
- 83. Brooker LGS, Keys CH, Heseltine DW (1951) J Am Chem Soc 73:5350
- 84. Reichardt C (2003) Solvents and solvent effects in organic chemistry, 3rd edn. Wiley, Weinheim
- 85. Reichardt C (1994) Chem Rev 94:2319
- 86. Morley JO, Morley RM, Docherty R, Charlton MH (1997) J Am Chem Soc 119:10192
- 87. Citterio D, Kawada T, Yagi J, Ishigaki T, Hisamoto H, Sasaki S, Suzuki K (2003) Anal Chim Acta 482:19
- 88. Strömberg N, Hulth S (2003) Sens Actuators B 90:308
- 89. Citterio D, Omagari M, Kawada T, Sasaki S, Suzuki Y, Suzuki K (2004) Anal Chim Acta 504:227
- 90. Rivera L, Puyol M, Miltsov S, Villuendas F, Alonso J (2006) Sens Actuators B 114:705
- 91. Furuki M, Tian M, Sato Y, Pu LS (2000) Appl Phys Lett 77:472
- 92. Bernas T, Dobrucki J (2002) Cytometry 47:236
- 93. Dai Z, Dähne L, Donath E, Möhwald H (2002) Langmuir 18:4553
- 94. Kobayashi T (ed) (1996) J-aggregates. World Scientific, Singapore
- 95. Harrison WJ, Mateer DL, Tiddy GJT (1996) J Phys Chem 100:2310
- 96. Hirano Y, Kawata J, Miura YF, Sugi M, Ishii T (1998) Thin Solid Films 345:327
- 97. Ray K, Nakahara H (2001) Jpn J Appl Phys 40:5095
- 98. Hirano Y, Okada TM, Miura YF, Sugi M, Ishii T (2000) J Appl Phys 88:5194
- 99. Hirano Y, Kamata KN, Inadzuki YS, Kawata J, Miura YF, Sugi M, Ishii T (1999) Jpn J Appl Phys 38:6024
- 100. Murata M, Villeneuve M, Nakahara H (2005) Chem Phys Lett 405:416
- 101. Murata M, Mori K, Sakamoto A, Villeneuve M, Nakahara H (2005) Chem Phys Lett 405:32
- 102. Ikegamia K, Mingotaud C, Lan M (2001) Thin Solid Films 393:193
- Fujimoto Y, Ozaki Y, Takayanagi M, Nakata M, Iriyama K (1996) J Chem Soc, Faraday Trans 92:413
- 104. Fujimoto Y, Ozaki Y, Iriyama K (1996) J Chem Soc, Faraday Trans 92:419
- 105. Kato N, Prime J, Katagiri K, Caruso F (2004) Langmuir 20:5718
- 106. Ostroverkhova O, Moerner WE (2004) Chem Rev 104:3267
- 107. Würthner F, Wortmann R, Meerholz K (2002) Chem Phys Chem 3:17
- 108. Dalton LR, Harper AW, Ghosen R, Steier WH, Ziari M, Fetterman H, Shi Y, Mustacich RV, Jen AK-Y, Shea KJ (1995) Chem Mater 7:1060
- 109. Marder SR, Cheng L-T, Tieman BG, Friedli AC, Blanchard-Desce M, Perry JW, Skindhoj J (1994) Science 263:511
- 110. Kanis DR, Ratner MA, Marks TJ (1994) Chem Rev 94:195
- 111. Pan F, Wong MS, Gramlich V, Bosshard C, Gunther P (1996) J Am Chem Soc 118:6315
- 112. Tsuboi K, Seki K, Ouchi Y, Fujita K, Kajikawa K (2003) Jpn J Appl Phys 42:607
- 113. Bublitz GU, Ortiz R, Runser C, Fort A, Barzoukas M, Marder SR, Boxer SG (1997) J Am Chem Soc 119:2311
- 114. Würthner F, Schmidt J, Stolte M, Wortmann R (2006) Angew Chem Int Ed 45:3842
- 115. Fujishima A, Honda K (1972) Nature 37:238

- 116. Lehn J, Sauvage J, Ziessel R, Hilaire L (1982) Isr J Chem 22:168
- 117. Kudo A, Domen K, Maruya K, Aika K, Onishi T (1988) J Catal 111:67
- 118. Abe R, Hara K, Sayama K, Domen K, Arakawa H (2000) J Photochem Photobiol A 137:63
- 119. Hara M, Waraksa CC, Lean JT, Lewis BA, Mallouk TE (2000) J Phys Chem A 104: 5275
- 120. Abe R, Sayama K, Domen K, Arakawa H (2001) Chem Phys Lett 344:339
- 121. Abe R, Sayama K, Arakawa H (2004) J Photochem Photobiol A 166:115
- 122. Abe R, Sayama K, Arakawa H (2003) Chem Phys Lett 379:230
- 123. Abe R, Sayama K, Arakawa H (2002) Chem Phys Lett 362:441
- 124. Abe R, Sayama K, Sugihara H (2005) J Solar Energy Eng 127:413
- 125. O'Regan B, Gratzel M (1991) Nature 353:737
- 126. Nazeeruddin MK, Kay A, Rodicio I, Humphrybaker R, Muller E, Liska P, Vlachopoulos N, Gratzel M (1993) J Am Chem Soc 115:6382
- 127. Brabe CJ, Arendse F, Comte P, Jirousek M, Lenzmann F, Shklover V, Gratzel M (1997) J Am Ceram Soc 80:3157
- 128. Sayama K, Sugihara H, Arakawa H (1998) Chem Mater 10:3825
- 129. Takahashi K, Nakanishi T, Yamaguchi T, Nakamura J, Murata K (2005) Chem Lett 34:714
- 130. Otaka H, Kira M, Yano K, Ito S, Mitekura H, Kawata T, Matsui F (2004) J Photochem Photobiol A 164:67
- 131. Wu J-Y, Lam Y-W, Falk CX, Cohen LB, Fang J, Loew L, Prechtl JC, Kleinfeld D, Tsau Y (1998) Histochem J 30:169
- 132. Matsuo T (2003) Acta Med Okayama 57:257
- 133. Wainwrigh M (1998) J Antimicrob Chemother 42:13
- 134. Staśkowiak E, Dudkowiak A, Hanyż I, Wiktorowicz K, Frąckowiak D (2004) J Photochem Photobiol A 163:127
- 135. Staśkowiak E, Dudkowiak A, Wiktorowicz K, Cofta J, Frackowiak D (2005) J Photochem Photobiol A 169:159
- 136. Dougherty TJ, Gomer CJ, Henderson BW, Jori G, Kessel D, Korbelik M, Moan J, Peng Q (1998) J Natl Cancer Inst 90:889
- 137. Zareba M, Niziolek M, Korytowski W, Girotti AW (2005) Biochim Biophys Acta 1722:51
- 138. Peng Q, Berg K, Moan J, Kongshaug M, Nesland JM (1997) Photochem Photobiol 65:235
- 139. Günther WHH, Searle R, Sieber F (1992) Sem Hematol 29:88
- 140. Krieg M, Bilitz JM, Srichai MB, Redmond RW (1994) Biochim Biophys Acta 1199:149
- 141. Anderson GS, Gunther WHH, Searle R, Bilitz JM, Krieg M, Sieber F (1996) Photochem Photobiol 64:683
- 142. Waggoner AS, Grinvald A (1997) Ann NY Acad Sci 303:217
- 143. Benniston AC, Gulliya KS, Harriman A (1994) J Chem Soc, Faraday Trans 90:953
- 144. Koya K, Wang YLH, Ukai T, Tatsuta N, Kawakami M, Shishido T, Chen LB (1996) Cancer Res 56:538
- 145. Modica-Napolitano JS, Koya K, Weisberg E, Brunelli BT, Li Y, Chen LB (1996) Cancer Res 56:544
- 146. Weisberg E, Koya K, Modica-Napolitano J, Li Y, Chen LB (1996) Cancer Res 56:551
- 147. Wadhwa R, Sugihara T, Yoshida A, Nomura H, Reddel RR, Simpson R, Maruta H, Kaul SC (2000) Cancer Res 60:6818

# Coumarin Polymethines, Their Boron Complexes and Analogs

Valerii F. Traven

D. Mendeleev University of Chemical Technology of Russia, Miusskaya pl. 9, 125047 Moscow, Russia traven@muctr.edu.ru

1	Introduction	107
2	Boron Complexes of Coumarin Polymethines	108
3	2-Pyrone Analogs of Coumarin Polymethines	114
4	2-Quinolone Analogs of Coumarin Polymethines	116
5	Coumarin Merocyanines Derived from Spiropyranes	117
5.1	Synthesis and Structure	117
5.2	Photochromism	119
5.3	Coumarin Merocyanines in Polymeric Matrices	127
Dofo	rences	130

**Abstract** Boron complexes of acyl(hydroxy)coumarins, their acyl(hydroxy)-2-pyrone, and acyl(hydroxy)-2-quinolone analogs are useful intermediates in the polymethine dyes synthesis. Such polymethine dyes show strong light absorption and strong fluorescent emission. Structures and properties of merocyanine forms derived from spiropyrans (coumarin derivatives) are also discussed. The compounds formed by the condensation of the indoline derivatives with 3-formyl-4-hydroxycoumarin exist only in open merocyanine forms. The effects of solvent, polymer matrix, and other factors on stability and color properties of merocyanines (derivatives of coumarino(indoline)spiropyrans) are summarized.

**Keywords** Color · Coumarins · Merocyanines · Polymethine dyes · Spiropyranes

### 1 Introduction

Many coumarin derivatives exhibit strong fluorescence [1]. This feature makes potential polymethine dyes interesting subjects for many applications. Few coumarin polymethine dyes were known a decade ago, since the most important synthetic routes to this class of compounds have been developed only recently. Sensitivity of the lactone ring to the bases used in polymethine dyes synthesis strongly hampered the early synthetic efforts.

However, there are examples of polymethine synthesis under acid catalysis [2, 3]. The use of boron complexes of acyl(hydroxy)arenes provides another convenient way for conducting condensation reactions. These complexes are characterized by high reactivity. For example, the methyl group in boron complexes of substituted *o*-hydroxyacetophenones, benzoylacetone, and acetylnaphthols is readily involved in condensation with carbonyl compounds and their equivalents, and in particular, with aldehydes, formamides, acetals, orthoesters, and anils [4–7]. The boron complexes procedures of polymethines have been successfully elaborated for coumarin derivatives and their analogs. These reactions are reviewed in this survey. Another novel method for coumarin polymethines preparation is based on spiropyranes photochromism. Open (merocyanine) forms, which are available by this method, differ in their stability depending on their structures, solvent, and polymer matrixes.

# 2 Boron Complexes of Coumarin Polymethines

3-Acetyl-4-hydroxycoumarin (1), 8-acetyl-7-hydroxy-4-methylcoumarin (2), and 7-hydroxy-4-methyl-8-propionylcoumarin (3) react easily with boron trifluoride etherate and 1,2-phenylenedioxaboryl derivative (4) to form complexes (5a-d) (Scheme 1) [8, 9].

The structures of the boron complexes were established by <sup>1</sup>H and <sup>11</sup>B nuclear magnetic resonance (NMR) spectroscopy. In the <sup>1</sup>H NMR spectra of the chelates, the signals for the protons of the methyl group of the acetyl fragment are shifted downfield compared to the signals of the starting acetylhydroxy-coumarins, due to a lower electron density on the carbonyl oxygen atom.

The  $^{11}B$  NMR spectra of compounds 5a-d show signals for the four-coordinate boron atom. The mass spectra of all these complexes show molecular ion peaks as the base peaks (100%). The structure of complex 5a has been studied by X-ray diffraction method and compared to the data obtained earlier for 3-acetyl-4-hydroxycoumarin (1) [10–13]. It has been demonstrated that molecule 1 in the crystal is planar, and the acetyl group is rotated relative to the 4-hydroxycoumarin fragment by  $6.2^{\circ}$ . Complexation of compound 1 with BF<sub>3</sub> leads to a pronounced change in the molecular geometry and the bond lengths in the O–C=C–C(O)Me fragment.

In order to estimate whether a distortion of the boron-containing ring in complex 5a is a characteristic feature of this compound or is caused by the crystal packing effects, quantum chemical calculations (B3LYP/6-311G\*) with the use of the G98W program have been performed [9]. The observed differences in the geometry of isolated molecule 5a (calculated data) and the molecule in the crystal (experimental data) are apparently attributed to both the difference in the degree of distortion of the boron-containing ring

### Scheme 1

and an elongation of the B–O bonds (1.532 and 1.515 Å), which is a general characteristic of donor-acceptor bonds involving the boron atoms [14, 15]. Therefore, it can be concluded that complexation with the boron atom is accompanied by equalization of the C–C and C=O bonds due to delocalization of  $\pi$  bonds.

Boron complexes **5a,b** differ in their hydrolytic stability and reactivity. Complex **5a** is stable during prolonged storage and does not undergo hydro-

lysis even on refluxing in water in neutral and acidic media. Hydrolysis was successfully performed only in an aqueous alcoholic solution of sodium carbonate, which produced compound 1 in quantitative yield. On the other hand, the phenylenedioxaboryl derivative 5b is much less stable and is hydrolyzed in aqueous solution at pH 7. It has been suggested that the high stability of 5a is due to its quasi-aromatic structure, as shown in Scheme 2.

Scheme 2

Due to high stability of complex 5a to hydrolysis and high proton acidity of its methyl group, this compound can be used in condensation reactions with different carbonyl derivatives (Scheme 2) for the polymethine dyes synthesis [16–18].

All these reactions provide dyes in high yield. For example, condensation of 5a with triethyl orthoformate in acetic anhydride in the presence of triethylamine furnishes symmetric dye 6 of high purity by direct crystallization from the reaction mixture. In a similar way, the reaction of 5a with Fisher's aldehyde 7 in acetic anhydride gives a non-symmetric dye 8. Condensation of 5a with N,N-dimethylformamide in acetic anhydride provides highly reactive enamine 9, which undergoes reactions with CH-acids, such as 1,4-dimethylquinolinium iodide or 1,2-dimethylquinolinium iodide. Polymethine dyes 10 and 11 have been prepared in good yields using this approach.

Coumarin polymethine dyes show electronic absorption in the visible region  $500-650\,\mathrm{nm}$  with high extinction coefficient ranging from  $96\,000\,\mathrm{M}^{-1}\,\mathrm{cm}^{-1}$  to  $145\,000\,\mathrm{M}^{-1}\,\mathrm{cm}^{-1}$ . These features are comparable to the absorption characteristics of analogous cyanines and suggest similarity in the frontier orbitals of these classes of chromophores. The electronic spectrum of 6 is illustrated in Fig. 1.

As shown in Fig. 1, the absorption spectrum of 6 is characterized by a remarkably narrow band with high extinction coefficient and a vibrational structure, which are specific for polymethine dyes. Compound 6 and its analogs are also fluorescent.

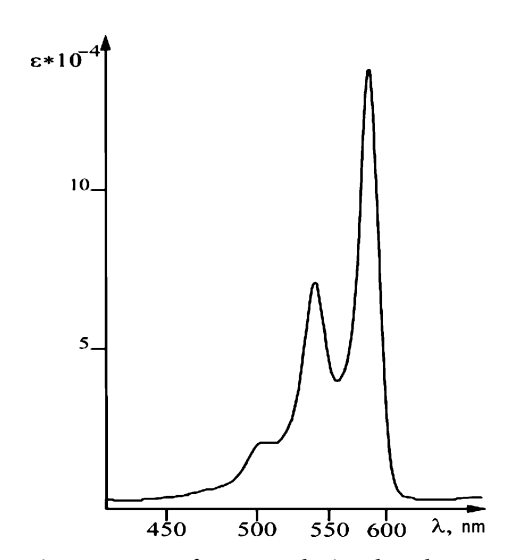


**Fig. 1** Electron absorption spectrum of compound **6** in ethanol:  $\lambda_{\text{max}} = 581$  nm,  $\varepsilon = 145000$  ( $c = 510 \times 10^{-5}$  M)

In spite of its hydrolytic instability, complex **5b** can also be reacted with triethyl orthoformate to give dye **12** (Eq. 1).

### **Equation 1**

The difluoroboron complexes of polymethine dyes are remarkably stable when stored in the solid state or in solution in the presence of air. For example, no changes were observed for solid samples of 6 and 10 stored under normal laboratory conditions for several months, and no changes were observed for their solutions in water or aqueous mineral acids heated under reflux for 1 h.

Scheme 3

Dyes 13–15 (Scheme 3), obtained by condensation of complex 5a with aldehydes possess narrow intensive bands in the region 430–600 nm of electron absorption spectra and are fluorescent [17, 18]. The condensations were carried out with benzaldehydes, cinnamic aldehydes, and heterocyclic aldehydes (Scheme 3).

Hydrolysis of boron complexes 13–15 produces the corresponding boron-free coumarin polymethines. Maxima in the visible absorption spectra (taken in ethanol) of the compounds 15a–c and the boron-free hydrolysis products of 15a,b (in parentheses) are as follows: 15a, 527 nm (475 nm); 15b, 500 nm (453 nm); 15c, 536 nm.

Unlike boron complexes of 3-acetyl-4-hydroxycoumarin 5a,b, complexes of 7-hydroxy-8-acylcoumarins 5c,d (Scheme 1) are colored and show fluorescence both in solution and in the solid state. In contrast to boron complexes 5a,b, complexes 5c,d are not stable during prolonged storage. Nevertheless, boron complexes 5c,d can be reacted with carbonyl compounds or their equivalents with the formation of polymethine dyes, such as 16 or 17 (Scheme 4) [16–18].

HC(OEt)<sub>3</sub>

$$Ac_2O$$
 $Et_3N$ 

Me

To Represent the second of the second o

### Scheme 4

The synthesis of a symmetric dye **16** involves condensation of **5c** with triethyl orthoformate. Complex **5d** undergoes a reaction with Fisher's aldehyde 7 to give a non-symmetric dye **17**. The hipsochromically shifted absorption of **17** ( $\lambda_{max} = 431$  nm,  $\varepsilon = 62\,000$  M<sup>-1</sup> cm<sup>-1</sup>), in comparison to that of its analog **8**, is due to the steric hindrance caused by the presence of the methyl group at the polymethine chain in **17**.

3

# 2-Pyrone Analogs of Coumarin Polymethines

Boron complexes of similarly substituted 2-pyrone derivatives possess similar reactivity [19]. The complex 19 has been synthesized from a pyrone 18 in the same manner as the coumarin analog 5a (Scheme 5).

#### Scheme 5

The structure of 19 has been studied by X-ray diffraction analysis. In contrast to complex 5a, the molecule 19 is planar. The lengths of the two B–O bonds are similar. In the <sup>1</sup>H NMR spectrum of the chelate 19, the signals for the protons of both methyl groups (acetyl fragment and 6-methyl) are shifted downfield, compared to the signals of the starting 3-acetyl-6-methyl-2-oxo-2*H*-pyran. The shifts (0.20 ppm and 0.14 ppm, respectively) show an increased CH-acidity of both methyl groups in the complex 19. As a result, the complex 19 easily undergoes condensations with aldehydes without base catalysis. These reactions are particularily facile with aromatic and heteroaromatic aldehydes containing electron-donating substituents. The synthesis of dye 20, by the reaction of 19 with aldehyde 21, is shown in Scheme 5 as an example.

Complex 19 can also be condensed with cinnamic aldehydes. For example, reaction with 4-dimethylaminocinnamic aldehyde provides dye 22, the subsequent hydrolysis of which gives a boron-free dye 23 (Scheme 6).

# Scheme 6

A facile condensation of complex 19 with heterocyclic aldehydes is illustrated in Scheme 7.

Scheme 7

Base-catalyzed condensation of 3-acetyl-6-methyl-2-oxo-2*H*-pyran with benzaldehyde has been shown to take place at the 6-methyl group of the pyran [20]. The more reactive complex **20** undergoes reaction with aldehydes at the 6-methyl group, even in the absence of a basic catalyst. The synthesis of a boron chelate **24** by the reaction of **20** with a benzaldehyde **21** is given in Scheme 8 for illustration.

#### Scheme 8

The boron chelate 24 has also been synthesized by one-pot condensation of the complex 19 with two equivalents of 21. A facile hydrolysis of 24 in diluted alcohol in the presence of sodium carbonate is also shown in Scheme 8.

# 4 2-Quinolone Analogs of Coumarin Polymethines

Very recently, we have shown that the boron complex 26 of 3-acetyl-4-hydroxy-1-methyl-2-quinolone (25) can also be utilized in the synthesis of polymethine dyes (Eq. 2) [21, 22].

The structure of **26** was solved by X-ray diffraction analysis. The introduction of a boron difluoride fragment into **25** leads to significant equalization of the lengths of the C–O bonds in the boron-containing ring in the complex **26**.

### **Equation 2**

As in the coumarin and 2-pyrone derivatives, this equalization is due to conjugation of  $\pi$ -O and n-O orbitals with vacant B-orbitals in the six-membered boron-containing ring. The molecule **26** is approximately planar (compared to **5a**), with deviation of atoms (other than H and F) from the molecular plane not exceeding 0.01 Å.

Complex 26 reacts easily with a variety of carbonyl compounds with the formation of polymethine dyes. This work is underway in our laboratories.

# 5 Coumarin Merocyanines Derived from Spiropyranes

# 5.1 Synthesis and Structure

Indoline spiropyrans, such as A in Eq. 3, and their heteroanalogs are photochromic compounds [23–32]. The photochromic transition involves a spiro derivative, such as A, and a merocyanine, such as B. The photoinduced opening of the pyran ring in A is followed by the thermal *cis-trans* isomerization of the open form with the formation of colored merocyanine and the subsequent thermal or photochemical recyclization of the open form B to the starting colorless spiro-compound A.

#### **Equation 3**

The important parameters of the photochromicity are the absorption wavelength of the merocyanine form, the lifetime of this form, and the

quantum yield of the photoreaction. A change in the structure of the spiroderivative exerts a substantial effect on these parameters. Spiropyranes derived from coumarin derivatives are of special interest, because both cyclic and open merocyanine forms are fluorescent.

The first syntheses of indoline spiropyrans of the coumarin series were patented nearly 20 years ago [33, 34], but were only recently reported in periodicals [35–37]. However, at the time, details of the syntheses and identification of the products were not presented adequately in the literature. The systematic studies, including the study on the influence of the coumarin component on the photochromic properties of indoline spiropyrans, have recently been undertaken in our laboratories. [38–40]. 8-Formyl-7-hydroxy-4-methylcoumarin and 5-formyl-6-hydroxy-4-methylcoumarin were used as coumarin components in the synthesis of spiro compounds 27a–e and 28a–c.

 $R = H (a), CH_3 (b), Br (c), NO_2 (d), OCH_3 (e)$ 

Spiropyrans 27 and 28 were synthesized by the Wizinger-Wennig method [41], which involves the condensation of Fischer's base (or its substi-

Scheme 9

tuted analog) with a formylhydroxycoumarin. A unified mechanism for the synthesis of spiropyrans 27 and 28 is suggested in Scheme 9.

The structures of compounds 27 and 28 have been studied by <sup>1</sup>H NMR and electronic absorption spectroscopy, taking into account that they can exist in both the cyclic (spiro) and open forms. The high field region of the <sup>1</sup>H NMR spectra of spiropyrans 27 and 28 exhibits two signals from the magnetically nonequivalent (due to the nonsymmetric spiro atom) geminal Me groups, which indicates the cyclic structure of these compounds. On the other hand, the analysis of the <sup>1</sup>H NMR spectra of compounds synthesized by condensation of 3-formyl-4-hydroxycoumarin and 5-substituted 1,3,3-trimethyl-2-methyleneindolines, showed that these compounds exist in the open form 30a-d, rather than in the spiro form 29. This conclusion comes from analysis of the <sup>1</sup>H NMR spectra. Thus, the methyl groups in position 3 of the indoline fragment of compound 30 give rise to one six-proton singlet at  $\delta$ 1.75–1.82. This absorption pattern unambiguously indicates the open form of these compounds in solution. A rather complicated absorption pattern for the two protons of the central vinylene group in 30, which is consistent with the presence of several isomers for these compounds in solution [38].

 $R = H (a), CH_3 (b), Br (c), NO_2 (d)$ 

# 5.2 Photochromism

The compounds 27a-e in toluene solutions ( $c = 210 \times 10^{-4}$  M) at room temperature exhibit the photochromic properties, which are observed as reversible changes in the absorption spectra [39]. For instance, when colorless solutions of spiro compound 27a are UV irradiated, a maximum at 584 nm and a shoulder at 620 nm appear in the long wave spectral region (Fig. 2, curve 1).

The highest values of the photoinduced absorbance are observed for the substances containing electron releasing substituents in the indoline derivatives 27. In particular, the presence of the methoxy group in the indoline moiety (compound 27e) results in the greatest increase in the absorption intensity in the long wave maximum of the absorption band (Fig. 2, curve 2).

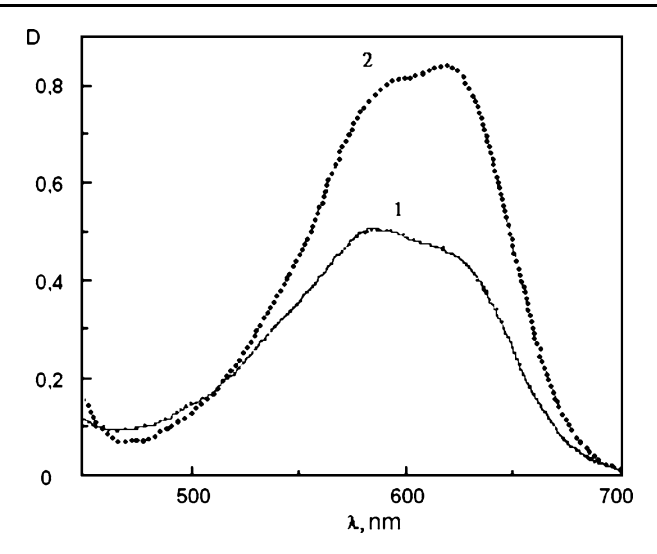


**Fig. 2** Electron absorption spectra of photoinduced merocyanine form **B** of compounds **27a** (1) and **27e** (2) in toluene ( $c = 210 \times 10^{-4}$  M); **D** denotes optical density

The efficiency of photochromic transformations of compounds 27a-e can be estimated from a comparison of the kinetic curves of photocolorization and spontaneous decolorization (not shown). The differences observed in the photochromic properties can be explained from the dependence of the kinetics of spontaneous relaxation of the photoinduced merocyanine form on the nature of the substituent in the indoline fragment. The introduction of electron releasing substituents increases the lifetime of the photoinduced form, while the lifetime is decreased with an enhancement of the electron withdrawing properties of the substituents. This agrees with the earlier revealed dependences of the properties of indoline spiropyrans on their structure. Electron releasing substituents in the indoline moiety favor the positive charge delocalization on the nitrogen atom, and the increase in the stability of compounds in the merocyanine form.

An important property of compounds 27a-e is the fluorescence of their solutions before and after irradiation. A comparison of the fluorescence spectra of compound 27a before and after irradiation (Fig. 3) shows that the initial colorless cyclic form of the compound is characterized by the fluorescence band at 475 nm (Fig. 3, curve 1). Upon UV irradiation of the solution, the intensity of this band decreases with the simultaneous appearance of a new fluorescence band with a maximum at 668 nm (Fig. 3, curve 2), which is caused by the formation of photoinduced colored merocyanine, as follows from the comparison of the absorption and fluorescence spectra.

Spiropyrans 28a-c are characterized by less pronounced photochromic changes in solution at room temperature compared to those of compounds

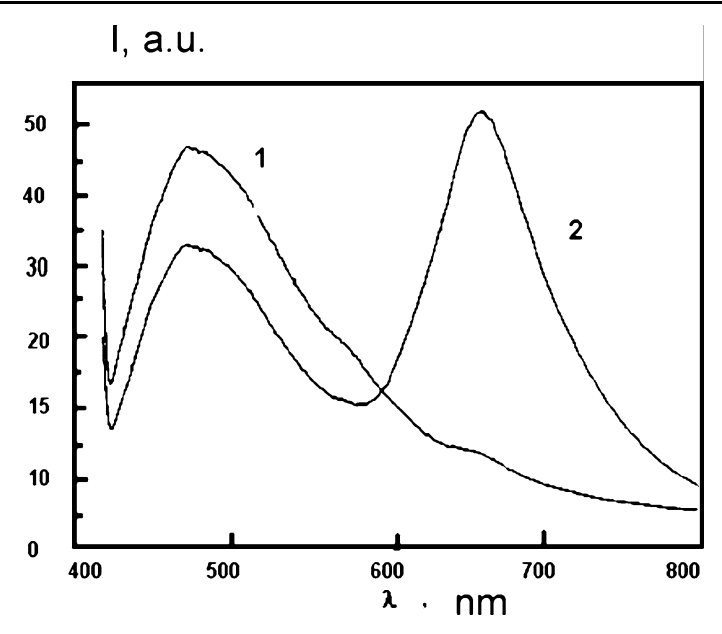


**Fig. 3** Fluorescence spectra of spiropyran **27a** in benzene ( $c = 210 \times 10^{-3}$  M) before (1) and after (2) UV irradiation; I denotes fluorescence intensity in arbitrary units (a.u.)

27a-e. This feature may be related to a sharp shortening of the lifetime of their photoinduced merocyanine form B (Eq. 3).

Distinct photochromic transformations were detected only for compound **28c**. As compared with compounds **27a**–**e**, the absorption maxima of the open forms of compounds **28a**–**c** are noticeably shifted hypochromically.

Unlike spiropyrans 27 and 28, compounds 30 exist in a stable merocyanine form B. The narrow shape of the absorption bands in the electronic absorption spectra of compounds 30a-d with a maximum at 498-500 nm (Fig. 4) is remarkable. As can be seen, the spectra contain a shoulder in the short wave region of the major band. The ratio of the intensities of these absorptions depends on the nature of the substituents at the molecular skeleton of 30. The intensity of the shoulder increases upon the introduction of electron releasing substituents into the molecule (Fig. 4, curve 2) and decreases for the electron withdrawing substituents (Fig. 4, curves 3 and 4), compared to the unsubstituted compound 30a (Fig. 4, curve 1). By contrast, the introduction of electron acceptors into position 5 of the indoline fragment increases the intensity of the long wave absorption band. These experimental data may indicate the presence of both monomeric and J-aggregated structures of the merocyanine forms of compounds 30a-d.

The analysis of the obtained spectral data for compounds 27a,b suggests that UV irradiation results in the J-aggregation of molecules of the merocyanine form, which is indicated by an increase in the intensities of ab-

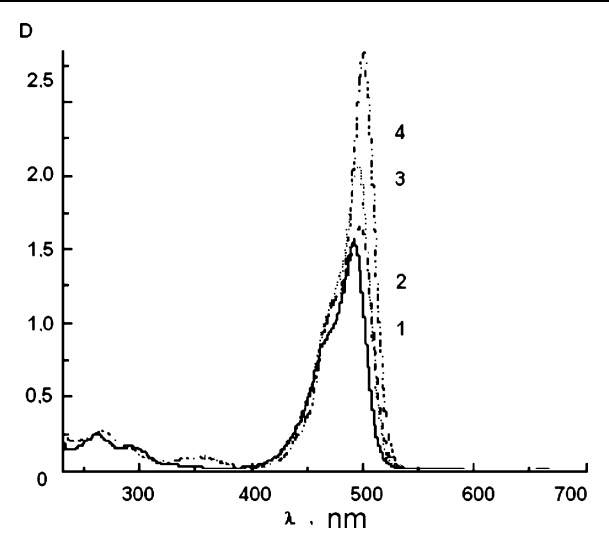


**Fig. 4** Electron absorption spectra of solutions of merocyanines **30a** (1), **30b** (2), **30c** (3), and **30d** (4) in chloroform ( $c = 110 \times 10^{-4} \text{ M}$ )

sorption and fluorescence bands due to the photoinduced increase in the number of molecules in the merocyanine form. The absorption and fluorescence spectra of a more concentrated solution of compound **27a** in benzene  $(c = 210 \times 10^{-3} \text{ M})$  are shown in Fig. 5.

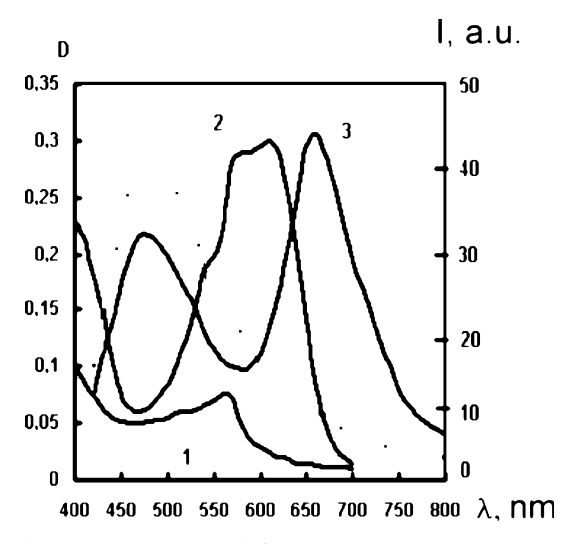


**Fig. 5** Electron absorption (1, 2) and fluorescence spectra at  $\lambda_{\rm exc} = 400$  nm (3) before (1) and after (2, 3) UV irradiation of solution of compound **27a** in benzene  $(c = 110 \times 10^{-3} \text{ M})$ 

The electronic absorption spectrum of compound 27a before irradiation (Fig. 5, curve 1) contains the absorption band of the initial spiro-form A in the UV spectral region and a band in the visible region with a maximum at 565 nm, which most likely belongs, to merocyanine form B of this compound (Eq. 3). The appearance of the latter band is caused by the partial shift of equilibrium in concentrated solutions toward the formation of an insignificant amount of the merocyanine form. UV irradiation of the solution increases the concentration and, hence, the intensity of the absorption band of merocyanine form B (Fig. 5, curve 2). In this case, the absorption band becomes broad and has two maxima at 575 and 618 nm.

The first maximum is close to the absorption maximum of the merocyanine form before irradiation, while the second maximum is shifted toward the long wave region by approximately 40 nm. As followed from the photoinduced absorption spectra, monomeric compounds and, possibly, dimeric aggregates are present in the solution along with the J-aggregates. The spectral interval between the long wave absorption maximum and photoinduced fluorescence maximum (668 nm) (Fig. 5, curve 3) is 50 nm (Stokes shift). Similar spectral changes are also observed for concentrated solutions of compound 27b in benzene.

It should be mentioned that the efficiency of aggregation of 27 depends on the polarity of the solvent. For instance, it decreases with an increase in the solvent polarity as a result of the replacement of benzene ( $\varepsilon$  = 2.25) by acetone ( $\varepsilon$  = 20.7). In addition, the aggregation decreases in the presence of the 5-methyl substituent in the indoline moiety compared to that for the unsubstituted compound.

Unlike in solution, a polymolecular layer of compound 27a is characterized by a large Stokes shift of 100 nm (Fig. 6). The spectral characteristics of the initial and photoinduced forms of compounds 27a,b in polymolecular layers and the large Stokes shift indicate that the J-aggregation process does not occur. The molecular packing probably prevents the aggregation of molecules in the polymolecular layer.

Unlike the indoline spiropyrans discussed above, compounds 30a,b are not photochromic in solution and in a solid state. The prolonged UV irradiation or visible irradiation of these compounds and/or heating of their solutions to 65 °C did not result in any noticeable spectral changes. The absorption and fluorescence spectra of compound 30a indicate that the starting solution of this compound contains J-aggregates. Efficient aggregation is also observed for merocyanine 30b. The replacement of nonpolar benzene by more polar acetone broadens the absorption and fluorescence bands, due to the appearance of monomeric and dimeric molecules.

Absorption and fluorescence spectra of the polymolecular layers of compound **30a** are shown in Fig. 7. The maxima of the absorption and fluorescence bands of this compound virtually coincide, which means that resonance fluorescence is observed. This feature is a convincing proof for the formation

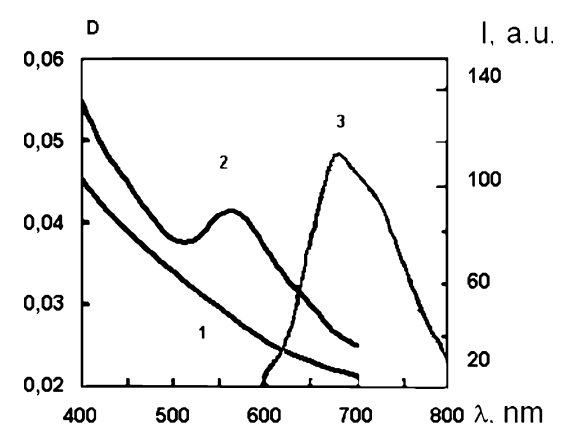


**Fig. 6** Electron absorption (1, 2) and fluorescence spectra at  $\lambda_{\rm exc} = 550$  nm (3) before (1) and after (2, 3) UV irradiation of the one-component polymolecular layer (nine monolayers), based on compound **27a** 

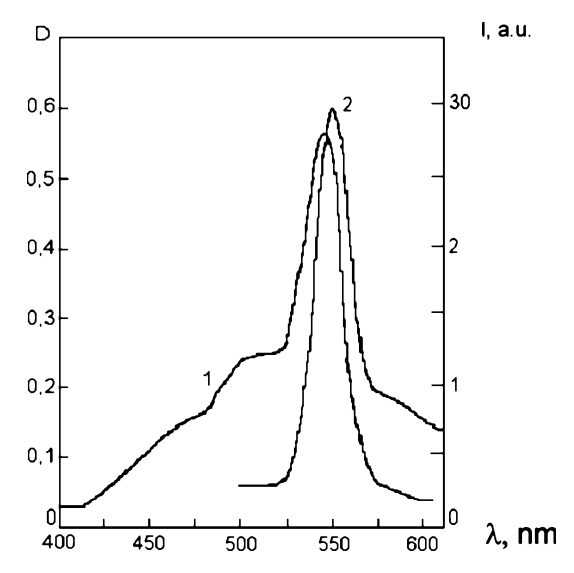


**Fig. 7** Electron absorption spectrum (1) and fluorescence spectrum (2) of compound **30a** in the polymolecular layer (nine monolayers)

of J-aggregates of molecules of the merocyanine form. The polymolecular layers of **30a** containing J-aggregates were used for studying their nonlinear optical properties [42].

As can be seen from analysis of the resonance structures of merocyanines 27 and 28 (Scheme 10) and 30 (Scheme 11), the conditions for negative charge

#### Scheme 10

### Scheme 11

delocalization differ in the fragments of 7-, 6- and 4-hydroxycoumarins. Each of the open forms (form B in Eq. 3) of compounds 27a-e and 30a-d has three resonance structures, and only two structures can be found for compounds 28a-c (Eq. 4).

The heat of formation  $\Delta H^{\circ}$  values for the cyclic (spiro, B) and open (A) forms of compounds 27a and 28a and merocyanine 30a, which were calculated by the standard procedure of AM1 calculations, are given in Table 1.

Table 1	Heat of formation $[\Delta H_f^{\circ} \text{ (kcal mol}^{-1})]$ values for the spiro (A) and merocyanine
(B) for	ns of unsubstituted indoline spirocoumarins

Compound	$\Delta H_{ m f}^{\circ}$ (A)	$\Delta H_{ m f}^{\circ}$ (B)	$\Delta \Delta H_{\rm f}^{\circ}$ $[\Delta H_{\rm f}^{\circ}(\mathbf{B}) - \Delta H_{\rm f}^{\circ}(\mathbf{A})]$
27a	-4.4676	-2.2853	+2.1823
28a	+2.0103	+6.0439	+4.0336
30a	+0.9123	-8.6327	-9.5450

#### **Equation 4**

The results of the calculations show that the 1,3-diketo form of compound 30a is the most stable. It is most likely that its spiro-form of structure 29a is not formed in the studied temperature interval just for this reason. Finally, according to the results of calculations, the open form B of 28a is less stable than its isomeric spiro form A. As can be seen, the heat of formation of open form B of 28a is higher than the heat of formation of the cyclic form A of this compound. The observed high rates of the thermal decolorization of compounds 28a-c may be due to the discussed feature. In summary, compounds 27a-e synthesized from 8-formyl-7-hydroxy-4-methylcoumarin have the most pronounced photochromic properties. The electron releasing substituents in the indoline fragment of 27a-e increase and the electron withdrawing substituents decrease the lifetime of the photoinduced form. Spiropyrans 28a-c synthesized using 5-formyl-6-hydroxy-4methylcoumarin are characterized by a shorter lifetime of the photoinduced merocyanine form at room temperature. Under normal conditions, compounds 30a-d based on 3-formyl-4 hydroxycoumarin are not photochromic and exist in the merocyanine form. According to the quantum chemical calculations, the experimental data can be explained by differences in the negative charge delocalization in the coumarin fragments of the corresponding merocyanines.

This stability pattern is also observed for dyes 31 and 32, which are derivatives of benzothieno[3,2-b]pyrrole. Only the open (merocyanine) forms 31 and 32 have been found [43].

**31**,  $\lambda_{max}$  = 502 nm

**32**,  $\lambda_{max}$  = 624 nm

# 5.3 Coumarin Merocyanines in Polymeric Matrices

The photoinduced merocyanine forms of spiropyrans 27 are more stable in polymeric matrices of poly(methyl methacrylate) than in solution [40]. In particular, UV irradiation of spiro compound 27e results in the appearance of a broad absorption band at 594 nm for the photoinduced merocyanine form, the intensity of which increases with an increase in the duration of UV irradiation. Similar results were obtained for compounds 27b,c. On the other hand, the photoinduced merocyanine form of the nitro derivative 27d shows two absorption maxima at 574 nm and 599 nm. Overall, the absorption for the photoinduced form of the nitro derivative 27d is much broader than the absorption of the open forms of 27a-c, especially in comparison to the absorption band of the methoxy derivative 27e. The increase in the absorption intensity in the long-wavelength region of the photoinduced absorption band of 27d in poly(methyl methacrylate) is apparently due to J-aggregation of the merocyanine form [44]. Irradiation of the merocyanine forms with a visible light causes photobleaching, which is a result of the formation of the spiro forms. This effect is illustrated in Fig. 8 for the transformations of 27a.

At ambient temperatures in the dark, the merocyanines derived from 27a-c undergo spontaneous transformation into the initial spiro form. However, unlike the fast processes in solution of tens of seconds [39], the spontaneous dark bleaching in a polymer matrix lasts for tens of minutes [40]. In addition, the process in the solid state is not exponential [45]. The comparison of the times of thermal bleaching corresponding to the spontaneous twofold decrease in the photoinduced absorbance suggests that the

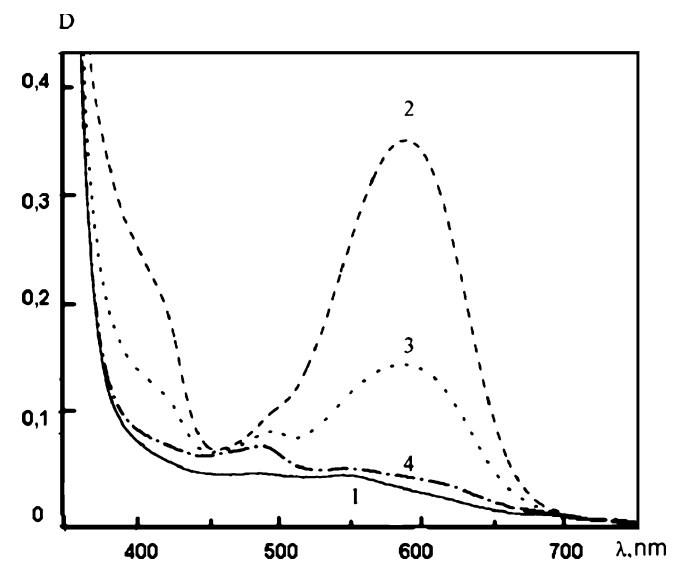


**Fig. 8** Electron absorption spectra of compound **27a** in block poly(methyl methacrylate) before UV irradiation (1), after UV irradiation (810 s) (2), and after visible light irradiation for 20.5 (3) and 35.5 min (4)

rate of thermal bleaching decreases with an increase in the electron-donor ability of substituents in the indoline system, as for solutions of these compounds.

Photochromic compounds 27a-c in the polymeric matrices exhibit photoinduced fluorescence (Fig. 9), which is due to the formation of the photoinduced merocyanine form [29, 46, 47]. The Stokes shift for the methoxy-substituted compound 27e under these conditions is 55 nm. By contrast, the Stokes shift for the nitro derivative 27d in the poly(methyl metacrylate) film is only 5 nm.

Compounds 30a,b, both in polymeric matrix and in solution [40], exhibit no photochromic transformations. As already mentioned, they exist in the fluorescent merocyanine form. The absorption and fluorescence spectra of dye 30b in the polymer matrix are shown in Fig. 10 for illustration. The Stokes shift of 38 nm for this compound is smaller than those for other photochromic analogs discussed above.

The strong fluorescence of the merocyanine dyes in polymer matrices is mimicked in their non-covalent complexes with proteins. Some of the coumarin polymethines have been studied for interaction with protein bovine serum albumin. For example, fluorescence of compounds 6 and 8 is increased about 1200-fold and 2500-fold, respectively, in the rigid complex with the protein, in comparison to fluorescence intensity of these dyes free in solution.

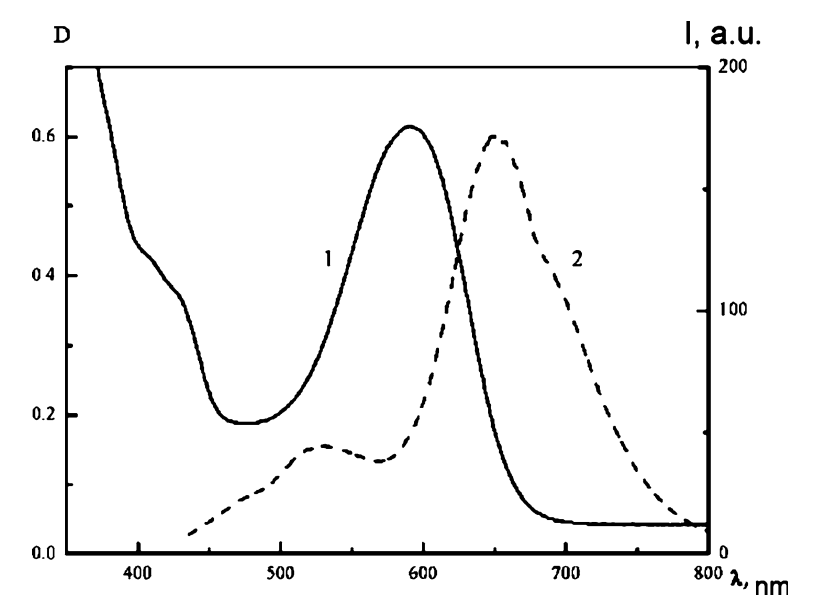


**Fig. 9** Electron absorption (1) and fluorescence (2) spectra upon irradiation (420 nm) of the photoinduced merocyanine form of compound **27e** in the poly(methyl methacrylate) film

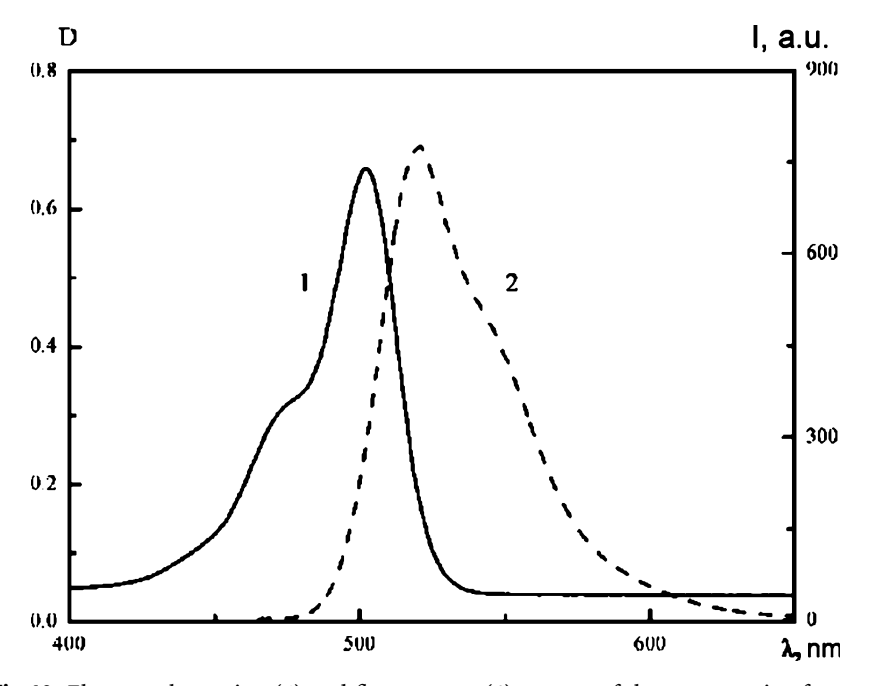


**Fig. 10** Electron absorption (1) and fluorescence (2) spectra of the merocyanine form of non-photochromic compound **30b** in the poly(methyl methacrylate) film

### References

 Brackman U (1997) Lamdachrome Laser Dyes Data Sheets, 2nd Ed. Lamda Physik GmbH, Göttingen

- 2. Dilthey W (1903) Ber 36:3207
- 3. Shizuri Y, Kato K, Hirata Y, Nurobushi A, Yamanura S (1969) J Chem Soc, p 2774
- 4. Reynolds GA, Van Allen JA (1969) J Het Chem 6:375
- 5. Reynolds GA, Van Allen JA (1971) J Org Chem 36:600
- Markin VS, Abramenko PI, Boiko II (1984) Zhurnal Vses Himich Obshestva (USSR) 29:457
- 7. Markin VS, Abramenko PI, Boiko II (1984) Mendeleev Chem J (Engl Transl), p 29
- 8. Manaev AV, Chibisova TA, Lyssenko KA, Antipin MY, Traven VF (2006) Izv Akad Nauk, Ser Khim 11:2012
- 9. Manaev AV, Chibisova TA, Lyssenko KA, Antipin MY, Traven VF (2006) Russ Chem Bull Int Ed 55:2091
- Traven VF, Manaev AV, Safronova OB, Chibisova TA, Lyssenko KA, Antipin MY (2000)
   Zhurnal Obshch Khim 70:853
- 11. Traven VF, Manaev AV, Safronova OB, Chibisova TA, Lyssenko KA, Antipin MY (2000) Russ J Gen Chem (Engl Transl), p 70
- 12. Lyssenko KA, Antipin MY (2001) Izv Akad Nauk, Ser Khim 400
- 13. Lyssenko KA, Antipin MY (2001) Russ Chem Bull Int Ed 50:418
- Korlyukov AA, Lyssenko KA, Antipin MY, Kirin VN, Chernyshev EA, Knyazev SP (2002) Inorg Chem 41:5043
- Lyssenko KA, Ponomarev VA, Gurskii ME, Antipin MY, Bubnov YN (2004) Mendeleev Commun, p 189
- 16. Traven VF, Chibisova TA, Manaev AV (2003) Dyes and Pigments 58:41
- 17. Manaev AV, Chibisova TA, Traven VF (2006) Izv Akad Nauk, Ser Khim 12:2245
- 18. Manaev AV, Chibisova TA, Traven VF (2006) Russ Chem Bull Int Ed 55:2226
- 19. Traven VF, Manaev AV, Tambov KV (2007) Unpublished results, Zhurnal Organ Khim 43:0000
- 20. Takeuchi N, Nakagawa H, Tobinaga S (1980) Chem Pharm Bull 28:3002
- 21. Traven VF, Manaev AV, Ohrimenko IN, Lyssenko KA (2007) Unpublished results, Izv Akad Nauk, Ser Khim: 0000
- 22. Traven VF, Manaev AV, Ohrimenko IN, Lyssenko KA (2007) Russ Chem Bull Int Ed 56:0000 (in print)
- 23. Bertelson RC (1971) In: Brown GH (ed) The Photochromism. Wiley Interscience, New York, p 45
- 24. Krongauz VA, Goldburt EI (1978) Nature 271:43
- 25. Barachevsky VA, Lashkov GI, Tsekhomskii VA (1977) Fotokhromizm i ego primenenie. Photochromism and Its Application, Khimiya, Moscow, p 279 (in Russian)
- 26. Chibisov AK, Gorner H (1998) Chem Phys 237:425
- 27. Bertelson RC (1999) In: Crano JC, Guglielmetti R (eds) Organic Photochromic and Thermochromic Compounds. Plenum Press, New York, p 11
- 28. Maeda S (1999) In: Crano JC, Guglielmetti R (eds) Organic Photochromic and Thermochromic Compounds. Plenum Press, New York, p 85
- 29. Barachevsky VA (2000) J Fluoresc 10:185
- Antipin SA, Petrukhin AN, Gostev FE, Marevtsev VS, Titov AA, Barachevsky VA, Strokach YP, Sarkisov OM (2000) Chem Phys Lett 331:378
- 31. Lokshin VA, Samat A, Metelitsa AV (2002) Usp Khim 71:1015
- 32. Lokshin VA, Samat A, Metelitsa AV (2002) Russ Chem Rev (Engl Transl), p 71

- 33. FR Patent 1555666 (1973) RZ Chim 7:755
- 34. JP Patent 89 203 388 (1990) Chem Abstr 112:45742
- 35. Metelitsa AV, Knyazhansky MI, Ivanitsky VV, Nikolaeva OG, Palchkov VA, Panina AP, Shelepin NE, Minkin VI (1994) Mol Cryst Liq Cryst 246:37
- 36. Traven VF, Kozakova LD, Fedorovsky OY, Uzhinov BM (2001) XX Intern Conf Photochem. Book of Abstracts, p 238
- 37. Traven VF, Miroshnikov VS, Chibisova TA, Barachevsky VA, Venidiktova OV, Strokach YP (2004) Proc 10th International Conf on Dyes, Pigments and Functional Dyes. Czech Republic, p L27
- 38. Traven VF, Miroshnikov VS, Chibisova TA, Barachevsky VA, Venidiktova OV, Strokach YP (2005) Russ Chem Bull Int Ed 54:2417
- 39. Barachevsky VA, Karpov RE, Venediktova OV, Valova TM, Strokach YP, Miroshnikov VS, Chibisova TA, Traven VF (2005) Russ Chem Bull Int Ed 54:2425
- Dolotov SM, Miroshnikov VS, Chibisova TA, Sin S-L, Venidiktova OV, Valova TM, Dunaev AA, Strokach YP, Barachevsky VA, Traven VF (2007) Russ Chem Bull Int Ed 56:904
- 41. Wizinger R, Wennig H (1940) Helv Chim Acta 23:247
- 42. Barachevsky VA, Karpov RE, Nagovitsin IA, Chudinova GK, Strokach YP, Miroshnikov VS, Chibisova TA, Traven VF (2004) Superlattices and Microstructures 36:73
- 43. Schimkin AA (2007) PhD Thesis, Institute Organ Chem RAS
- 44. Eckhardt H, Bose A, Krongauz VA (1987) Polymer 28:1959
- 45. Smets G, Thoen J, Aerts F (1975) J Polym Sci Polym Symp 51:119
- 46. Ignatin AA, Strokach YP Barachevsky VA (1998) Zhur Nauchn Prikl Fotografii. J Sci Appl Photogr 43:33 (in Russian)
- 47. Ignatin AA, Barachevsky VA, Strokach YP, Alfimov MV, Samat A, Guglielmetti Z (2003) Zhur Nauchn Prikl Fotografii. J Sci Appl Photography 48:28 (in Russian)

# **Squarylium Dyes and Related Compounds**

Shigeyuki Yagi (☒) · Hiroyuki Nakazumi

Department of Applied Chemistry, Graduate School of Engineering, Osaka Prefecture University, 1-1 Gakuen-cho, Naka-ku, Sakai, 599-8531 Osaka, Japan yagi@chem.osakafu-u.ac.jp

1	Introduction	134
2	Synthesis and Optical Properties of Squarylium Dyes	135
2.1	Conventional Synthesis of Squarylium Dyes	135
2.2	Unsymmetrical Squarylium Dyes	139
2.3	Modification of Squarylium Dyes	145
2.4	$\pi$ -Extended Squarylium Dyes and Analogues	147
2.5	Bis-squarylium Dyes	153
2.6	Squarylium Analogues Derived from Bisquarate	156
3	Applications of Squarylium Dyes	160
3.1	Squarylium Dyes as Photo-conducting Materials	160
3.2	Squarylium Dyes as Photosensitizers in Photovoltaic Devices	162
3.3	Squarylium-based Conjugated Polymers as Conductive Materials	165
3.4	Application of Squarylium Dyes to Biological and Environmental Analyses	168
3.5	Supramolecular Systems Based on Squarylium Dyes	174
4	Concluding Remarks	178
Refe	erences	178

Abstract Squarylium dyes, first synthesized in the 1960s, consist of an oxocyclobutenolate core with aromatic or heterocyclic components at both ends of the molecule. As squarylium dyes show intense absorption and often fluorescence emission, they have attracted much attention from the viewpoint of technological applications. Efforts have been made to develop new synthetic methods for constructing squarylium-based chromophores. Here novel synthetic protocols for construction of novel squaryliums and related chromophores are reviewed. The present chapter starts with modification of squarylium dyes affording amino- and dithio-substituted dyes, and then the synthesis of unsymmetrical squarylium dyes is introduced. The syntheses of methine- and arene-bridged bis-squarylium dyes are next reviewed, and the bisquarylbased analogues are also discussed. Applications of squarylium dyes and related compounds are discussed, including xerographic devices utilizing photoconductive properties of squarylium dyes, photovoltaic devices employing the dyes as photosensitizers, and biolabeling and chemosensory materials for analytical uses. Low band-gap electroconductive materials are available by polymerization of squarylium skeletons. As a future aspect, supramolecular systems based on squaryliums are also introduced.

# 1 Introduction

The chemistry and industrial use of synthetic organic dyes started in the 19th century, and numerous classes of dyes and pigments have so far been investigated. Polymethine dyes have seldom been used for dyeing purposes due to low photo and chemical stability. However, they have been practically used as photosensitizers in photography [1]. Thereafter, the development of optoelectronics has brought about great demand for various types of dyes with suitable optical properties for device performances. In particular, optical recording technology using diode lasers such as Ga-Al-As (emission at 780 nm) and YAG (emission at 1064 nm) facilitated investigation of new  $\pi$ -based structural backbones because of needs of near-infrared (NIR) light absorbers [2]. Nowadays, polymethine dyes are placed at the center of studies on functional organic dyes and have also been receiving much interest as advanced materials for applications to optical recording media, sensitizers of inorganic semiconductors for photography and photoenergy conversion, and display devices, among others [3-7]. They have also been employed as colorimetric and fluorometric labeling reagents in clinical and bioanalytical fields [8].

Squarylium dyes, which are often called squaraines, possess polymethine structures and are occasionally classified as cyanine dyes. They exhibit intense light absorption and sometimes fluorescence emission, similar to cyanine dyes. There is, however, an important difference between the electronic structures of cyanine and squarylium dyes (Fig. 1). As already discussed in Chap. 1, the cyanine dye is cationic and its two terminal nitrogen atoms are linked by an odd number of methine carbons. One of the nitrogen atoms is a positively charged iminium, and the other is an amine. Thus, the cyanine dyes is cationic and the other is an amine.

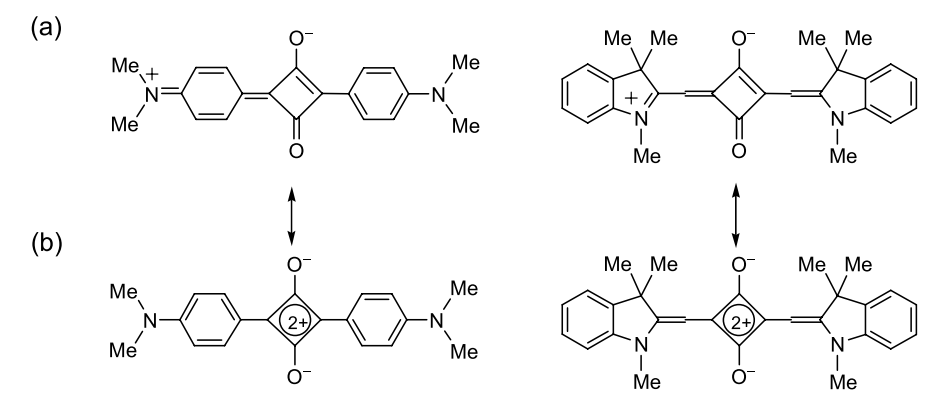


Fig. 1 Resonance structures of typical squarylium dyes

nine dye has a push-pull electronic conjugation structure which enhances the electronic transition dipole. As shown in Fig. 1a, the squarylium dye also consists of the polymethine structure with amine and iminium terminals, and this is the reason why squarylium dyes are sometimes classified as cyanines. However, the squarylium dye has an oxocyclobutenolate core, affording a neutral, zwitterionic structure that is often represented by a resonance structure with a cyclobutenediyliumdiolate core (Fig. 1b). As the central four-membered ring intensely pulls the electrons, the squaryliums have a donor-acceptor-donor charge transfer structure. Therefore, the squarylium dyes should be classified as compounds that are different from the classical cyanine dyes.

Squarylium dyes are generally stable, and heterocyclic or aromatic components introduced at the both ends result in various optical properties. Recently, they have received increased attention from scientific as well as technological viewpoints. In the present chapter, new aspects in squarylium chemistry are reviewed, especially focused on the syntheses and technological applications. We start with the conventional synthesis of squarylium dyes because the historical aspect is necessary to see how the syntheses of squaryliums and related compounds have been developed. We next discuss the syntheses of unsymmetrical squarylium dyes, and then move to the syntheses of various squarylium analogues. The optical properties are also shown. We also review the recent development of technological applications of squarylium dyes. The potential application of squarylium dyes in supramolecular systems is also an area of focus.

# 2 Synthesis and Optical Properties of Squarylium Dyes

# 2.1 Conventional Synthesis of Squarylium Dyes

The first synthesis of squarylium dyes was reported by Treibs and Jacob in 1965 (Scheme 1) [9, 10]. The condensation of squaric acid (3,4-dihydroxy-3-cyclobutene-1,2-dione) with two equivalents of electron-rich aromatics such as  $\alpha$ -unsubstituted pyrrole and phloroglycinol (1,3,5-trihydroxybenzene) under acidic conditions yielded the squarylium dyes 1 and 2, respectively. Similar reactions producing a series of azuleno-squarylium 3 and anilino-squarylium 4 were reported by Sprenger and Ziegenbein [11,12]. They used condensation of nucleophilic aniline or azulene derivatives with squaric acid in a 1-butanol-benzene mixed solvent with azeotropic removal of water. These conditions were used afterwards as a generic synthetic protocol to prepare squarylium dyes. The proposed reaction mechanism in the squarylium synthesis has been discussed by Sprenger and Ziegenbein in their review

#### Scheme 1

(Scheme 2) [13]. The condensation starts with the nucleophilic attack of the aromatic molecule (Ar–H) on the carbonyl carbon of the half ester of squaric acid, and the elimination of the alcohol affords a mono-substituted squaric

$$R^{5}$$
 $R^{4}$ 
 $R^{2}$ 
 $R^{2}$ 
 $R^{2}$ 
 $R^{3}$ 
 $R^{3}$ 

**3a**:  $R^1 - R^5 = H$ 

**3b**:  $R^1$ ,  $R^2$  = Me;  $R^4$  = *i*-Pr;  $R^3$ ,  $R^5$  = H

**3c**:  $R^1$ ,  $R^4 = H$ ;  $R^2$ ,  $R^3$ ,  $R^5 = Me$ 

$$R^1$$
 $R^2$ 
 $R^2$ 
 $R^2$ 
 $R^2$ 

**4a**:  $R^1$ ,  $R^2 = Me$ 

**4b**:  $R^1$ ,  $R^2 = (CH_2)_2OH$ 

**4c**:  $R^1$ ,  $R^2 = CH_2Ph$ 

**4d**:  $R^1$ ,  $R^2 = (CH_2)_2 O(CH_2)_2$ 

$$+BuOH$$
 $+BuOH$ 
 $+BuOH$ 
 $+Ar-H$ 
 $+Ar-$ 

#### Scheme 2

Table 1 Electronic absorption data of the squarylium dyes 1 and 3-8

Compound	Solvent	$\lambda_{max}$ (nm)	$\varepsilon$ (M <sup>-1</sup> cm <sup>-1</sup> )	Refs.
1 3a 3b 3c 4a 4b 4c 4d 5	CHCl <sub>3</sub> MeOH CHCl <sub>3</sub> MeOH CHCl <sub>3</sub>	550 680 770 720 628 (627) <sup>b</sup> 640 624 621 630 (633) <sup>b</sup>	230 000 110 000 132 000 -a 309 000 b -a -a -a 321 000 c	[9, 10] [11] [11] [11] [12] [12] [12] [12] [14]
6 7 8	CHCl₃ DMF CHCl₃	670 (667) <sup>c</sup> 678 730	160 000 <sup>d</sup> _ a _ a	[14] [14] [14]

<sup>&</sup>lt;sup>a</sup> No data is listed in the literature

b Data from [15]

<sup>&</sup>lt;sup>c</sup> Data from [16]

d Data from [17]

acid as an intermediate product. The subsequent reaction of another aromatic molecule followed by removal of a water molecule gives a squarylium dye. Although this mechanism has not been experimentally verified, the synthesis of unsymmetrical squarylium dyes, as discussed later, is fully consistent with this pathway. As summarized in Table 1, the representative squarylium dyes are colored blue to green, and their molar absorptivities can be as large as those observed for cyanine dyes.

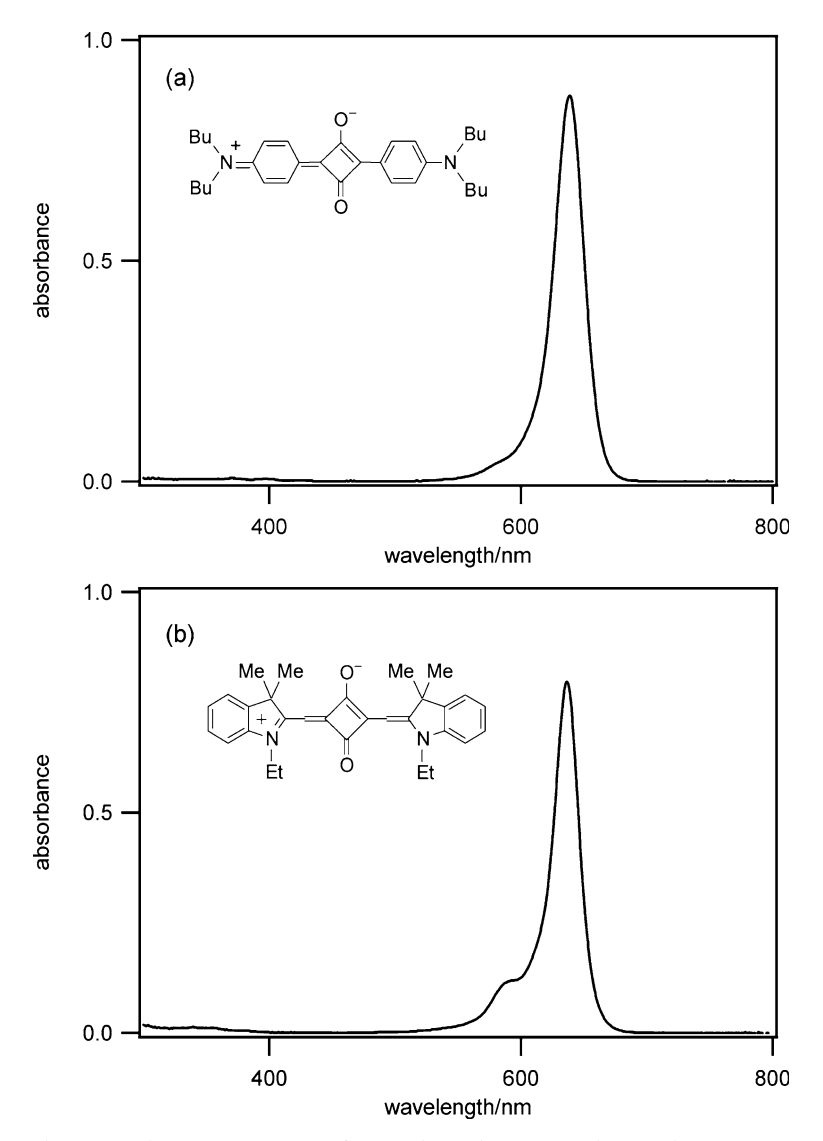


Fig. 2 Electronic absorption spectra of squarylium dyes in CHCl $_3$  at ambient temperature; a 4e and b 5:  $R=C_2H_5$ 

It did not take long to find that it is possible to prepare squarylium dyes with heterocyclic components in addition to those with electron-rich aromatic moieties. Sprenger and Ziegenbein reported the synthesis of a series of squarylium dyes 5-8, where the corresponding heterocyclic quaternary salts with an activated methyl group 9-12 were used as starting materials [14]. Elimination of a proton from the methyl group is essential to convert the quaternary salts to the nucleophilic enamines, and quinoline was added to the reaction mixture to facilitate the enamine formation. Light absorption properties of these squarylium dyes depend on the constituent heterocycles, as summarized in Table 1. The absorption maxima range from 630 to 730 nm, and their solutions are deeply colored. As an example, the electronic absorption spectrum of 5 (R = Et) is shown in Fig. 2 together with that of the anilino-squarylium dye 4e.

## 2.2 Unsymmetrical Squarylium Dyes

Although the synthetic protocol for symmetrical squarylium dyes was developed as early as the 1960s, the methodology could not be applied nor modified to the preparation of unsymmetrical squarylium dyes. Only two decades later in the 1980s did Law and Bailey report a rational approach to the synthesis of unsymmetrical squarylium dyes (Scheme 3) [18, 19]. Thus, the organic salt consisting of a mono-substituted squaric acid and an aniline derivative was heated in 2-propanol containing a small amount of tributyl orthoformate (method A) or in a 1-butanol/benzene mixture (method B). As can

### Scheme 3

**Table 2** Structures and electronic absorption data in  $CHCl_3$  of the squarylium dyes 13–15 (data abstracted from [19])

		0 <sup>-</sup> R <sup>1</sup> —(2+)—R <sup>2</sup>		
Compound	$\mathbb{R}^1$	$\mathbb{R}^2$	λ <sub>max</sub> (nm)	$\log arepsilon^a$
13a	MeO-	$-$ NMe $_2$	578.8	5.37
13b		$NMe_2$	563.6	5.20
13c		NMe <sub>2</sub>	583.5	5.32
13d		NMe <sub>2</sub>	581.1	5.40
13e		$NMe_2$	583.6	5.23
14a	MeO MeO	$-$ NMe $_2$	587.0	5.34
14b		$NMe_2$	572.1	5.20
14c		$NMe_2$	592.4	5.35
14d		NMe <sub>2</sub>	590.6	5.32
14e		NMe <sub>2</sub>	582.4	5.08
15a	MeO MeO	$-$ NMe $_2$	583.1	5.39
15b	ivieO	NMe <sub>2</sub>	562.4	5.12

<sup>&</sup>lt;sup>a</sup>  $\varepsilon$  in [M<sup>-1</sup> cm<sup>-1</sup>]

be seen from the mechanistic Scheme 2, the monosubstituted squaric acid was postulated previously to be an intermediate product in the synthesis of symmetrical dyes. Thus, it is reasonable to employ mono-substituted squaric acid as a dye precursor for the preparation of unsymmetrical dyes. It should be noted, however, that the mono-substituted squaric acid was not derived from squaric acid by Law and Bailey. They prepared the precursors by the [2 + 2] cycloaddition reaction of tetraethoxyethane with arylacetylchloride according to the method reported by Belluš [20]. Three precursors were reported, which were allowed to react with a series of substituted anilines to afford the squarylium dyes 13–15. The structures and optical properties are listed in Table 2. The yields of the squarylium dyes obtained by either method ranged from 32% to 87%. These were the first examples of the synthesis of squarylium dyes without using unsubstituted squaric acid as a starting material.

Mono-substituted squaric acids are key precursors for the synthesis of unsymmetrical squarylium dyes. The first preparation of an aryl-substituted squaric acid derivative was described by Green and Neuse. They reacted benzene with 3,4-dichloro-3-cyclobutene-1,2-dione in the presence of AlCl<sub>3</sub> and obtained 3-chloro-4-phenyl-3-cyclobutene-1,2-dione [21]. Thereafter, this type of reaction was found to occur without any Lewis acids when electron-rich aromatic compounds were employed [22]. The obtained squaryl chlorides were easily hydrolyzed under acidic conditions to afford the monosubstituted squaric acids. As the dichloride of squaric acid is easily obtained by the reaction of squaric acid with SOCl<sub>2</sub> [23], this is a versatile method for preparing the precursors for unsymmetrical squarylium dyes.

(b)
$$Me \xrightarrow{\hspace{1cm} Ph} Or Me \xrightarrow{\hspace{1cm} Ph} CIO_4^- + 16-18 \xrightarrow{\hspace{1cm} BuOH/C_6H_6} Quinoline reflux \qquad O^-$$

### Scheme 4

**Table 3** Structures and optical data in CHCl<sub>3</sub> of the unsymmetrical squarylium dyes 19–24 (data abstracted from [24])

		$R^1$ $Q^ R^2$		
Compound	$\mathbb{R}^1$	R <sup>2</sup>	Yield (%)	$\lambda_{ m max}$ (nm) (log( $arepsilon/{ m M}^{-1}$ cm <sup>-1</sup> ))
19	Bu <sub>2</sub> N—	N C <sub>6</sub> H <sub>13</sub>	58	729 (4.92) 794 (5.03)
20	Bu <sub>2</sub> N-	Ph O	20	712 (4.99) 782 (5.18)
21	N-	N C <sub>6</sub> H <sub>13</sub>	71	751 (4.92) 821 (4.96)
22	N-	Ph	19	725 (5.01) 800 (5.10)
23	Me Me	N C <sub>6</sub> H <sub>13</sub>	55	720 (4.97) 774 (5.00)
24	Me Me	Ph	73	682 (5.02) 739 (4.98)

Yagi and Nakazumi prepared a series of unsymmetrical squarylium dyes using the precursors 16–18 shown in Scheme 4a [24]. This method is applicable to the synthesis of the mono-substituted squaric acid with a heterocyclic component. For example, the reaction of the indolenine-derived enamine with squaryl dichloride followed by acidic hydrolysis yielded the precursor 18. Using this protocol, one obtains various NIR-absorbing dyes 19–24 which consist of a squarylium skeleton with an aromatic-heterocycle or a heterocycle-heterocycle combination (Scheme 4b). The structures and optical data of 19–24 are summarized in Table 3. Employing the benzindolium

**Fig. 3** Molecular structure of the squarylium dye **21**. One water and 0.5 benzene molecules are included in a unit cell. Hydrogen atoms are omitted for clarity

Ėt

28

**27a**: 
$$R^1 = Et$$
,  $R^2 = H$ , ,  $R^3 = H$ ,  $X = S$   
**27b**:  $R^1 = Et$ ,  $R^2 = H$ ,  $R^3 = H$ ,  $X = Se$   
**27c**:  $R^1 = Et$ ,  $R^2 = H$ ,  $R^3 = CI$ ,  $X = S$   
**27d**:  $R^1 = Et$ ,  $R^2 = H$ ,  $R^3 = CI$ ,  $X = Se$   
**27e**:  $R^1 = Me$ ,  $R^2 = CI$ ,  $R^3 = H$ ,  $X = CMe_2$ 

Scheme 5

and benzopyrylium salts afforded large  $\pi$ -conjugation systems exhibiting low energy gaps of electronic transition. This feature is consistent with the X-ray crystallographic analysis of 21, which shows a highly planar structure of the  $\pi$ -electron system (Fig. 3). In contrast to the single absorption band of symmetrical dyes, the unsymmetrical dyes 19–24 show two broadened absorption bands. Indeed, the introduction of aromatic or heterocyclic components with different electronic contributions to the chromophoric system should result in two or more electronic transitions with different energy-gaps, as observed.

Unsymmetrical squarylium dyes were also reported by Terpetschnig and Lacowics (Scheme 5), who employed diethyl squarate as a starting material [25, 26]. Similar to 3,4-dichloro-3-cyclobutene-1,2-dione, the squarate was reacted with quaternary heterocyclic salts to afford the compounds 25a-c, which were converted to 26a-c by hydrolysis under basic conditions. The unsymmetrical squarylium dyes 27 and 28 were prepared by condensation of 26 with a series of quaternary heterocyclic salts. In the preparation of the quinaldine-based unsymmetrical squarylium dyes without a hydrolysis step, as reported by Ramaiah et al. [27], the mono-substituted squarate 29 was employed as a dye precursor (Scheme 6). In this case, it appeared that the substituent at the 6-position significantly affected the reactivity of the squarate 29. As shown in Scheme 6, the reactions of the 6-hydroxy- and 6-iodo-2-methylquinaldiniums with 29 were examined, and the reaction of the former compound did not afford any squarylium dyes, whereas the reaction of the latter compound yielded the unsymmetrical squarylium dye. It was also found that the reaction of squaric acid with the 2-methylquinaldinium with an electron-withdrawing substituent at the 6-position (X = H, Br, I, NO<sub>2</sub> or CN) yielded a squarylium dye, whereas the reaction with the 2-methylquinaldinium substrate with an electron-

Scheme 6

### Scheme 7

donating substituent (X = OH or OEt) afforded only a squarate (half-dye) (Scheme 7).

## 2.3 Modification of Squarylium Dyes

In order to develop new squarylium-based chromophores, introduction of hetero atoms such as nitrogen and sulfur in the central four-membered ring in place of oxygen has been examined. Kim et al. synthesized the aminosquarylium dyes 31, as shown in Eq. 1 [28]. The key starting material was the aminosquarate 30 which was prepared by the reaction of a dialkyl

### **Equation 1**

squarate with a primary amine. Then, condensation of **30** with 1-ethyl-2,3,3-trimethylindolium iodide afforded the aminosquarylium derivatives **31** in 9–15% yield. These dyes possess a cationic chromophore like a cyanine dye, with the light absorption maxima ranging from 650 to 653 nm in CHCl<sub>3</sub>, which is somewhat red-shifted compared to the absorption of indolino-squarylium dye **5**. In the IR spectrum, the aminosquarylium **31** exhibits absorption at 1730 cm<sup>-1</sup>. Squarylium dyes usually exhibit the C=O stretching vibration at ca. 1600 cm<sup>-1</sup> showing significant delocalization of the  $\pi$ -system

in the cyclobutene core, and such a conjugated double bond character has been indicated by X-ray crystallographic analyses [29, 30]. Therefore, the result from the IR spectra of the aminosquarylium dye indicates the existence of the localized double bond in the central four-membered ring. Kim et al. also reported that the photostability of 31 under exposure of a high-pressure Hg lamp was improved by the counter anion exchange from iodide

**34a-c**: R = H, R<sup>1</sup> = Me **35a-c**: R = R<sup>1</sup> = Et

### Scheme 8

**Table 4** Electronic absorption data of the squarylium derivatives 32–35 (data abstracted from [31])

Compound	X	$\lambda_{max} (nm)^a$	$\log(\varepsilon/\mathrm{M}^{-1}~\mathrm{cm}^{-1})$
32a	S	650	5.24
32b	Se	665	5.49
32c	CH=CH	707	5.39
33a	S	632	5.27
33b	Se	647	5.28
33c	CH = CH	671	5.62
34a	S	659	5.23
34b	Se	674	5.26
34c	CH = CH	707	5.43
35a	S	668	5.27
35b	Se	686	5.22
35c	CH=CH	719	5.55

<sup>&</sup>lt;sup>a</sup> Data obtained in MeOH/CH<sub>2</sub>Cl<sub>2</sub> (99/1, v/v)

to a bis(dithiolate)copper(II) anion. Nevertheless, the aminosquarylium dyes are photochemically less stable than squarylium dyes.

An improved synthesis of aminosquarylium dyes involves methylation of the oxygen atom in the cyclobutene core of the squarylium dye 32 followed by nucleophilic displacement of the resultant methoxy group in the intermediate product 33 by a primary or secondary amine, as shown in Scheme 8 [31]. The yields of the methylation steps were 76–95%, and the aminosquarylium dyes 34 and 35 were obtained from the corresponding squarylium dyes in overall yields of 44–89%. Optical properties of the dyes 32–35 are listed in Table 4.

Synthesis of a dithiosquarylium analogue 36 by the reaction of the corresponding squarylium dye with the Lawesson's reagent or  $P_4S_{10}$  was also reported by Kim et al. (Eq. 2) [32]. The dye 36 exhibits red-shifted electronic absorption by 27 nm in comparison to absorption of the corresponding squarylium dye. The shape of the absorption is similar to that of the squarylium, showing a large and narrow band. The molecular structure of 36 was confirmed by X-ray crystallographic analysis [33].

**Equation 2** Method A; Lawesson's reagent/HMPA, reflux. Method B; P<sub>4</sub>S<sub>10</sub>/pyridine, reflux

# 2.4 $\pi$ -Extended Squarylium Dyes and Analogues

From the technological viewpoint, color tuning of dyes has been an important objective because the absorption properties of the dyes involved in photonic and optoelectronic devices are closely related to the light sources in determining the device performance. In particular, the design of NIR-absorbing chromophoric systems is of immense current interest because the inexpensive Ga-As-Al diode lasers are used as light sources in applications such as xerography, optical recording, and sensory devices. In the present section, construction of extended  $\pi$ -conjugation systems using squarylium-based chromophores is reviewed. Using a variety of starting materials with large  $\pi$ -conjugation structures and taking into account reactivity of a squarylium dye enables us to design novel NIR-absorbing chromophores.

In order to obtain  $\pi$ -extended electronic structures, stilbenoid compounds have been used as starting materials. The stilbenoid substrates are available employing Wittig-type reactions. Meier and Dullweber prepared the stilbenederived squarylium dyes 37–42 (Eq. 3), the absorption maxima of which

Compound	$R^1$	$\mathbb{R}^2$	$\mathbb{R}^3$	Yield (%)	λ <sub>max</sub> (nm) <sup>a</sup>
37 38 39 40 41 42	$\begin{array}{c} H \\ H \\ OC_6H_{13} \\ OC_6H_{13} \\ OC_6H_{13} \\ OC_6H_{13} \end{array}$	$\begin{array}{c} OC_6H_{13} \\ OH \\ OC_6H_{13} \\ H \\ OC_6H_{13} \\ OMe \end{array}$	$H$ $H$ $OC_{6}H_{13}$ $OC_{6}H_{13}$	33 49 28 16 20 21	714 696 730 680 727 735

**Table 5** Structures, yields, and electronic absorption data of the squarylium derivatives 37–42 (data abstracted from [34])

ranged from 680 nm to 735 nm in CHCl<sub>3</sub> solutions (Table 5) [34]. Meier et al. also prepared dendric molecules of the stilbenoid-based squaryliums 43–47, achieving construction of chromophoric assemblies with large light absorptivity [35]. It is interesting to note that the stilbene-linked bis-squarylium dye 43 exhibits the electronic absorption maximum at 778 nm, which matches the output of the commercial Ga-As-Al diode laser.

HO

OH

HO

$$R^1$$
 $R^2$ 
 $R^3$ 

BuOH/toluene

reflux

 $R^3$ 
 $R^3$ 
 $R^4$ 
 $R^3$ 
 $R^4$ 
 $R^3$ 
 $R^4$ 
 $R^4$ 

#### **Equation 3**

The stilbenoid-based squarylium dye with electrochromic activity 48 was reported by Ajayaghosh et al. [36]. The dye 48 can be oxidized to the radical cation and dication and reduced to the radical anion. The electrochemical interconversion occurs reversibly. The dye exhibits absorption at 678 nm, and upon the one-electron oxidation, it shows NIR absorption bands at 1000 and 1600 nm. Further oxidation leads to disappearance of these absorption bands, and new light absorption appeared at 850 nm, assignable to the electronic absorption of the dication of 48. On the other hand, significant bleaching of the absorption of the neutral dye occurs upon one-electron reduction.

<sup>&</sup>lt;sup>a</sup> Data obtained in CHCl<sub>3</sub>

The unique cationic squarylium analogue **49** was synthesized by Nakazumi et al. [37]. The cationic dye **49a** was produced by the reaction of 1-butyl-2-benzothiazolium iodide with squaric acid under azeotropic conditions (a 1-butanol/benzene mixture, reflux) (Scheme 9). This dye is deeply colored, exhibiting an intense absorption band in the NIR region ( $\lambda_{\text{max}} = 797 \text{ nm}$ ,  $\log \varepsilon = 5.44$ , in CHCl<sub>3</sub>). By anion exchange with tetraphenylborate BPh<sub>4</sub> $^-$ , a single crystal suitable for X-ray crystallographic analysis was obtained and, thus, the molecular structure of the dye **49b** was confirmed (Fig. 4). The  $\pi$ -conjugation system is extended from one benzothiazolino-squaryl moiety

#### Scheme 9

Fig. 4 Molecular structure of the cationic squarylium analogue 49b. Hydrogen atoms and tetraphenylborate anion are omitted for clarity

to the other via the central methine carbon with the help of intramolecular hydrogen bonding. On the other hand, the central benzothiazolium subunit is barely involved in the  $\pi$ -conjugation because the dihedral angle between the carbon-bridged bis-squarylium subunit and the benzothiazolium subunit is 62.5°. Upon treatment of **49a** with sodium hydroxide, a di-zwitterionic neutral dye was obtained (not shown).

A series of unsymmetrical analogues of the cationic dye 49 was prepared by the reaction of the benzothiazolino-squarylium dye 6 with monosubstituted squaric acid derivatives 50 or 52 (Eqs. 4 and 5) [38]. Two methods were examined for the dye preparation. The precursors 50a and 50b were allowed to react with the squarylium dye 6 under azeotropic conditions (a 1-butanol/benzene mixture, reflux) in the presence of HI, yielding the

cationic dyes **51a** and **51b** in 72% and 35% yields, respectively, as iodides (method A). In method B, the diethyl squarates **52a–c** were used as the starting materials. The unsymmetrical dyes **53a–c** were obtained as tetraphenylborates in yields of 10-17% after anion exchange. The dyes **51** and **53** exhibit NIR absorption in the range from 771 nm ( $\log \varepsilon = 5.02$ ) for **51a** to 815 nm ( $\log \varepsilon = 5.43$ ) for **51b**. In the <sup>1</sup>H NMR spectra of these dyes, the signal of the

### Method A

### **Equation 4**

#### Method B

### **Equation 5**

OH proton is observed at  $\delta$ 18–19, indicating that the OH group is involved in hydrogen bonding. Thus, the intramolecular hydrogen bonding should keep high planarity of the bis-squarylium  $\pi$ -conjugation system.

Related dyes 54a-c were reported by Yagi and Nakazumi (Eq. 6) [39]. These dyes were obtained in 3-10% yields by the reaction of an anilino-substituted squaric acid with an excess of tributyl orthoformate in 2-propanol under reflux. In comparison with the cationic dyes 51 and 53, the dyes 54 are neutral. The structure of 54a was confirmed by X-ray crystallographic analysis (Fig. 5), where the methine-bridged bis-squarylium skeleton shows high planarity, indicating an extensively  $\pi$ -conjugated structure. Intramolecular hydrogen bonding bridging the squaryl moieties was also found, and this noncovalent interaction was also indicated in solution by  $^1$ H NMR spectrum showing a large downfield shift of the OH proton to ca.  $\delta19$ . The unique electronic structure of the dyes 54 is reflected in the intense light absorption in the NIR region.

**54a**:  $R^1$ ,  $R^2$  = Bu  $\lambda_{max}$ = 828 nm (log  $\epsilon$  = 5.44)

**54b**:  $R^1$  = Me,  $R^2$  =  $C_{12}H_{25}$   $\lambda_{max}$ = 815 nm (log  $\epsilon$  = 5.59)

**54c**:  $R^1$  =Me,  $R^2$  =  $C_{16}H_{33}$   $\lambda_{max}$ = 815 nm (log  $\epsilon$  = 5.40)

### **Equation 6**

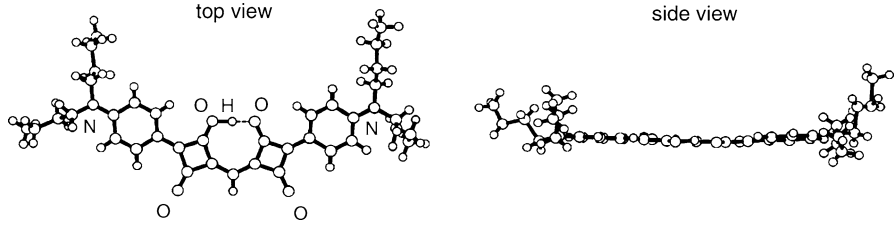


Fig. 5 Molecular structure of the neutral squarylium analogue 54a

### 2.5 Bis-squarylium Dyes

Yagi and Nakazumi reported the synthesis of a series of arene-bridged bis-squarylium dyes [40–42] (Scheme 10). The key substrates are arene-bridged bis-squaric acids, which react with hetrocyclic quaternary salts at both squaric acid moieties. These compounds are available, employing the palladium-promoted cross-coupling reaction of tributylstannylsquarate with dihalogenated arenes followed by hydrolysis. This Stille-type reaction has been developed by Liebeskind [43]. As shown in Scheme 10, the m- and p-phenylene-bridged and 4,4'-biphenylene-bridged bis-squaric acids 55a-c

Scheme 10

were prepared and allowed to react with a series of heterocyclic quaternary salts under typical conditions for squarylium synthesis to yield bissquarylium dyes 56-59 [40]. The yields and optical properties of the obtained dyes are summarized in Table 6. The optical properties depend on the spacer, with the electronic absorption maxima in CHCl<sub>3</sub> solution ranging from 543 nm to 768 nm. The p-phenylene-bridged dyes exhibit more redshifted absorption and large molar absorptivity ( $\log \varepsilon > 5.0$ ) relative to the m-bridged dyes. The X-ray diffraction analysis of the dye 56a is shown in Fig. 6. The structure is planar with the  $\pi$ -conjugation system extended over the whole molecule. The possible resonance structure of the p-phenylenebridged dye 56a is shown in Scheme 11a, where the  $\pi$ -conjugation is extended across the phenylene spacer. On the other hand, the m-bridged dye **56b** exhibits blue-shifted absorption relative to the *p*-bridged analogues. This hypsochromic effect of 127–198 nm is explained by the resonance structures shown in Scheme 11b, where the  $\pi$ -conjugation is terminated at the central phenylene moiety. The bathochromic shifts in the biphenylene-bridged dyes **56c** and **57c** relative to the *m*-bridged dyes **56b** and **57b** are modest because the biphenylene spacer is not planar, partially inhibiting  $\pi$ -conjugation. The fluorescence emission properties of 56-59 were also investigated. Some com-

**Table 6** Yields and electronic absorption and emission data of squarylium analogues 56–59 (data abstracted from [40])

Compound	Yield (%)	$\lambda_{\max}$ (nm) $(\log \varepsilon)^a$	$\lambda_{em}$ (nm) (relative intensity)
56a	75	699 (5.25) 635 (4.93)	714 (126)
56b	<b>5b</b> 22		587 (56)
56c	45	618 (5.28)	656 (226)
57a	90	685 (5.28) 623 (4.99)	706 (206)
57b	30	543 (5.15) 479 (4.71)	586 (34)
57c	60	609 (5.01)	651 (157)
58a	8	704 (5.29) 641 (4.98)	736 (77)
59a	8	768 (5.13) 692 (4.80)	809 (15)
59b 4e	12	570 (5.30) 640 (5.50)	571 (3.4) 667 (2000)

 $<sup>^{\</sup>rm a}~\varepsilon~{\rm in}~{\rm M}^{-1}~{\rm cm}^{-1}$ 

Fig. 6 Molecular structure of the bis-squarylium dye 56a

pounds show emission in the visible-to-NIR regions (571–809 nm), although the intensity is lower than that of the dye 4 (Table 6).

Yagi and Nakazumi also employed polycyclic arene spacers such as anthracene and pyrene to prepare bis-squarylium dyes 60-63 [41, 42]. The anthracene- and pyrene-bridged dyes 60 and 61 have lower energy gaps of the electronic transitions compared to the phenylene- and biphenylene-bridged dyes with the same heterocyclic components (56a and 56c, respectively) and, as a consequence, exhibit absorption maxima in the NIR region with the absorption bands broadened. The absorption maxima of the reference squarylium dyes 64 and 65 are significantly blue-shifted compared to the corresponding bis-squarylium dyes. Thus, the anthracene and pyrene spacers give rise to extension of the  $\pi$ -conjugation system over the whole molecule.

In further development of the bis-squarylium dyes, the thiophene-bridged dyes 66-68 were investigated. Their optical properties are summarized in

#### Scheme 11

Table 7. It is interesting to note that the mono-thiophene-bridged dyes exhibit electronic absorption in the NIR region in spite of relatively short  $\pi$ -conjugation of the thiophene. As the number of the thiophene unit increases, the absorption maxima shift hypsochromically. This can be explained in terms of the inhibition of the  $\pi$ -conjugation by non-planarity of the thiophene subunits, as mentioned for the biphenylene-bridged dyes 56c and 57c.

## 2.6 Squarylium Analogues Derived from Bisquarate

As shown in Sect. 2.3, modification of the central 4-membered ring of squarylium dyes results in variation of optical properties. Nakazumi and Yagi reported the preparation of a series of new squarylium analogues 70–73 by employing bisquarate in place of squaric acid [44] (Scheme 12 and Table 8). The preparation of isopropyl bisquarate 69 was reported by Liebeskind

et al. [45] by a coupling reaction of isopropyl tributylstannylsquarate with chlorosquarate in the presence of a palladium catalyst. An attempted reaction of bisquaric acid, obtained by hydrolysis of 69, with heterocyclic enamines was not successful, whereas the condensation of the bisquarate 69 with a het-

Compound	$\lambda_{\max}$ (nm) $(\log \varepsilon)^a$	
66a	785 (5.4), 708 (5.0)	
66b	771 (5.1), 705 (5.0)	
66c	735 (5.1), 695 (5.1)	
67a	772 (5.2), 696 (4.8)	
67b	725 (4.9), 687 (5.0)	
67c	717 (5.0), 784 (5.0)	
68a	807 (5.4), 728 (5.0)	

Table 7 Electronic absorption data of the squarylium homologues 66-68

### Scheme 12

erocyclic quaternary salt in the presence of triethylamine yielded squarylium analogues 70–73 in 36–67% yields. The structure of the bisquarate-based dye 70 was confirmed by X-ray crystallographic analysis (Fig. 7). Spectral data for 70–73 are given in Table 8.

The preparation of unsymmetrical derivatives of this class was achieved by using mono-substituted bisquarates (Scheme 13). Typical synthesis is shown in Scheme 13. The reaction of 3,4-dichloro-3-cyclobutene-1,2-dione with 1-butyl-2,3,3-trimethylindolium followed by a palladium-promoted cross-coupling reaction of the resultant product with isopropyl tributylstannylsquarate afforded

 $<sup>^{\</sup>rm a}~\varepsilon~{\rm in}~{\rm M}^{-1}~{\rm cm}^{-1}$ 

**Table 8** Structures, yields, and electronic absorption data in CHCl<sub>3</sub> solutions of the symmetrical dyes 70–73 (data abstracted from [44])

	0	Y Y	0
Compound	R	Ö R Yield (%)	$\lambda_{max}$ (nm) (log( $\epsilon/M^{-1}$ cm <sup>-1</sup> ))
	Me Me		
70		39	657 (4.87)
	N Bu		601 (4.73)
71	S	67	653 (4.92)
	N     Bu		595 (4.73)
72		41	692 (5.04)
	Bu N—		628 (4.79)
73	——N−Bu	36	757 (5.14)
			682 (4.76)

**Fig. 7** Molecular structure of the bisquarate-based squarylium analogue **70**. Hydrogen atoms are omitted for clarity

the intermediate bisquarate 74a. The subsequent reaction of 74a with 1-butyl-2-methylbenzothiazolium iodide in the presence of triethylamine yielded the unsymmetrical bisquarate-based dye 75a. Employing 1-butyl-2-methyl and 1-butyl-4-methylquinolinium salts yielded 75b and 75c, respectively (Table 9). Aniline derivatives 74b–d were also used to obtain the unsymmetrical dyes 76–78. These dyes are characterized in Table 9. The absorption maxima of these unsymmetrical dyes varied from 640 nm to 705 nm in CHCl<sub>3</sub>. The  $\lambda_{\rm max}$  of the unsymmetrical dye is an averaged value of the absorption bands of the symmet-

#### Scheme 13

rical dyes possessing the corresponding aromatic or heterocyclic components. For instance, the value of  $\lambda_{max}$  of 75c (705 nm) is approximately half of the sum of 657 nm for 70 and 757 nm for 73. Thus, it is possible to predict absorption of the bisqurate-based dyes without using theoretical methods.

# 3 Applications of Squarylium Dyes

# 3.1 Squarylium Dyes as Photo-conducting Materials

As copying and printing technology has evolved, organic photoconductive materials have received much attention as xerographic photoreceptors. The

Table 9 Structures, yields, and electronic absorption data in CHCl<sub>3</sub> solutions of the unsymmetrical dyes 75–77 (data abstracted from [44])

		0 R <sup>1</sup> 0	=0	
Compound	$\mathbb{R}^1$	$R^2$	Yield (%)	$\lambda_{\mathrm{max}}$ (nm) (log( $\varepsilon/\mathrm{M}^{-1}\mathrm{cm}^{-1}$ ))
75a	Me Me	S N Bu	70	653 (5.01) 598 (4.85)
75b			50	672 (5.02) 613 (4.82)
75c		N-Bu	50	705 (5.10) 641 (4.82)
76a	$-$ \bigset NEt <sub>2</sub>	S N Bu	38	640 (4.71) 600 (4.68)
76b			70	648 (4.73) 620 (4.72)
77a	$-$ \bigsim NBu <sub>2</sub>	S N Bu	33	642 (4.70) 604 (4.67)
77b			30	649 (4.73) 620 (4.72)
78a	-\sqrt{\sqrt{N}}	S N Bu	35	656 (4.70) 620 (4.61)
78b		N-	30	673 (4.73) 630 (4.67)

availability of Ga-Al-As diode lasers emitting in the NIR region (ca. 780 nm) has facilitated the demand for organic photoconductors with response to the NIR light. The photoconductivity of squarylium dyes was found in 1974 [46]. Thereafter, aniline-derived squarylium dyes have been intensively studied because they exhibit broad and intense absorption bands from the visible to

$$Me_2N$$
 $NMe_2$ 
 $NMe_$ 

the NIR region. The major studies of photoconductive squarylium dyes, including synthesis, solid-state chemistry, and xerographic performance, have been carried out by Law and coworkers [47-51]. Representative examples of photoconductive squarylium dyes are 4a and 79a-c. These dyes exhibit visible-to-NIR absorption in the solid state, but they show narrow and intense absorption bands at ca. 625-645 nm in solution. It has been suggested that the vis-to-NIR absorption, suitable to the diode laser-based xerography, is due to the intermolecular charge transfer (CT) interaction. In X-ray powder diffraction and single-crystal studies [52, 53], the stacking between the anilino moiety of one molecule and the central ring of the neighboring molecule was found to be ca. 3.5 Å, indicating that the intermolecular donor-acceptor CT interaction results in a specific arrangement of the dye molecules. Introduction of N-alkyl substituents longer than ethyl diminishes the intermolecular CT interaction, and the bathochromic effect in the solid-state absorption is small. Indeed, in the X-ray structure of the anilinosquarylium dye 4e (Sect. 2.1), the dibutylamino group of one molecule is located over the central ring of the other molecule, but the mean-plane distance of the  $\pi$ -conjugated planes (ca. 3.9 Å) is longer than that observed for 79c [54].

In an attempt to improve the xerographic performance of squarylium dyes, Law et al. synthesized a series of unsymmetrical dyes (Sect. 2.2). Low dark-decay ( $\Delta V/\Delta t$ ; the decrease in the electric potential per unit time upon the dark-discharge process) as well as high sensitivity, i.e., a low  $E_{0.5}$  ( $E_{0.5}$ ; the energy required to discharge the initial electric potential to half upon photoir-radiation), are required to develop good xerographic devices. In particular, the unsymmetrical dye 14d exhibits very low values of  $\Delta V/\Delta t$  (-15 V s<sup>-1</sup>) and  $E_{0.5}$  (3.1 and 1.9 erg cm<sup>-2</sup> upon exposure to 600 nm and 790 nm light, respectively), showing high xerographic performance among the photoconductive squarylium dyes studied by Law et al. [55].

## 3.2 Squarylium Dyes as Photosensitizers in Photovoltaic Devices

Because of the global fuel energy shortage, sunlight has been receiving increasing attention as an alternative energy. The greenhouse gas problem,

mainly caused by combustion of fossil fuels, also has made us consider the use of solar energy. In this respect, solar energy conversion devices have been developed, and those based on inorganic photoconductors, such as silicon devices, have been commercialized. From the viewpoint of the low cost of preparation, photoenergy conversion devices based on organic materials, i.e., organic solar cells, have been attracting an increasing interest. The application of squarylium dyes to organic solar cells is described as follows.

In the early work, a squarylium dye was applied to a Schottky barrier-type solar cell, taking advantage of its photoconductive properties. In such a device, the anilino-squarylium dye  $80\ [56]$  was sandwiched by two electrodes (transparent  $In_2O_3$  and metal electrodes). The photo-initiated generation of the hole–electron pair enabled photoenergy-to-electricity conversion, but the efficiency was less than 1%. Thereafter, squarylium dyes have been used mainly as photosensitizers for inorganic semiconductors such as  $TiO_2$  and ZnO. Organic dye-sensitized solar cells (DSSCs) using ruthenium complexes as the sensitizers for  $TiO_2$  electrodes have realized relatively high energy conversion efficiencies (more than 10%) and have been widely studied

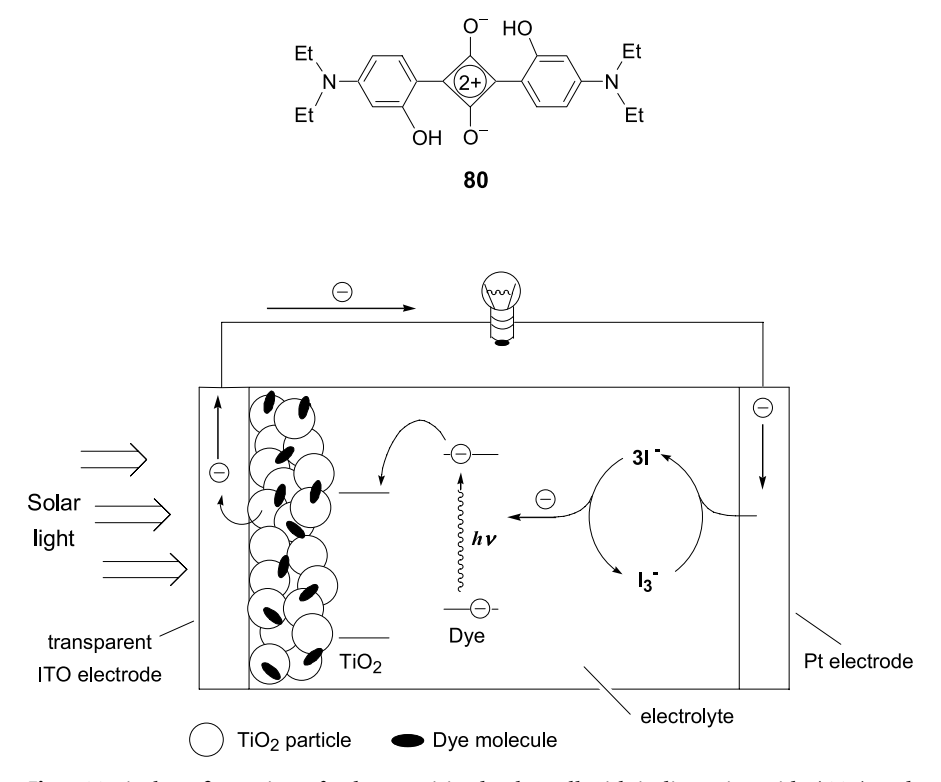


**Fig. 8** Typical configuration of a dye-sensitized solar cell with indium-tin-oxide (ITO) and platinum electrodes

(Fig. 8) [57-59]. From the viewpoints of low-cost fabrication and saving of precious metal resources, organic dyes have been increasingly focused on. In order to have organic dyes adsorbed on a TiO2 surface, a carboxyl anchor group forming a titanate bond is required. Hence, squarylium dyes with carboxylate groups have been investigated. Wang and Zhang applied a series of anilino-squarylium dyes 81-84 to DSSC [60], and the photoelectric conversion efficiencies of the solar cells employing 83 and 84 were 3.2 and 3.4%, respectively. Development of the synthesis of unsymmetrical squarylium dyes has extended the availability of squarylium-based sensitizers. Das et al. improved the photoelectric conversion efficiency employing the unsymmetrical dyes 89-91 [61]. Although the solar cells with the symmetrical dyes 85-88  $(\lambda_{\text{max}} = 630-670 \text{ nm in MeOH})$  showed conversion efficiencies of 0.06-1.04%, those with 89-91 ( $\lambda_{\text{max}} = 600-630 \text{ nm}$  in MeOH) afforded conversion efficiencies of 1.25-2.08% upon exposure to visible-NIR light. The results of molecular orbital calculations have suggested that the intramolecular charge transfer upon the HOMO-LUMO transition gives rise to the directional flow

Me Me O Me Me Me 92: 
$$\lambda_{max} = 663 \text{ nm}$$
HN<sup>+</sup>Et<sub>3</sub> COO OC HN<sup>+</sup>Et<sub>3</sub>

of the electron from the anilino moiety to the carboxyl-anchored heterocycle to achieve effective electron injection to TiO<sub>2</sub>, leading to relatively high conversion efficiencies.

In order to improve the performance of solar cells, the efficient use of NIR solar illumination has been receiving increased interest. Current dyesensitizers for photoenergy conversion are effective only with visible light, but solar light ranges from the visible to the NIR regions. Squarylium dyes are suitable candidates for harvesting the NIR light. Recently, Grätzel et al. developed a solar cell with the squarylium dye 92 absorbing red light [62]. They prepared liquid and solid cells (the cells composed of liquid and solid electrolytes, respectively), and achieved photoelectric conversion efficiencies of 3.7 and 1.5%, respectively. It is noteworthy that these conversion efficiencies for both types of cells are the highest values of the squarylium-based DSSCs so far reported. In a further attempt to improve DSSC performance, sensitization of TiO<sub>2</sub> by a co-adsorbed mixture of ruthenium complex and squarylium dye has also been examined (so-called "cock-tail cells") [62–64].

# 3.3 Squarylium-based Conjugated Polymers as Conductive Materials

Low band-gap  $\pi$ -conjugated polymers have received much attention with respect to application in electroconductive devices [65-67]. Conjugated squarylium-based polymers were first reported by Treibs and Jacob in their report on the synthesis of the pyrrole-derived squarylium dyes [9]. The synthesis and conducting properties of squarylium-based polymers have been developed by Ajayaghosh et al. [68-71]. Thus, polymerization of electronrich pyrroles without substituents at the 2- and 5-positions with squaric acids yielded the squarylium-based  $\pi$ -conjugated polymers 93–96 [68, 69] (Scheme 14). Depending on the reaction conditions, two types of resonancestabilized zwitterionic polymers were selectively obtained as shown. Polymers 93 and 95 constitute the first class of products, and block copolymers 94 and 96 are the second type of products. Broad electronic absorption spectra in which shoulders reach the NIR region are observed for thin films of these polymers, with  $\lambda_{\text{max}}$  around 630-640 nm. The low band-gap features result in electrical conductivity without any chemical doping. The block copolymers 94 and 96 exhibit higher conductivity  $(2.5 \times 10^{-6})$  and

### Scheme 14

 $2.3\times10^{-5}~{\rm S~cm^{-1}}$  for **94** and **96**, respectively) than the polymers **93** and **95** ( $2.4\times10^{-6}$  and  $2.5\times10^{-6}~{\rm S~cm^{-1}}$ , respectively). Doped with iodine, the conductivities of these polymers were significantly improved and reached values of  $2.5\times10^{-4}~{\rm S~cm^{-1}}$  for **93**,  $1\times10^{-3}~{\rm S~cm^{-1}}$  for **94**,  $6.0\times10^{-4}~{\rm S~cm^{-1}}$  for **95**, and  $1.8\times10^{-3}~{\rm S~cm^{-1}}$  for **96**.

Employing electron-rich bienamine heterocycles yielded low band-gap polymers 97 and 98, as reported by Havinga et al. (Eq. 7) [72]. These polymers exhibit small band-gaps in the solid state, 1.15 eV for 97 and

$$\begin{array}{c} X \\ N \\ N \\ N \end{array} \begin{array}{c} X \\ N \end{array} \begin{array}{c} X \\ N \\ N \end{array} \begin{array}{c} X \\ N \end{array} \begin{array}{c} X \\ N \\ N \end{array} \begin{array}{c} X \\ N \\ N \end{array} \begin{array}{c} X \\ N \end{array} \begin{array}{c$$

### **Equation 7**

Scheme 15

 $0.8 \, \mathrm{eV}$  for 98, as estimated by the cut-off of their absorption bands, and exhibit electric conductivity on the order of  $10^{-7} \, \mathrm{S \, cm^{-1}}$ . The solid samples heavily doped with iodine as well as the thin cast films doped with 2,3-dichloro-4,5-dicyanobenzoquinone exhibit extraordinary conductivities reaching  $1 \, \mathrm{S \, cm^{-1}}$ .

Ajayaghosh et al. prepared another type of squarylium-based  $\pi$ -conjugated polymers, employing a stilbenoid dipyrryl monomer [71]. Thus, condensation of **99a-g** with two equivalents of squaric acid afforded the squarylium-based polymers **100a-g** (Scheme 15, route A). The same polymers were obtained by starting with the squarylium derivatives **101** which were obtained by condensation of two equivalents of **99** with one equivalent of squaric acid (Scheme 15, route B). These polymers exhibit broad electronic absorption in the visible-to-NIR region, showing low band-gap optical features (band gaps of

Compound	Inter-column distance (Å) $d_1$	Inter-layer (Å) d <sub>2</sub>	distance $d_3$	Intrinsic conductivity (S cm <sup>-1</sup> )	Iodine-doped conductivity (S cm <sup>-1</sup> )
100a 100b 100c 100d 100e 100f 100g	11.0 14.7 19.2 17.0 18.4 20.5 21.0	5.3 4.6 4.6 4.4 4.2 4.3 4.5	3.4 3.4 3.8 - -	$5.30 \times 10^{-4}$ $8.75 \times 10^{-4}$ $4.21 \times 10^{-6}$ $2.20 \times 10^{-5}$ $4.40 \times 10^{-6}$ $6.20 \times 10^{-6}$ $6.30 \times 10^{-7}$	$5.20 \times 10^{-2}$ $2.98 \times 10^{-2}$ $6.17 \times 10^{-2}$ $1.10 \times 10^{-2}$ $2.80 \times 10^{-2}$ $5.10 \times 10^{-2}$ $1.10 \times 10^{-2}$

**Table 10** X-ray diffraction and electric conductivity data of the polymer **100** (data abstracted from [71])

0.7-1.1 eV). Their intrinsic electric conductivity ranges from  $6.3 \times 10^{-7}$  S cm<sup>-1</sup> to  $5.3 \times 10^{-4}$  S cm<sup>-1</sup>, depending on the length of the N-alkyl groups at the pyrrole units. As the length of the alkyl group increases, the band-gap increases also, resulting in a decrease in conductivity (Table 10). The X-ray diffraction analysis of the polymers 100 revealed that the inter-column distance ( $d_1$  in Table 10) in the molecular packing geometry of the polymer backbone is tuned by the alkyl side chains although the stacking of the polymer layers is present for all polymers ( $d_2$  and  $d_3$  in Table 10). Hence, the intrinsic conductivity is affected by the polymer chain packing, modulated between  $10^{-7}-10^{-4}$  S cm<sup>-1</sup>. By exposing the polymer samples to iodine vapor the conductivity was significantly improved, up to  $10^{-2}$  S cm<sup>-1</sup>. Thus, squarylium-based  $\pi$ -conjugated polymers are good candidates for low band-gap polymers.

# 3.4 Application of Squarylium Dyes to Biological and Environmental Analyses

Organic dyes have frequently been used as labeling and sensing materials to detect biologically and environmentally important molecules and ions because their optical properties such as light absorption and fluorescent emission are often sensitively perturbed by electrostatic interactions or chemical reactions with those molecules and ions. For such analytical uses, the following types of dye-based sensing materials have been investigated: (1) dyes that bind to the analyte, (2) dyes that are conjugated with the synthetic receptor of the analyte, and (3) dyes that undergo a selective binding reaction with the analyte. These dyes should exhibit dramatic changes of their optical properties detectable by the naked eye or spectroscopic methods, when affected by external chemical stimuli. In this section, recent developments in the area of analytical chemistry using materials based on squarylium chromophores and fluorophores are described.

In attempts to develop non-destructive detection methods for proteins, squarylium-based labeling materials have been investigated. Since squarylium dyes are fluorescent from the far-visible to the NIR region, read-out of fluorescent signals from squarylium chromophores is free of background emission from analytes, leading to accurate quantitative analysis. Lakowicz et al. attempted to apply symmetrical and unsymmetrical squarylium dyes 102a-e to fluorometric analysis of bovine serum albumin (BSA) [26]. In methanol, the dyes exhibit electronic absorption at 628-635 nm and fluorescence at 644-662 nm (quantum yield  $\Phi_{\text{MeOH}}$  = 0.07-0.10), as shown in Table 11. The addition of 102a-e to aqueous solutions of BSA resulted in a dramatic enhancement of fluorescence ( $\Phi_{RSA} = 0.34$ -0.78), although only slight bathochromic shifts of the electronic absorption spectra were observed. The fluorescence enhancement could be caused by specific complexation of the dyes to the hydrophobic binding site of BSA. The indolenine-based symmetrical squarylium dyes 102a and 102b exhibited large emission enhancement of up to  $\Phi_{BSA}$  = ca. 0.7 and showed high photostability upon exposure to ambient light (< 10% bleaching in BSA-H<sub>2</sub>O, after 120 h) in the presence of BSA. The indolenine-based unsymmetrical

$$R^{2}$$

$$X$$

$$Q^{-}$$

$$R^{1}$$

$$Q^{-}$$

$$R^{3}$$

$$R^{4}$$

**102a**:  $X = CMe_2$ ,  $R^1 = R^3 = Et$ ,  $R^2 = R^4 = H$ 

**102b**:  $X = CMe_2$ ,  $R^1 = R^3 = Me$ ,  $R^2 = R^4 = CI$ 

**102c**:  $X = CMe_2$ ,  $R^1 = R^3 = Me$ ,  $R^2 = CI$ ,  $R^4 = H$ 

**102d**: X = S,  $R^1 = Me$ ,  $R^3 = Et$ ,  $R^2 = R^4 = H$ 

**102e**: X = S,  $R^1 = Me$ ,  $R^3 = Et$ ,  $R^2 = H$ ,  $R^4 = CI$ 

**Table 11** Electronic absorption and fluorescence data of the squarylium dyes 102a-e in alcohol and BSA aqueous solutions (data abstracted from [26])

Com-	λ <sub>max</sub> (nı	n)	λ <sub>em</sub> (nm	n)	Quantur	n yield	Mean lif	Tetime (ns)
pound	MeOH	BSA	MeOH	BSA	<i>i</i> -PrOH	BSA	MeOH	BSA
102a	628	636	644	669	0.09	0.70	0.20	3.25
102b	632	642	653	652	0.10	0.68	0.21	2.80
102c	629	643	648	655	0.07	0.34	0.20	2.29
102d	635	647	651	662	0.10	0.78	0.24	3.53
102e	634	651	653	661	0.08	0.34	0.26	3.01

dye 102c also showed high photostability upon complexation with BSA, but the fluorescence was less efficient ( $\Phi_{\rm BSA}=0.34$ ). On the other hand, the unsymmetrical dye 102d, composed of indolenine and benzothiazole heterocycles, exhibited less photostability (55% bleaching in BSA-H<sub>2</sub>O, after 120 h) although the fluorescence enhancement was most effective. Another spectroscopic feature of the squarylium dyes 102 is prolonged fluorescent lifetime upon binding to BSA. The lifetime of these dyes in the presence of BSA in aqueous solution was one order of magnitude longer than that in methanol without the analyte. Thus, the BSA detection by time-resolved fluorometric technique is possible taking advantage of such particular photophysical properties [73,74].

From a practical viewpoint, the low solubility of squarylium dyes in aqueous solvents is a serious problem in analyses of water-soluble biomolecules.

**Table 12** Electronic absorption and fluorescence data and stability constants  $K_s$  of the squarylium dyes 103 and 104 upon complexation with HSA (data abstracted from [75])

Com- pound	without HSA a $\lambda_{max}$ (nm) $(\log \varepsilon)^e$	$\Phi_{ m em}$	λ <sub>max</sub> (nm)	with HSA <sup>b</sup> $\lambda_{em}$ (nm) <sup>c</sup>	$\Phi_{ m em}$	$K_s (M^{-1})^d$
103a 103b 103c 103d	564 (4.81) 550 (4.89) 604 (4.96) 558 (4.66)	0.05 0.05 0.03 0.04	621 550 643 656	656 618 654 677	0.70 0.39 0.92 0.06	$8.7 \times 10^{5}$ $1.1 \times 10^{6}$ $8.0 \times 10^{5}$ $1.7 \times 10^{5}$
104	658 (5.08)	0.01	658	680	0.34	$5.8 \times 10^6$

 $<sup>^{\</sup>rm b}$  5.0  $\times$  10  $^{\rm -7}$  M solution of the dye dissolved in trizma buffer (pH 7.4) with 5.0  $\times$  10  $^{\rm -6}$  M HSA at 298 K

 $<sup>^{\</sup>text{c}}$  The  $\lambda_{\text{em}}$  in the presence of HSA was the same as that in the absence of HSA for each dve

<sup>&</sup>lt;sup>d</sup> Obtained by fluorescence titration experiments

<sup>&</sup>lt;sup>e</sup>  $\varepsilon$  in M<sup>-1</sup> cm<sup>-1</sup>

Nakazumi and Yagi introduced a carboxyl tail to a squarylium skeleton to improve the solubility in water [75]. The reported unsymmetrical dyes 103 and 104 exhibit high solubility in polar solvents (see Sect. 2.2 for preparation). A small volume of a methanolic solution of the dye can be diluted in a trizma buffer solution without precipitation. For all the dyes except 103d, fluorescence enhancement was observed upon binding to human serum albumin (HSA), as shown in Table 12. In particular, the quantum yield of 103c reached 0.92, giving the limit detection of 2 nM HSA under the signal-to-noise ratio of 15. Job's analysis based on fluorescence changes revealed that the complexation stoichiometry was 1:1, and the binding constant, also determined by fluorescene spectroscopy, ranged from  $1.7 \times 10^5$ to  $5.8 \times 10^6 \,\mathrm{M}^{-1}$ . HSA has three substrate-binding sites, namely digitoxin, warfarin, and diazepam sites. From the results of the competitive binding experiments, it was concluded that these squarylium dyes bind to the warfarin site. The emission enhancement of 103a was also observed in the presence of BSA. Using the water-soluble squarylium dyes, researchers have analysed proteins by capillary electrophoresis with laser-induced fluorescence detection [76, 77].

Inspired by the development of crown ethers, many chemists became interested in the design of chemosensory systems based on ionophore-dye conjugates [78-80]. The development of squarylium-based ionophores has also been focused on selective sensing of metal ions [81-85]. In order to maximize electronic perturbation between the chemosensor and an analyte, the binding site should be included in the squarylium chromophore. Akkaya et al. developed the squarylium dye 105, in which monoazacrown ethers were integrated into the aniline moieties [81, 82]. The chromoionophore 105 was prepared by one-pot synthesis using 1,3,5-trihydroxybenzene, aza-18crown-6, and squaric acid (Eq. 8). The addition of a series of alkaline earth metal ions to an acetonitrile solution of 105 (free ligand:  $\lambda_{max} = 640 \text{ nm}$ ,  $\varepsilon = 240\,000\,\mathrm{M}^{-1}\,\mathrm{cm}^{-1}$ ), caused blue shifts and hypochromic effects in light absorption and a decrease in fluorescence intensity. Significant changes were observed in the presence of a Ba<sup>2+</sup> ion, and Na<sup>+</sup> and K<sup>+</sup> ions were much less effective. It was concluded that such spectral changes upon binding to alkaline earth metal ions resulted from formation of the H-aggregated dimer. Thus, 105 is a potential chemosensor selective to alkaline earth metal ions, especially to Ba<sup>2+</sup>. For a Ca<sup>2+</sup> ion, the non-crowned chemosensor with chelating moieties 106 was developed [83]. Upon addition of Ca<sup>2+</sup> in an aqueous buffer solution of 106, hypochromic effects on electronic absorption as well as bleaching of fluorescence emission were observed, whereas the addition of Mg<sup>2+</sup> had no effect on the optical properties. As Ca<sup>2+</sup> and Mg<sup>2+</sup> ions are the alkaline earth metal cations existing in biological systems, the ligand 106 may be applicable to bio-analytical and clinical uses. Akkaya also developed a squarylium-based fluorescent sensor 107 that is selective for a Zn<sup>2+</sup> ion [85].

The ligand 108 is a chemosensor for selective detection of Na<sup>+</sup> ion [84]. This diazacrown-derivatized squarylium dye was prepared in a one-pot synthesis similar to the preparation of 105. The complexation of a Na<sup>+</sup> ion by 108 was monitored by bleaching of the original absorption band ( $\lambda_{max} = 642$  nm) and a decrease in fluorescence ( $\lambda_{em} = 651$  nm). On the other hand, a K<sup>+</sup> ion had no effect on the electronic absorption and fluorescence of 108.

### **Equation 8**

$$\frac{\mathsf{Ag}^+}{\mathsf{disaggregation}} \overset{\mathsf{Ag}^+}{\longleftarrow} \overset{\mathsf{O}^-}{\bigvee} \overset{\mathsf{O}^-}{$$

bleaching of monomer and H-aggregate absorption bands

Fig. 9 Metal ion-sensing protocol using the squarylium-based chromoionophore 109

For analysis of transition metal ions, Martínes-Máñes et al. developed the squarylium-based chemosensor **109** (structure in Fig. 9), which had sulfurcontaining azacrowns as metal binding sites [86]. The chromoionophore **109** exhibits monomer and H-aggregate absorption bands at 647 and 560 nm, respectively, in an acetonitrile-H<sub>2</sub>O solution. The intensities of these bands depend on the concentration of **109** and the composition of the solvent. When a Hg<sup>2+</sup> ion was added to a H<sub>2</sub>O-enriched solution (e.g., 20: 80, CH<sub>3</sub>CN/H<sub>2</sub>O, v/v) of **109**, complete bleaching of both the monomer and H-aggregate bands was observed. This spectral change was fully reversible as confirmed by the addition of EDTA. On the other hand, the addition of a Ag<sup>+</sup> ion induced bleaching of the H-aggregate band, and the monomer band was enhanced. Other cations such as Li<sup>+</sup>, Na<sup>+</sup>, K<sup>+</sup>, Mg<sup>2+</sup>, Ca<sup>2+</sup>, Ba<sup>2+</sup>, Fe<sup>3+</sup>, Ni<sup>2+</sup>, Cu<sup>2+</sup>, Zn<sup>2+</sup>, and Cd<sup>2+</sup> did not give rise to any spectral changes of either the monomer or

**Equation 9** 

H-aggregate bands. Therefore, utilizing the monomer-H-aggregate equilibrium of 109 provides the  $Hg^{2+}$ -sensing protocol for aqueous media (Fig. 9). It is worth noting that  $Hg^{2+}$  could be detected at nM levels. This analytical limit meets well the practical level of the analysis of drinking water.

Taking advantage of electrophilic reactivity of a squarylium dye, "chemodosimeter" was developed for selective detection of biorelevant thiol compounds. Martínes-Máñes et al. employed water-soluble squarylium dyes 110a and 110b for this purpose [87]. They studied the reactivity of these dyes with a series of naturally occurring  $\alpha$ -amino acids in aqueous solutions (CH<sub>3</sub>CN/H<sub>2</sub>O, 20/80, v/v, buffered at pH 6). Among 19 amino acids examined, only cysteine induced remarkable decoloration and fluorescence quenching of 110a and 110b. Although it is known that a cyanide anion reacts with an anilino-squarylium dye under basic conditions [88], the present squarylium dyes do not exhibit any reactivity toward cyanide at the neutral pH. Thus, the squarylium dyes 110a and 110b are selective for thiols. The bleaching process was tentatively assigned to the nucleophilic addition of a thiol to the central four-membered ring, as shown in Eq. 9. Using the squarylium dyes 110, quantitative analysis of low-molecular mass aminothiols in human plasma was successfully achieved [87].

### 3.5 Supramolecular Systems Based on Squarylium Dyes

Dye molecules often form aggregates under specific conditions because their planar structures tend to stack through electrostatic and/or solvophobic interactions. The aggregation significantly affects optical, electrochemical, and photochemical properties of the dyes due to excitonic interaction among the constituent chromophores [89-91]. Two types of dye aggregates, Hand J-types, are known, where the dye molecules are aligned in card-pack and slipped-stack manners, respectively. These special arrangements of dye molecules result in different types of excitonic interactions of the chromophores. The H-type aggregation, in which transition dipole moments of the chromophores are arranged in a parallel manner, yields a hypsochromic shift of the electronic absorption band. On the other hand, the J-type aggregation, in which the transition dipoles are arranged in a head-to-tail manner, yields a bathochromic shift. Squarylium dyes also form aggregates [92-97], and taking advantage of aggregate formation of squaryliums, new types of molecular-scale materials as well as nano-scale self-assembled materials are expected to be developed.

Ajayaghosh et al. prepared the polyether-tethered squarylium dimer 111 to apply the intramolecular aggregate formation to sensing devices for metal ions [98]. The metal-free dimer is expected to exhibit optical properties ascribed to the monomeric chromophores, whereas the metal-bound dimer is forced to adopt a folded structure through the conformational change with

$$\begin{array}{c} \text{Me} \\ \text{Me} \\ \text{N} \end{array} \begin{array}{c} \text{O}^- \\ \text{N} \end{array} \begin{array}{c} \text{O}^- \\ \text{Me} \\ \text{O} \\ \text{O} \end{array} \begin{array}{c} \text{O}^- \\ \text{Me} \\ \text{O} \\ \text{O} \end{array} \begin{array}{c} \text{O}^- \\ \text{Me} \\ \text{O} \\ \text{O} \\ \text{O} \end{array} \begin{array}{c} \text{O}^- \\ \text{Me} \\ \text{O} \\ \text{O$$

111

a metal ion surrounded by the polyether chain, and the chromophores electronically perturb each other. Indeed, the addition of a Ca<sup>2+</sup> ion to CH<sub>3</sub>CN solution of 111 resulted in the decrease of the monomer absorption at 630 nm along with the generation of the H-aggregate absorption at 552 nm, accompanied by considerable fluorescence quenching where the quantum yield decreased from 0.03 to 0.008. These spectral changes in electronic absorption as well as fluorescence emission were ascribed to the complexation-induced intramolecular H-aggregate formation (i.e., "H-foldamer" formation), as shown in Eq. 10. Modest spectral changes were observed upon addition of other alkaline earth metal ions, and alkali metal ions such as Na<sup>+</sup> and K<sup>+</sup> had no effect on the optical properties of 111. Therefore, the metal ion-induced H-aggregate formation is specific for Ca<sup>2+</sup>, and the squarylium dimer 111 is potentially applicable to Ca<sup>2+</sup> sensing.

Another type of metal ion-induced H-aggregate formation of squarylium dimers was reported by Yagi and Nakazumi, using alkyl dimeric dyes 112a and 112b [99]. Upon addition of a Ca<sup>2+</sup> ion to CHCl<sub>3</sub>/CH<sub>3</sub>CN solution (3/1,

v/v) of 112a, the absorbance at 645 nm assigned to the monomer band de-

**Equation 10** 

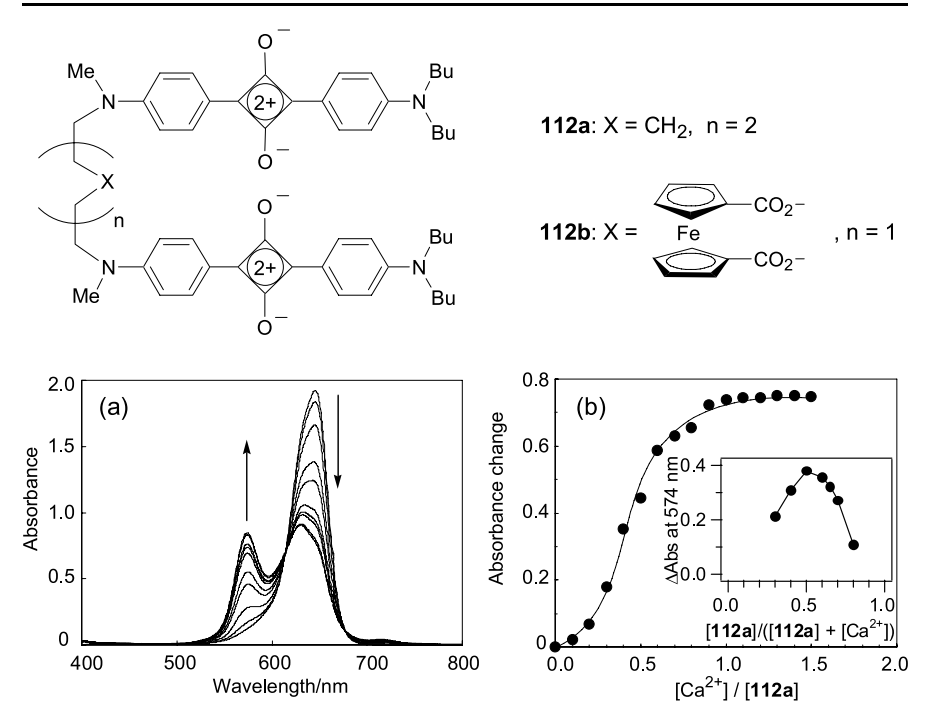


**Fig. 10 a** Electronic absorption spectral changes of  $112a~(4.0\times10^{-6}~M)$  in CHCl<sub>3</sub>/CH<sub>3</sub>CN (3/1, v/v) upon addition of increasing amounts of Ca(ClO<sub>4</sub>)<sub>2</sub> ([Ca<sup>2+</sup>]/[112a] = 0, 0.1, 0.2, 0.3, 0.4, 0.5, 0.6, 0.7, 0.8, 0.9, 1.0). **b** Absorbance changes of a CHCl<sub>3</sub>/CH<sub>3</sub>CN solution (3/1, v/v) of 112a at 574 nm titrated with Ca(ClO<sub>4</sub>)<sub>2</sub>; [112a] =  $4.0\times10^{-6}~M$ . The *inset* is the Job's plot for the 112a-Ca<sup>2+</sup> system; [112a] + [Ca<sup>2+</sup>] =  $4.0\times10^{-6}~M$ 

creased, and this was accompanied by appearance of a new absorption band at 574 nm, as shown in Fig. 10a. From the result of the Job's analysis indicating a 1:1 stoichiometry of the dimer and Ca<sup>2+</sup>, this blue shift was ascribed to the H-foldamer formation similar to the 111-Ca<sup>2+</sup> complex. Furthermore, the sigmoidal profile of the spectral changes implied Ca<sup>2+</sup>-induced cooperative supramolecular assembly of 112a (Fig. 10b). Such a Ca<sup>2+</sup> ioninduced allosteric assembling of the squarylium dimer was confirmed by electrospray ionization mass (ESI-MS) measurements showing the formation of metallo supramolecular complexes, that is the H-aggregate composed of at least three units. In addition, the IR study revealed coalescence of the absorption bands of the C=O stretching at 1582-1616 cm<sup>-1</sup> into one at ca. 1590 cm<sup>-1</sup>, showing that the complexed Ca<sup>2+</sup> ions interact with the oxygen atoms of the cyclobutenolate core of the squarylium skeletons. More specifically, the H-foldamer is formed first by chelation of two squarylium moieties to Ca<sup>2+</sup> (Fig. 11a), and then reorganization of the other chelating site facilitates the allosteric binding of Ca<sup>2+</sup> resulting in complexation of the next dimer (Fig. 11b). Finally, successive alternations of the unit H-

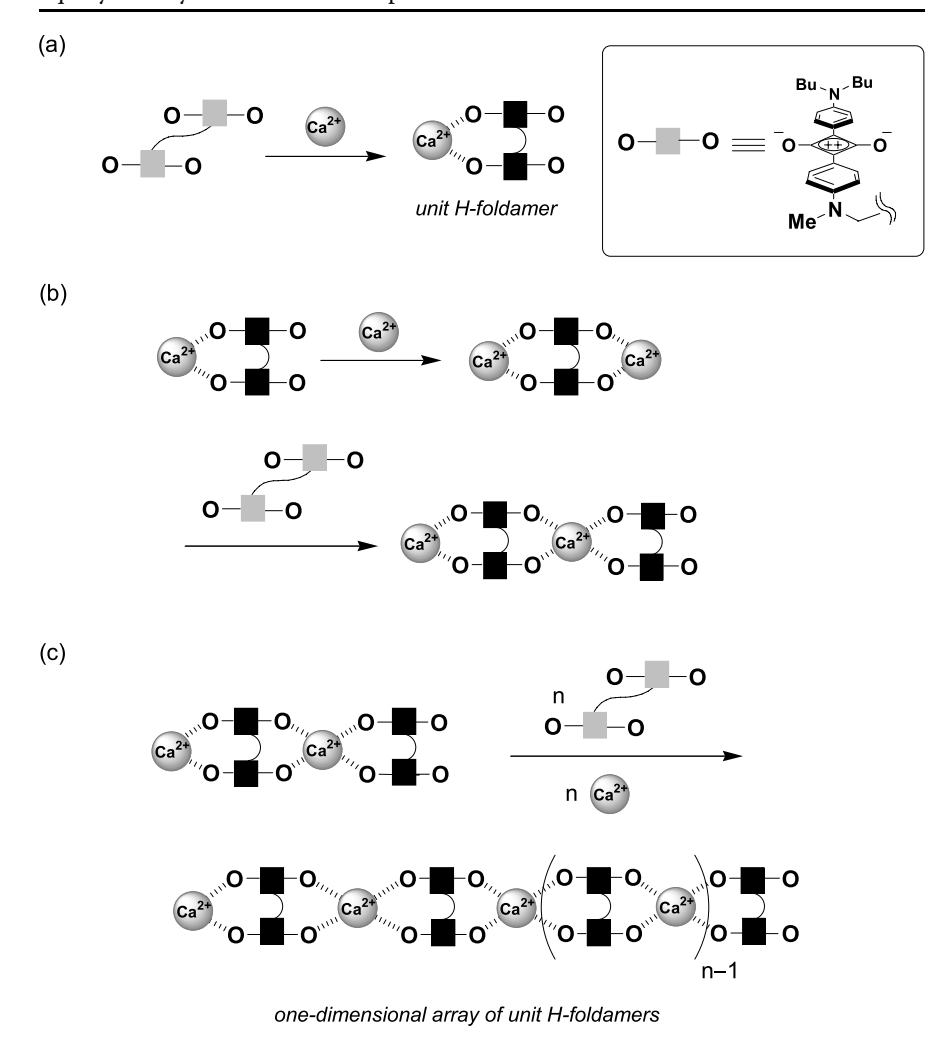


Fig. 11 Schematic illustration of the formation of the supramolecular H-aggregate of the squarylium dimer 112 with  $\text{Ca}^{2+}$ 

aggregates and Ca<sup>2+</sup> ions yield a one-dimensional metallo supramolecular array of the H-foldamers (Fig. 11c). Such a complexation mechanism was also supported by the fact that the ferrocene-linked squarylium dimer 112b [100], which has no podand linker, showed effective formation of the metallo supramolecular assembly upon addition of Ca<sup>2+</sup>. Coordination of the oxygens of the central four-membered ring to metal ions was also found in an inclusion complex composed of a crown ether-bridged molecular cage and an anilino-squarylium dye, yielding a pseudorotaxane supramolecular complex [101].

### 4 Concluding Remarks

Novel syntheses of squarylium-based chromophoric systems such as aminoand dithio-substituted squaryliums, unsymmetrical squaryliums, methineand arene-bridged bis-squaryliums, and bisquaryl-based squarylium analogues have been reviewed. In most cases, the key intermediates are monosubstituted squaric acid (or squarate) derivatives, which show specific electrophilicity to heterocyclic enamines and electron-rich aromatics to afford substituted squarylium skeletons. Establishment of synthetic protocols for the squarylium-based chromophores allows one to obtain a wide range of optical properties such as light absorption and fluorescence emission, especially responsive to far visible-to-NIR light. These achievements should open the door to specific syntheses of functional squaryliums and related compounds by rational molecular designs. Applications of squarylium dyes were also reviewed. The unique optical and electrochemical properties provide numerous opportunities to develop a wide range of materials for photonics and optoelectronics applications such as xerographic and photovoltaic devices. Polymerization of squarylium chromophores led to construction of low band-gap conjugated polymers with intrinsic electric conductivity. Squarylium dyes have also been applied to labeling of biological polymers and as chemosensory materials. By using electronic perturbation to squarylium chromophores upon binding to analytes, drastic changes of electronic absorption and fluorescence emission spectra can be induced. Along with the advance in host-guest chemistry, squarylium-based chemosensory systems selective to various metal ions have been successfully developed. As a new aspect of squarylium chemistry, supramolecular systems of squarylium dyes were also reviewed. Squarylium chromophores are important cornerstones for the development of advanced materials with various functionalities. There is no doubt that the chemistry of squarylium and related compounds will greatly contribute to further development of organic optics devices in the near future.

### References

- 1. Tani T (1998) J Imaging Sci Technol 42:1
- 2. Fabian J, Nakazumi H, Matsuoka M (1992) Chem Rev 92:1197
- 3. Emmelius M, Pawlowski G, Vollmann HW (1989) Angew Chem Int Ed 28:1445
- 4. Mishra A, Behera RK, Behera PK, Mishra BK, Behera GB (2000) Chem Rev 100:1973
- 5. Ehret A, Stuhl L, Spitler MT (2001) J Phys Chem B 105:9960
- 6. Meng FS, Chen KC, Tian H, Zuppiroli L, Nüesch F (2003) Appl Phys Lett 82:3788
- Nüesch F, Tornare G, Zuppiroli L, Meng FS, Chen KC, Tian H (2005) Sol Energ Mater Sol Cells 87:817
- 8. Licha K (2002) Top Curr Chem 222:1
- 9. Treibs A, Jacob K (1965) Angew Chem Int Ed 4:694
- 10. Treibs A, Jacob, K (1966) Liebigs Ann Chem 153

- 11. Ziegenbein W, Sprenger HE (1966) Angew Chem Int Ed 5:893
- 12. Sprenger HE, Ziegenbein W (1966) Angew Chem Int Ed 5:894
- 13. Sprenger HE, Ziegenbein W (1968) Angew Chem Int Ed 7:530
- 14. Sprenger HE, Ziegenbein W (1967) Angew Chem Int Ed 6:553
- 15. Law KY, Bailey FC (1986) Can J Chem 64:1607
- 16. Kim SH, Hwang SH (1997) Dyes Pigm 35:111
- 17. Kuramoto N, Natsukawa K, Asao K (1989) Dyes Pigm 11:21
- 18. Law KY, Bailey FC (1990) J Chem Soc Chem Commun 863
- 19. Law KY, Bailey FC (1992) J Org Chem 57:3278
- 20. Belluš D (1978) J Am Chem Soc 100:8026
- 21. Green BR, Neuse EW (1974) Synthesis 46
- 22. Kazmaier, PM, Burt R, Baranyi G (1986) US Patent 4624904
- 23. de Selms RC, Fox CJ, Riordan RC (1970) Terrahedron Lett 10:781
- 24. Yagi S, Hyodo Y, Matsumoto S, Takahashi N, Kono H, Nakazumi H (2000) J Chem Soc Perkin Trans 1:599
- 25. Terpetschnig E, Lakowicz JR (1993) Dyes Pigm 21:227
- 26. Terpetschnig E, Szmacinski H, Lakowicz JR (1993) Anal Chim Acta 282:633
- 27. Jyothish K, Arun KT, Ramaiah D (2004) Org Lett 6:3965
- 28. Kim SH, Hwang SH, Kim JJ, Yoon CM, Keum SR (1998) Dyes Pigm 37:145
- 29. Bernstein J, Tristani-Kendra M, Eckhardt CJ (1986) J Phys Chem 90:1069
- 30. Kobayashi Y, Goto M, Kurahashi M (1986) Bull Chem Soc Jpn 59:311
- 31. Reis LV, Serrano JPC, Almeida P, Santos PF (2002) Synlett 1617
- 32. Kim SH, Han SK, Kim JJ, Hwang SH, Yoon CM, Keum SR (1998) Dyes Pigm 39:77
- 33. Kim SH, Han SK, Kim JJ, Lim WT, Heo NH, Koh KN (1998) Dyes Pigm 39:259
- 34. Meier H, Dullweber U (1997) J Org Chem 62:4821
- 35. Gerold J, Holzenkamp U, Meier H (2001) Eur J Org Chem 2757
- 36. Buschel M, Ajayaghosh A, Arunkumar E, Daub J (2003) Org Lett 5:2975
- 37. Nakazumi H, Natsukawa K, Nakai K, Isagawa K (1994) Angew Chem Int Ed 33:1001
- 38. Yagi S, Nakai K, Hyodo Y, Nakazumi H (2002) Synthesis 413
- 39. Yagi S, Fujie Y, Hyodo Y, Nakazumi H (2002) Dyes Pigm 52:245
- 40. Yagi S, Murayama S, Hyodo Y, Fujie Y, Hirose M, Nakazumi H (2002) J Chem Soc Perkin Trans 1:1417
- 41. Nakazumi H, Ohta T, Etoh H, Uno T, Colyer CL, Hyodo H, Yagi S (2005) Syn Metal 153:33
- 42. Yagi S, Ohta T, Akagi N, Nakazumi H (2008) Dyes Pigm 77:525
- 43. Liebeskind LS, Fengl RW (1990) J Org Chem 55:5359
- 44. Hyodo Y, Nakazumi H, Yagi S, Nakai K (2001) J Chem Soc Perkin Trans 1:2823
- 45. Liebeskind LS, Yu MS, Yu RH, Wang J, Hagen KS (1993) J Am Chem Soc 115:9048
- 46. Champ RB, Shattuck MD (1974) US Patent 3 824 099
- 47. Law KY, Bailey FC (1986) Can J Chem 64:1607
- 48. Law KY, Bailey FC (1986) Can J Chem 64:2267
- 49. Law KY (1987) J Phys Chem 91:5184
- 50. Law KY, Bailey FC, Yanus JF (1990) J Imaging Sci 34:31
- 51. Law KY, Bailey FC (1993) Dyes Pigm 21:1
- 52. Wingard RE (1982) IEEE Ind Appl 37:1251
- 53. Tristani-Kendra M, Eckhardt CJ (1984) J Chem Phys 81:1160
- 54. Ashwell GJ, Bahra GS, Brown CR, Hamilton DG, Kennard CHL, Lynch DE (1996) J Mater Chem 6:23
- 55. Law KY (1992) Chem Mater 4:605
- 56. Merritt VY, Hovel HJ (1976) Appl Phys Lett 29:414

- 57. Grätzel M (2003) J Photochem Photobiol C 4:145
- 58. O'Regan B, Grätzel M (1991) Nature 353:737
- Nazeeruddin MK, Péchy P, Renouard T, Zakeeruddin SM, Humphry-Baker R, Comte P, Liska P, Cevey L, Costa E, Shklover V, Spiccia L, Deacon GB, Bignozzi CA, Grätzel M (2001) J Am Chem Soc 123:1613
- 60. Li C, Wang W, Wang X, Zhang B, Cao Y (2005) Chem Lett 34:554
- 61. Alex S, Santhosh, Das S (2005) J Photochem Photobiol A 172:63
- 62. Burke A, Schmidt-Mende L, Ito S, Grätzel M (2007) Chem Commun 234
- 63. Zhang D, Wang W, Liu Y, Xiao X, Zhao W, Zhang B, Cao Y (2000) J Photochem Photobiol A 135:235
- 64. Zhao W, Hou YJ, Wang XS, Zhang BW, Cao Y, Yang R, Wang WB, Xiao XR (1999) Sol Energ Mater Sol Cells 58:173
- 65. McQuade DT, Pullen AE, Swager TM (2000) Chem Rev 100:2537
- 66. MacDiarmid AG (2002) Synth Met 125:11
- 67. Heeger AJ (2001) J Phys Chem B 105:8475
- 68. Ajayaghosh A, Chenthamarakshan CR, Das S, George MV (1997) Chem Mater 9:644
- 69. Chenthamarakshan CR, Eldo J, Ajayaghosh A (1999) Macromolecules 32:251
- 70. Chenthamarakshan CR, Ajayaghosh A (1998) Chem Mater 10:1657
- 71. Eldo J, Ajayaghosh A (2002) Chem Mater 14:410
- 72. Havinga EE, Hoeve WT, Wynberg H (1992) Polymer Bull 29:119
- 73. Thompson RB, Lakowicz JR (1993) Anal Chem 65:853
- 74. Szmacinski H, Lakowicz JR (1993) Anal Chem 65:1668
- 75. Nakazumi H, Colyer CL, Kaihara K, Yagi S, Hyodo Y (2003) Chem Lett 32:804
- 76. Welder F, Paul B, Nakazumi H, Yagi S, Colyer CL (2003) J Chromatogr B 793:93
- 77. Yan W, Sloat AL, Yagi S, Nakazumi H, Colyer CL (2006) Electrophoresis 27:1347
- 78. Löhr HG, Vögtle F (1985) Acc Chem Res 18:63
- Bissell RA, de Silva AP, Gunarante HQN, Lynch PLM, Maguire GEM, Sandanayake KRAS (1992) Chem Soc Rev 21:187
- 80. de Silva AP, Gunarante HQN, Gunnlaugsson T, Huxley AJM, McCoy CP, Rademacher JT, Rice TE (1997) Chem Rev 97:1515
- 81. Oguz U, Akkaya EU (1997) Tetrahedron Lett 38:4509
- 82. Oguz U, Akkaya EU (1998) J Org Chem 63:6059
- 83. Akkaya EU, Turkyilmaz S (1997) Tetrahedron Lett 38:4513
- 84. Oguz U, Akkaya EU (1998) Tetrahedron Lett 38:5857
- 85. Dilek G, Akkaya EU (2000) Tetrahedron Lett 41:3721
- Ros-Lis JV, Martínes-Máñes R, Rurack K, Sancenón F, Soto J, Spieles M (2004) Inorg Chem 43:5183
- 87. Ros-Lis JV, Garcia B, Jiménez D, Martínes-Máñes R, Sancenón F, Soto J, Gonzalvo F, Valldecabres MC (2004) J Am Chem Soc 126:4064
- 88. Ros-Lis JV, Martínes-Máñes R, Soto J (2002) Chem Commun 2248
- 89. Jelly EE (1936) Nature 138:1009
- 90. Brooker LGS, White FL, Heseltine DW, Keyes GH, Dent SG, VanLare EJ (1953) J Photogr Sci 1:173
- 91. McRae EG, Kasha M (1958) J Chem Phys 28:721
- 92. Chen H, Law KY, Whitten DG (1996) J Phys Chem 100:5949
- 93. Chen H, Herkstroeter WG, Perlstein J, Law KY, Whitten DG (1994) J Phys Chem 98:5138
- 94. Das S, Thanulingam TL, Thomas KG, Kamat PV, George MV (1993) J Phys Chem 97:13620
- 95. Buncel E, MacKerrow A, Kazmaier PM (1992) J Chem Soc Chem Commun 1242

- 96. Law KY (1987) J Phys Chem 91:5184
- 97. Kim S, Furuki M, Pu LS, Nakahara H, Fukuda K (1987) J Chem Soc Chem Commun 1201
- 98. Ajayaghosh A, Arunkumar E, Daub J (2002) Angew Chem Int Ed 41:1766
- 99. Yagi S, Hyodo Y, Hirose M, Nakazumi H, Sakurai Y, Ajayaghosh A (2007) Org Lett 9:1999
- 100. Hyodo Y, Nakazumi H, Yagi S (2002) Dyes Pigm 54:163
- 101. Hsueh SY, Lai CC, Liu YH, Peng SM, Chiu SH (2007) Angew Chem Int Ed 46:2013

Top Heterocycl Chem (2008) 14: 183–220 DOI 10.1007/7081\_2008\_122 © Springer-Verlag Berlin Heidelberg Published online: 14 May 2008

# Polymethine Dyes as Fluorescent Probes and Visible-Light Photoinitiators for Free Radical Polymerization

Jerzy Paczkowski (≥) · Janina Kabatc · Beata Jędrzejewska

University of Technology and Life Sciences, Faculty of Chemical Technology and Engineering, Seminaryjna 3, 85-326 Bydgoszcz, Poland paczek@utp.edu.pl

1	Introduction	184
2	Polymethine Dyes as Fluorescent Probes	185
2.1	Asymmetric Polymethine Dyes as Fluorescent Probes	
	for Monitoring of Polymerization Process	185
2.1.1	Probing of Thermally Initiated Polymerization of Methyl Methacrylate	188
2.1.2	Probing of Photoinitiated Polymerization of Multifunctional Acrylate	197
3	Dye-Based Photoinitiators for Visible Light Polymerization	200
3.1	General Information	200
3.2	Dyes as Photoinitiators	200
3.3	Dyes/Coinitiator Photoinitiating Systems	201
3.4	Polymethine Dyes as Sensitizers	
	in Two-Component Photoinitiating Systems	202
3.4.1	Cyanine Dye/Alkyltriphenylborate Salt	202
3.4.2	Symmetrical Cyanine Borate Photoredox Pairs	
	as Visible-Light Photoinitiators	203
3.4.3	Hemicyanines as Photoinitiators for Free Radical Polymerization	206
3.4.4	Modified Hemicyanines as Component	
	of Effective Photoinitiating Photoredox Systems	207
3.4.5	Influence of Coinitiator Concentration	209
3.5	Cyanine Dye/N-Alkoxypyridinium Salt	
	as Three-Component Photoinitiating Systems	209
3.6	Thermodynamics of Photoinitiation	212
3.7	Marcus Theory Applied to Kinetics Study	
	of Multifunctional Acrylates Polymerization	214
3.8	The Photobleaching Reaction of the Dye	216

**Abstract** One of the most important applications of asymmetric cyanines is related to their use as fluorescence probes for monitoring the progress of polymerization. Independently, cyanine dyes paired with organoborate anions are very effective visible-light photoinitiators of vinyl monomer polymerization. This chapter is focused on the influence of different factors on polymethine dye properties applied as fluorescence probes, and on the kinetics of free radical polymerization.

**Keywords** Fluorescence probes · Dyeing photoinitiators · Photoinduced electron-transfer reaction · Polymethine dyes · Radical polymerization

#### **Abbreviations**

IR Infrared

NLO Nonlinear optical properties

VIS Visible UV Ultraviolet CT Charge transfer

HOMO Highest occupied molecular orbital LUMO Lowest unoccupied molecular orbital TICT Twisted intramolecular charge transfer

PMM Poly(methyl methacrylate)

FTIR Fourier transform infrared spectroscopy

TMPTA 2-Ethyl-2-(hydroxymethyl)-1,3-propanediol triacrylate

MP 1-Methyl-2-pyrrolidinone

D Electron donor
A Electron acceptor
DMF N,N-Dimethylformamide

PET Photoinduced electron-transfer process

#### 1

#### Introduction

Photopolymerization is a field undergoing significant growth because it is an efficient, energy-saving, economical and environmentally friendly method for the formation of high molecular weight polymers [1]. There is one striking point when considering the thermodynamics of polymerization photosensitization by dyes. The photophysical energy transfer between an excited state of the dye and another chromophore, which is able to generate free radicals, is generally disfavored due to the fact that the energy needed to dissociate a bond is larger than the energy transferred to the chromophore. However, with hydrogen or electron transfer involved, it is possible to generate free radicals from molecules with low excitation energy [2, 3]. There are numerous studies on dye photoinitiators in which a free radical is formed via the photoinduced electron-transfer process. These dyes include acridines, xanthenes and thiazines, first reported by Oster [4], a wide group of fluorone dyes [5-8], cyanine dyes [9-11], and dyes based on pyrene [12, 13], safranine T [14], and quinaxolin-2-one [15, 16], among others [17, 18]. It is noteworthy that only cyanine borates [11] are "tunable photoinitiators", that is, their color change can be achieved by altering the number of conjugated vinylene units separating the aromatic parts of cyanine dye. Cyanine dyes are not only widely used as photoinitiators, but also as fluorescence probes of free-radical polymerization. Fluorescence probes are spectroscopic tools used in chemistry for monitoring specific properties of the medium in which they are incorporated. It is possible because their fluorescence is sensitive to changes in temperature, polarity or rigidity of the environment. Therefore, one can use them to estimate polarity of medium or degree of cure by measuring the changes in their emission intensity or value of the emission maximum shift. New photoinitiating systems based on cyanine borate salts operating in the visible-light region and fluorescence probes used for monitoring the progress of acrylate polymerization are described in this chapter.

### 2 Polymethine Dyes as Fluorescent Probes

## 2.1 Asymmetric Polymethine Dyes as Fluorescent Probes for Monitoring of Polymerization Process

Asymmetric cyanine dyes consist of an electron-donating moiety and a different electron-deficient acceptor that are conjugated via a mono- or polymethine  $\pi$ -system. The acceptor moiety itself can be charged or uncharged [19]. The asymmetric cyanine dyes with electron donor-acceptor moieties on opposite sides of the styryl bond are particularly attractive for their spectral sensitivity towards the local host environment, and can be used as probing fluorophores. Fluorescent probes are, perhaps, the most popular and powerful tools that can be used in order to understand the physical and chemical processes that occur at the molecular level. It is possible because their fluorescence is sensitive to the mobility and/or viscosity of the molecular environment in which the probe molecules are located. This sensitivity can be achieved via a number of physical interactions such as intramolecular reorientation [20], intramolecular excimer formation process [21], diffusioncontrolled interaction [22], and solvent stabilization of the probe's excited state [23, 24]. It is important to note that the physical origin of the sensitivity to the molecular environment, for a given probe molecule, can be determined by several of the above-mentioned interactions [25]. One of the most important applications of fluorescence probes in polymer chemistry is monitoring of a polymerization process. The local and macroscopic viscosities of polymers are often different. The local viscosity combines the effect of solvent and interaction of polymer segments surrounding the relaxing fluorophore. The difference between local and macroscopic viscosity can be measured by commonly used viscometric techniques, as shown by Nishijama and coworkers [26-28]. They compared the local viscosity measured by the depolarization of fluorescence to the melt viscosity of polyethylene. It was documented that the local viscosity increases linearly up to a certain degree of polymerization and then becomes independent of molecular weight. Flu-

orescence probes, in polymer chemistry, are used to observe the changes in properties of a polymerization mixture that occur during polymerization by measuring the changes in the fluorescence intensity and spectral characteristics of a small molecular probe incorporated in the polymerizing formulation. Changes in fluorescence yield [20, 29–33], the position of fluorescence maximum [24], changes in fluorescence polarization [27, 28] and the efficiency of intramolecular [34, 35] or intermolecular [22] excimer formation have been related to the local viscosity changes occurring during polymerization. More detailed discussion covering various aspects of this problem can be found in other reviews [36, 37].

A very important group of fluorophores are fluorescent organic salts that can undergo a photoinduced intramolecular electron-transfer process (PET). The asymmetric cyanine dyes, which are organic salts of the D- $\pi$ -A<sup>+</sup>X<sup>-</sup> type, where D and A denote donor and acceptor, respectively, belong to this class of compounds. They are called charge-resonance probes because they resemble charge-transfer (CT) probes D- $\pi$ -A or D- $\sigma$ -A [38–41]. However, the spectroscopic behavior of the charge-resonance probes is quite different. They display blue shift in their emission maximum during polymerization, but their fluorescence is only slightly dependent on changes in solvent polarity. That is why they are essentially nonsolvatochromic probes. The structures presented in Chart 1 exemplify the hemicyanine dyes investigated by our research group [39, 40, 42].

Similar dyes have been reported [43–46]. Fluorescing molecules of this type can exist as *trans* and *cis* isomers, as exemplified in Chart 2.

The electronic absorption spectra of these dyes contain absorption bands that correspond to the  $S^0 \to \mathrm{CT}$  transition, which appears at the blue-energy side of the absorption spectrum. A well-separated CT absorption band is observed for almost all dyes. The position and intensity of the CT absorption band strongly depend on the molecular structure. In particular, the presence of a planar conformation of a molecule increases the probability of the radiative transition in comparison to a molecule in which coplanarity is decreased for steric reasons. This feature is supported by the data obtained by Gawinecki et al. during the study on the resonance substituent constants of *para*-substituted benzaldoximes [39, 40, 47]. The CT character of the longwavelength absorption band is additionally reflected by the values of the ground state dipole moments.

The asymmetric cyanine dyes show large Stokes shifts. This indicates that an emitting state is not the Franck–Condon  $S_1$  state reached in the absorption transition but the solvent relaxed state. It cannot be assumed that the excited state dipole moment remains unchanged during transition from the Franck–Condon state to the emitting state. The nature of the emitting state in D- $\pi$ -A molecules may change with the solvent or can be changed with the dye structure that is forcing or precluding the excited-state relaxation via selected channels or that may be controlled by viscosity of the medium [48, 49].

Chart 1

$$C_2H_5$$

R

Trans

R

Cis

#### Chart 2

Considering the influence of dye structure on the CT fluorescence, one should take into account the nature of the electron donor part of the molecule. Theoretically, the energy level of the molecule excited CT state, relative to its ground state, can be expressed by Eq. 1, where  $E_{\rm ox}(D)$  and  $E_{\rm red}(A)$  are one-electron oxidation and reduction potentials of donor and acceptor and C is a constant that depends on the degree of charge separation [50]

$$E_{\rm CT} = E_{\rm ox}({\rm D}) - E_{\rm red}({\rm A}) + C.$$

#### **Equation 1**

Verhoeven [51], analyzing the properties of rod-shaped donor–acceptor systems, illustrated that the fluorescence frequency of intermolecular exciplexes and excimers, as well as intramolecular donor–acceptor systems, is linearly dependent on the value of  $E_{\rm ox}({\rm D})$  –  $E_{\rm red}({\rm A})$ . Dyes described in this chapter fulfil this dependence, and their emission occurs from the excited CT state [39]. The effect of the media on the absolute and relative energies of the electronic states of solute molecules is of considerable importance in photophysics and photochemistry [39, 40, 42, 52–66].

Using Bakshiev's solvatochromic method [58] for determination of the dipole moments of the excited state, the linear relationship between the spectral shift and the polarity parameters (dielectric constant and refractive index) of solvents should be observed [64]. The dipole moments estimated from the obtained linear relationships and the calculated Onsager's cavity radius [59–63] for selected dyes are summarized in Table 1 [64].

### 2.1.1 Probing of Thermally Initiated Polymerization of Methyl Methacrylate

The hemicyanine dyes used as fluorescence probes for monitoring of a polymerization reaction are involved in the electron-transfer process and show

**Table 1** Calculated Onsager's cavity radius, the ground state dipole moments  $(\mu_{\rm g})$  and estimated excited state dipole moments  $(\mu_{\rm e})$  of selected dyes [64]

	Dye	Onsager's radius [Å]	$\mu_{g}$ [D]	$\mu_{e}$ [D]
F1	$H_3C$ $H_3C$ $C_2H_5$ $C_1$ $C_2$ $C_3$	5.27	2.47	5.85
F2	$H_5C_2$ $H_5C_2$ $C_2H_5$	5.27	1.81	4.93
F3	$S$ $C_2H_5$	5.72	1.78	4.94
F13	$H_3C'$ $S$ $C_2H_5$	5.49	2.63	4.77
F18	$S$ $C_2H_5$	5.56	1.90	5.78
F19	$_{\text{H}_{3}\text{C}}$ C <sub>2</sub> H <sub>5</sub> $_{\text{C}}$ C <sub>H<sub>3</sub></sub>	5.19	2.37	5.06
F20	$H_5C_2$ $C_2H_5$ $C_3$	5.48	3.89	9.19

### Table 1 (continued)

	Dye	Onsager's radius [Å]	$\mu_{ m g}$ [D]	μ <sub>e</sub> [D]
F21	- so <sub>3</sub>	5.78	7.40	11.7
	$ \begin{array}{c c} S \\ \downarrow \\ C_2H_5 \end{array} $ $ \begin{array}{c} C_{13} \end{array} $			
F22	s - 1	5.52	3.00	8.8
	$\downarrow$ HO $\downarrow$			
F23	-so <sub>3</sub>	6.10	5.26	6.11
	$H_5C_2O$ $C_2H_5$ $C_3$			
F25	$\begin{array}{c} \begin{array}{c} \\ \\ \\ \\ \\ \\ \end{array} \\ \begin{array}{c} \\ \\ \\ \end{array} \\ \begin{array}{c} \\ \\ \\ \\ \end{array} \\ \begin{array}{c} \\ \\ \\ \\ \end{array} \\ \begin{array}{c} \\ \\ \\ \end{array} \\ \begin{array}{c} \\ \\ \\ \\ \end{array} \\ \begin{array}{c} \\ \\ \\ \end{array} \\ \begin{array}{c} \\ \\ \\ \\ \\ \\ \end{array} \\ \begin{array}{c} \\ \\ \\ \\ \\ \\ \end{array} \\ \begin{array}{c} \\ \\ \\ \\ \\ \end{array} \\ \begin{array}{c} \\ \\ \\ \\ \\ \end{array} \\ \begin{array}{c} \\ \\ \\ \\ \\ \\ \end{array} \\ \begin{array}{c} \\ \\ \\ \\ \\ \\ \end{array} \\ \begin{array}{c} \\ \\ \\ \\ \\ \\ \end{array} \\ \begin{array}{c} \\ \\ \\ \\ \\ \\ \end{array} \\ \begin{array}{c} \\ \\ \\ \\ \\ \\ \end{array} \\ \begin{array}{c} \\ \\ \\ \\ \\ \\ \end{array} \\ \begin{array}{c} \\ \\ \\ \\ \\ \\ \end{array} \\ \begin{array}{c} \\ \\ \\ \\ \\ \\ \\ \end{array} \\ \begin{array}{c} \\ \\ \\ \\ \\ \\ \end{array} \\ \begin{array}{c} \\ \\ \\ \\ \\ \\ \\ \end{array} \\ \begin{array}{c} \\ \\ \\ \\ \\ \\ \\ \end{array} \\ \begin{array}{c} \\ \\ \\ \\ \\ \\ \\ \end{array} \\ \begin{array}{c} \\ \\ \\ \\ \\ \\ \\ \end{array} \\ \\ \begin{array}{c} \\ \\ \\ \\ \\ \\ \\ \end{array} \\ \begin{array}{c} \\ \\ \\ \\ \\ \\ \\ \\ \\ \\ \end{array} \\ \begin{array}{c} \\ \\ \\ \\ \\ \\ \\ \\ \\ \\ \\ \\ \\ \\ \end{array} \\ \begin{array}{c} \\ \\ \\ \\ \\ \\ \\ \\ \\ \\ \\ \\ \\ \\ \\ \\ \\ \\ \\$	5.24	8.55	13.85
F26	S	4.99	4.24	8.6
	$F \longrightarrow \begin{array}{c} + \\ N \\ C_2H_5 \end{array}$			
F27	S	5.37	9.35	12.2
	$ \begin{array}{cccccccccccccccccccccccccccccccccccc$			
F28	S T T	5.19	12.31	13.28
	$O_2N$ $\downarrow$			

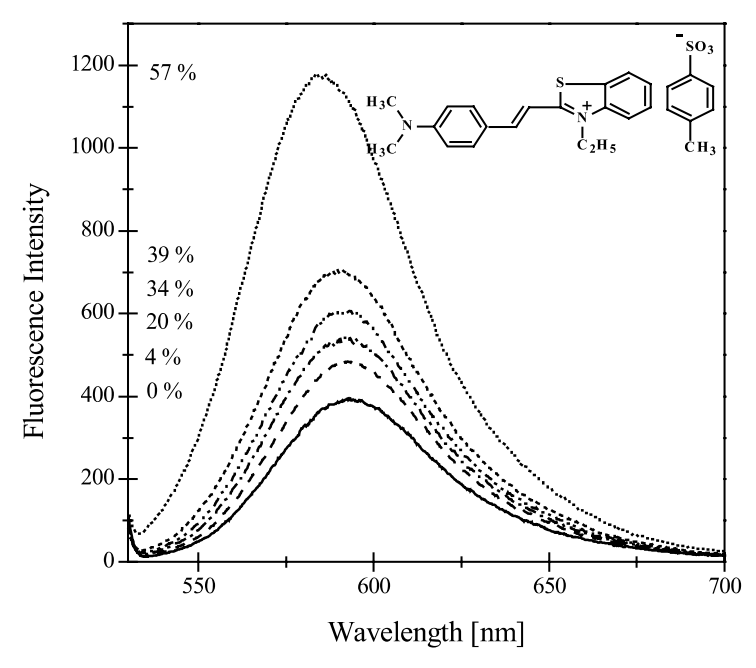


**Fig. 1** Changes in the fluorescence spectra of hemicyanine dye F1 during thermally initiated polymerization of methyl methacrylate recorded for the conversion below the transition point of the liquid sample into a rigid polymer matrix [41]. (Reprinted from John Wiley & Sons, Inc.)

fluorescence spectra that depend on the environment in which the probe molecules are located. Figures 1 and 2 illustrate the changes in the emission spectra recorded for selected dye F1 during thermally initiated polymerization of methyl methacrylate. A gradual increase in intensity of the probe fluorescence is observed for a low degree of monomer conversion, whereas there is a distinct blue shift and a strong increase in the fluorescence intensity during a subsequent conversion of the sample into a rigid polymer matrix. An increase in medium rigidity causes essential reduction in the rates of all processes controlled by diffusion [39–42].

Two mechanisms have been put forward to explain the observed photophysical behavior of D- $\pi$ -A salt. Using the chromophore shown in Fig. 3 as an example, Neckers et al. [38] assumed that the positive charge in the cation is localized on the pyridinium ion in the ground state, but changes its location in the excited state. Based on the calculation of the highest occupied molecular orbital (HOMO) and the lowest unoccupied molecular orbital (LUMO), it can be concluded that in the excited state the positive charge is transferred from the pyridinium ion to the (N,N-dimethylamino)phenyl group. It is also assumed that the positive charge is primarily stabilized by the counterion.

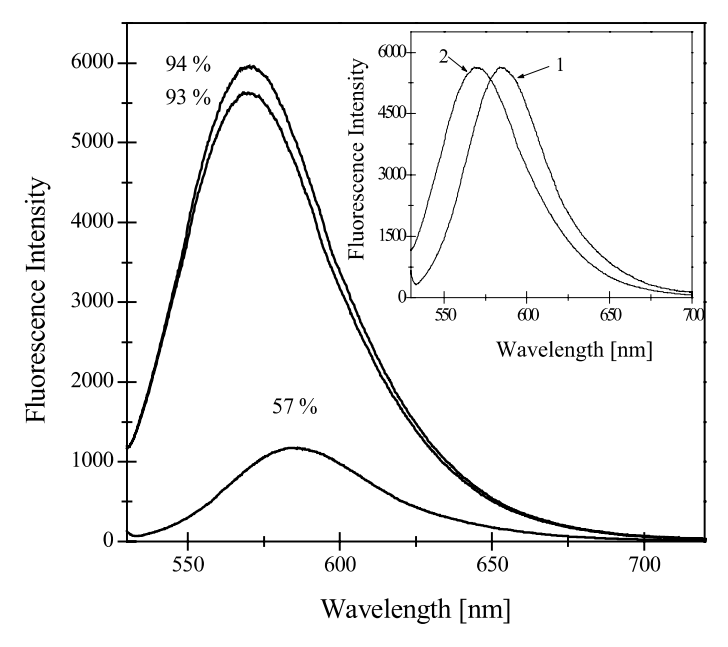


**Fig. 2** Changes in the fluorescence spectra of hemicyanine dye F1 during thermally initiated polymerization of methyl methacrylate recorded above the point of transition of the liquid sample into a rigid polymer matrix. The *inset* shows normalized emission curves illustrating a blue shift observed during thermally initiated polymerization recorded at a high degree of monomer conversion: 1 57%, 2 94% of degree of polymerization [41]. (Reprinted from of John Wiley & Sons, Inc.)

The lack of solvatochromism is consistent with the fact that the ground state and the fully relaxed excited state are roughly equivalent. Therefore, the polarity of the solvent does not influence the emission wavelength of the probe. The ability of these types of probes to monitor the rigidity of their environment is explained by the low mobility of the counterion, which is not able to follow the cation in rigid media, which in turn destabilizes the excited molecule (see Fig. 4).

A more convincing explanation of the specific photophysical properties of stilbazolium salts was provided by Rettig et al. [23, 67, 68]. These authors applied the global analysis technique to construct the spectral profile of several emitting states. A global fit of the emission data, obtained from time-resolved fluorescence spectroscopy, showed that a three-exponential model was necessary to obtain an acceptable fit. The well-known model of twisted intramolecular CT states (TICT) [23, 67, 69–71] can be a good basis for the description of the multiple fluorescence of tested molecules. According to Rettig [67, 68], the excited and ground states energies for the selected probe A9 can be presented as plotted in Fig. 5.

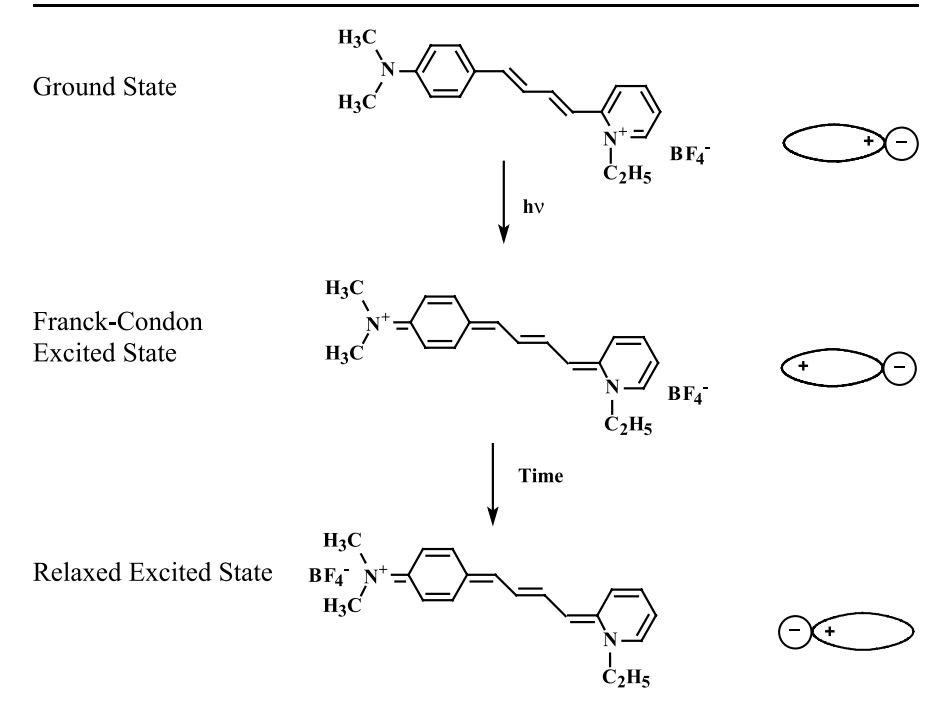


**Fig. 3** Schematic representation of the ground state, the Franck-Condon excited state, and the fully relaxed excited state proposed for  $D-\pi-A^+X^-$  type of probes. (Reprinted from [38])

Figure 5 shows that simultaneous fluorescence can occur from the states E,  $A^2$ , and  $A^3$ , and this explains the broad steady-state spectra. The twist of the N,N-dialkylamino group leads to a TICT state  $A^1$ . However, its energy level is considerably higher than that for the nontwisted conformation E and, therefore, it cannot be easily thermally activated to contribute in the emission spectra. A twist of the double bond gives a state P with a relatively narrow  $S_1$ – $S_0$  gap. The deactivation of this state should be radiationless in character because of the small energy gap to the ground state. An emission from  $A^2$  and  $A^3$  should be possible because their energies are similar to that of the E state. The suggested mechanism of multiple fluorescence is consistent with the data for probe **D8** shown in Fig. 6.

The S-shaped curve shows a distinct transition from fluid to a rigid glass and demonstrates that the probe emission intensity increases as polymerization propagates. In other words, as monomer concentration decreases due to polymerization, probe molecules are starting to be trapped in the rigid poly(methyl methacrylate) (PMM) environment and, as a result, the emission intensity increases. In general, the specific behavior of the probes in the transition area of fluid monomer to a rigid polymer is explained by the dra-

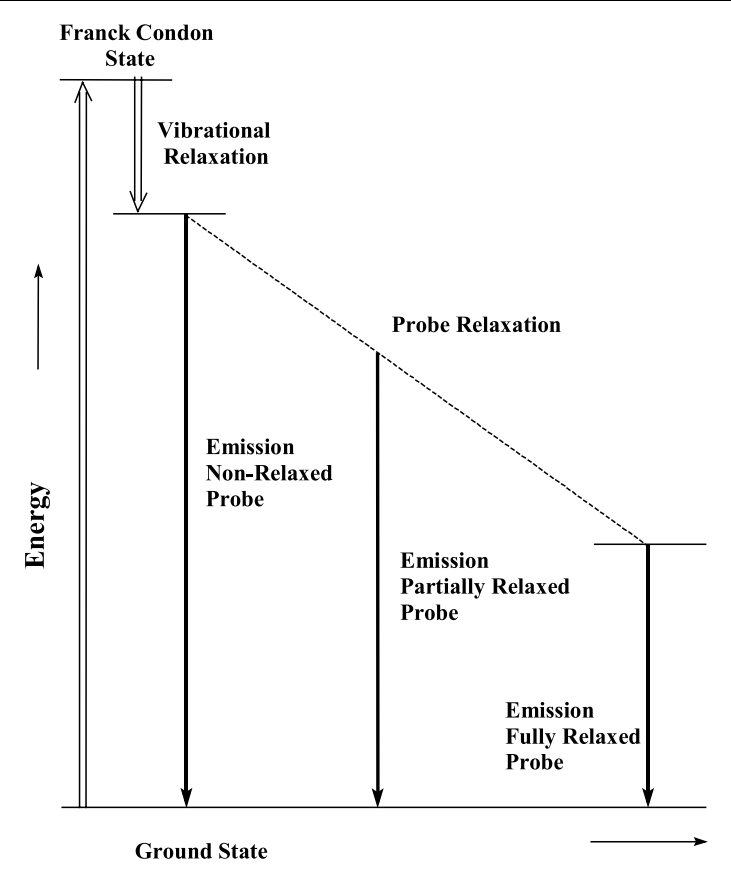
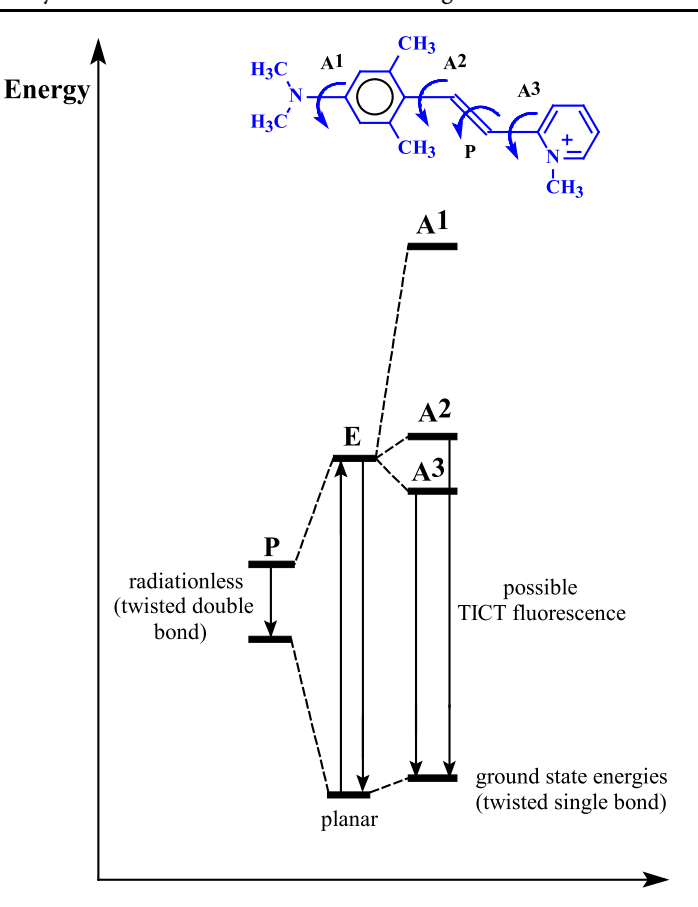


Fig. 4 Schematic representation of the probe's emission as a function of the medium relaxation [38]. 2007 the American Chemical Society

matic increase in viscosity that, in turn, rapidly decreases the efficiency of nonradiative deactivation of the emitting state.

Changes in the probe emission intensity can be used to characterize a degree of polymerization. The relationship is linear for low degrees of polymerization (Fig. 7). At higher degrees of conversion, a sudden increase in fluorescence intensity occurs, which is caused by the conversion of polymer solution into the rigid polymer matrix [39–42].

The increase in the fluorescence intensity during polymerization is also consistent with the reduced efficiency of the *trans-cis* isomerization about the C = C bond as the viscosity increases. This, in turn, decreases efficiency of the formation of the radiationless state P and, as a result, causes more effective emission from E,  $A^2$  and  $A^3$  states. This effect can be rationalized in terms of the activation energy needed for isomerization of aromatic imines, which is on the order of 20 kcal/mol or less [71-74].



**Fig. 5** Conceptual presentation of energy gaps between the ground state energy and the lowest excited states for probe A9. The indexes 1, 2 and 3 denote the states reached after the twist of a single bond, P corresponds to the state after the twist of the double bond and E is the lowest excited state for the planar conformation [68]. (The American Chemical Society)

Linearity of the fluorescence intensity versus a degree of monomer conversion into polymer for low degrees of polymerization can be used for analysis of polymerization progress by using the factor called the "probe sensitivity parameter". This parameter is also an approximate characteristic of probe response, as shown in Fig. 8 [39–41].

Several parameters that describe the sensitivity of selected pyridinium probes together with values of the blue shifts in their emission maxima observed during methyl methacrylate polymerization have been published [39–41]. The quantitative explanation of the specific probe sensitivity comes from the estimation of a reorganization energy that is related to the solvent and solute motions and the reorganization energy corresponding to the changes

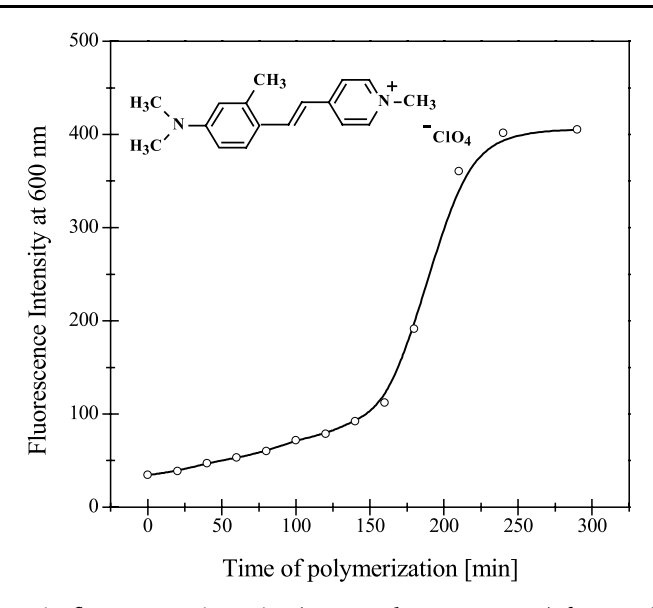


**Fig. 6** Changes in fluorescence intensity (measured at  $\lambda = 600$  nm) for styrylpyridinium probe **D8** during thermally initiated polymerization of methyl methacrylate in the presence of  $\alpha$ ,  $\alpha'$ -azobisisobutyronitrile (AIBN) [40]

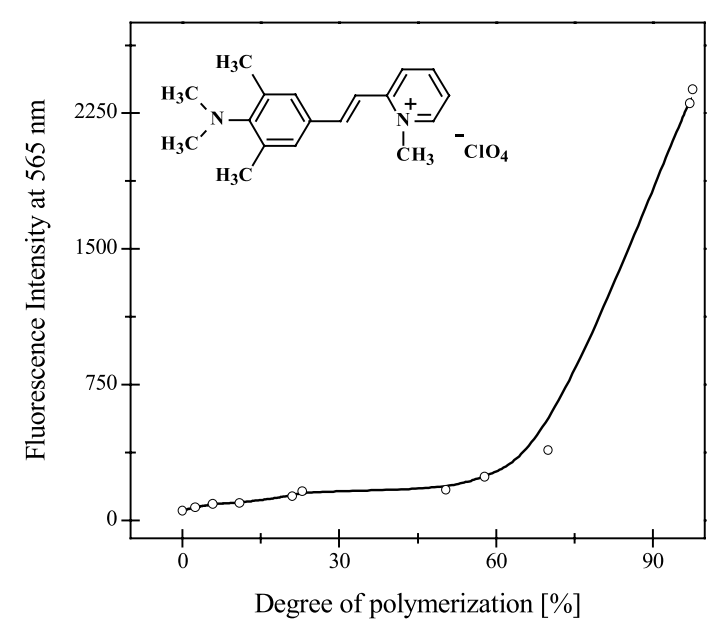


**Fig. 7** Relationship between the probe emission intensity A7 (recorded at  $\lambda = 565$  nm) versus degree of monomer conversion into polymer during methyl methacrylate polymerization [39]. (Reproduced by permission of the Royal Society of Chemistry)

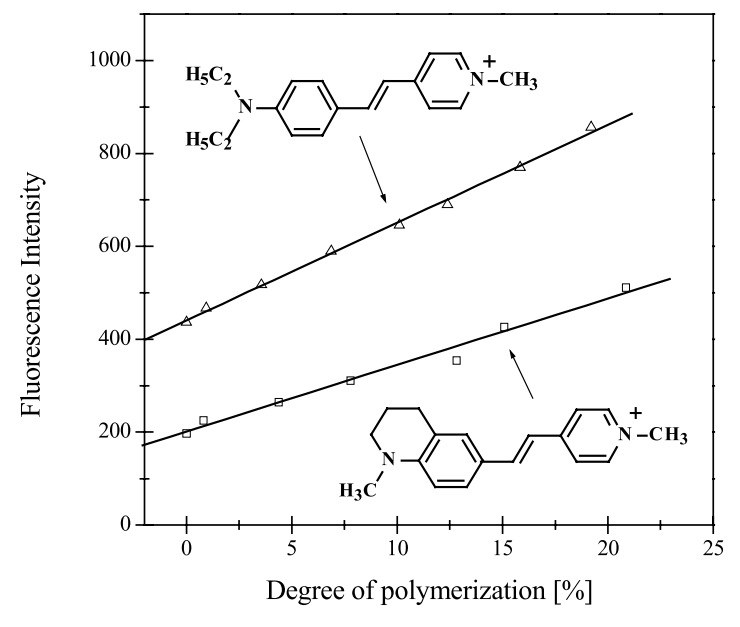


**Fig. 8** Linear relationships between the fluorescence intensity and a degree of polymerization for selected probes **D4** (*top*) and **D15** (*bottom*) illustrating their sensitivity [40]

in the solute bond lengths and angles accompanying the excited-state electron transfer [75–77]. The lowest sensitivity is often observed for molecules possessing the highest value of reorganization energies. Replacement of perchlorate anion by iodide decreases the probe sensitivity. This observation supports the mechanism proposed by Neckers et al., in which a change in anion size causes a change in the excited state stabilization efficiency [38]. Another explanation of the counterion size influence is the possibility of its effect on the relationship between solvation and CT fluorescence. Thus, an increase of a counterion size increases the effective Onsager's cavity radius [78], and this effect, according to Lippert [79] and Mataga [80], can change the energy of the emitting state.

### 2.1.2 Probing of Photoinitiated Polymerization of Multifunctional Acrylate

The real-time kinetics of photopolymerization can be investigated by using a system that is schematically presented in Fig. 9 [81].

The laboratory studies on the changes of probe fluorescence during polymerization initiated photochemically can be carried out using a suitable alkene monomer, a photoinitiator absorbing UV light and a fluorescence probe that does not absorb in the same range as the pho-

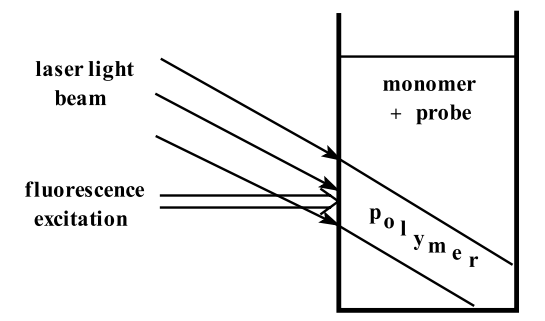


**Fig. 9** Measurements of kinetics of a photoinitiated polymerization by using a fluorescent probe

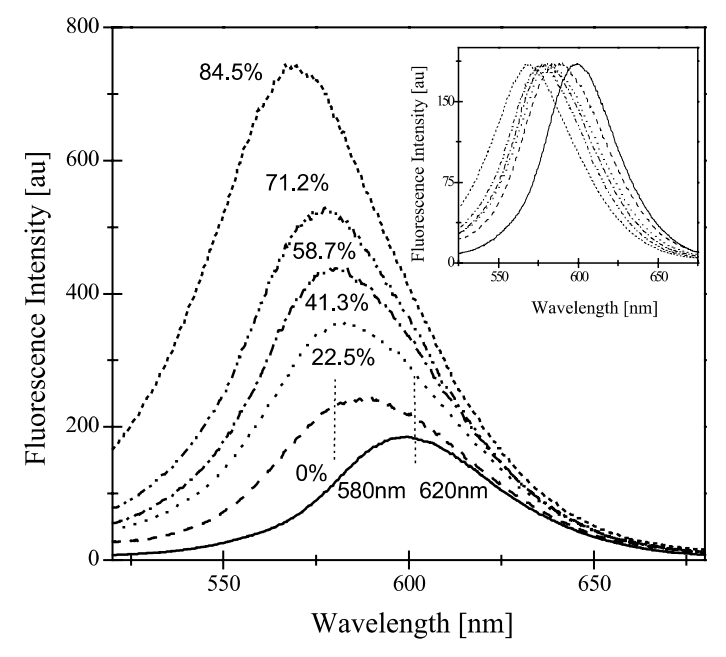


**Fig. 10** Emission spectra of pyridinium salt **A16** (structure of the dye market in Fig. 11) for different degrees of photoinitiated of 2-ethyl-2-(hydroxymethyl)-1,3-propanediol triacrylate (TMPTA)-1-methyl-2-pyrrolidinone (MP) (9:1) mixture. The degree of polymerization was calculated using Fourier transform infrared spectroscopy (FTIR) spectroscopy. *Inset* Normalized fluorescence spectra of the probe illustrating a blue shift of fluorescence  $\lambda_{max}$  during polymerization of TMPTA-MP (9:1) mixture [39]. (Reproduced by permission of the Royal Society of Chemistry)

toinitiator (visible-light probe). The emission spectra of the probe and Fourier transform infrared spectroscopy (FTIR) spectra of the alkene (to monitor a decrease in the monomer concentration) are measured after

subsequent irradiations. Examples of the emission spectra are presented in Fig. 10.

As can be seen, an increase in the intensity of the probe fluorescence during a photochemically initiated polymerization parallels the degree of monomer double-bond conversion. This effect is accompanied by a blue shift in the emission maxima. No sudden increase caused by formation of the rigid gel is observed. However, the increase in the probe's emission intensity versus monomer double-bond conversion is not usually a well-defined linear function. On the other hand, the relationship between the ratio of emission intensities at two selected wavelengths and degree of vinyl monomer double-bond conversion is a linear function with a high correlation coefficient (Fig. 11).

Additional effects that cause changes in the intensity of fluorescence are a decrease in temperature when polymerization is completed and a strong increase in viscosity as a result of a transition of a liquid monomer into solid polymer matrix. Reduction of a probe may also be a factor if the probe is used as a photoinitiator [82].

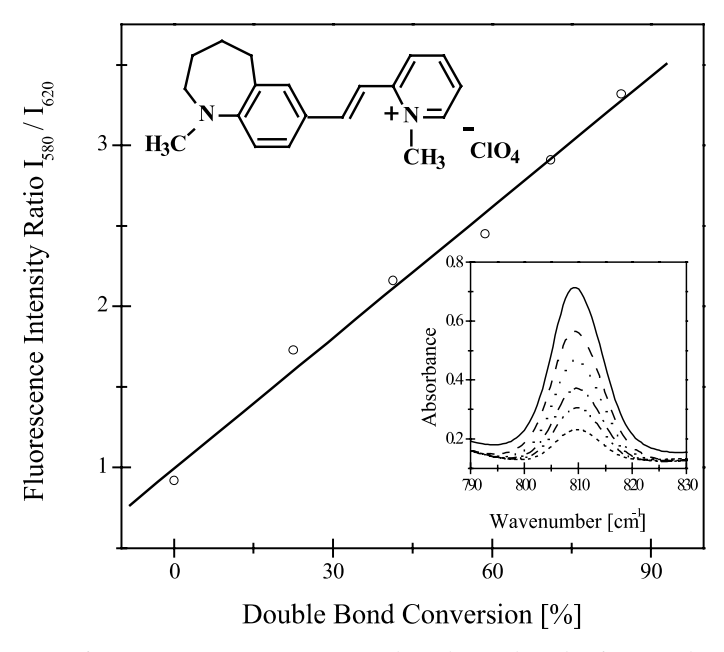


**Fig. 11** Ratio of emission intensity at two selected wavelengths for styrylpyridinium probe A16 versus degree of double bond conversion during photoinitiated polymerization of TMPTA-MP (9:1) mixture. The *inset* shows changes in the infrared (IR) absorption of -C = C - of TMPTA recorded at 810 cm<sup>-1</sup> [39]. (Reproduced by permission of the Royal Society of Chemistry)

3 Dye-Based Photoinitiators for Visible Light Polymerization

### 3.1 General Information

Polymer photoinitiating systems, introduced by Dupont in the 1950s [83], are an important application of photochemical technology [84]. Polymerization reactions can be carried out in an image-forming fashion, as a thin film or layers [85–87].

The photoinitiator system generates free radicals that initiate radical chain polymerization of the unsaturated monomer or monomers. It may be a single compound, typically called a photoinitiator, rather than a photoinitiator system that absorbs light and undergoes unimolecular reactions to form radicals, or it may consist of several different compounds that undergo a complex series of reactions to produce the initiating radicals [88].

### 3.2 Dyes as Photoinitiators

A few photoreducible dyes, such as xanthene and acridine dyes, can directly photoinitiate polymerization of methyl methacrylate, styrene and acrylonitrile, with low efficiency [84, 89, 90]. Photoinitiation occurs by electron-transfer between the singlet excited dye molecule and the monomer (Scheme 1).

$$dye^{+}X^{-} \xrightarrow{hv} {}^{1}(dye^{+}X^{-})^{+} + R \longrightarrow CH = CH_{2} \longrightarrow dye^{-} + [R - CH \longrightarrow CH_{2}^{+}X^{-}]$$

$$M \downarrow \qquad M \downarrow$$

Polymerization Polymerization

$$dye^{-}X^{+} \xrightarrow{hv} {}^{3}(dye^{-}X^{+})^{+} + R \xrightarrow{CH} CH_{2} \xrightarrow{M} {}^{\bullet} + [R \xrightarrow{\bullet} CH \xrightarrow{CH} CH_{2} X^{+}]$$

Scheme 1

Electron-deficient monomers (like acrylates) react preferentially as electron acceptors, whereas polymerization of electron-rich monomers occurs by monomer oxidation [84, 87].

### 3.3 Dyes/Coinitiator Photoinitiating Systems

Usually, photoinitiation of polymerization does not occur upon interaction of the excited singlet or triplet state of the dye with a monomer molecule [84]. In most practical applications of photoinduced radical polymerization, the sensitizers are UV-absorbing compounds that undergo unimolecular fragmentation in an excited state to form the initiating radicals. It has proven difficult to extend this feature far into the visible region of the spectrum. Most of the useful initiating systems that respond to visible light are based on quite different, usually bimolecular chemistry. For example, a sensitization that is useful in the blue region requires a bimolecular electron-transfer reaction between an excited compound and an electron-donor compound. In the case of neutral reactants, a radical anion and a radical cation are formed. Subsequent proton transfer results in the formation of radicals that are capable of initiating polymerization [91]. Two types of sensitization of free radical polymerization can occur, namely photoreducible dye sensitization, reported first by Oster in 1954 [4], and photooxidizable dye sensitization [3, 84]. Initiation of polymerization by photoreducible dyes in the presence of different coinitiators (electron donors) is very common, whereas polymerization initiated by photooxidation of a dye in the presence of an electron acceptor is very rare. For example, thiazine dyes such as methylene blue can react either as electron acceptor in the presence of N-phenylglycine [92] as electron donor, or as electron donor in the presence of benzyltrimethylstannane as electron acceptor [84, 93].

### Methylene blue

The secondary reaction following the electron-transfer process involves either a proton transfer or a fragmentation reaction (cleavage). The latter type of reaction can occur as reductive cleavage (Eq. 2) or as oxidative cleavage (Eq. 3), depending on whether the compound that undergoes the cleavage reaction has been initially reduced or oxidized. Here, D\* represents an excited state of an electron donor, A\* represents an excited state of an electron acceptor and X-Y is the compound that undergoes cleavage. When the X-Y molecule is charged, the most likely photoinduced electron-transfer reaction is either reduction if the molecule is a cation, or oxidation if the molecule is

an anion. Both processes form a neutral radical X-Y', the fragmentation of which generates a radical X' and a neutral species Y [91]

$$D^* + X - Y^+ \to D^{*+} + X - Y^* \to X^* + Y$$

**Equation 2** 

$$A^* + X - Y^- \rightarrow A^{-} + X - Y^{-} \rightarrow X^{-} + Y$$
.

#### **Equation 3**

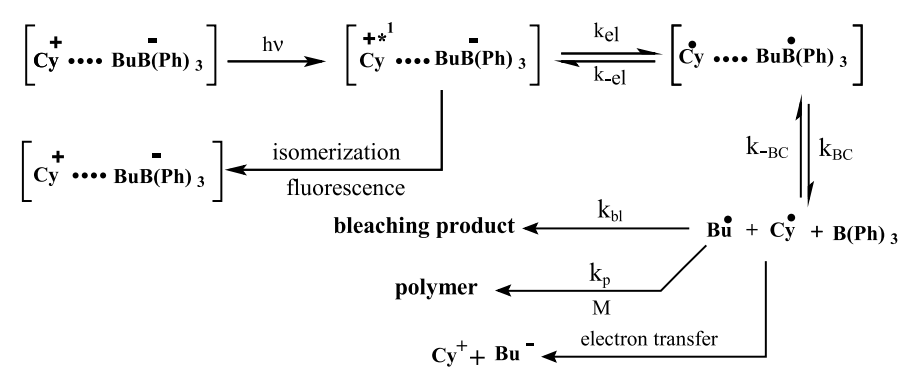
A number of examples of reductive cleavage of cationic acceptors (Eq. 2) and oxidative cleavage of anionic donors (Eq. 3) have been reported [91].

Most photoreducible dyes absorb in the visible region. A suitable dye/co-initiator system must exhibit a high absorption in the wavelength delivered by visible light sources (lasers) in order to efficiently generate the reactive initiating radicals [91].

### 3.4 Polymethine Dyes as Sensitizers in Two-Component Photoinitiating Systems

### 3.4.1 Cyanine Dye/Alkyltriphenylborate Salt

Cyanine dyes act as a primary absorber of the visible light in many photoinitiator systems. The ion pair composed of a cyanine dye cation and an alkyltriarylborate anion was first described by G.B. Schuster et al. [9, 10]. Work on the photochemistry of cyanine borates led to the preparation of commercial photoinitiators that are color-tunable and operate in the visible region [94-99]. The cyanine cation and borate anion exist as an ion pair even in medium polarity solvents, and some of them even form penetrated ion pairs for which the center-to-center distance between the ions is less than the sum of their individual radii [100-103]. Since the lifetime of the excited singlet state of a cyanine dye is too short to allow for an efficient diffusive encounter at an achievable concentration of the borate, self-association of the cyanine cation and borate anion is a prerequisite for efficient photoinduced reaction. The mechanism of free radical formation from cyanine borates was established using photolytic studies including laser flash photolysis [100]. Laser flash photolysis of a cyanine benzyltriphenylborate salt showed very fast bleaching of the cyanine absorption and the formation of a transient cyanine dye radical. Similar experiments



Scheme 2

performed with a vinyltriphenylborate analogue showed that the process occurs with significantly less efficiency than that of the benzyltriphenylborate salt. On the other hand, in the photolysis of a tetraphenylborate salt, the cyanine radical is not generated and the excited singlet state of the dye is nearly completely returned to the cyanine ion ground state at the end of the pulse.

The laser flash photolysis data helped delineate the mechanism of the polymerization initiation process. The initiation step of the reaction involves alkyl radical formation as a result of photoinduced electron transfer from the borate anion to the excited singlet state of cyanine dye, followed by a rapid cleavage of the carbon-boron bond of the boranyl radical (Scheme 2). Possible processes for free radical photoinitiated polymerization with the use of cyanine borate initiators are presented in Scheme 2, where  $k_{\rm BC}$  denotes the rate of the carbon-boron bond cleavage, the reverse step is designated as  $k_{\rm -BC}$ , and  $k_{\rm bl}$  is the rate constant of the free radicals cross-coupling step yielding bleached dye.

### 3.4.2 Symmetrical Cyanine Borate Photoredox Pairs as Visible-Light Photoinitiators

In this section, the experimental results describing the application of the cyanine borate salts as the photoinitiators of polymerization of acrylic monomers are presented [11, 42, 105–118]. The effect of the photoinitiating ion-pair structure on the rate of photoinitiated free radical polymerization is also considered.

The structures of symmetrical polymethine dyes as n-butyltriphenylborate salts tested as visible light photoinitiators for free radical polymerization are shown in Chart 3.

#### Chart 3

The choice of the photoinitiator is essential in laser-induced polymerization, since even the most reactive acrylic monomers polymerize slowly when exposed in pure form to the laser beam (less than 3% conversion after 1 min.). In our studies, the polymerizations in the presence of cyanine borate salts were performed under irradiation at 514 nm by using an argon-ion laser.

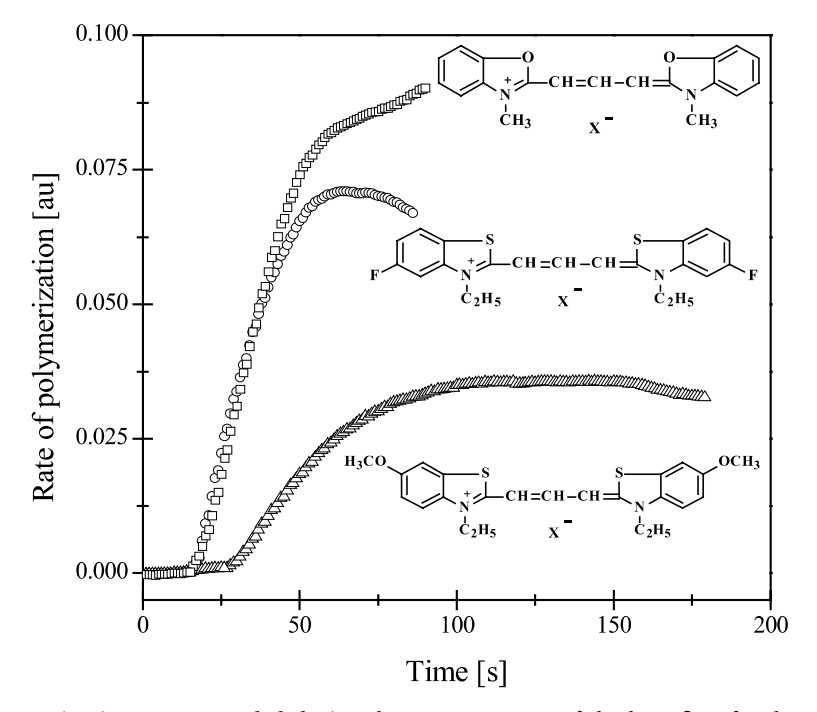


**Fig. 12** Kinetic curves recorded during the measurements of the heat flow for the photoinitiated polymerization of the TMPTA/MP (9:1) mixture initiated by the tested borate salts ( $X^- = n$ -butyltriphenylborate). The dye concentration was  $1 \times 10^{-3}$  M,  $I_a = 64$  mW/cm<sup>2</sup> [105]. (Reprinted with permission of John Wiley & Sons, Inc.)

The benzothiazolium trimethine dyes (X=S) are characterized by an intense absorption at 550–600 nm and a second, less intense, hypsochromically shifted absorption. For the corresponding benzoxazolium analogues (X=O), the absorption bands are hypsochromically shifted by about 60–70 nm. The two bands are assigned to the 0,0 and 0,1 vibronic transitions within the first excited state of the dye. The position of absorption  $\lambda_{max}$  essentially does not depend on the type of borate ion. The series of symmetrical polymethine dyes also contain several *meso*-substituted analogues (R<sup>9</sup> = alkyl). The principal difference between the *meso*-substituted and nonsubstituted dyes is reflected in the value of the molar absorption coefficient, which is smaller for *meso*-alkyl substituted derivatives. The introduction of *meso*-alkyl substitution is known to destabilize the all-*trans* isomer of cyanine dye in solution, which is normally the preferred ground state isomer [11, 105, 106, 110, 111, 118, 119].

The sensitivity of cyanine borate salts to the photoinitiation of free radical polymerization of a solution composed of 1-methyl-2-pyrrolidinone (MP), 2-ethyl-2-(hydroxymethyl)-1,3-propanediol triacrylate (TMPTA) and initiating cyanine borate with a concentration of  $1 \times 10^{-3}$  M depends on the structure of the dye (Fig. 12) and on the structure of the borate anion (Fig. 13).

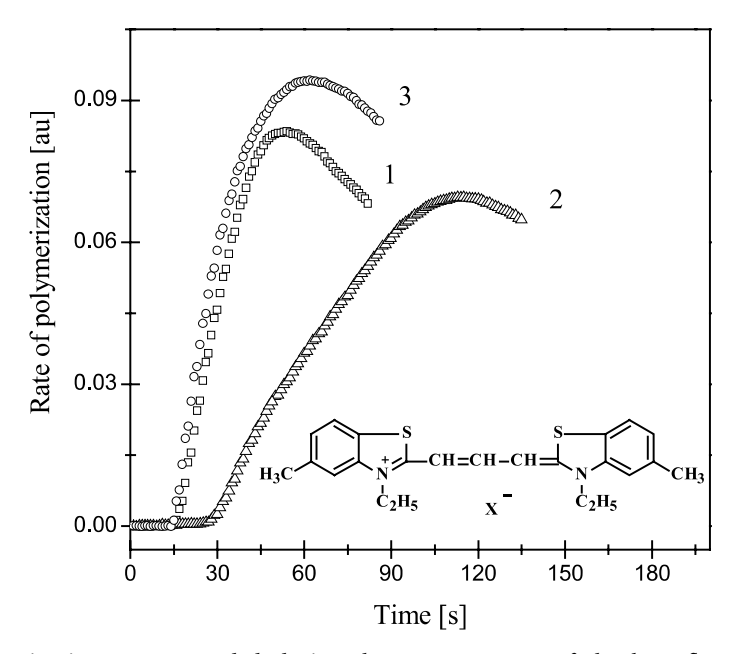


**Fig. 13** Kinetic curves recorded during the measurements of the heat flow for the photoinitiated polymerization of the TMPTA/MP (9:1) mixture initiated by the tested borate salts. (1)  $X^-=$  *n*-butyltriphenylborate, 2  $X^-=$  *sec*-butyltriphenylborate, 3  $X^-=$  *tert*-butyltriphenylborate. The dye concentration was  $1 \times 10^{-3}$  M,  $I_a = 64$  mW/cm<sup>2</sup> [105]. (Reprinted with permission of John Wiley & Sons, Inc.)

High rates of free radical polymerization are observed for symmetrical polymethine dyes without substituents at the end-heterocyclic units. The introduction of an electron-withdrawing atom, e.g., chloride and fluoride, into the heterocyclic system causes an increase in the rate of polymerization. On the other hand, electron-donating substituents such as methyl, methoxy and phenyl groups cause a decrease in the rate of free radical polymerization.

### 3.4.3 Hemicyanines as Photoinitiators for Free Radical Polymerization

Several photoredox pairs consisting of an asymmetric cyanine dye (acting as electron acceptor) and *n*-butyltriphenylborate anion (acting as electron donor) were tested as a photoinitiating system for the polymerization of the multiacrylate monomer. Their structures were presented earlier in Chart 1. The kinetic curves obtained for the photoinitiated polymerization of TMPTA-MP (9:1) mixture in the presence of selected hemicyanine borate salts, under irradiation with a visible light, are shown in Fig. 14 for illustration.

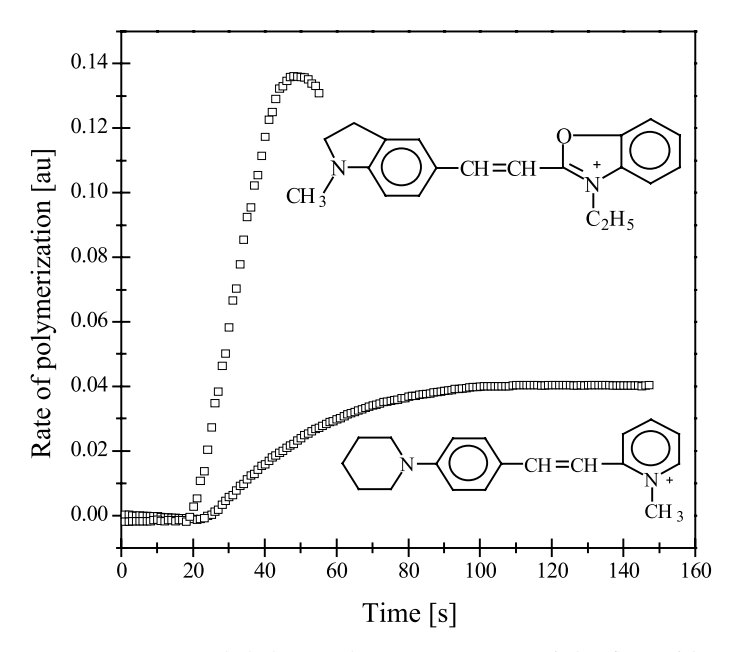


**Fig. 14** Kinetic curves recorded during the measurements of the flow of heat for the photoinitiated polymerization of the TMPTA/MP (9:1) mixture initiated by the tested borate salts. The dye concentration was  $1 \times 10^{-3}$  M,  $I_a = 64$  mW/cm<sup>2</sup>. The dyes are **E13** (*top*) and **A11** (*bottom*), and the anion is *n*-butyltriphenylborate [107]. (Reprinted with permission of John Wiley & Sons, Inc.)

Generally, the initiators with electron-donating groups other than dialkylamino groups or with electron-withdrawing groups induce somewhat higher rates of heat evolution (slope of the linear part of kinetic curve) in comparison to the photoredox pairs with the dyes possessing dialkylamino electrondonating substituents.

### 3.4.4 Modified Hemicyanines as Component of Effective Photoinitiating Photoredox Systems

Chart 4 shows dicationic styryl dyes (series **K**–**M**) and *N*-methoxypyridinium styryl dyes (series **N**) as novel photoinitiating systems for free radical polymerization of acrylate monomers.

Properties of the dicationic hemicyanine dyes of the series K-M as polymerization initiators have been compared to the properties of other monocationic styryl dyes of the series A-H discussed previously [41, 105, 107, 108, 120, 121]. These hemicyanines paired with borate electron donors are not the most sensitive reagents for inducing photopolymerization. For example, a rose bengal derivative is much more efficient [122].

#### Series K

$$R^3$$
 $N$ 
 $CH_2$ 
 $CH_2$ 
 $R^3$ 
 $R^3$ 

#### Series L

Series M Series N

Chart 4

The photoinitiation efficiency of a dicationic hemicyanine of the series M ( $R = NMe_2$ ,  $X^- = n$ -butyltriphenylborate) is comparable to the sensitivity of the rose bengal-based initiation systems (a triplet state photoinitiator [122]) and is the best of all the two-component photoinitiating systems described here.

Experiments with dyes of the series K and L revealed that these photoinitiators possess better photoinitiating abilities than their monocationic equivalents [123–126]. On the other hand, they initiate free radical polymerization with lower rates than monochromophoric dicationic hemicyanine borates, despite a similar value of degree of dissociation (about 45%). However, the specific spectroscopic properties make those symmetrical dicationic bischromophoric polymethine dyes good candidates for two-photon-induced initiators for free radical polymerization.

The third group of modified hemicyanine dyes as photoinitiators constitutes substituted N-methoxypyridinium borate salts (series N).

The replacement of an *N*-methyl group by *N*-methoxy group at the pyridine ring sharply increases the rate of photoinitiation of TMPTA free radical polymerization (Fig. 15). The better photoinitiating ability of the *N*-

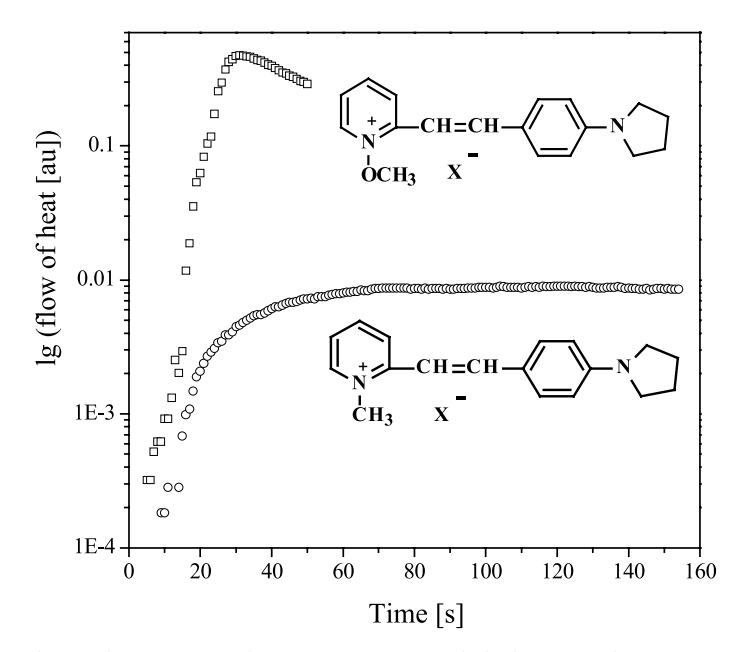


**Fig. 15** Photopolymerization kinetic traces recorded during polymerization of the TMPTA/MP (9:1) mixture initiated by  $N\alpha$  (top) and A10 (bottom) n-butyltriphenylborate salts. The dye concentration was  $4.5 \times 10^{-2}$  M,  $I_a = 64$  mW/cm<sup>2</sup>. For clarity of presentation the rate of polymerization is expressed in logarithmic form [113]. (Elsevier (or appropriate Society name))

methoxy derivatives is a consequence of an increase in the quantum yield of free-radical formation, caused by the fragmentation of the electron-acceptor radical obtained after electron transfer. The type of N-methoxypyridinium substitution  $(\alpha, \beta \text{ or } \gamma)$  does not significantly affect the photoinitiation efficiency [113].

### 3.4.5 Influence of Coinitiator Concentration

Initiation of polymerization via photoinduced intermolecular electrontransfer process may involve many steps such as photoinduced electron transfer from an electron donor to the excited state of a dye or from an excited electron donor to the ground state of an electron acceptor followed by secondary reactions yielding a neutral radical initiating polymerization. The steps determining the reaction rate of the free-radical-initiated polymerization via intermolecular electron-transfer process (PET) are dependent on the nature of the dye and the electron donor (or acceptor). It has been suggested that symmetrical cyanine borate salts [10, 102] in nonpolar or medium polarity solvents can be treated as ion pairs. However, our studies on the influence of the borate anion concentration on the rate of photoinitiated polymerization showed a distinct increase in the rate of polymerization as the concentration of borate anion increased [41, 107, 108]. This finding suggests that at the concentration of borate anion that is equal to the concentration of cyanine cation, only a part of the photoredox pairs exists as ion pairs. Since the electron transfer in cyanine dyes occurs in their singlet state, the existence of a cyanine cation and borate anion as an ion pair is the basic prerequisite for effective electron transfer. It can be suggested that the additional amount of borate anion in the polymerizing composition should shift the equilibrium between free ions and ion pairs to a higher ion-pair concentration and cause an increase in the photoinitiation efficiency of the dye-borate salt. Indeed, a study of the influence of borate concentration on the rate of photoinitiated polymerization revealed a distinct increase in the rate of photopolymerization with the increase in concentration of borate anion [11, 105, 106, 115].

## 3.5 Cyanine Dye/N-Alkoxypyridinium Salt as Three-Component Photoinitiating Systems

N-alkoxypyridinium salts are useful sources of radicals for photoinitiated polymerization. Single-electron transfer from cyanine chromophore to N-alkoxypyridinium salt results in N – O bond cleavage and the formation of an alkoxy radical (Scheme 3).

210 J.Pączkowski et al.

Scheme 3

The driving force for the fragmentation reaction is the formation of a stable pyridine molecule. *N*-alkoxypyridinium salts have proven to be effective as photoinitiators with a wide range of sensitizers [91]. When the reduction potential of the donor molecule is more negative than that of *N*-alkoxypyridinium salt (i.e., it is more difficult to reduce), the photochemical electron-transfer reaction will be exothermic. Thus, the energetics of electron transfer from an excited hemicyanine dye to *N*-alkoxypyridinium salt, and thus the efficiency of forming initiating radicals, can be a function of the difference in the reduction potentials of the two reactants [91]. Dyes used in combination with *N*-methoxypyridinium *n*-butyltriphenylborate in our studies to photoinitiate polymerization are the unsymmetrical benzothiazolium derivatives (Chart 1). From these studies it was concluded that the reduction potential of the dye is the main factor controlling the initiation efficiency of polymerization.

From the laser flash photolysis measurements performed for a model triplet state chromophore, it was concluded that the chromophore radical is quenched by *N*-alkoxypyridinium cation (+PyOR) [104, 109].

The lifetime of a chromophore radical in MeCN solution is about 10 µs and it decreases as the concentration of +PyOR increases. The Stern-Volmer plots obtained from the Py' lifetime measurements are linear over the whole range of the quencher concentration used [109]. Therefore, it appears that the alkoxypyridinium cation is reduced by dye radical. This reaction generates alkoxypyridinium radical that undergoes fragmentation giving neutral pyridine and alkoxy radical. Gould et al. have documented that exothermic photochemical electron-transfer reaction requires the reduction potential of the donor molecule to be more negative in comparison to the reduction potential of the alkoxypyridinium cation [91]. The dyes F1 and F10 (Chart 1) in combination with N-methoxy-4-phenylpyridinium n-butyltriphenylborate were studied. The dyes F1 and F10 undergo reduction at about - 1.06 V and at about - 0.73 V, respectively (versus Ag - AgCl). The measured value of reduction potential for N-methoxy-4-phenylpyridinium cation is about - 0.67 V. Thus, in the presence of the methoxypyridinium cation, only dye F1 can initiate polymerization because the energy of its photoredox pair is close to the region where the electron transfer becomes exothermic. It is commonly assumed that the oxidation potential of the dye radical is approximately equal to the reduction potential of the dye cation. Thus, the

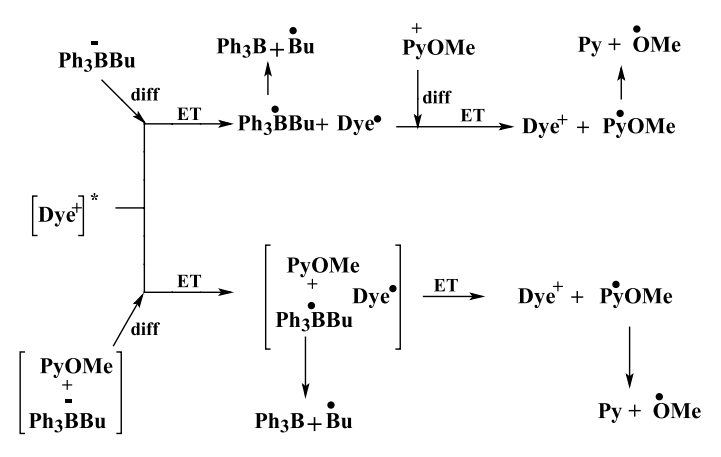
reduction potentials for the dye radicals under study are – 1.06 V for F1' and – 0.73 for F10', respectively. The reduction potential of the N-methoxy-4-phenylpyridinium cation is about – 0.67 V. Thus, the driving force of electron transfer between the dye radical and N-methoxy-4-phenylpyridinium cation is 0.42 eV (– 40.5 kJ mol $^{-1}$ ) for dye F1 and – 0.06 eV (– 5.8 kJ mol $^{-1}$ ) for dye F10. The negative values indicate that the electron transfer between dye radicals and N-methoxy-4-phenylpyridinium cation is thermodynamically allowed [109]. It was found that in the presence of F1, the polymerization rate increases with increasing concentration of N-methoxy-4-phenylpyridinium n-butyltriphenylborate.

As mentioned above, Gould and Farid described reactions of photoinitiated polymerization that apply the electron transfer occurring between the excited state of dye and N-alkoxypirydinium salts, acting as the efficient ground-state electron acceptors [91]. The photochemistry of such electrontransfer reactions was, in part, clarified by Schuster et al. [9, 10, 127], who concluded that for the singlet state reaction, the nitrogen-oxygen bond cleavage competes successfully with the back electron transfer. When reaction occurs in an overall triplet state, back electron transfer cannot occur and solvation and nitrogen-oxygen bond cleavage to form an alkoxy radical become competitive. Following the Schuster and Gould studies we have compared the reactivity of systems composed of positively charged hemicyanine dye acting as light absorber, n-butyltriphenylborate (Ph<sub>3</sub>BBu<sup>-</sup>) anion acting as electron donor and methoxypyridinium (+PyOMe) cation acting as ground-state electron acceptor. Salts Ph<sub>3</sub>BBu<sup>-</sup>Me<sub>4</sub>N<sup>+</sup>, <sup>+</sup>PyOMe F<sub>4</sub>B<sup>-</sup> or +PyOMe Ph<sub>3</sub>BBu<sup>-</sup> were used in the polymerizing formulations. There are two significant structural differences between the main system studied by us and that reported by Schuster [9, 10, 127]. First, the absorbing dyes are positively charged and this feature allows the obtaining of a neutral radical after an electron transfer. Second, we use coinitiators paired either with different counterions or in the form of an ion pair, which allows substrates of electron-transfer reactions in a specific form to organize. As a result, the diffusion effect on overall efficiency of photoinitiation is minimized [109, 113].

The highest rate of polymerization is observed for the formulation in which a n-butyltriphenyl borate and N-methoxy-4-phenylpyridinium ion pair acts as coinitiating pair. The relative rate of photoinitiated polymerization is the lowest for the system containing only n-butyltriphenylborate salt as electron donor [109, 113].

On the basis of the photochemistry of the borate anion [9, 10] and the photochemistry of N-alkoxypyridinium cation [91, 109, 113] the following unified mechanism was proposed (Scheme 4).

J.Paczkowski et al.



**Scheme 4** (Reprinted with permission from [109])

Two possible pathways of free radical generation are considered. The upper path describes the processes that can occur when all initiating components are not organized, e.g., they are present in formulation as salts of photochemically inert counterions. After excitation, in order to make an electron transfer effective the electron donor and electron acceptor must diffuse to each other to form an encounter complex, in which an electron-transfer reaction takes place. The resulting boranyl radical undergoes decomposition generating neutral triphenylboron and butyl radical [9, 10, 127]. The other product of the electron-transfer reaction is dye radical that could participate in a second electron-transfer reaction with alkoxypyridinium cation to form alkoxypyridinium radical and in this way to generate a second radical.

It was suggested that for the photoinitiation occurring via the singlet excited state, the diffusion of photoinitiator components and the back electron transfer limit an overall efficiency of photoinitiation. The simplest way to eliminate the diffusion effect is to covalently link a dye with either an electron donor or electron acceptor. An example of such a dye is N1 (Chart 4) as *n*-butyltriphenylborate salt. The mechanism of free-radical generation was clarified with the use of laser flash photolysis experiments. Electron transfer to the dye N1 generates radical localized on the pyridine nitrogen atom. Then this radical undergoes fragmentation forming methoxy radical and reduced dye.

# 3.6 Thermodynamics of Photoinitiation

Discussion of the cyanine borates photochemistry should include the estimation of the thermodynamic driving force of photoinduced electron-transfer

reaction (PET). The main prerequisite for PET reactions is described by the Rehm–Weller equation, Eq. 4, which states that the free energy of activation for the PET ( $\Delta G_{\rm el}$ ) process should have negative value [128, 129]

$$\Delta G_{\rm el}^0 = E_{\rm ox} \left( {\rm D/D}^{\, \cdot +} \right) - E_{\rm red} \left( {\rm A}^{\, \cdot -} / {\rm A} \right) - Z e^2 / \varepsilon a - E_{\rm oo} \; . \label{eq:delta_General}$$

#### **Equation 4**

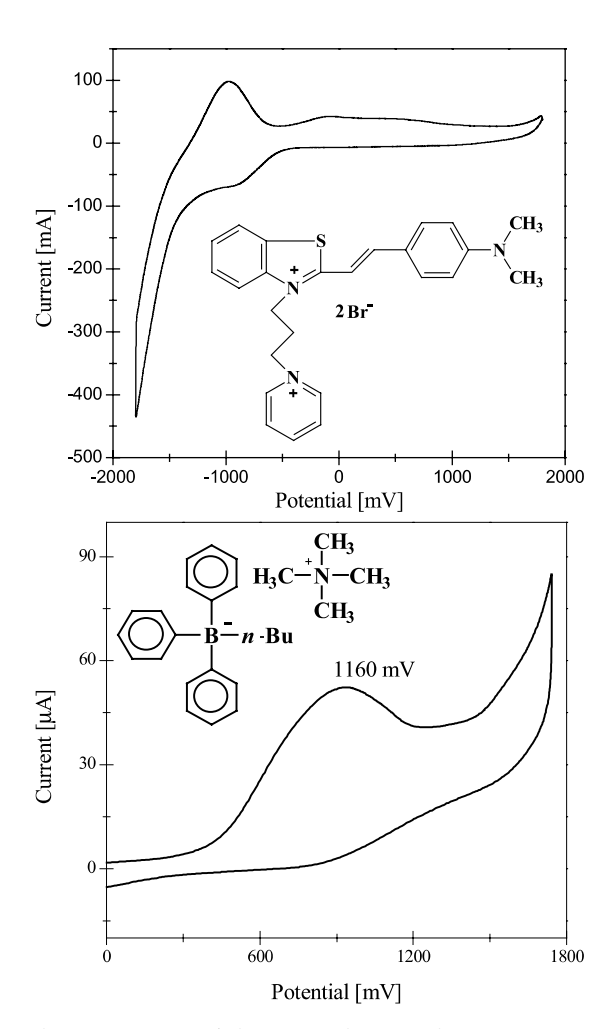


**Fig. 16** Cyclic voltamperograms of dicationic dye M (Chart 4, R=H) and tetramethylammonium n-butyltriphenylborate in 0.1 M tetrabutylammonium perchlorate solution in dry acetonitrile as the supporting electrolyte [115]. (Reprinted with permission of John Wiley & Sons, Inc.)

J.Paczkowski et al.

**Fig. 17** Oxidation potentials  $(E_{ox})$  of borate salts

In this function,  $E_{\rm ox}$  (D/D<sup>\*+</sup>) is the oxidation potential of the electron donor,  $E_{\rm red}$  (A<sup>\*-</sup>/A) is the reduction potential of the electron acceptor,  $E_{\rm oo}$  is the energy of the excited state and  $Ze^2/\varepsilon a$  is the Coulombic energy associated with the process.

Usually the electrochemical data are measured in acetonitrile solution. The electrochemical reduction of dye M (Chart 4, R=H) in acetonitrile solution is reversible (Fig. 16). However, the oxidation of n-butyltriphenylborate is dissociative, which causes the electrochemical process to be irreversible.

The thermodynamically meaningful oxidation potential can also be estimated using an indirect kinetic method described by Murphy and Schuster [102]. The oxidation potentials measured electrochemically and kinetically differ by about 0.3 V [106, 115].

In spite of the fact that the obtained electrochemical values for both components of photoredox pairs are only approximate, they allow estimation the free energy of activation ( $\Delta G_{\rm el}$ ) for the PET. The experimental values of the oxidation potentials of three isomeric borate salts are presented in Fig. 17.

# 3.7 Marcus Theory Applied to Kinetics Study of Multifunctional Acrylates Polymerization

The rate of the photoinitiated polymerization  $(R_p)$  can be described by Eq. 5 [17, 58, 59, 63, 105, 130]

$$\ln R_{\rm p} = A - (\lambda + \Delta G_{\rm el})^2 / 8\lambda RT,$$

#### **Equation 5**

where A combines all constant data for the initial time of polymerization,  $\lambda$  is defined as the total reorganization energy, and  $\Delta G_{\rm el}$  is the free energy of activation for PET as expressed by Eq. 4. It is apparent from Eq. 5 that for the photoinduced polymerization occurring via the electron- transfer pro-

cess, the relationship between the rate of polymerization  $R_{\rm p}$  and free energy of activation  $\Delta G_{\rm el}$  should present a classical, Marcus parabolic relationship. Equation 5 predicts that the rate of polymerization may be controlled, in part, by the rate of photoinduced electron transfer. As a consequence, the Marcus equation can be applied for the description of the rate of the polymerization photoinitiated via the photoinduced intermolecular electron transfer. Experimental verification of Eq. 5 for the tested ion pairs is possible by measuring the rate of the primary process of the polymerization initiation process, e.g., the rate of the electron transfer between the borate and cyanine ions.

As already noted, Schuster and coworkers [9, 10] established that the single-electron transfer from the alkyltriphenyl borate to the excited cyanine dye occurs at a rapid rate. These authors also established that the unassociated cyanine cations fluoresce and there is no (or very little) fluorescence from the cyanine borate ion pair. Finally, they concluded that the fluorescing state of the cyanine is not the state that is reduced by the borate [9, 10]. In order to clarify the relationships between the rate of the polymerization and the photophysical properties of cyanine dyes, fluorescence lifetime measurements were performed. The fluorescence lifetimes were measured for the cationic dyes with a variety of counteranions. Surprisingly, these measurements revealed mostly two-exponential fits with the experimental residual very close to the theoretical one.

For a few dyes, a three-exponential model was necessary in order to obtain the acceptable fits. There are also examples, mostly for *meso*-substituted cyanines, of single-exponential decay [127, 131–134]. The alkyl substitution in the *meso* position of the polymethine chain dramatically decreases the fluorescence lifetime, which is attributed to faster torsional relaxation to the ground state of the excited dye [135]. The exchange of ethyl sulfate or iodide anion for borate ion also strongly decreases the cyanine ion fluorescence lifetime.

Theoretical calculations of the cyanine ground states in the *trans* and *cis* forms of the polymethine chain have been conducted [106, 110, 133, 136]. The spectroscopic properties of the *cis* form of cyanine dyes should be clarified here. In literature, there is controversy about the interpretation of the transient absorption spectra of cyanine dyes. Indolium trimethine cyanines display characteristic transient absorption (apparent absorption maximum at 580 nm) that decays in a nanosecond time scale and which, according to Schuster [127], can be attributed to mono-*cis* excited isomer. On the other hand, Serpone et al. [135], in their study of benzothiazolium trimethine dyes (Chart 3) attributed this transient absorption to the triplet excited state of the dye. However, it is necessary to emphasize that the heavy atom effect creates a transient with an apparent absorption maximum recorded at 620 nm [127] and that the triplet energy transfer sensitization of benzothiazolium trimethine dyes also gives an absorption band with a maximum at 630 nm [127, 137]. These observations allow us to anticipate that the nonemit-

J.Paczkowski et al.

ting state exhibiting a transient absorption band in the range 480–580 nm can be assigned to the absorption related to the presence of the excited *mono-cis* isomer.

The occurrence of the electron transfer between cyanine and borate ions leads to quenching and simultaneous shortening of the fluorescence lifetime of cyanine. Under the assumption that the electron transfer is the only additional quenching route available in the ion pair (lifetime  $\tau_{\text{CyB}}$ ), as compared to the parent dye (lifetime  $\tau_{\text{CyX}}$ ), the rate of the electron transfer ( $k_{\text{el}}$ ) for the ion pair can be obtained from Eq. 6

$$k_{\rm el} = \frac{1}{\tau_{\rm CyB}} - \frac{1}{\tau_{\rm CyX}} \ .$$

#### **Equation 6**

The calculated rate constants for the symmetrical polymethine dyes are in the range  $2.74 \times 10^8~\rm s^{-1}$  to  $6.6 \times 10^{10}~\rm s^{-1}$  [106, 110]. The main question arising during the quenching experiments is whether the fluorescing state of the cyanine is the state that is quenched and reduced by the borate. It is well known that the rate of the electron transfer is related to the free energy of the reaction through the classical Marcus equation [75]. It has been suggested that the quenched state is the fluorescing state [106, 110]. It is important to emphasize that the relationship predicted by the Marcus equation is fulfilled only for cyanines without substitution in the *meso* position. Accordingly, it can be suggested that *meso*-substituted cyanines are not quenched in their fluorescing state.

# 3.8 The Photobleaching Reaction of the Dye

It is evident from Scheme 2 that the photochemical reactions occurring after irradiation of the photoinitiator redox pair with visible light involve, besides the initiation of free radical polymerization, the color loss of the light absorber.

The colorless product obtained during polymerization originates from a cross-coupling reaction between an alkyl radical and a cyanine radical formed from an electron donor or an electron acceptor [9–11, 107, 122, 131, 138]. The above-mentioned reaction may decrease the efficiency of free radical photopolymerization.

The quantum yields of the dye photoreduction processes range from 0.005 to 0.3 [11, 105–108, 110, 111]. The efficiency of the bleaching process can be described using the Marcus relationship.

**Acknowledgements** This work was supported by Ministry of Science and Higher Education (MNiSW) (Grants No. 3 T09B 101 28, N N204 219734, and BS 13/2006).

### References

- 1. Eaton DF (1986) Adv Photochem 13:427
- 2. Eaton DF (1990) Top Curr Chem 156:199
- Paczkowski J, Kucybała Z, Ścigalski F, Wrzyszczyński A (2003) J Photochem Photobiol A 159:115
- 4. Oster G (1954) Nature 173:300
- 5. Shi J, Zhang X, Neckers DC (1992) J Org Chem 57:4418
- 6. Shi J, Zhang X, Neckers DC (1993) J Org Chem 58:2614
- 7. Polykarpov AY, Hassoon S, Neckers DC (1996) Macromolecules 29:8274
- 8. Hassoon S, Neckers DC (1995) J Phys Chem 99:9416
- 9. Chatterjee S, Gottschalk P, Davis PD, Schuster GB (1988) J Am Chem Soc 110:2326
- Chatterjee S, Davis PD, Gottschalk P, Kurz B, Yang X, Schuster GB (1990) J Am Chem Soc 112:6329
- 11. Kabatc J, Pietrzak M, Paczkowski J (1998) Macromolecules 31:4651
- 12. Encinas MV, Majmund C, Lissi EA, Scaiano JC (1991) Macromolecules 24:2111
- 13. Encinas MV, Lissi EE, Majmund C, Cosa JJ (1993) Macromolecules 26:6284
- Previtali CM, Bertolotti SG, Neumann MG, Pastre IA, Rufs AM, Encinas MV (1994)
   Macromolecules 27:7454
- 15. Kucybała Z, Pietrzak M, Pączkowski J (1998) Chem Mater 10:2555
- 16. Kucybała Z, Pączkowski J (1999) J Photochem Photobiol A 128:135
- 17. Paczkowski J, Neckers DC (2001) Photoinduced electron transfer initiating system for free radical polymerization. In: Gould IR (ed) Electron transfer in chemistry, vol 5. Wiley, Weinheim, p 516
- 18. Linden L-A, Pączkowski J, Rabek JF, Wrzyszczyński A (1999) Polimery 44:161
- Bricks JL, Slominski JL, Kudinova MA, Tolmachev AI, Rurack K, Resch-Genger U, Rettig W (2000) J Photochem Photobiol A 132:193
- 20. Loutfy RO (1986) Pure Appl Chem 58:1239
- 21. Jing D (1990) Polymer 31:110
- 22. Valdes-Aquilera O, Pathak CP, Neckers DC (1990) Macromolecules 23:689
- 23. Rettig W (1986) Angew Chem Int Edn 25:971
- Van Ramesdonk HJ, Vos M, Verhoeven JV, Möhlmann GR, Tissink NA, Meesen AW (1987) Polymer 28:951
- 25. Frahn MS, Luthjens LH, Warman JM (2003) Polymer 44:7933
- 26. Nishijama Y, Mito Y (1967) Rep Prog Polym Phys Jpn 10:139
- 27. Nishijama Y (1970) J Polym Sci C 31:353
- 28. Nishijama Y (1974) Fluorescence methods for studying molecular motion. In: Geil PH, Baer E, Wada Y (eds) The solid state of polymer. Dekker, New York, p 1
- 29. Loutfy RO (1981) Macromolecules 14:270
- 30. Loutfy RO (1982) J Polym Sci B 20:825
- 31. Cho D, Mattice WL, Porter LJ, Hemingway RW (1989) Polymer 30:1955
- 32. Kamat PV (1987) Anal Chem 59:1636
- 33. Kamat PV, Gupta SK (1988) Polymer 29:1329
- 34. Wang FW, Lowry RE, Grant WH (1984) Polymer 25:690
- 35. Wang FW, Lowry RE, Fanconi BM (1986) Polymer 27:1529
- 36. Pączkowski J, Neckers DC (1992) Chemtracts Macromol Chem 3:75
- 37. Morawetz H (1989) J Luminesc 43:59
- 38. Jager WF, Kudasheva D, Neckers DC (1996) Macromolecules 29:7351
- 39. Wróblewski S, Trzebiatowska K, Jędrzejewska B, Pietrzak M, Gawinecki R, Paczkowski J (1999) J Chem Soc Perkin Trans 2 1909

J.Paczkowski et al.

 Bajorek A, Trzebiatowska K, Jędrzejewska B, Pietrzak M, Gawinecki R, Pączkowski J (2004) J Fluoresc 14:295

- 41. Kabatc J, Jędrzejewska B, Pączkowski J (2006) J Appl Polym Sci 99:207
- 42. Kabatc J, Jędrzejewska B, Bajorek A, Pączkowski J (2006) J Fluoresc 16:525
- 43. Mishra A, Behera PK, Behera RK, Mishra BK, Behera GB (1998) J Photochem Photobiol A 116:79
- 44. Koti ASR, Bhattacharjee B, Haram NS, Das R, Periasamy N, Sonawane ND, Rangnekar DW (2000) J Photochem Photobiol A 137:115
- 45. Loew LM, Simpson LL (1981) Biophys J 34:353
- 46. Ephardt H, Fromherz P (1989) J Phys Chem 93:7717
- 47. Gawinecki R, Kolehmainen E, Kauppinen R (1998) J Chem Soc Perkin Trans 2:25
- 48. Fromherz P, Heileman A (1992) J Phys Chem 96:6864
- 49. Strehmel B, Younes M, Strehmel V, Wartewig S (1992) Prog Colloid Polym Sci 90:1
- 50. Foster R (1969) Organic Charge Transfer Complexes. In: Organic CT complexes. Academic Press, London, p 384
- 51. Hermant RM, Bakker NAC, Scherer T, Krijnen B, Verhoeven JW (1990) J Am Chem Soc 112:1214
- 52. Porter G, Suppan P (1965) Trans Faraday Soc 61:1664
- 53. Ghazy R, Azim SA, Shaheen M, El-Mekawey F (2004) Spectrochim Acta A 60:187
- 54. Sheng SJ, El-Sayed MA (1977) Chem Phys 20:61
- 55. Cyrii P, Maged SA, Aaron JJ, Michaela B, Alphonse T, Lamine C (1994) Spectrosc Lett 27:439
- 56. Kawski A (1991) Z Naturforsch A 54:379
- 57. Kawski A, Kukliński B, Bojarski P (2001) Z Naturforsch A 56:407
- 58. Bakshiev NG (1964) Opt Spectrosc 16:821
- 59. Chamma P, Viallet CR (1970) C R Hebd Sean Acad Sci 270:1901
- 60. Sharma VK, Saharo PD, Sharma N, Rastogi RC, Ghoshal SK, Mohan D (2003) Spectrochim Acta A 59:1161
- 61. Inamdar SR, Nadaf YF, Mulimani BG (2003) J Mol Struct 624:47
- 62. Bilot L, Kawski A (1962) Z Naturforsch A 17:621
- 63. Kawski A, Rabek JF (eds) (1992) Progress in photochemistry and photophysics, vol. 5. CRC, Boca Raton, p 1
- 64. Kabatc J, Ośmiałowski B, Pączkowski J (2006) Spectrochim Acta A 63:524
- 65. Koti SR, Bhattacharjee B, Haram NS, Das R, Periasamy N, Sonawane ND, Rangnekar DW (2000) J Photochem Photobiol A 137:115
- 66. Jager WF, Lungu A, Chen DY, Neckers DC (1997) Macromolecules 30:780
- 67. Rettig W (1994) Photoinduced electron transfer. In: Mattay J (ed) Topics in current chemistry. Springer, Berlin, p 93
- 68. Strehmel H, Seifert W, Rettig W (1997) J Phys Chem 101:2232
- 69. Rotkiewicz K, Grellman KH, Grabowski ZR (1973) Chem Phys Lett 19:315
- 70. Grabowski ZR, Rotkiewicz K, Siemiarczuk A, Cowley D, Baumann W (1979) Nouv J Chim 2:443
- 71. Herstroeter WG (1973) J Am Chem Soc 95:8686
- 72. Herstroeter WG (1975) J Am Chem Soc 97:3090
- 73. Smith WF, Herstroeter WG, Eddy KL (1975) J Am Chem Soc 97:2764
- 74. Herstroeter WG (1976) J Am Chem Soc 98:6210
- 75. Marcus RA (1989) J Phys Chem 93:3078 and references cited therein
- 76. Kapturkiewicz A, Herbich J, Karpiuk J, Nowacki J (1997) J Phys Chem A 101:2332
- 77. Herbich J, Kapturkiewicz A (1998) J Am Chem Soc 120:1014
- 78. Onsager L (1936) J Am Chem Soc 58:1486

- 79. Lippert E (1955) Z Naturforsch A 10:541
- 80. Mataga N, Kaqifu Y, Kouzumi M (1955) Bull Chem Soc Jpn 28:690
- 81. Pączkowski J, Neckers DC (1992) Macromolecules 25:548
- 82. Lis S, Konarski J, Hnatejko Z, Elbanowski M (1994) J Photochem Photobiol A 79:25
- 83. Plambeck LF (1956) US Patent 2760 863
- 84. Cohen AB, Walker P (1989) Imaging processes and materials. In: Sturge J, Walworth V, Shepp A (eds) Neblett's, 8th edn. Van Nostrand Reinhold, New York, p 240
- 85. Neckers DC, Jager W (1998) Photoinitiation or photopolymerization: UV and EB at the millennium. Wiley, Chichester
- 86. Lowe C, Webzter G, Kessel S, McDonald I (1997) Formulation. chemistry and technology for UV and EB formulation for coatings, inks and points. Wiley, Chichester
- 87. Reiser A (1989) Photoreactive polymers: the science and technology of resists. Wiley, New York
- 88. Monroe BM (1993) Chem Rev 93:435
- 89. Katley AD (1982) J Radiat Curing 3:35
- 90. Eaton F (1984) Pure Appl Chem 56:1191
- 91. Gould R, Shukla D, Giesen D, Farid S, (2001) Helv Chim Acta 83:2796
- 92. Matsumoto S (1962) Bull Chem Soc Jpn 35:1860
- 93. Eaton DF (1979) Photogr Sci Eng 23:150
- 94. Gottschalk P, Neckers DC, Schuster GB (1980) US Patent 4772 530
- 95. Gottschalk P, Neckers DC, Schuster GB (1987) Chem Abstr 107:187434n
- 96. Gottschalk P, Neckers DC, Schuster GB (1988) US Patent 4842980
- 97. Gottschalk P, Neckers DC, Schuster GB (1987) Chem Abstr 107:187434n
- 98. Gottschalk P (1989) US Patent 4874450
- 99. Weed G, Monroe BM (1992) US Patent 5 143 818
- 100. Lan LY, Schuster GB (1986) Tetrahedron Lett 27:4261
- 101. Yang X, Zaitsev A, Sauerwein B, Marphy S, Schuster GB (1992) J Am Chem Soc 114:793
- 102. Murphy S, Yang X, Schuster GB (1995) J Org Chem 60:2411
- 103. Owen DJ, Schuster GB (1996) J Am Chem Soc 118:259
- 104. Griller D, Ingold KU, Patterson LK, Scaino JC, Small RD (1979) J Am Chem Soc 101:3780
- 105. Kabatc J, Jędrzejewska B, Pączkowski J (2000) J Polym Sci A Polym Chem 38:2365
- 106. Kabatc J, Pietrzak M, Paczkowski J (2002) J Chem Soc Perkin Trans 2 2:287
- 107. Kabatc J, Jędrzejewska B, Pączkowski J (2003) J Polym Sci A Polym Chem 41:3017
- 108. Jędrzejewska B, Kabatc J, Pietrzak M, Pączkowski J (2002) J Polym Sci A Polym Chem 40:1433
- 109. Kabatc J, Pączkowski J (2005) Macromolecules 38:9985
- 110. Kabatc J, Pączkowski J, Karolczak J (2003) Polimery 48:425
- 111. Kabatc J, Pączkowski J (2003) Polimery 48:321
- 112. Kabatc J, Kucybała Z, Pietrzak M, Ścigalski F, Pączkowski J (1999) Polymer 40:735
- 113. Kabatc J, Paczkowski J (2006) Polymer 47:2699
- 114. Kabatc J, Jędrzejewska B, Pączkowski J (2005) Polym Bull 54:409
- 115. Kabatc J, Jędrzejewska B, Pączkowski J (2006) J Polym Sci A Polym Chem 44:6345
- 116. Kabatc J, Jędrzejewska B, Gruszewska M, Pączkowski J (2007) Polym Bull 58:691
- 117. Bajorek A, Kabatc J, Paczkowski J (2007) Polimery 52:556
- 118. Jędrzejewska B, Kabatc J, Paczkowski J (2005) Polimery 50:418
- 119. Kabatc J, Paczkowski J (2004) Dyes Pigm 61:1
- 120. Jedrzejewska B, Kabatc J, Pietrzak M, Paczkowski J (2003) Dyes Pigm 58:47
- 121. Kabatc J, Jędrzejewska B, Orliński P, Pączkowski J (2005) Spectrochim Acta A 62:115

J.Pączkowski et al.

122. Valdes-Aquilera O, Pathak CP, Shi J, Watson D, Neckers DC (1992) Macromolecules 25:541

- 123. Jędrzejewska B, Kabatc J, Pączkowski J (2007) Dyes Pigm 73:361
- 124. Jędrzejewska B, Kabatc J, Pączkowski J (2007) Dyes Pigm 74:262
- 125. Jędrzejewska B, Kabatc J, Ośmiałowski B, Paczkowski J (2007) Spectrochim Acta A 67:306
- 126. Jędrzejewska B, Jeziórska J, Pączkowski J (2008) J Photochem Photobiol A: Chem 195:105
- 127. Sauerwein B, Schuster GB (1991) J Phys Chem 95:1903
- 128. Rehm DA, Weller (1969) Ber Bunsenges Phys Chem 73:834
- 129. Rehm DA, Weller (1970) Isr J Chem 8:259
- 130. Pączkowski J, Pietrzak M, Kucybała Z (1996) Macromolecules 29:5057
- 131. Schuster GB (1991) Adv Electron Transfer Chem 1:163
- 132. Sahyun MR, Serpone N (1997) J Phys Chem 101:9877
- 133. Khlimenko V, Chibisov AK, Görner H (1997) J Phys Chem 101:7304
- 134. Murphy S, Sauerwein B, Drickamer HG, Schuster GB (1994) J Phys Chem 98:13476
- 135. Serpone N, Sahyun MRV (1994) J Phys Chem 98:734
- 136. Sanchez-Galvez A, Hunt P, Robb MA, Olivucci M, Vreven T, Schlegel HB (2001) J Am Chem Soc 122:2911
- 137. O'Brien DF, Kelly T, Costa LFA (1974) Photogr Sci Eng 18:76
- 138. Previtali CM, Bertolotti SG, Neumann MG, Pastre IA, Rufs AM, Encinas MV (1994) Macromolecules 27:7454

# Stability and Reactivity of Polymethine Dyes in Solution

Maged Henary¹ (⋈) · Mariusz Mojzych¹,²

1	Introduction	221
2	Photodegradation	222
2.1	Mechanism	222
2.2	Structural Effects	225
2.2.1	Rigidization	225
2.2.2	Inhibition of Aggregation and Steric Protection	226
2.2.3	Miscellaneous	229
3	Dark Reactions	232
3.1	General	232
3.2	Nucleophile Addition	232
3.2.1	Reactions of Cyanines with Hydride and Cyanide Ions	232
3.2.2	Reactions with Hydroxide and Alkoxide Ions	234
Dofor	on cas	23

**Abstract** The widespread use of polymethine dyes in high-technology applications such as optical recording, thermal displays, laser printers, laser filters, and infrared photography involves a solid state of the dyes. The polymethine dyes are relatively stable in the solid state. By contrast, a common limitation of the application of the polymethine dyes in solution, especially those with long-wavelength absorption bands, is their susceptibility to chemical and photochemical degradation. The features that affect stability of the dyes in solution under dark and light conditions are the subject of this review. The reactivity of polymethine dyes, that can be used in synthetic modifications, is also discussed.

 $\label{eq:keywords} \begin{tabular}{ll} \textbf{Keywords} & Cyclodextrin \cdot Encapsulation \cdot NIR \cdot Pyroninocyanine dyes \cdot Rigidization \cdot Rotaxane \cdot pH-sensitive dyes \end{tabular}$ 

# Introduction

As shown in other parts of this volume, solid polymethine dyes are widely used in many commercial products. They serve as active ingredients in semi-conducting materials, laser materials, optical recording media, paints, and are used in infrared photography, among others. Polymethine dyes are relatively stable in the solid state. The last decade has seen an increase in the applications of the dyes in solution, such as labeling of nucleic acids and proteins

<sup>&</sup>lt;sup>1</sup>Department of Chemistry, Georgia State University, Atlanta, Georgia 30302-4098, USA chemmh@langate.gsu.edu

<sup>&</sup>lt;sup>2</sup>Department of Chemistry, University of Podlasie, 08-110 Siedlce, Poland

and for use in medicine, as described by other authors in this volume. The first efforts of the use of these dyes in solution were strongly hampered by relatively low stability when compared to stability in the solid state. Subsequently, numerous studies have been undertaken to better understand the factors behind the instability. As a result, improved dyes for use in bioanalytical chemistry and medicine are being synthesized. As shown in other parts of this volume, the modern synthetic chemistry permits an easy preparation of various polymethine dyes, the absorption and fluorescence of which range from visible to near-infrared regions. The use of near-infrared dyes in the biological sciences is especially advantageous because of the low interference from background absorption and fluorescence [1]. More specifically, the interaction of a near-infrared dye with a biomolecule of interest can be studied directly without prepurification of the complex biological sample. Unfortunately, certain near-infrared dyes have been known to be much less stable in solution than their visible counterparts. The factors responsible for this low stability and the synthetic modifications that are known to increase stability of polymethine dyes are discussed herein. Degradation of the dyes in the presence of light and molecular oxygen and under dark conditions is discussed. Then, structural modifications of the dyes to improve their stability are presented. Since it is known that dyes in the aggregated state in solution are especially prone to photodegradation, special attention is given to a decrease in aggregation of polymethine dyes in solution. Specifically, bulky groups and cyclodextrin inclusion [2] of the cationic polymethine chain have been shown to inhibit aggregation by limiting the dye's self-sensitizing photooxidation [3]. Aggregation is also decreased for dyes containing sulfonate or sulfonatoalkyl groups attached to the heterocyclic subunits [4].

Reactivity of the dyes in relation to synthetic transformations for a facile introduction of various functional groups at the chromophore is also discussed. Overall, the conditions under which the chromophore is stable or not stable are analyzed.

# 2 Photodegradation

# 2.1 Mechanism

Degradation of polymethine dyes in solution in the presence of light and air has been a recurrent and troublesome problem over the years. The essential agents that contribute to this degradation process are molecular oxygen and light. However, these two components are ubiquitous and, in order to improve the chemical and light stability, a synthetic chemist must understand the mechanism of the photodegradation process. The major pathway of photodecomposition involves the reaction of singlet oxygen  $^1O_2$  with the chromophore [5–7]. Specifically, upon light absorption the molecule undergoes intersystem-crossing from the excited singlet state  $S_1$  to the excited triplet state  $T_1$  followed by interaction of  $T_1$  with endogeneous ground state triplet oxygen  $^3O_2$  to generate the destructive singlet species  $^1O_2$ . Subsequent attack on the polymethine chain by  $^1O_2$  results in fragmentation of the chromophore. Another reactive species is superoxide anion  $O_2$  which is also generated in the photochemical process.

Lepaja et al. have studied the main degradative pathway of indolium heptamethine cyanine 1 in aerated solution using sensitization techniques and specific quenchers [6].

Their results established that the photooxidation reaction proceeds, in part, with the involvement of  $^1O_2$  and the regioselectivity is controlled by the electrophilic centers of the chromophore. One major photoproduct in the degradation pathway of the indolium heptamethine dye 1 was identified by  $^1H$  NMR and IR analysis as 1,3,3-trimethyl-2-indolinone 2. This photoproduct is the result of the oxidation of the C1'-C2 or C7'-C2'' bond. Because of the electropositivity of the 2 or 2'' carbon relative to the electron-rich position 1' or 7' [8] of the cationic chromophore, singlet oxygen ( $^1O_2$ ) is directed towards the polymethine chain. Thus, the formation of the major photoproduct 2 is consistent with addition reaction of  $^1O_2$  to the cyanine C1'-C2 or C7'-2'' bond followed by fragmentation of the resultant adduct to the carbonyl compound 2.

Photosensitization in the presence of methylene blue and molecular oxygen also leads to degradation and oxidation of many cyanine dyes [9]. For example, the photoproducts obtained during such oxidation of the benzothiazolium trimethine cyanine dye 3 (Eq. 1) are a 3-penten-2-one 4 and

**Equation 1** 

a 2-benzothiazolone 5. These results are consistent with the addition of singlet oxygen to the polymethine chain before the bonds fragment to the corresponding carbonyl compounds.

A brief study of the mechanism of the photooxidation of heptamethine cyanine dye 6 (Scheme 1) was conduced by Chen et al. [7] utilizing VIS/NIR absorption and electron-spin resonance (ESR) techniques. The main photoproducts were characterized by <sup>1</sup>H NMR spectroscopy and fast-atom bombardment (FAB) mass spectrometry. The results of the experiments using spin-trapping probes 5,5-dimethyl-1-pyrroline N-oxide (DMPO) and 2,2,6,6tetramethyl-4-piperidone (TEMP) in conjunction with ESR were consistent with the formation of singlet oxygen  $({}^{1}O_{2})$  and superoxide anion  $(O_{2}^{-})$  as the reactive species responsible for the photofading process. Spectrophotometric analysis of the decrease of the absorption maximum at 756 nm in acetonitrile indicated that the rate of photooxidation follows first-order kinetics with a rate constant of 0.39 min<sup>-1</sup>. This degradation process follows the mechanism shown in Scheme 1 where benzothiazolium heptamethine cyanine dye 6 undergoes an addition reaction of singlet oxygen (1O2) or superoxide anion (O<sub>2</sub><sup>-</sup>) to the C1' - C2 or C7' - C2" bond to give a precursor to the conjugated aldehyde 7 and 3-ethyl-2-benzothiazolone 8. Subsequent oxidation of aldehyde 7, apparently by superperoxide anion, furnishes the carboxylic acid 9.

### Scheme 1

To enhance the chemical and light stability of cyanine dyes, synthetic chemists have made various structural modifications [3, 10] to the chromophore. Most of these modifications include rigidization of the polymethine chain to inhibit radiationless internal conversion (IC) and subsequent isomerization [3, 5]. Further modifications to instill durability on the chromophore rely on limiting the intermolecular interactions by altering the steric and/or ion-pair properties of the dye.

### 2.2 Structural Effects

# 2.2.1 Rigidization

The longer the polymethine chain the lower the stability, and starting with nonamethine dyes such as 10 the stability is marginal. However, the stability of 10 in solution was enhanced by incorporating the central portion of the polymethine chain into a ring system to instill rigidization of the chromophore [11]. It was found that the unbridged nonamethine cyanine 10 decomposes by approximately 70% in a 45 min period, while the rigidized nonamethine analog 11 decomposes by only 5% in a 24 h period.

Another example is dye 12, where the 11-methine chain is partially rigidized by incorporating part of the chain into two six-membered rings. Stable, structural analogs of 12 are also known [12].

In a similar way, the stability of heptamethine cyanine dyes is dramatically increased by incorporating all but two of the methine groups into a ring system [13, 14]. As an added benefit, rigidization increases fluorescence quantum yield with a concomitant decrease in the efficiency of the internal conversion (IC) process for cyanine dyes [5, 15]. The IC process is problematic for near-infrared absorbing cyanine dyes due to the linear correlation of the rate of IC to excitation energy [5]. In addition, the IC process proceeds more efficiently if twisted intramolecular charge-transfer (TICT) structures are formed. These TICTs result in photoisomerization of the chromophore and a subsequent degradation. However, the process of radiationless deactivation through torsional release is reduced and subsequent photoisomerization of the chromophore is inhibited if the skeleton of the chromophore is modified by rigidization [5].

# 2.2.2 Inhibition of Aggregation and Steric Protection

Modification of the chromophore to include bulky  $\beta$ -cyclodextrins (CDs) has been found to not only inhibit intermolecular association but also to lend to the enhancement of emission intensity and lifetime of the excited state [4]. Guether et al. analyzed the photostabilities of a series of indolium pentamethine cyanines in aqueous solution [2]. These studies included a substituted dye 13 and the parent dye devoid of the dextrin substitution. The chromophore of 13 apparently forms an intramolecular inclusion complex with the cyclodextrin.

The inclusion process inhibits photodegradation of the chromophore but the effect is dye dependent. For example, photodecomposition of benzothiazolium dyes occurs even after complexing with cyclodextrin, whereas analogous indolium dyes become more resistant to photobleaching upon cyclodextrin complexation.

An alternative way to form a permanently encapsulated chromophore is to construct an interlocked structure with a rotaxane. Smith et al. reported that encapsulation of a squaraine dye 14 with rotaxanes to form complexes 15 greatly increases the dark and photochemical stability of the dye [16, 17]. The enhanced stability of 15 may be due to two factors. First, the surrounding macrocycle that sits perfectly over both faces of the electrophilic cyclobutane

core of the squaraine blocks nucleophilic attack [17]. Second, aggregation of 15 is hindered in comparison to the aggregation of 14, which results in enhanced stability, as observed. The rotaxane inclusion complexes 15 exhibit the same photophysical properties as the precursor squaraine 14.

Encapsulation of dyes, so that their aggregation is inhibited for steric reasons, provides a means to increase photostability. Another way to hinder aggregation is to modify dyes with sterically bulky groups. Such groups do not have to be as large as the cyclodextrin portion of 13. For example, the profound increase in stability of 11 in comparison to 10 and the remarkable stability of 12 may be attributed, at least in part, to the steric protection effect. By simply utilizing a 3,3-dimethylindolium moiety as the end-heterocyclic unit of the dye, in comparison to benzothiazolium, benzoxazolium and similar planar heteroaromatic systems, the aggregation is inhibited by unfavorable steric interactions between the chromophores. More specifically, the molecules with bulky substituents overlap inefficiently their molecular orbitals to form a triplet dye species. Another structural factor that increases stability of the chromophore is the presence of anionic moieties at the periphery of the molecule [2, 4]. These moieties are normally

sulfonatoalkyl groups, and they are generally affixed to the nitrogen atoms of the end-heterocyclic units. Dye **16** is shown for illustration [3]. Most dyes of this class contain one sulfonate group as part of the internal salt with the cationic  $\pi$ -system and the second sulfonate group is neutralized by a metal counter ion such as Na<sup>+</sup> or K<sup>+</sup>. The two alkylsulfonate substituents are in a constant dynamic motion, shielding the chromophore from intermolecular interactions with other chromophores and attack by degradative species. This prominent stabilizing factor is further enhanced by the presence of additional sulfonate groups at the heterocyclic end-units of the dye molecule. This stabilizing effect can be explained in terms of the inhibition of aggregation of polyanionic molecules. An added benefit to the use of polysulfonated dyes is their increased solubility in aqueous solvents relative to the solubility of unsubstituted parent compounds. It should be noted that dyes with and without sulfonate substituents exhibit similar absorption and fluorescence properties.

These structural features that affect stability of cyanine dyes are illustrated by an unstable compound 17 and its relatively stable analog 16 [4]. After a four-day period of exposure to light, the indolium pentamethine dye 16 containing the *N*-propylsulfonate moieties decomposed by 21%, while the *N*-methyl pentamethine analog 17 decomposed by 98%. On the other hand, the benzothiazolium pentamethine dye 18 decomposed by 67% under the same conditions. Thus, the indolium cyanines are less susceptible to photodegradation than their benzothiazolium counterparts, as already discussed.

Waggoner et al. reported that polyfluorination of cyanine dyes inhibits aggregation and concomitant photobleaching. The structure of stable dye 19 is provided for illustration [18].

Brichkin et al. have studied the influence of surfactants, such as cationic CTAB, anionic SDS, AOT, and nonionic Triton X-100, on the spectral properties and aggregation of benzothiazolium cyanine dyes and found that the result significantly depends on the surfactant type and concentration. They found that the addition of surfactants to aqueous solutions of these dyes at concentrations below the critical micelle concentration (CMC) favors the formation of aggregates, whereas surfactant concentrations above CMC cause dissociation of the aggregates [19]. As already noted, photostability of cyanine dyes increases with a decrease in the polymethine length [20]. However, substituents on the terminal heterocyclic units do not have much effect on the photostability of the dyes. On the other hand, photostability of the dyes in solution can be greatly affected by solvent polarity. The greater the polarity, the smaller the rate of the generation of singlet oxygen and the related rate of the photooxidation reaction [20].

### 2.2.3 Miscellaneous

Kim et al. reported squarylium dyes 20–22 with dihydroperimidine end-units that are additionally modified with other groups. The authors claimed that the introduction of a quinoline moiety into the squarylium dye afforded considerable protection against fading [21]. The order of photostability for these squarylium dyes is 22 > 20 > 21.

Symmetrical and unsymmetrical pyroninocyanine dyes 23–25 reported by Shandura et al. are photostable long-wavelength dyes [22]. However, they are not stable in the presence of nucleophiles under dark conditions. They undergo nucleophilic addition at the position 9 of the xanthylium moiety.

Peng et al. studied photostability of near-infrared indolium dyes **26a**–**f** [23]. After irradiation for 6 h in ethanol, the nitro-substituted dye **26d** showed

100% photofading, but dye **26e** (R = H) showed only 24% decrease in maximal absorbance. The authors claimed that photostabilities decrease in the order of 26e > 26b > 26c > 26a > 26f > 26d. The quite low stability of the 5-(carboxy)pentyl-substituted dye **26f** is unfortunate because this dye is widely used for labeling of biomolecules.

In a recent study, Strekowski and coworkers [14] synthesized a series of merocyanines 27-30 that absorb in the visible region in a neutral or basic solution. In acidic solution (pH < 5) these merocyanines undergo protonation at the central oxygen atom to give hydroxy-substituted cyanine dyes that absorb in the near-infrared region. The authors studied relative stabilities of methanolic solutions of these dyes in the presence of molecular oxygen under dark and light conditions. After 1 day the samples exposed to sunlight of an average intensity decomposed completely, except for compound 28 which exhibited exceptional stability. The relative stabilities are in the order of  $30 > 27 \sim 28 > 29$  (Table 1).

**Table 1** Half-lives  $(t_{1/2})$  for decomposition of dyes 27–30 (0.1 mM) in methanol at pH 7 in the presence of air under dark and light conditions (light intensity of 0.08 W/cm<sup>2</sup>)

<i>t</i> <sub>1/2</sub> (h) Dark	Light	
45	2.3	
45	2.3	
21	1.8	
836	59	
	45 45 21	45 2.3 45 2.3 21 1.8

# 3 Dark Reactions

# 3.1 General

Stability of polymethine dyes in the presence of common reactive species under dark conditions is reviewed in this section. Facile synthetic modifications that are related to reactivity of the dyes, that is "controlled instability" for a specific transformation, are also included to give an interested reader a more complete picture of the chemical properties of this important class of molecules.

# 3.2 Nucleophile Addition

# 3.2.1 Reactions of Cyanines with Hydride and Cyanide Ions

Studies by Khanna et al. on Basic Violet 21 and Basic Red 14 (31 and 33, Eqs. 2 and 3) indicated that a cyanide or hydride ion undergoes a regioselective addition to the position C2 of the indolium system of these styryl dyes to give an adduct 32 or a reduced derivative 34, respectively [24]. These and similar addition reactions were studied using mass spectrometry and <sup>1</sup>H NMR.

#### **Equation 2**

### **Equation 3**

Briks et al. studied the reactions of symmetrical and unsymmetrical trimethine and pentamethine cyanine dyes and trinuclear dicationic pentamethine indocarbocyanine dyes with sodium borohydride as the source of the hydride ion [25]. They showed that the reduction of asymmetrical cyanines containing two different end-heterocyclic units is regioselective and takes place at the more electron-positive heterocyclic system. Two examples of the reduction of dye 35 (Scheme 2) and dye 38 (Scheme 3) are given for illustration. As can be seen, these reactions produce the respective products 37 and 40, and the alternative products 36 and 39 were not found.

#### Scheme 2

#### Scheme 3

A similar treatment of the dicationic pentamethine indolium cyanine 41 resulted in addition of hydride at both cationic centers to produce the dihydro derivative 42 (Eq. 4).

On the other hand, an entirely different reduction pattern was observed when certain symmetrical cyanine dyes were allowed to react with sodium borohydride in methanol. Thus, *meso*-addition of hydride was observed with

**Equation 4** 

both benz[c,d] indolium and pyrylium trimethine cyanine dyes to give the respective adducts 43 and 44.

# 3.2.2 Reactions with Hydroxide and Alkoxide Ions

In addition to the reactions described above, the  $\pi$ -framework of the polymethine dyes is also prone to the addition reaction of hydroxide and alkoxide ions. This addition takes place at the alternating electrophilic carbons of the polymethine chain. For example, the telluropyrylium dye 45 undergoes a reaction with hydroxide ion at the central *meso*-carbon [26]. The resultant adduct 46 subsequently undergoes fragmentation with the formation of the telluropyrylium aldehyde 47 and 4-methylidenetelluropyran 48 (Scheme 4). The final product 49 is apparently formed by the reaction of 48 with substrate 45.

Gray et al. [27] observed a hydrolytic breakdown of the commercial near-infrared dye IR140 50 upon treatment with aqueous NaOH in a mixture with dichloromethane in the presence of tributylammonium bromide as a phase-transfer catalyst. This reaction converts the benzothiazolium heptamethine cyanine 50 (Scheme 5) to the unexpected merocyanine derivative 52, apparently through the intermediary of an adduct 51.

#### Scheme 4

#### Scheme 5

The addition reaction of hydroxide or ethoxide ion with benzindolium heptamethine cyanine dyes was studied by Strekowski et al. and the reactivity pattern of a benz[c,d]indolium derivative 53 is given in Eq. 5 for illustration [28]. An interesting feature of this addition reaction is the formation of an ethoxy or hydroxy adduct in aqueous ethanol or methanol, respectively. A similar addition of hydroxide ion to a 3,3-dimethyl-1H-benz[e]indolium analog of 53 was also observed. The parent dye is regenerated quantitatively upon treatment of the corresponding adduct with a weak acid, including silica gel.

CI CI CI CI CI CI 
$$ROH/H_2O$$
  $ORD R$   $R = Et (in EtOH/H_2O)$   $ROH/H_2O$   $ROH/H_2O$ 

### **Equation 5**

The treatment of indolium heptamethine cyanines such as 56 with sodium methoxide in the presence of methanol- $d_4$  results in a highly selective hydrogen-deuterium exchange at positions C1′ and C7′ [8]. The reaction can conveniently be monitored by  $^1\mathrm{H}$  NMR when conducted in deuteriochloroform. The mechanism is suggested in Scheme 6. As can be seen, the methoxide adducts 57-59 are the suggested precursors to the final product such as 60. On the other hand, all hydrogens of the polymethine chain can be displaced by deuterium atoms upon treatment of a cyanine dye with deuterium chloride.

Heptamethine indolium cyanines containing a chlorine atom at the central meso position, such as **61** in Eq. 6, are easily synthesized, and recently they became important substrates for modification of the heptamethine indolium chromophore [14, 28–36]. Specifically, treatment of **61** with nucleophiles results in derivatization of the chromophore at the central meso position, as illustrated in Eq. 5 by a facile preparation of cyanines **62–68**. Importantly,

#### Scheme 6

### **Equation 6**

the reaction of 61 with 4-(isothiocyanato)benzenethiol directly gives compound 67 which is a useful reagent for labeling of proteins with a nearinfrared chromophore. The mechanism of these highly efficient transformations involves a S<sub>RN</sub>1 pathway which starts with a single-electron-transfer (SET) from a nucleophilic species to the dye. These transformations are essentially instant for nucleophiles that are good single-electron donors, such as phenoxide or benzenethiolate ions, when conducted in a solvent that supports the SET process, such as dimethyl sulfoxide or N,N-dimethylformamide. Conversely, the synthesis of derivatized dyes is strongly inhibited in solvents, such as water and alcohols, that do not support the SET process. This analysis of the reactivity of dye 61 and analogs has important ramifications for future design, synthesis, and application of functionalized indolium heptamethine cyanines. Thus, dyes 61 and similar chloro-substituted chromophores are readily available, and their chlorine atom can be displaced by the reaction with nucleophiles under S<sub>RN</sub>1 conditions. When used for labeling of biomolecules in aqueous media, the derivatized dyes are stable at neutral pH but may undergo a nucleophile addition reaction with the chromophore under basic aqueous conditions, as discussed above. However, the resultant adducts are quantitatively decomposed to the starting near-infrared dyes by weak acid.

#### References

- 1. Patonay G, Kim JS, Kodagahally R, Strekowski L (2005) Appl Spectrosc 59:682
- 2. Guether R, Reddington MV (1997) Tetrahedron Lett 38:6167
- 3. Strekowski L, Lipowska M, Patonay G (1992) Synth Commun 22:2593
- 4. Rao TVS, Huff JB, Bieniarz C (1998) Tetrahedron 54:10627
- 5. Tyutyulkov N, Fabian J, Mehlhorn A, Dietz F, Tadjer A (1991) Polymethine Dyes. Structure and Properties. St. Kliment Ohridski University Press, Sofia, Bulgaria
- 6. Lepaja S, Strub H, Lougnot DJ (1982) Z Naturforsch 38A:56
- 7. Chen P, Li J, Qian Z, Zheng D, Okasaki T, Hayami M (1998) Dyes Pigm 37:213

- 8. Lipowska M, Patterson SE, Patonay G, Strekowski L (1993) J Heterocycl Chem 30:1177
- 9. Raue R (1990) Methine Dyes and Pigments. In: Ullman's Encyclopedia of Industrial Chemistry. VCH, Weinheim, p 491
- Strekowski L, Lipowska M, Gorecki T, Mason JC, Patonay G (1996) J Heterocycl Chem 33:1685
- 11. Monich NV, Krasnaya ZA, Levkoev VF (1980) Khim Geterotsikl Soedin 12:16
- 12. Fabian J (1992) Chem Rev 92:1197
- 13. Reynolds GA, Drexhage KH (1977) J Org Chem 42:885
- 14. Strekowski L, Lee H, Mason JC, Say M, Patonay G (2007) J Heterocycl Chem 44:475
- 15. Raue R, Harnisch H (1984) Heterocycles 21:167
- 16. Arunkumar E, Forbes CC, Noll BC, Smith BD (2005) J Am Chem Soc 127:3288
- 17. Arunkumar E, Fu N, Smith BD (2006) Chem Eur J 12:4684
- 18. Renikuntla BR, Rose HC, Eldo J, Waggoner AS, Armitaga BA (2004) Org Lett 6:909
- 19. Brichkin SB, Kurandina MA, Nikolaeva TM, Razumov VF (2004) High Energ Chem 38:373
- 20. Chen P, Sun S, Hu Y, Qian Z, Zheng D (1999) Dyes Pigm 41:227
- 21. Kim S-H, Kim J-H, Cui J-Z, Gal Y-S, Jin S-H, Koh K (2002) Dyes Pigm 55:1
- 22. Shandura MP, Poronik YM, Kovtun YP (2005) Dyes Pigm 66:171
- 23. Chen X, Peng X, Cui A, Wang B, Wang L, Zhang R (2006) J Photochem Photobiol A 181:79
- 24. Khana IK, Vekataraman K (1978) Indian J Chem 16B:755
- 25. Briks YL, Romanov NN, Turov AV (1990) Zh Org Khim 26:2591
- 26. Young DN, Detty MR (1997) J Org Chem 62:4692
- 27. Gray R, Walton D, Brickerton J, Richards P, Hepinstall J (1998) Dyes Pigm 38:97
- 28. Strekowski L, Mason JC, Britton JE, Lee H, Aken KV, Patonay G (2000) Dyes Pigm 46:163
- 29. Strekowski L, Lipowska M, Patonay G (1992) J Org Chem 57:4578
- 30. Strekowski L, Lipowska M, Patonay G (1992) Synth Commun 22:2593
- 31. Lipowska M, Patonay G, Strekowski L (1993) Synth Commun 23:3087
- 32. Strekowski L, Gorecki T, Mason JC, Lee H, Patonay G (2001) Heterocycl Commun 7:117
- 33. Strekowski L, Mason JC, Lee H, Gupta R, Sowell J, Patonay G (2003) Heterocycl Commun 40:913
- 34. Strekowski L, Mason JC, Lee H, Patonay G (2004) Heterocycl Commun 10:381
- 35. Strekowski L, Mason JC, Lee H, Say M, Patonay G (2004) J Heterocycl Chem 41:227
- 36. Strekowski L, Mason JC, Say M, Lee H, Gupta R, Sowell J, Hojjat M (2005) Heterocycl Commun 11:129

# **Subject Index**

3-Acetyl-4-hydroxycoumarin 108 8-Acetyl-7-hydroxy-4-methylcoumarin	-, spiropyranes 117 Coumarin polymethines 107
108	-, 2-pyrone analogs 114
Acrylates, multifunctional, Marcus theory	-, quinolone analogs 116
214	Covalent labeling 33
-, probing of photoinitiated polymerization	Cyanine borates 184
197	-, photoredox pairs, visible-light
Acyl(hydroxy)arenes, boron complexes	photoinitiators 203
108	Cyanine dyes 11
Acyl(hydroxy)coumarins 107	–, <i>N</i> -alkoxypyridinium salt 209
N-Alkoxypyridinium salt 209	-, alkyltriphenylborate salt 202
Alkyltriphenylborate salt 202	-, Arg-Gly-Asp sequence (RGD) conjugates
Anilinosquarylium 135	54
Azuleno-squarylium 135	-, cathepsin-D-sensitive 59
Tizateno oquarynam 100	-, endostatin conjugates 58
Barbituric acid anilinomethylene	-, folic acid conjugates 61
derivatives 84	-, hydrophilic, carbohydrate moieties 51
Benzothiazole 13	-, nucleophile addition 232, 235
Benzothiazolium 12	-, photodynamic therapy (PDT) 62
Benzothiazolium heptamethine cyanine	-, reduction 232
dye 224	-, small peptide conjugates 49
Benzothiazolium trimethine dyes 205	-, symmetrical 14
Benzoxazolium 12	-, synthesis 1
Bisquarate-based squarylium 159	-, tumor-targeted 48
Bis-squarylium dyes 153	-, unsymmetrical 17
	•
	-, water-soluble 46
<i>n</i> -Butyltriphenylborate 203	Cyanine–DNA conjugates 24
Cook a service a description	Cyclodextrins 221, 226
Carbocyanine dyes 94	12 Dil + 12 di 1 di + 11 00
Cathepsin-D-sensitive cyanine dyes 59	1,3-Dibutyl-2-thiobarbituric acid 88
CE-LIF, proteins 35	Dibutylthiobarbituric acid 86
Charge-resonance probes 186	Dimethyl-1-pyrroline <i>N</i> -oxide (DMPO)
Charge-transfer (CT) probes 186	224
Cholesteryl laurates 60	Dimethylindole 13
Chromen-4-one 80	DNA nanotag concept 21
Circular dichroism (CD) 36	DNA-dye assembly 21
Coinitiator concentration 209	Dye aggregates, H-/J-types 38, 94, 124,
Coumarin merocyanines, polymeric	174, 222, 227
matrices 127	Dyeing photoinitiators 183

240 Subject Index

7-Hydroxy-4-methyl-8-propionylcoumarin Dyes 11 -, dimeric 13, 22, 96, 174 -, DNA-conjugated 24 -, near-infrared 7, 31, 43, 48, 57, 148, 158 ICG analogs, modified 45 -, peptide-/protein-conjugated 26 Immunoassays 35 -, photobleaching 216, 223 Indocyanine green 41 -, pH-sensitive 221 Indolium pentamethine cyanines 226 -, PNA-conjugated 25 Integrated waveguide fluorescence optodes -, unsymmetrical 18 (IWFOs) 94 Dyes/coinitiator photoinitiating systems Intercalation 11 Ion sensors, merocyanines Encapsulation 221 Ketocyanines 83, 86, 94, 231 Endostatin 2-Ethyl-2-(hydroxymethyl)-1,3-Labeling, covalent 33 propanediol triacrylate (TMPTA) -, noncovalent 36 205 Fluorescence 7, 11, 31, 53, 67, 129 Magnetic resonance Fluorescence probes 183 Malachite green 17 Fluorescent fiberoptic immunosensor Medicine, merocyanines 99 Merocarbocyanines 77, 79 (FFOI) 36 Fluorodeoxyglucose 41 Merocyanines 78, 234 3-Formyl-4-hydroxycoumarin 107 -, long-bridge 86 Förster resonance energy transfer (FRET) -, medicines 99 20 Meropolycarbocyanines 77 N-Methoxypyridinium borate salts 208 Glioma tumors, in vivo fluorescence Methyl methacrylate, probing of thermally imaging/PDT efficacy 67 initiated polymerization 188 Glutacondialdehyde dianil -, pyridinium probes, blue shifts 195 monohydrochloride 88 1-Methyl-2-pyrrolidinone (MP) 205 Methylene blue 201 Hemicyanines 19, 186, 207 4-Methylidenetelluropyran 234 –, modified, photoinitiating photoredox 2-(Methylmercapto) benzothiazole 78 systems 207 Monomethine cyanines 2 -, photoinitiators, free radical Multifunctional dyes 41 polymerization 206 Heptamethine cyanines 6, 31 Near-infrared (NIR) dyes 31, 41, 221 Heptamethine indolium cyanines 7, 43, Noncovalent interaction 36 48, 57, 236 Non-linear optics, merocyanines 97 -, S<sub>RN</sub>1 reaction 6, 53 Nucleic acids 11 3-(1'-Hexyloxyethyl)-3-devinylpyropheophorbide-a (HPPH) 41, Organic dye-sensitized solar cells (DSSCs) HSA-dye conjugate, fluorescent lymph Oxazole yellow 25 tracer 35 Hummel-Dreyer method 36 Hybridization probes, fluorogenic dye Pentamethine cyanines 4, 14, 16, 46, 50, 54 Peptide-conjugated dyes

Photobleaching reaction 216, 223

Hydrogen energy, merocyanines 98

Subject Index 241

Photochromism 119 Rhodanine 78 Photodynamic antimicrobial Rigidization 221 chemotherapy 100 Rose bengal 207 Photodynamic therapy (PDT) 41, 76, 99 Rotaxane 221 Photoinduced electron-transfer reaction (PET) 183, 212 Sandwich assay 35 Solar cells, merocyanines Photoinitiation, thermodynamics 212 Photoinitiators, visible light -, squarylium dye 163 polymerization 200 Solvatochromism, merocyanines 91 Photomerocyanines 77 Spiropyranes 77, 117 Photooxidizable dye sensitization Squaraine dye 226 Squaric acid (3,4-dihydroxy-3-cyclobutene-201 Photophysics 17 1,2-dione) Photoreducible dye sensitization 201 135 Photosensitizers, tumor-avid 41 Squarylium dyes (squaraines) 133, 229 Pinacyanol 14 -, analogues bisquarate 156 Poly(3-hexylthiophene-2,5-diyl) (P3HT), -, biological/environmental analyses 168 TiO<sub>2</sub>/P3HT solar cell 98 -, diazacrown-derivatized 172 Poly(methyl methacrylate), trapping of -,  $\pi$ -extended probe molecules 193 -, optical properties 135 Polymethine dyes 75, 183 -, photoconductivity 160 -, coumarins 107 -, photosensitizers, photovoltaic devices -, dark reactions 232 -, fluorescent probes 185 -, supramolecular systems -, -, monitoring of polymerization process -, synthesis 135 185 -, unsymmetrical 139 –, hydroxide/alkoxide ions 234 Squarylium-based conjugated polymers, conductive materials 165 -, inhibition of aggregation/steric protection 226 Styryl dyes 20 -, nucleophile addition 232 Styrylpyridinium probe 196, 199 -, photodegradation 222 -, rigidization 225 Tellurazole 85 Telluropyrylium dye 234 -, sensitizers, two-component photoinitiating systems 202 Tetramethyl-4-piperidone (TEMP) 224 Porphyrin-based photosensitizer-cyanine Tetraphenylborate 203 Thiazole orange 13, 17 dye conjugates 63 Probe fluorescence 199 Thiobarbituric acid 87 Probe sensitivity parameter 195 Thiochromen-4-one 80 Protein labeling 32 Tricarbocyanine-cholesteryl laurates Protein-conjugated dyes 26 Trimethine cyanines 3, 204 3,5,5-Trimethylcyclohex-2-enone Pseudoisocyanine 14 Pyroninocyanine dyes 221, 230 Tumor imaging 41 Tumor-avid photosensitizers 41 Tumor-targeted cyanine dyes 48 Quantum dots (QDs) Quinolinium 12 Twisted intramolecular charge-transfer 192, 225 Radical polymerization 183 Tyrian (Royal purple) Rhodacyanine derivatives, Plasmodium falciparum 101 Vinyltriphenylborate 203